Improved Exact Strip Postbuckling Analysis of Anisotropic Plate With Combined Load and Edge Cases

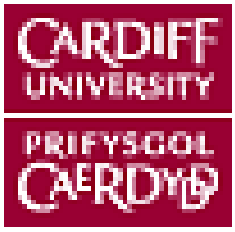

Bin Che

Cardiff School of Engineering

Cardiff University

A thesis submitted for the degree of

PhilosophiæDoctor (PhD)

October 2012

DECLARATION

This work has not previously been accepted in substance for any degree and is not concurrently submitted in candidature for any degree.

Signed.....(Candidate) Date.....

STATEMENT 1

This thesis is being submitted in partial fulfillment of the requirements for the degree of.....(insert MCh, MD, MPhill, PhD etc, as appropriate)

Signed.....(Candidate) Date.....

STATEMENT 2

This thesis is the result of my own independent work/investigation, except where otherwise stated. Other sources are acknowledged by explicit references.

Signed.....(Candidate) Date.....

STATEMENT 3

I hereby give consent for my thesis, if accepted, to be available for photocopying and for inter-library loan, and for the title and summary to be made available to outside organisations.

Signed.....(Candidate) Date.....

STATEMENT 4: PREVIOUSLY APPROVED BAR ON ACCESS

I hereby give consent for my thesis, if accepted, to be available for photocopying and for inter-library loans **after expiry of a bar on access previously approved by the Graduate Development Committee.**

Signed.....(Candidate) Date.....

I would like to dedicate this thesis to my loving families ...

Acknowledgements

I would like to gratefully thank my supervisors Prof. David Kennedy and Dr. Carol Featherston for their patient and continuous guidance and support throughout my entire PhD study. Their critical advices lead this thesis on the direction which it should pursue. Moreover, their dedicated attitude towards research encourages and inspires me to do my best on my PhD study. In particular, they introduced me to the interesting field of computational mechanics.

Also I would like to appreciate my Master supervisors Prof. Carlo Sansour and Dr. Sebastian Skatulla who encouraged and supported me to make the decision of being a PhD student.

This thesis is not possible to be completed without the support from my loving families. I would like to thank my parents who never lost passion and confidence on me, which encourages me all the time in my PhD study. Meanwhile, thanks for everything my wife did throughout my study especially last few months. She brings me encouragement, understanding and emotional support which makes me confident on my research.

Abstract

Minimisation of the mass of aerospace structures has been investigated by researchers and designers for many years. It is an efficient means to reduce the manufacturing costs, fuel consumption and environmental impact. To achieve this objective, high performance composite materials and optimised configurations are utilised in modern aircraft design. Additionally, use of the postbuckling reserve of strength has been considered during the preliminary design stage to obtain more efficient structures.

The exact strip analysis and optimum design software VICONOPT has been developed and used in postbuckling analysis. VICONOPT is able to give a good initial evaluation of load versus end shortening when compared with experimental and finite element results. However it provides poor predictions of the stress and strain distributions in the postbuckling range. This is due to its assumptions concerning the longitudinal invariance of stress and the sinusoidal variation of buckling modes in the longitudinal direction. These assumptions are appropriate for initial buckling analysis but they limit the accuracy of subsequent postbuckling analysis.

This thesis outlines some developments which improve the existing exact strip postbuckling analysis by improving the accuracy of mode shape prediction and stress and strain distributions. Based on previous research by Von Kármán, improved governing equations are derived and solved for general anisotropic plates with different in-plane edge conditions. Implementation of the improved analysis in VICONOPT enhances the accuracy of mode shapes and stress and strain distributions in the postbuckling analysis.

Contents

List of Figures

Nomenclature

$\mathbf{A_i}$,$\mathbf{B_i}$,$\mathbf{C_i}$	membrane, bending-membrane and flexural stiffness matrices for node i
a	length of plate
b_i	width of strip i
$\mathbf{D}$	displacement vector
f	eigenparameter, i.e. load factor
f^*	trial value of f
$\mathbf{I_5}$	unit matrix of order 5
J	number of eigenvalues below f^*
J_0	number of fixed end eigenvalues below f^*
J_m	number of fixed end eigenvalues of member m below f^*
$\mathbf{k}_m$	member stiffness matrix
$\mathbf{K}(\mathbf{f})$	global stiffness matrix
n	number of strips
N_{xij},N_{yij},N_{xyij}	stress resultants at node i
$\mathbf{O_5}$	null matrix of order 5
$\mathbf{P}$	perturbation force vector
$s\{\mathbf{K}(\mathbf{f})\}$	sign count of $\mathbf{K}(\mathbf{f})$
u_{ij},v_{ij}	in-plane displacements at node i
V_{xi},V_{yi},V_{xyi}	work done by applied loads
w_{ij},ψ_{ij}	out-of-plane displacements and rotations at node i
x,y,z	longitudinal, transverse and lateral directions
ε_{xij},ε_{yij},γ_{xyij}	membrane strains at node i
η_{xij},η_{yij},η_{xyij}	parameters used in effective stress resultant calculations
κ_{xij},κ_{yij},η_{xyij}	curvatures at node i

λ	longitudinal half-wavelength
ω_i	coefficient,$=\frac{\pi b_i}{\lambda}$

Subscripts

i	node reference number
j	solution case: $j = 0, c, s, C, S$ give terms to be multiplied by factors 1,$cos\frac{\pi x}{\lambda}$,$sin\frac{\pi x}{\lambda}$,$cos\frac{2\pi x}{\lambda}$,$sin\frac{2\pi x}{\lambda}$
m	member
x,y,xy	longitudinal, transverse, shear

Chapter 1

Introduction

1.1 Background

The design and manufacture of modern commercial aircraft is of major research interest due to their complexity and technical challenge. Aircraft structural design has become more complicated and significant due to recent developments in technology and considerations of safety and financial and environmental factors. Aircraft structures which are the focus of design and academic research mainly include wings and fuselage. Figure 1.1 shows typical sections of an aircraft wing and fuselage of Airbus A380. For the complex task of aircraft design, the design process normally consists of three stages, a conceptual design phase, a preliminary design phase and detailed design phase. In the conceptual design phase, a variety of possible aircraft configurations that meet all the requirements in the design specifications are collected to sketch up a basic concept of the aircraft. Then the design specifications established in the conceptual design phase will be used to fit design parameters in the preliminary design phase. The optimisation of the aircraft, structural analysis and control design are also carried out in this phase. Moreover, wind tunnel testing and computational calculations are required to determine the structural stability and mechanical characteristics. As a result of high speed computers, a variety of computer software is utilised to complete a great number of tests and analyses, which bring benefits in reducing

Figure 1.1: Typical section of A380 wing and fuselage [1]

computational consumption and therefore saving money in the preliminary design phase. Finally in the detailed design stage, determinations of component design and fabrication aspects are completed.

In modern aircraft design, lightweight aircraft structures are essential due to the consideration of financial factors and environmental impact. Therefore minimisation of weight of aircraft is taken into account by both researchers and designers. High performance composite material is regarded as an alternative to traditional metalic material (e.g. aluminium and titanium) in parts of aircraft such as the wings and the fuselages. Composite material can bring advantages in lighter weight structures due to its higher strength-weight ratios, moreover it also offers resistance to fatigue and corrosion. Figure 1.2 shows two modern commercial jets, Boeing 777 and Airbus A380, which utilise a great amount of composite materials. With a combination of efficient analysis and optimisation tools, high performance materials can lead to significant increases in stiffness, strength and reliability, while minimising the weight of aircraft structures.

Another way of minimising the weight of aircraft structures is to take into account the postbuckling reserve of strength. A plate structure can often carry loads far in excess of its critical buckling loads in a stable manner before it collapses. This phenomenon is known as postbuckling and was first investigated by Euler [4] in 1744. By taking advantage of the postbuckling properties of a material, structures can carry more loads within a safe range, further reducing the weight of aircraft structures.

Figure 1.2: Boeing 787 and Airbus A380 [2]

Owing to the rapid development of computer technology, computer analysis software has been widely accepted and used in aircraft engineering in the past few decades. Researchers and designers have obtained great benefits from high speed computers in computational analysis. In the preliminary and detailed phases of aircraft design, finite element analysis (FEA) software (e.g. ABAQUS, NASTRAN and ANSYS) have numerous advantages in terms of easy modelling and accurate analysis. However, researchers and designers keep seeking for more efficient computational approach to reduce the computation time of the software. Finite strip analysis (FSA) which was introduced by Cheung [5] in 1968 has proved to be a powerful and efficient tool in the analysis of structural components. Later on Stein [3] provided an analytical solution to postbuckling of isotropic and orthotropic plates in compression and shear. In 1990, Williams *et al.* [6] presented a buckling and vibration analysis and optimum design software VICONOPT based on an 'exact strip' approach, which provided an reliable efficient approach for analysing anisotropic plates in the preliminary design phase.

VICONOPT is not only an analysis software but also an optimisation tool which deals with anisotropic plates in combined load cases and edge conditions. It has been shown to be a reliable, fast tool compared with FEA and FSA while providing adequate accuracy in the preliminary design phase. This thesis is based on existing theory of Kennedy [7] and Stein [3], while developing the improved exact strip analysis theory and implementing improvements to VICONOPT in postbuckling analysis. The features of this improved analysis in VICONOPT lead

to accurate solutions in postbuckling analysis and keep efficiency advantages in preliminary design.

1.2 Thesis motivation, aims and objectives

The motivation for this thesis is to enable reliable, efficient, and accurate postbuckling analysis in the software VICONOPT. VICONOPT has been utilised as an analysis tool and optimum design software in both research and industry for many years. It was developed for typical aircraft structure components, such as aircraft wing and fuselage panels made from both isotropic (e.g. metallic) materials and anisotropic (e.g. composite) materials with combined load cases. VICONOPT is an efficient tool in the preliminary design phase having been proved to be up to two orders of magnitude faster than FEA software such as ABAQUS [8] and NASTRAN [9]. VICONOPT has been validated as a reliable tool in initial buckling analysis for preliminary design of aircraft. However it loses accuracy in postbuckling analysis, notably in the calculation of stress and strain distributions. The improvement of the postbuckling accuracy of VICONOPT is therefore an attractive objective. To improve the postbuckling prediction of stress and strain distributions, previous work by Stein [3], who presented an analytical solution, provides inspiration for the project accomplished in this thesis. More importantly, by combining with Kennedy's [7] work, coupling of different sine and cosine terms and consideration of anisotropic plates have been implemented into the improved postbuckling analysis, which enables analysis of anisotropic plates under more general and complicated load and edge conditions. Meanwhile, features which enable fast analysis in VICONOPT are also kept to retain the advantage in the preliminary design phase.

VICONOPT analysis assumes longitudinal invariance of stress and the sinusoidal variation of buckling modes in the longitudinal direction. These assumptions are proper and accurate enough for initial buckling analysis. However they limit the accuracy of subsequent postbuckling analysis. VICONOPT is able to give a good evaluation of load versus end shortening in initial buckling analysis when compared with FEA and experimental results. However VICONOPT shows

poor prediction of stress and strain distributions in the postbuckling range. The aims and objectives of the project are mainly concentrated on improving postbuckling predictions of stress and strain distributions. The work involved roughly consists of three stages to meet these objectives. First of all, the improved exact strip postbuckling analysis is investigated based on Stein's [3] work. In this stage, the theoretical work is done and improved governing equations are derived and solved. Then in the second stage, the relevant formulations and calculations are compiled in a Fortran 77 program which makes possible the implementation of the improved exact strip postbuckling analysis into VICONOPT. Finally the improved analysis is implemented into VICONOPT so that it can produce accurate postbuckling analysis by using the improved exact strip postbuckling analysis.

1.3 Layout of the thesis

Section 1.1 in Chapter 1 presents an introduction of background relevant to the research topic. In section 1.2 the motivations, aims and objectives of the project have been outlined. Finally, a synopsis of the following chapters is described in detail as below.

Chapter 2 provides a brief review of initial buckling and postbuckling theory for prismatic plates. The basic theory and formulation of buckling and postbuckling is introduced. Moreover, relevant research concerning postbuckling behaviour of plate structures is critically reviewed and evaluated. As a crucial reference to this project, Stein's [3] method is introduced and demonstrated in detail.

Chapter 3 gives a detailed description of exact strip analysis and the Wittrick-Williams algorithm, which provides a theoretical background to the remainder of the thesis including VICONOPT and improved exact strip postbuckling analysis.

In Chapter 4, the exact strip analysis software VICONOPT is presented with an emphasis on the development of its analysis features. The earlier programs VIPASA and VICON are introduced in detail in order to describe the main analysis features. The development and main features of VICONOPT are then briefly discussed followed by the presentation of the optimum design capacity. Moreover, the process of the existing postbuckling analysis in VICONOPT is also examined.

Chapter 5 is dedicated to the new theory developed in this project which deals with the problem of inaccurate postbuckling prediction of stress and strain distribution. The so-called improved exact strip postbuckling analysis is introduced in detail with the improved governing differential equilibrium equations and solutions.

Chapter 6 presents the illustrative numerical results obtained from improve exact strip analysis. The results are shown for an isotropic square plate with various edge conditions. The finite element results from software ABAQUS are used to compare with those from the improved analysis to validate the current approach. Old VICONOPT results are also compared with improved postbuckling analysis and ABAQUS analysis in some cases to show the improvement of improved postbuckling analysis. Relevant discussions of improvements and errors made by the improved analysis are introduced and evaluated with the demonstration of results.

Chapter 7 shows illustrative results from the improved postbuckling analysis for other cases of problem, including isotropic plate with different aspect ratio (0.5 and 1.5 respectively), symmetric balanced composite square plate, unsymmetric unbalanced composite square plate and isotropic square plate with shear. The results from improved postbuckling analysis are compared with those from software ABAQUS to validate the accuracy. Discussion of results and evaluation of error are also presented following the demonstration of results.

Chapter 8 concludes the main objectives of this thesis and briefly summarises the processes of achieving these targets. The additional capabilities provided by improved analysis are reviewed and concluded. Recommendations for further extension and development based on improved analysis are critical evaluated and proposed for the future work.

Chapter 2

Initial buckling and postbuckling theory of prismatic plates

The buckling behaviour of a range of commonly used structures has been predicted and investigated for centuries. Regarding the history of buckling research, the first study contributing to the buckling problem is the so-called 'Euler column'. Euler [4] presented the theory of obtaining the equilibrium equation and critical buckling load of a compressed elastic column. Besides buckling research on column, Bryan [10] is recognised as the pioneer researcher who investigated the buckling behaviour of plates in 1890. Following researchers like Donnell [11], Von Kármán and Tsien [12], and Batdorf [13] then extended the buckling analysis and investigation to shell structures. Moreover, the instability buckling analysis of columns was carried out by Von Kármán [14], who investigated plastic deformation of columns and beams. Later on, the classical nonlinear bifurcation theory was developed by Koiter [15], which motivated the nonlinear buckling analysis of continuous elastic structures. Further research by Hutchinson [16] brought important contributions to nonlinear post-bifurcation/post-buckling analysis in the plastic range.

When a slender structure is loaded in compression, a point is reached where any deformation in geometry causes loss of load carrying ability. At this stage, the structure is considered to have buckled and is unstable. Therefore, buckling is

generally known as structural instability leading to failure. In practice, buckling is regarded as a sudden failure of a member of a structural component subject to compression, where the actual compressive stress at the point of failure is found to be lower than the ultimate compressive stress that the material is theoretically able to carry. Prediction of such buckling behaviour is regarded as crucial to structures subject to compression, and also to shear and dynamic loading. Basically, postbuckling problems involve nonlinear analysis rather than linear analysis, and are therefore more complicated to resolve. This chapter introduces buckling and postbuckling phenomena, and investigates this behaviour by presenting several existing plate theories. Meanwhile, recent work on the postbuckling of plates is reviewed.

2.1 Phenomenon of buckling

A buckled structure is normally known as unstable in engineering, and therefore buckling is also regarded as structural instability. To better understand the concept of buckling, the definition of instability therefore needs to be mentioned. Jones [17] provides a rigorous definition for instability which is "*An equilibrium state or configuration of a structural element, structure, or mechanical system is* ***unstable*** *if any 'small' disturbance of the system results in a sudden change in deformation mode or displacement value after which the system does not return to its original equilibrium state*". Therefore a buckling configuration can be regarded as a loss of the stable equilibrium state of a structure. To examine the state of a structure, it is essential to distinguish the types of equilibrium. In Fig.2.1 two spheres are placed on surfaces which are concave and convex respectively. In Fig.2.1(a) the sphere will move back to its original stable position (solid line) after it has been moved to another place (dashed line) due to its gravity. The condition is hence called stable equilibrium, and the potential energy is a minimum. In Fig.2.1(b) once the sphere is placed on the convex surface, it moves away from its original place and is not able to move back. This is a condition of unstable equilibrium, and the potential energy is a maximum. The phenomenon of stability as described above is similar to real buckling behaviour of structures

(a) (b)

Figure 2.1: Types of equilibrium (a) stable (b) unstable

subject to combined loadings. Engineers and researchers who study buckling behaviour of structures tend to establish the point when structures become unstable, namely, the onset of structural buckling.

According to Galambos [18] and Chen and Lui [19], buckling can be classified into two categories which are buckling into an adjacent stable equilibrium state and buckling into a non-adjacent stable equilibrium state. For buckling into an adjacent stable equilibrium state, the load versus deflection behaviour of structural elements suddenly changes at the critical buckling load from a stable equilibrium to an adjacent buckled stable equilibrium. In this type of buckling, the structure starts to buckle when the compression load exceeds the critical buckling load at which the bifurcation occurs in the load-deflection graph. For example, an Euler column with axial loading will buckle when the loading exceeds the critical buckling load P_{cr} (Fig.2.2(a)). The load versus deflection behaviour follows the deflection path when the compression increases, and otherwise follows the path in the opposite direction when the column is unloaded. For buckling into a non-adjacent stable equilibrium state, if the load is increased infinitely beyond the the critical load, the structure will deform into a different stable configuration which is not adjacent to the previous configuration. In Figure 2.2 (b), the deflection path achieves a maximum at point A which is known as the limit point, then suddenly jumps from point A to C which is not an adjacent stable equilibrium. A typical example of this type of buckling is snap-through buckling of a toggle frame shown in Fig.2.2(b).

From the load-deflection graph, the critical buckling load can be found at the point where bifurcation occurs. In the design of structures, a structure may become unstable and buckled before the ultimate strength has been reached.

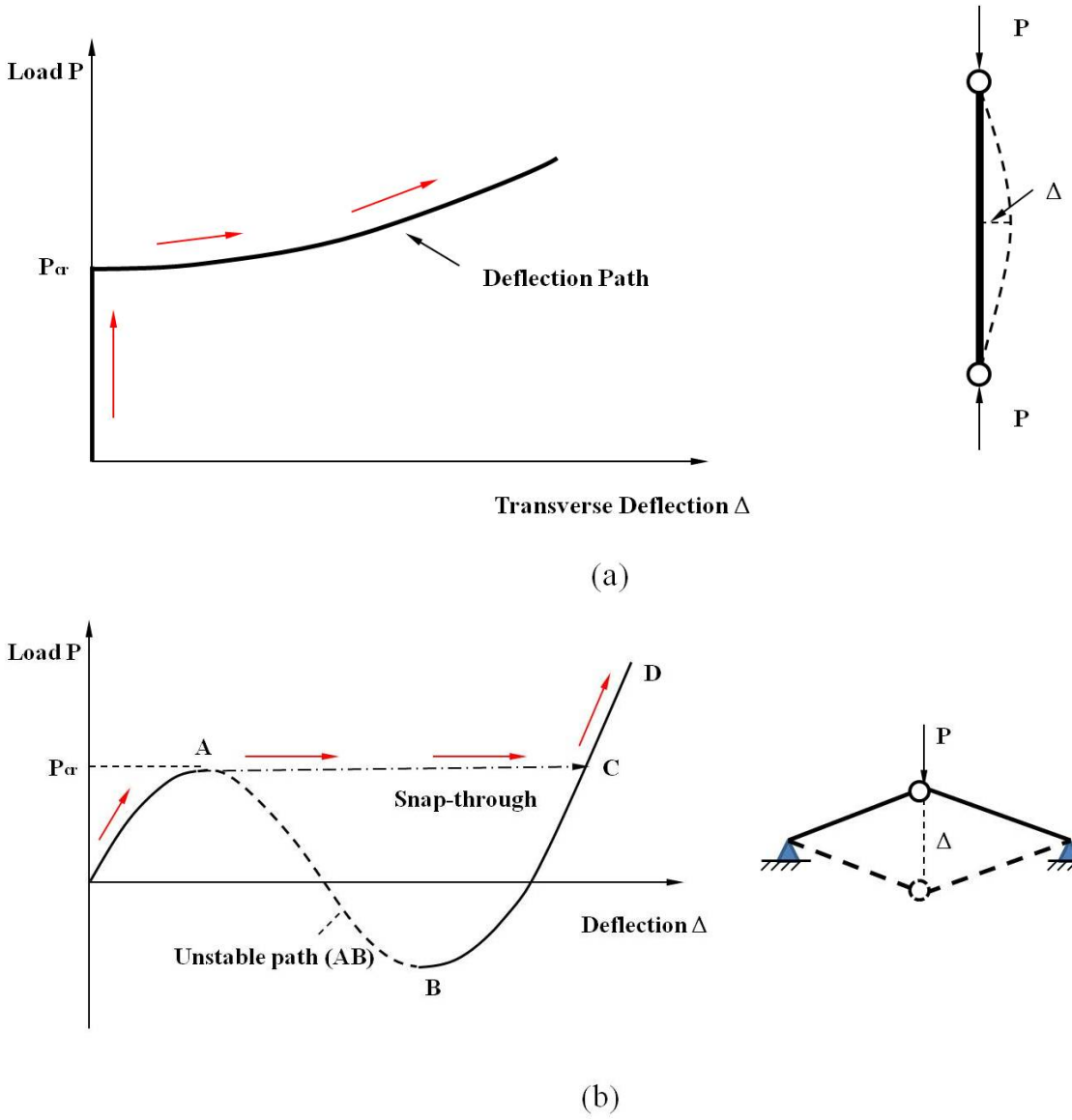

Figure 2.2: (a) Buckling with a pitchfork bifurcation point (b) Snap-through buckling

Therefore, buckling behaviour and the critical buckling load of structure is very important in both design and academic research.

2.2 Buckling theory of thin plates

2.2.1 Classical plate theory

A plate structure is a typical structure which is commonly used in aircraft engineering. The plate structure can be classified as either a thin plate or a thick plate structure depending on the width to thickness ratio. A plate can be defined as a thin plate when the thickness to width ratio is less than 0.1, otherwise it will be defined as a thick plate. The mechanical properties of the plate also have an effect. In the following section, plate theories will be introduced for isotropic, orthotropic and anisotropic plates, where isotropic materials have the same properties in all directions (e.g. glass and metal), orthotropic materials have two or three mutually orthogonal twofold axes of rotational symmetry so that their mechanical properties are different along each axis and anisotropic materials have mechanical properties which are different in any direction, namely, directional dependent. Classical plate theory (CPT) considers a plate which is sufficiently thin to assumes the transverse shear force is small compared to the bending force. The theory assumes the Kirchhoff hypothesis that: normals to the mid-surface of plate remain straight and normal after deformation. The neglection of shear deformation effects in classical plate theory satisfies the analysis of thin isotropic elastic plates. However for thick plates and anisotropic plates which have a modulus relationship of $E_{11}/E_{22} > 25$, the shear deformation effects cannot be ignored. Other plate theories concerning this will be discussed in the following section. In this section, assumptions and general formulations of CPT are introduced and referenced to the thin plate buckling theory presented by Leissa [20] and Reddy [21].

Fig.2.3 shows a typical thin plate with length, width and thickness of a, b and h respectively, and a plate element. From the Kirchhoff hypothesis the

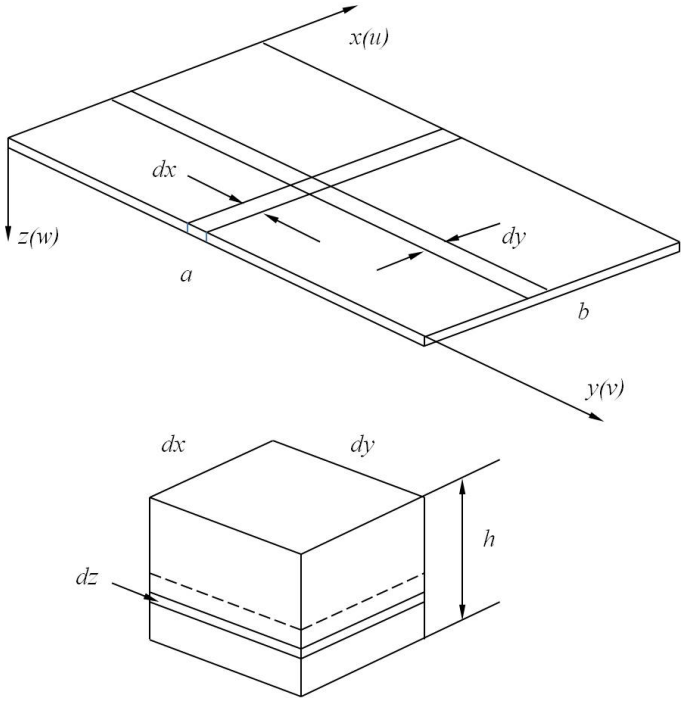

Figure 2.3: Thin plate notation
[22]

displacement for the kinematic behaviour of the plate can be written in the form

$$u = u_0 - z\frac{\partial w}{\partial x}, v = v_0 - z\frac{\partial w}{\partial y} \tag{2.1}$$

where u, v, w are displacements of a typical point in the plate, while u_0, v_0 are in-plane displacements of the mid-surface. Furthermore, all the above quantities are functions with respect to x and y only. Using the strain-displacement relationship of plane elasticity theory, the in-plane normal strain ε_x, ε_y and shear strain γ_{xy} may take the form

$$\varepsilon_x = \frac{\partial u}{\partial x}, \varepsilon_y = \frac{\partial v}{\partial y}, \gamma_{xy} = \frac{\partial u}{\partial y} + \frac{\partial v}{\partial x} \tag{2.2}$$

Substituting equation (2.1) enables equation (2.2) to be rewritten as

$$\varepsilon_x = \varepsilon_x^0 - z\kappa_x, \varepsilon_y = \varepsilon_y^0 - z\kappa_y, \gamma_{xy} = \gamma_{xy}^0 - z\kappa_{xy}, \tag{2.3}$$

where ε_x^0, ε_y^0 and γ_{xy}^0 are the mid-surface strains and κ_x, κ_y and κ_{xy} are the changes of curvature during deformation. These quantities are given as

$$\varepsilon_x^0 = \frac{\partial u_0}{\partial x}, \varepsilon_y^0 = \frac{\partial v_0}{\partial y}, \gamma_{xy}^0 = \frac{\partial u_0}{\partial y} + \frac{\partial v_0}{\partial x} \tag{2.4}$$

$$\kappa_x = \frac{\partial^2 w}{\partial x^2}, \kappa_y = \frac{\partial^2 w}{\partial y^2}, \kappa_{xy} = 2\frac{\partial^2 w}{\partial x \partial y} \tag{2.5}$$

By calculating force and moment integrals through the thickness of the plate, the in-plane force resultants N_x, N_y, N_{xy} and moment resultants M_x, M_y, M_{xy} can be obtained as follows

$$N_x = \int_{-h/2}^{h/2} \sigma_x dz, N_y = \int_{-h/2}^{h/2} \sigma_y dz, N_{xy} = \int_{-h/2}^{h/2} \gamma_{xy} dz \tag{2.6}$$

$$M_x = \int_{-h/2}^{h/2} \sigma_x z dz, M_y = \int_{-h/2}^{h/2} \sigma_y z dz, M_{xy} = \int_{-h/2}^{h/2} \gamma_{xy} z dz \tag{2.7}$$

where σ_x and σ_y are the in-plane normal stresses and γ_{xy} is the in-plane shear stress. Rewriting the relationships between force and moment resultants and mid-surface strains and curvature in matrix form, the following expression is given

$$\begin{bmatrix} N_x \\ N_y \\ N_{xy} \\ M_x \\ M_y \\ M_{xy} \end{bmatrix} = \begin{bmatrix} A_{11} & A_{12} & A_{16} & B_{11} & B_{12} & B_{16} \\ A_{12} & A_{22} & A_{26} & B_{12} & B_{22} & B_{26} \\ A_{16} & A_{26} & A_{66} & B_{16} & B_{26} & B_{66} \\ B_{11} & B_{12} & B_{16} & D_{11} & D_{12} & D_{16} \\ B_{12} & B_{22} & B_{26} & D_{12} & D_{22} & D_{26} \\ B_{16} & B_{26} & B_{66} & D_{16} & D_{26} & D_{66} \end{bmatrix} = \begin{bmatrix} \varepsilon_x^0 \\ \varepsilon_y^0 \\ \gamma_{xy}^0 \\ -\kappa_x \\ -\kappa_y \\ -\kappa_{xy} \end{bmatrix} \tag{2.8}$$

where A_{ij}, B_{ij} and D_{ij} are the in-plane, coupling and out-of-plane stiffness respectively. To obtain the differential equations which govern the buckling behaviour of plates, the equilibrium equations are given as

$$\frac{\partial N_x}{\partial x} + \frac{\partial N_{xy}}{\partial y} = 0$$

$$\frac{\partial N_{xy}}{\partial x} + \frac{\partial N_y}{\partial y} = 0$$

$$\frac{\partial^2 M_x}{\partial x^2} + 2\frac{\partial^2 M_{xy}}{\partial x \partial y} + \frac{\partial^2 M_y}{\partial y^2} + N_x \frac{\partial^2 w}{\partial x^2} + 2N_{xy}\frac{\partial^2 w}{\partial x \partial y} + N_y \frac{\partial^2 w}{\partial y^2} = 0 \tag{2.9}$$

The above equilibrium equations are the fundamental form for the buckling problem and describe the state of neutral stability for plate structures. To explore the equilibrium equations in the buckled configuration for isotropic, orthotropic and anisotropic plates respectively, a simplified form of the above governing equilibrium equations can be obtained by the following procedure. Substituting equations (2.4), (2.5) and (2.8) into equation (2.9) and rewriting the equations in matrix form gives

$$\begin{bmatrix} L_{11} & L_{12} & L_{13} \\ L_{21} & L_{22} & L_{23} \\ L_{31} & L_{32} & (L_{33} - F) \end{bmatrix} \begin{bmatrix} u \\ v \\ w \end{bmatrix} = \begin{bmatrix} 0 \\ 0 \\ 0 \end{bmatrix} \tag{2.10}$$

where L_{ij} are differential operators in terms of plate stiffness

$$L_{11} = A_{11}\frac{\partial^2}{\partial x^2} + 2A_{16}\frac{\partial^2}{\partial x \partial y} + A_{66}\frac{\partial^2}{\partial y^2}$$

$$L_{22} = A_{22}\frac{\partial^2}{\partial y^2} + 2A_{26}\frac{\partial^2}{\partial x \partial y} + A_{66}\frac{\partial^2}{\partial x^2}$$

$$L_{33} = D_{11}\frac{\partial x^4}{\partial x^4} + 4D_{16}\frac{\partial^4}{\partial x^3 \partial y} + 2(D_{12} + 2D_{66})\frac{\partial^4}{\partial x^2 \partial y^2} + 4D_{26}\frac{\partial^4}{\partial x \partial y^3} + D_{22}\frac{\partial^4}{\partial y^4}$$

$$L_{12} = L_{21} = A_{16}\frac{\partial^2}{\partial x^2} + (A_{12} + A_{66})\frac{\partial^2}{\partial x \partial y} + A_{26}\frac{\partial^2}{\partial y^2}$$

$$L_{13} = L_{31} = -B_{11}\frac{\partial^3}{\partial x^3} - 3B_{16}\frac{\partial^3}{\partial x^2 \partial y} - (B_{12} + 2B_{66})\frac{\partial^3}{\partial x \partial y^2} - B_{26}\frac{\partial^3}{\partial y^3}$$

$$L_{23} = L_{32} = -B_{16}\frac{\partial^3}{\partial x^3} - 3B_{26}\frac{\partial^3}{\partial x \partial y^2} - (B_{12} + 2B_{66})\frac{\partial^3}{\partial x^2 \partial y} - B_{22}\frac{\partial^3}{\partial y^3} \tag{2.11}$$

and F is the differential operator representing the in-plane loading

$$F = N_x\frac{\partial^2}{\partial x^2} + 2N_{xy}\frac{\partial^2}{\partial x \partial y} + N_y\frac{\partial^2}{\partial y^2} \tag{2.12}$$

Just before buckling, the in-plane equilibrium equations yield $u = v = 0$. For symmetrically laminated cross-ply plates, $B_{ij} = 0$ and hence the operators L_{13} and L_{23} in equation (2.11) are null. Moreover, the absence of stiffnesses D_{16} and D_{26} cancels the corresponding terms in operator L_{33}, which gives the out-of-plane governing equation as

$$D_{11}\frac{\partial^4 w}{\partial x^4} + 2(D_{12} + 2D_{66})\frac{\partial^4 w}{\partial x^2 \partial y^2} + D_{22}\frac{\partial^4 w}{\partial y^4} - (N_x\frac{\partial^2 w}{\partial x^2} + 2N_{xy}\frac{\partial^2 w}{\partial x \partial y} + N_y\frac{\partial^2 w}{\partial y^2}) = 0 \tag{2.13}$$

For homogeneous orthotropic plates the governing equation is in the same form as for equation (2.13) above.

For symmetrically laminated plates, the coupling between bending and twisting can not be ignored therefore stiffnesses D_{16} and D_{26} are non-zero. Hence the governing equation is written as

$$D_{11}\frac{\partial^4 w}{\partial x^4} + 4D_{16}\frac{\partial^4 w}{\partial x^3 \partial y} + 2(D_{12} + 2D_{66})\frac{\partial^4 w}{\partial x^2 \partial y^2} + 4D_{26}\frac{\partial^4 w}{\partial x \partial y^3} + D_{22}\frac{\partial^4 w}{\partial y^4} - (N_x\frac{\partial^2 w}{\partial x^2} + 2N_{xy}\frac{\partial^2 w}{\partial x \partial y} + N_y\frac{\partial^2 w}{\partial y^2}) = 0 \tag{2.14}$$

For a homogeneous anisotropic plate the governing equation has the same form as equation (2.14) but the only difference is in how the stiffnesses D_{ij} are calculated. The complex problem of unsymmetrically laminated plates, is not discussed in this thesis and therefore the equilibrium equation is not given here.

Once the out-of-plane governing equilibrium equations are derived, the solution can be subsequently obtained from them with in-plane equilibrium equations using an analytical approach.

2.2.2 First-order shear deformation plate theory

As described above, considerations of shear deformation cannot be ignored when the plate thickness increases significantly (width to thickness ratio greater than 0.1). Moreover for laminated composites, the shear flexibility is particularly crucial because the moduli of elasticity in transverse shear are much lower than the in-plane moduli. In these cases, the so-called first-order shear deformation plate theory (FSDPT) which considers the shear deformation as having an important effect on buckling behaviour is introduced briefly. To start with the Kirchhoff hypothesis mentioned in Section 2.2.1, the assumption of no consideration of transverse shear deformation is relaxed by allowing the transverse normals perpendicular to the mid-surface to rotate after deformation. The theory concerning shear deformation effects was first developed by Reissner [23], [24] and Mindlin [25] in the 1940s and 1950s on isotropic elastic plates, and later extended to

anisotropic plates by Ambartsumyan [26]. Because the shear deformation effects need only be considered when the thickness of plate is big enough, the theory basically deals with the analysis of thick plates. In this section, first-order shear deformation plate theory is introduced briefly with basic formulations which are attributed to Leissa [20], Reddy [21] and Wang *et al.* [27].

In shear deformation plate theory the rotations about x and y axes of a certain point on the mid-surface can be written as

$$\frac{\partial w}{\partial x} = \psi_x + \phi_x, \frac{\partial w}{\partial y} = \psi_y + \phi_y \tag{2.15}$$

where ψ_x and ψ_y are the rotations about the x and y axes respectively, and ϕ_x and ϕ_y are the changes in rotation due to shear. The in-plane displacements at an arbitrary point in the plate are rewritten as

$$u = u_0 - z\psi_x, v = v_0 - z\psi_y \tag{2.16}$$

where u_0 and v_0 are displacements on the mid-surface of plate as mentioned in classical plate theory. Meanwhile, the curvature changes are also rewritten as

$$\kappa_x = \frac{\partial \psi_x}{\partial x}, \kappa_y = \frac{\partial \psi_y}{\partial y}, \kappa_{xy} = \frac{\partial \psi_y}{\partial x} + \frac{\partial \psi_x}{\partial y} \tag{2.17}$$

Owing to the consideration of the shear deformation effect, it is essential to derive additional stiffness relationships as

$$\begin{bmatrix} Q_x \\ Q_y \end{bmatrix} = k \begin{bmatrix} A_{44} & A_{45} \\ A_{45} & A_{55} \end{bmatrix} \begin{bmatrix} \phi_y \\ \phi_x \end{bmatrix} \tag{2.18}$$

where Q_x and Q_y are shear forces determined by integrating transverse shear stresses over the thickness of the plate, while A_{44}, A_{45} and A_{55} are additional stiffnesses which describe the relationships between shear forces and stresses. The coefficient k is a so-called 'shear correction factor' which is usually taken as either $k = 5/6 = 0.833$ [23] or $\pi^2/12 = 0.822$ [24] for homogeneous isotropic plates as well as for composite plates.

Shear forces are then included in the equilibrium equations so that equation (2.9) is rewritten as

$$\frac{\partial N_x}{\partial x} + \frac{\partial N_{xy}}{\partial y} = 0$$

$$\frac{\partial N_{xy}}{\partial x} + \frac{\partial N_y}{\partial y} = 0$$

$$\frac{\partial Q_x}{\partial x} + \frac{\partial Q_y}{\partial y} + N_x\frac{\partial^2 w}{\partial x^2} + 2N_{xy}\frac{\partial^2 w}{\partial x \partial y} + N_y\frac{\partial^2 w}{\partial y^2} = 0 \tag{2.19}$$

Substituting equations (2.4) and (2.18) into the stiffness equations (2.8) and (2.19), and then substituting these expressions into equation (2.20), gives the governing equilibrium equation as

$$\begin{bmatrix} L_{11} & L_{12} & L_{13} & L_{14} & 0 \\ L_{21} & L_{22} & L_{23} & L_{24} & 0 \\ L_{31} & L_{32} & L_{33} & L_{34} & L_{35} \\ L_{41} & L_{42} & L_{43} & L_{44} & L_{45} \\ 0 & 0 & L_{53} & L_{54} & L_{55} \end{bmatrix} \begin{bmatrix} u \\ v \\ -\psi_x \\ -\psi_y \\ w \end{bmatrix} = \begin{bmatrix} 0 \\ 0 \\ 0 \\ 0 \\ 0 \end{bmatrix} \tag{2.20}$$

where

$$L_{11} = A_{11}\frac{\partial^2}{\partial x^2} + 2A_{16}\frac{\partial^2}{\partial x \partial y} + A_{66}\frac{\partial^2}{\partial y^2}$$

$$L_{22} = A_{22}\frac{\partial^2}{\partial y^2} + 2A_{26}\frac{\partial^2}{\partial x \partial y} + A_{66}\frac{\partial^2}{\partial x^2}$$

$$L_{33} = D_{11}\frac{\partial^2}{\partial x^2} + 2D_{16}\frac{\partial^2}{\partial x \partial y} + D_{66}\frac{\partial^2}{\partial y^2} - kA_{55}$$

$$L_{44} = D_{66}\frac{\partial^2}{\partial x^2} + 2A_{26}\frac{\partial^2}{\partial x \partial y} + D_{22}\frac{\partial^2}{\partial y^2} - kA_{44}$$

$$L_{55} = -k(A_{55}\frac{\partial^2}{\partial x^2} + A_{45}\frac{\partial^2}{\partial x \partial y} + A_{44}\frac{\partial^2}{\partial y^2}) - F$$

$$L_{12} = L_{21} = A_{16}\frac{\partial^2}{\partial x^2} + (A_{12} + A_{66})\frac{\partial^2}{\partial x \partial y} + A_{26}\frac{\partial^2}{\partial y^2}$$

$$L_{13} = L_{31} = B_{11}\frac{\partial^2}{\partial x^2} + 2B_{16}\frac{\partial^2}{\partial x \partial y} + B_{66}\frac{\partial^2}{\partial y^2}$$

$$L_{14} = L_{41} = L_{23} = L_{32} = B_{16}\frac{\partial^2}{\partial x^2} + (B_{12} + B_{66})\frac{\partial^2}{\partial x \partial y} + B_{26}\frac{\partial^2}{\partial y^2}$$

$$L_{24} = L_{42} = B_{66}\frac{\partial^2}{\partial x^2} + 2B_{26}\frac{\partial^2}{\partial x \partial y} + B_{22}\frac{\partial^2}{\partial y^2}$$

$$L_{34} = L_{43} = D_{16}\frac{\partial^2}{\partial x^2} + (D_{12} + D_{66})\frac{\partial^2}{\partial x \partial y} + D_{26}\frac{\partial^2}{\partial y^2}$$

$$L_{35} = L_{53} = -k(A_{55}\frac{\partial}{\partial x} + A_{45}\frac{\partial}{\partial y})$$

$$L_{45} = L_{54} = -k(A_{45}\frac{\partial}{\partial x} + A_{44}\frac{\partial}{\partial y}) \tag{2.21}$$

where

$$F = N_x\frac{\partial^2}{\partial x^2} + 2N_{xy}\frac{\partial^2}{\partial x \partial y} + N_y\frac{\partial^2}{\partial y^2} \tag{2.22}$$

The equilibrium equation governs the configuration when a plate has just buckled, which gives $u = v = 0$. For an isotropic plate, the absence of stiffnesses B_{ij} leads to the vanishing of operators $L_{13} = L_{31}$, $L_{14} = L_{41}$, $L_{23} = L_{32}$ and $L_{24} = L_{42}$. Also the absence of stiffnesses A_{16}, A_{26}, D_{16}, D_{26} and A_{45} is under consideration, therefore the governing equilibrium equation for first-order shear deformation theory for isotropic, orthotropic plates or cross-ply symmetrically laminated plates can be written as

$$D_{11}\frac{\partial^2 \psi_x}{\partial x^2} + D_{66}\frac{\partial^2 \psi_x}{\partial y^2} + (D_{12} + D_{66})\frac{\partial^2 \psi_y}{\partial x \partial y} + kA_{55}(\frac{\partial w}{\partial x} - \psi_x) = 0$$

$$D_{66}\frac{\partial^2 \psi_x}{\partial x^2} + D_{22}\frac{\partial^2 \psi_x}{\partial y^2} + (D_{12} + D_{66})\frac{\partial^2 \psi_y}{\partial x \partial y} + kA_{44}(\frac{\partial w}{\partial y} - \psi_y) = 0$$

$$kA_{55}\frac{\partial}{\partial x}(\frac{\partial w}{\partial x}-\psi_x)+kA_{44}\frac{\partial}{\partial y}(\frac{\partial w}{\partial y}-\psi_y)+N_x\frac{\partial^2}{\partial x^2}+2N_{xy}\frac{\partial^2}{\partial x\partial y}+N_y\frac{\partial^2}{\partial y^2}=0 \tag{2.23}$$

Further for the general case of anisotropic plates or symmetrically laminated plates, stiffness D_{16}, D_{26} and A_{45} are considered and therefore the governing equilibrium out-of-plane equations can be given in matrix form as

$$\begin{bmatrix} L_{33} & L_{34} & L_{35} \\ L_{43} & L_{44} & L_{45} \\ L_{53} & L_{54} & L_{55} \end{bmatrix} \begin{bmatrix} -\psi_x \\ -\psi_y \\ w \end{bmatrix} = \begin{bmatrix} 0 \\ 0 \\ 0 \end{bmatrix} \tag{2.24}$$

2.3 Phenomenon of postbuckling

Postbuckling is normally known as the non-linear process which occurs after the critical buckling load has been reached. Slender plate structures can carry load far exceeding the critical buckling load in the postbuckling range, which brings great benefits if utilized saving materials. However, the non-linear characteristic of postbuckling behaviour brings some uncertainty in predicting the behaviour of structures in postbuckling. For example from Shen [28], plates loaded in compression have a stable postbuckling path and are insensitive to initial geometrical imperfection, however for cylindrical shells under pressure, the postbuckling path is unstable and the structures are found to be sensitive to initial geometrical imperfection. Due to this kind of uncertainty for structures in the postbuckling range, postbuckling analysis is a major concern for both engineers and researchers.

Figure 2.4 shows a typical load-displacement curve which demonstrates the behaviour of structures in buckling and postbuckling ranges. For classical buckling theory, the bifurcation behaviour of plate follows paths A, B and C in Figure 2.4. With increasing in-plane load P, the curve follows path A which shows no displacement with increased load until a critical buckling load is reached. After this bifurcation point the curve theoretically keeps moving on path B, or may follow a buckling path C for linear idealization. However, for large displacement analysis, the curve follows path D which is non-linear with increasing slope. Path

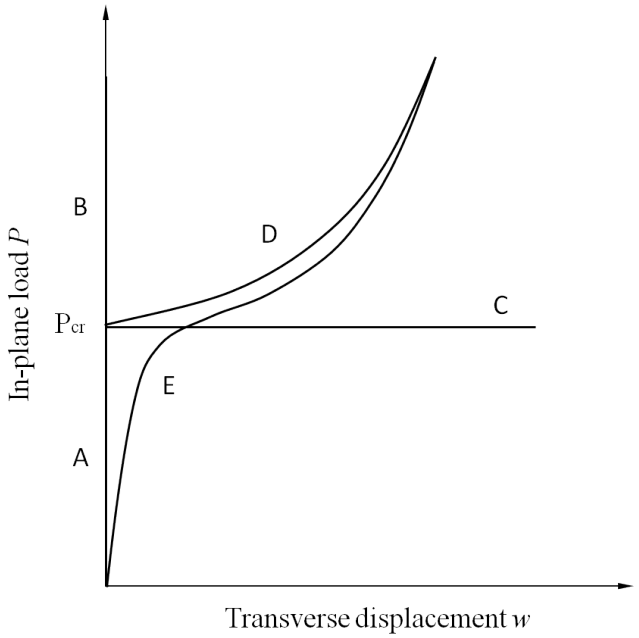

Figure 2.4: Curves of in-plane load versus transverse displacement showing typical buckling and postbuckling behaviour
[17]

D actually represents the postbuckling behaviour of plate which indicates that the plate is able to carry more load far in excess of the critical buckling load P_{cr} before it goes into unstable equilibrium. Path E shows the buckling and postbuckling behaviour of an imperfect plate as no plate is initially perfect. The decrease of imperfection magnitude will make path E increasingly kinked to path D.

To further understand the postbuckling behaviour of structures, a review of the types of buckling is given here, based on a classic review of postbuckling theory by Hutchinson and Koiter [29] and a brief description of postbuckling types by Jones [17]. Figure 2.5 illustrates four types of postbuckling behaviour for both perfect (solid line) and imperfect structures (dash line). Figure 2.5 (a) shows neutral postbuckling behaviour which gives a horizontal line for load-deflection curve for perfect structure. Points along the line are all in a neutral equilibrium state as no lower or higher energy state can be assumed for this postbuckling behaviour. This type of postbuckling behaviour indicates that structures cannot

carry load in excess of the critical buckling load P_{cr}. The dash line shows the postbuckling behaviour for imperfect structures which makes the curve approach P_{cr} asymptotically. Figure 2.5 (b) shows unsymmetric postbuckling behaviour which gives a straight line that is inclined to the horizontal for a perfect structure. The structure can only carry more load in excess of P_{cr} if it is constrained to buckle with a positive w. Otherwise the structure can only carry loads much less than P_{cr} until collapse. Figure 2.5 (c) shows symmetric stable postbuckling behaviour which gives a concave curve for a perfect structure. This type of postbuckling behaviour ensures a load carrying capacity far in excess of P_{cr} on both sides of the vertical axis, and hence it is in a stable equilibrium configuration. Moreover, due to symmetry about the vertical axis, the postbuckling behaviour is the same no matter whether the displacement w is positive or negative. Figure 2.5(d) shows symmetric unstable postbuckling behaviour which gives a convex curve for a perfect structure. This type of postbuckling behaviour indicates that the structure cannot carry load higher than P_{cr}, and hence it is in a unstable equilibrium configuration for both positive and negative displacements w. Figure 2.5(e) shows another type of postbuckling behaviour, for some structural elements which changes suddenly from a stable equilibrium configuration at point C to an immediately non-adjacent stable equilibrium configuration at point E, so the structural element 'jumps' from C to E.

2.4 Postbuckling theory of thin plates

2.4.1 Postbuckling plate theory

After the critical buckling load has been reached, a plate may start to buckle and undergo out-of-plane displacement, which is relatively large compared to the thickness. Moreover, the plate may have transverse displacement due to the buckling of the plate. Therefore, for the analysis of postbuckling additional terms have to be added to the expressions of strain due to stretching. To find the expressions for so-called Von Kármán strain, it would be useful to examine the geometric background for the strains. The following figures and derivation

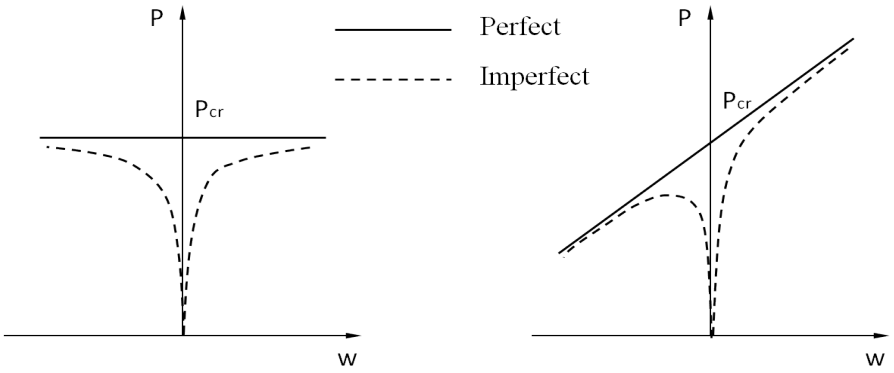

(a) Neutral Postbuckling Behaviour (b) Unsymmetric Postbuckling Behaviour

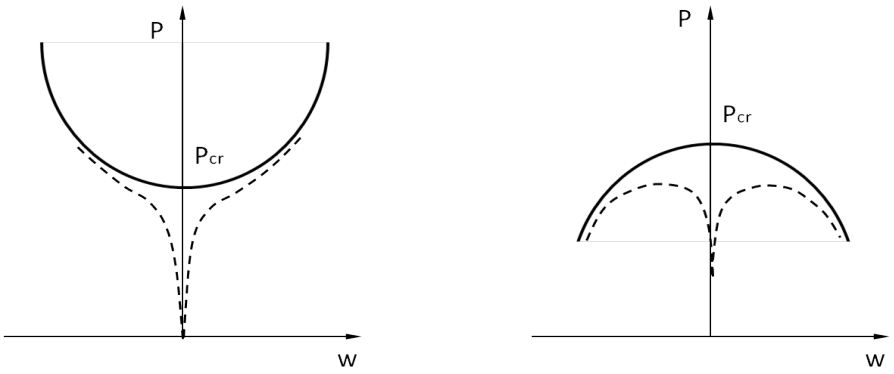

(c) Symmetric Stable Postbuckling Behaviour (d) Symmetric Unstable Postbuckling Behaviour

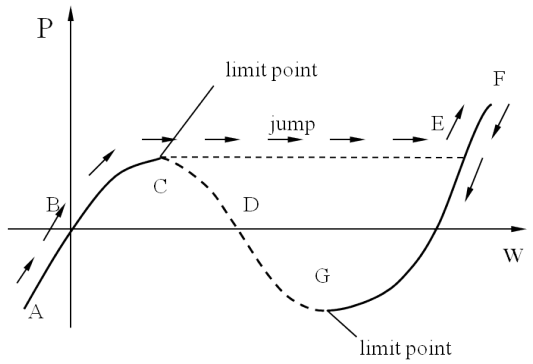

(e) Buckling into a Non-Adjacent Stable Equilibrium State

Figure 2.5: Types of Postbuckling Behaviour for perfect and imperfect structure [17]

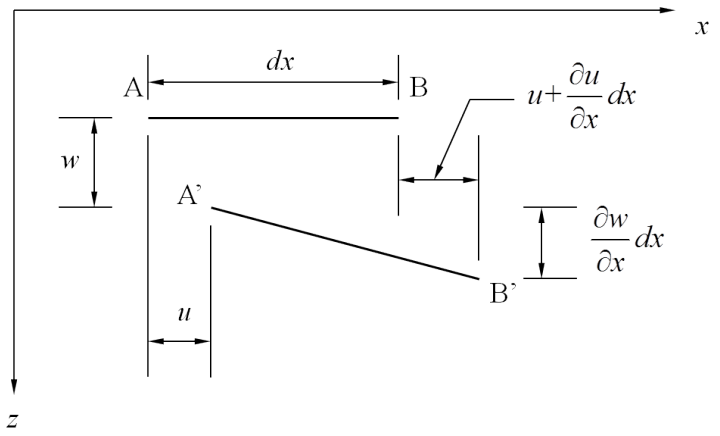

Figure 2.6: Calculation of axial strain

of strains are attributed to Yoo and Lee [22]. Consider a linear element AB of the middle surface of the plate as shown in Figure 2.6. After deformations, the length and position of AB has changed and is denoted A'B'. The length change of the element is due to effects of both in-plane displacement u and transverse displacement w. According to Figure 2.6, the elongation of the element due to u displacement is

$$\frac{\partial u}{\partial x}dx \tag{2.25}$$

The length change due to displacement w is calculated from the Pythagorean theorem as

$$A'B' = \left[dx^2 + \left(\frac{\partial w}{\partial x}dx\right)^2\right]^{1/2} \simeq \left[1 + \frac{1}{2}\left(\frac{\partial w}{\partial x}\right)^2\right]dx \tag{2.26}$$

Therefore the elongation due to the displacement w is

$$\frac{1}{2}\left(\frac{\partial w}{\partial x}\right)^2 dx \tag{2.27}$$

And the total elongation is the sum of above two

$$\frac{\partial u}{\partial x}dx + \frac{1}{2}\left(\frac{\partial w}{\partial x}\right)^2 dx \tag{2.28}$$

Hence the strain ε_x equals the total elongation divided by the original length of the element dx. Then the expression of ε_x is written as

$$\varepsilon_x = \frac{\partial u}{\partial x} + \frac{1}{2}\left(\frac{\partial w}{\partial x}\right)^2 \tag{2.29}$$

Likewise the expression of ε_y has the form

$$\varepsilon_y = \frac{\partial v}{\partial y} + \frac{1}{2}\left(\frac{\partial w}{\partial y}\right)^2 \tag{2.30}$$

The shear strain γ_{xy} which is actually an angular change consists of both the in-plane contribution and an out-of-plane contribution due to bending. Figure 2.7 illustrates the in-plane angle change and out-of-plane angle change. From Figure 2.7(a), the in-plane contribution for γ_{xy} is

$$\frac{\partial u}{\partial y} + \frac{\partial v}{\partial x} = \gamma_n \tag{2.31}$$

The bending contribution is

$$\gamma_w = \angle BOA - \angle B'O'A' = \frac{\pi}{2} - \left(\frac{\pi}{2} - \gamma_w\right) \tag{2.32}$$

Based on the law of cosines

$$(A'B')^2 = (O'A')^2 + (O'B')^2 - 2(O'A')(O'B')cos\left(\frac{\pi}{2} - \gamma_w\right) \tag{2.33}$$

where

$$(O'A')^2 = dx^2 + \left(dx\frac{\partial w}{\partial x}\right)^2$$

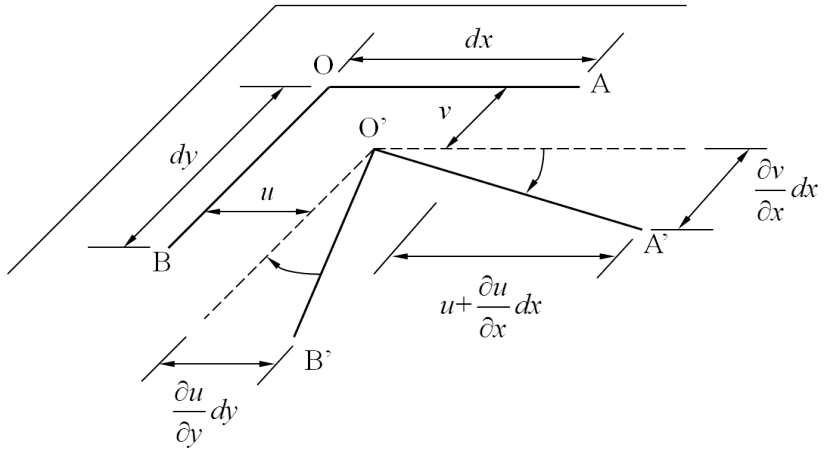

(a)

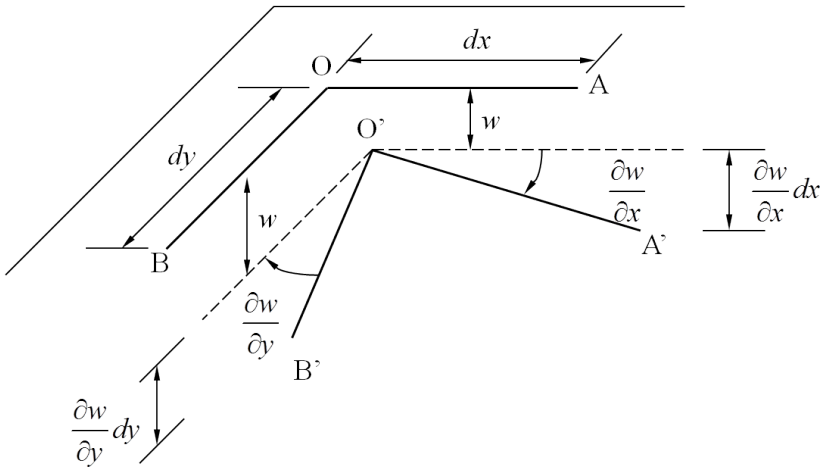

(b)

Figure 2.7: (a) in-plane angle change (b) out-of-plane angle change

$$(O'B')^2 = dy^2 + \left(dy\frac{\partial w}{\partial y}\right)^2$$

$$(A'B')^2 = dx^2 + dy^2 + \left(\frac{\partial w}{\partial x}\right)^2 dx^2 + \left(\frac{\partial w}{\partial y}\right)^2 dy^2 + \left(dy\frac{\partial w}{\partial y} - dx\frac{\partial w}{\partial x}\right)^2 \quad (2.34)$$

Neglecting higher order terms gives

$$(O'A')(O'B') = dxdy \quad (2.35)$$

For small angles $cos((\pi/2) - \gamma_w)$ can be computed as γ_w, therefore

$$\begin{aligned}(A'B')^2 &= dx^2 + \left(dx\frac{\partial w}{\partial x}\right)^2 + dy^2 + \left(dy\frac{\partial w}{\partial y}\right)^2 - 2\gamma_w dxdy + \left(\frac{\partial w}{\partial x}\right)^2 dx^2 + \left(\frac{\partial w}{\partial y}\right)^2 dy^2 \\ &= dx^2 + dy^2 + \left(dy\frac{\partial w}{\partial y} - dx\frac{\partial w}{\partial x}\right)^2 + \left(\frac{\partial w}{\partial x}\right)^2 dx^2 + \left(\frac{\partial w}{\partial y}\right)^2 dy^2\end{aligned}$$

which gives

$$\gamma_w = \frac{\partial w}{\partial x}\frac{\partial w}{\partial y} \quad (2.36)$$

Adding both in-plane and out-of-plane angle changes gives

$$\gamma_{xy} = \gamma_n + \gamma_w = \frac{\partial u}{\partial y} + \frac{\partial v}{\partial x} + \frac{\partial w}{\partial x}\frac{\partial w}{\partial y} \quad (2.37)$$

The Von Kármán strains are therefore written as

$$\varepsilon_x = \frac{\partial u}{\partial x} + \frac{1}{2}(\frac{\partial w}{\partial x})^2, \varepsilon_y = \frac{\partial v}{\partial y} + \frac{1}{2}(\frac{\partial w}{\partial x})^2, \gamma_{xy} = \frac{\partial u}{\partial y} + \frac{\partial v}{\partial x} + \frac{\partial w}{\partial x}\frac{\partial w}{\partial y} \quad (2.38)$$

and the additional terms, which involve w, are non-linear. The expression for curvature changes remains as equation (2.5) for buckling analysis, however, in the case of very large displacements, additional terms have to be added to better represent the postbuckling behaviour. To obtain the general form of the governing equilibrium equation for postbuckling analysis, equations (2.1), (2.5) and (2.8)

into (2.9) are substituted, expressed in matrix form in terms of displacements as

$$\begin{bmatrix} L_{11} & L_{12} & L_{13} \\ L_{21} & L_{21} & L_{23} \\ L_{31} & L_{32} & L_{33} \end{bmatrix} \begin{bmatrix} u \\ v \\ w \end{bmatrix} = \frac{\partial w}{\partial x} \begin{bmatrix} L_{11}w \\ L_{12}w \\ L_{13}w \end{bmatrix} + \frac{\partial w}{\partial y} \begin{bmatrix} L_{12}w \\ L_{22}w \\ L_{23}w \end{bmatrix} + \begin{bmatrix} 0 \\ 0 \\ \psi \end{bmatrix} \tag{2.39}$$

where L_{ij} are the operators defined by equation (2.22) and further

$$\begin{aligned} \psi = &\left[\tfrac{\partial u}{\partial x} + \tfrac{1}{2}(\tfrac{\partial u}{\partial x})^2\right] L_7 w + \left[\tfrac{\partial v}{\partial y} + \tfrac{1}{2}(\tfrac{\partial w}{\partial y})^2\right] L_8 w + \left[\tfrac{\partial v}{\partial x} + \tfrac{\partial u}{\partial y}\right] L_9 w \\ &-2(B_{12} - B_{26})(\frac{\partial^2 w}{\partial x \partial y}) + 2(B_{12} - B_{66}) \left[\tfrac{\partial^2 w}{\partial x^2}\tfrac{\partial^2 w}{\partial y^2} - (\tfrac{\partial^2 w}{\partial x \partial y})^2\right] \end{aligned}$$

with

$$\begin{aligned} L_7 &= A_{11}\frac{\partial^2}{\partial x^2} + 2A_{16}\frac{\partial^2}{\partial x \partial y} + A_{12}\frac{\partial^2}{\partial y^2} \\ L_8 &= A_{12}\frac{\partial^2}{\partial x^2} + 2A_{26}\frac{\partial^2}{\partial x \partial y} + A_{22}\frac{\partial^2}{\partial y^2} \\ L_9 &= A_{16}\frac{\partial^2}{\partial x^2} + 2A_{66}\frac{\partial^2}{\partial x \partial y} + A_{26}\frac{\partial^2}{\partial y^2} \end{aligned} \tag{2.40}$$

Equation (2.39) gives a general form of the postbuckling equilibrium equations for unsymmetrical composite plate, and some simplifications are possible to represent certain cases. For instance, for symmetrical laminated angle-ply plate $L_{13} = L_{31} = L_{23} = L_{32} = 0$ due to $B_{ij} = 0$, and therefore simplifications can be made in equation (2.39). For a symmetrically laminated cross-ply plate, further simplifications can be applied in addition, since $A_{16} = A_{26} = D_{16} = D_{26} = 0$.

2.4.2 Review of postbuckling analysis of plate structure

To review the work on postbuckling analysis of plates, some remarkable names who contributed greatly in raising this subject at an early stage ought to be mentioned. The first pioneer of plate buckling and postbuckling theory may be regarded as Von Kármán, who derived the basic differential equations for plate structures undergoing large deflection [14] in 1910. Later Von Kármán and other co-researchers developed and presented the concept of effective width in 1932

[30]. Later on, various approximate solutions based on energy considerations for postbuckling analysis of plates were presented by Cox [31], Timoshenko [32], Marguerre and Trefftz [33] and Van der Neut [34]. Furthermore, the work by Marguerre and Trefftz [33] was extended for simply supported infinitely long plates in compression by Kromm and Marguerre [35]. Further work by Koiter [15] enabled analysis of plate behaviour far beyond where buckling occurs. Based on Von Kármán's large deflection theory, Levy [36] derived the 'exact solution' of the equations for square plates. Further researches included Mayers and Budiansky [37], who presented the plastic behaviour of a simply supported flat plate loaded in compression. Smith [38], moreover, derived and applied rigorous plasticity theory to the analysis of plate buckling. To introduce Von Kármán large deflection theory to laminated composites, Reissner and Stavsky [39] and Stavsky [40, 41] extended Von Kármán's formulations. Further extensions for dynamic buckling problems for general elastic and imperfection-sensitive structures was investigated by Budiansky [42], Budiansky and Hutchinson [43] and Hutchinson and Budiansky [16]. Thompson [44] presented a work which starts from the point of view of elastic stability, then the buckling and snapping behaviour of an elastic structure subjected to a single generalised load is discussed. The theoretical predictions of elastic instability of structures and structural components are discussed to reveal the equilibrium state at which the stability of structure is lost. Further extension of a previous study from Thompson [45] gave the basic concepts and theories of elastic stability, both buckling and snapping conditions are examined at which the equilibrium state loses stability. More development concerning instability and postbuckling behaviour of structure are included in Thompson [46] and Thompson and Walker [47]. The first literature from Thompson presented a complete general statistical theory of imperfection-sensitivity in elastic post-buckling. The structural system has been described by n generalised coordinates, a loading parameter and an imperfection parameter. The behaviour of structures and structural components beyond which stability is lost has been investigated. In the second literature from Thompson and Walker, a non-linear perturbation analysis for discrete non-linear structural system is presented. Sewell [48] presented a general theory to investigate the bifurcation phenomena of elastic and inelastic thin plates from the standpoint of Hill's [49] bifurcation theory. The basic

differential equation is obtained for non-linear analysis of a thin plate under compression. Further extension of Sewell [50] showed the application to rectangular plates with four edges simply supported and uniaxial compression applied on two edges. Sewell [51] also investigated a method of postbuckling analysis which is based on some work of Koiter, and the differences of starting data and convergence technique with previous research from Sewell were discussed. Allen [52] presented his research on buckling analysis of sandwich plate and panels, and indicated the significance of shear deformation effects for finding the buckling loads.

In the past few decades, the postbuckling behaviour of plate structures has been paid great attention due to the increasing application of lightweight structures and composite materials in aerospace and military engineering. In recent years, a large amount of research on the postbuckling of plate structures has been carried out and published in particular looking at develop faster processes particularly for preliminary design. Wang and Dawe [53] presented a semi-analytical finite strip analysis to investigate the large deflection problem and overall postbuckling behaviour of a geometrically non-linear prismatic plate. In the context of classical plate theory and shear deformation plate theory, an enhanced stress-strain relationship was derived including modification of initial curvatures and the effect of initial imperfections. Furthermore, particular attention has been paid to a proper representation of longitudinal displacement which better represents the problem. These results show good comparison with finite element software and advantages in terms of efficiency. However, this concern with the accuracy of stress and strain distributions leads to a significant increase in solution time while only improving the accuracy for postbuckling problems with similar magnitudes of transverse displacement v and out-of-plane displacement w for a little. Later Wang and Dawe [54] generalised their previous research and considered the shear deformation effect in postbuckling problems. The governing equilibrium equations and solutions were obtained and results for symmetric and unsymmetric composite laminates were shown. Further extension of their research by Ge *et al.* [55] investigated thermomechanical postbuckling behaviour of composite laminates by including the thermal-elastic effects in their previous work. Rhodes [56] presented a brief review of two analysis methods to investigate

the postbuckling behaviour of plates and thin-walled members. The so-called 'lower bound' method provides an analytical solution which can be easily used to obtain the critical buckling load, while in the other methods based on non-linear differential equations from Von Kármán [14] and Marguerre [57] are taken into account to give a more rigorous postbuckling analysis. Librescu and Lin [58] discussed the postbuckling behaviour of flat and shallow curved panels based on high-order shear deformation plate theory with linear and non-linear Winkler elastic foundations. The research also took account of the effects of transverse shear, geometric non-linearities and geometrical initial imperfection. Everall and Hunt [59] reduced the Von Kármán plate equations to a series of ordinary differential equations, and investigated the postbuckling reserve and secondary buckling for a rectanglar plate with simply supported edges under uniaxial compression.

Singh and Kumar [60] contributed work which integrates first-order shear deformation plate theory and geometrical non-linearity by using Von Kármán's equilibrium equation with finite element procedures. The postbuckling behaviour and progressive failure response of thin, symmetric laminates under uniaxial compression and uniaxial compression with in-plane shear loading has been examined, and the buckling and failure loads of anisotropic laminates in various cases have been compared to determine their postbuckling behaviour. A similar theory has been extended by Srikanth and Kumar [61] by considering an energy approach and introducing temperature effects for postbuckling response of plates. Later on, Jain and Kumar [62] and Singh and Kumar [63] continued their research on evaluating the postbuckling behaviour of a plate with a central cutout. Similarly, the governing equilibrium equations were derived based on Von Kármán's plate theory with consideration of geometrical non-linearity, and the solutions were given by using the Newton-Raphson method. Liew *et al.* [64] presented the first-order shear deformation theory for isotropic and laminated composite plates in postbuckling with the Ritz method. The meshfree Ritz method introduced the kernel particle approximation for the field variables to discretise the non-linear equilibrium equations for the theory. Results for isotropic and laminated composites in postbuckling have been validated to retain accuracy comparing with the finite element method. Further, the research has been continued by Yang *et al.* [65]

for higher-order shear deformation theory with consideration of geometrical imperfection sensitivity. Higher-order shear deformation theory and Von Kármán's theory were explored to obtain the non-linear equilibrium equations which were solved to give a semi-analytical solution by involving a one-dimensional differential quadrature method and the Galerkin technique. The method was applied to functionally graded plates with imperfections, and the postbuckling behaviour of plates was tested and presented. More research based on higher-order shear deformation was extended by Liew *et al.* [66] and Woo *et al.* [67] with consideration of thermo-mechanical and thermo-electro-mechanical loadings with various boundary conditions. Other types of thermo-mechanical postbuckling plate analysis have been provided by Shen and Williams [68], Shen [69] and Shen [70]. Higher-order shear deformation plate theory was utilised to derive the governing differential equations, and a perturbation technique was used to find the buckling load and postbuckling equilibrium path. Results were given for laminated composite plates with consideration of initial imperfections. Kere and Lyly [71], using Reissner-Mindlin-Von Kármán type equilibrium equation for plates, investigated the postbuckling behaviour of laminated composite plates subject to large deflections. Diaconu and Weaver [72] presented an approximate solution to the postbuckling analysis of infinitely long and unsymmetrically laminated composite plates. The Von Kármán large deflection theory was used to represent the postbuckling mode with application of the Galerkin method. To obtain efficient approximate solutions, non-dimensional parameters have been introduced by referring to Stein's [73] work to simplify the formulations. The results have been found to be efficient for analysing the postbuckling behaviour of infinitely long and unsymmetrically laminated composite plates. Muradova and Stavroulakis [74] described a method based on Von Kármán's plate theory with the use of the spectral method for discretisation of boundary value problems and results were presented for buckling and postbuckling behaviour of rectangular plates.

Further types of analysis and solution techniques for the postbuckling behaviour of plates have been presented recently, which are worth mentioning and reviewing here. Chen and Yu [75] however, presented an asymptotically correct, geometrically non-linear theory which rigorously gives the governing differential equations for the postbuckling analysis of laminated composite plates. Results

showed good comparison with finite element analysis in the primary postbuckling range while also showing the advantage of convergence deep into postbuckling in various plate configurations and load and boundary conditions. Han *et al.*[76] introduced an element-based Lagrangian formulation for postbuckling analysis of laminated composite plates. Results were given for cases with combinations of in-plane compression, shear and lateral loads and showed the advantage of fast convergence.

2.5 Review of Stein's work on postbuckling

In an early work of Stein [77], a perturbation analysis is introduced in detail and postbuckling results are given for a plate under longitudinal compression and temperature effects. The perturbation analysis converts the Von Kármán large-deflection equations for a plate given below, a set of three non-linear partial differential equations, into an infinite set of linear partial differential equations.

$$\frac{\partial N_x}{\partial x} + \frac{\partial N_{xy}}{\partial y} = 0$$

$$\frac{\partial N_{xy}}{\partial x} + \frac{\partial N_y}{\partial y} = 0$$

$$D\nabla^4 w + N_x \frac{\partial^2 w}{\partial x^2} + 2N_{xy}\frac{\partial^2 w}{\partial x \partial y} + N_y \frac{\partial^2 w}{\partial y^2} = 0 \tag{2.41}$$

where $D = Gh^3/12(1-\nu)$, $\nabla^4 = (\partial^4/\partial x^4 + 2\partial^4/\partial x^2 \partial y^2 + \partial^4/\partial y^4)$ To achieve the above conversion, the displacements which are function of only x and y are expanded into a power series in terms of an arbitrary parameter ϵ (at buckling $\epsilon = 0$). The power series is assumed to start from zero power and have only odd powers for u and v but start from the first power and have only even powers for w as

$$u = \sum_{n=0,2,..}^{\infty} u^{(n)}\epsilon^n, v = \sum_{n=0,2,..}^{\infty} v^{(n)}\epsilon^n, w = \sum_{n=1,3,..}^{\infty} w^{(n)}\epsilon^n \tag{2.42}$$

For a plate without any initial imperfections and subject to in-plane loading, the out-of-plane displacement w is zero in the loading range prior to buckling but in-plane displacements u and v have values other than zero. Thus, the series for u and v are expected to start from zero power but for w is expected to start from the first power. To convert Von Kármán's equation into an infinite set, it is also essential to rewrite the applied force into a series. Writing the force-strain and strain-displacement relationships below as

$$N_x = \frac{Eh}{1-\mu^2}(\varepsilon_x + \mu\varepsilon_y), N_y = \frac{Eh}{1-\mu^2}(\varepsilon_y + \mu\varepsilon_x), N_{xy} = \frac{Eh}{2(1+\mu)}\gamma_{xy} \tag{2.43}$$

$$\varepsilon_x = \frac{\partial u}{\partial x} + \frac{1}{2}(\frac{\partial w}{\partial x})^2, \varepsilon_y = \frac{\partial v}{\partial y} + \frac{1}{2}(\frac{\partial w}{\partial y})^2, \gamma_{xy} = \frac{\partial u}{\partial y} + \frac{\partial v}{\partial x} + \frac{\partial w}{\partial x}\frac{\partial w}{\partial y} \tag{2.44}$$

where μ is Poisson's ratio. Substituting the power series in equation (2.5.2) into the above relationships, the following power series for applied forces can be obtained as

$$\begin{aligned} N_x &= \sum_{n=0,2,..}^{\infty} N_x^{(n)}\epsilon^n + \sum_{m=1,3,..}^{\infty}\sum_{n=1,3,..}^{\infty} N_x^{(mn)}\epsilon^{(m+n)} \\ N_y &= \sum_{n=0,2,..}^{\infty} N_y^{(n)}\epsilon^n + \sum_{m=1,3,..}^{\infty}\sum_{n=1,3,..}^{\infty} N_y^{(mn)}\epsilon^{(m+n)} \\ N_{xy} &= \sum_{n=0,2,..}^{\infty} N_{xy}^{(n)}\epsilon^n + \sum_{m=1,3,..}^{\infty}\sum_{n=1,3,..}^{\infty} N_{xy}^{(mn)}\epsilon^{(m+n)} \end{aligned} \tag{2.45}$$

where

$$\begin{aligned} N_x^{(n)} &= \frac{Eh}{1-\mu^2}[\frac{\partial u^{(n)}}{\partial x} + \mu\frac{\partial v^{(n)}}{\partial y}] \\ N_y^{(n)} &= \frac{Eh}{1-\mu^2}[\frac{\partial v^{(n)}}{\partial y} + \mu\frac{\partial u^{(n)}}{\partial x}] \\ N_{xy}^{(n)} &= \frac{Eh}{2(1+\mu)}[\frac{\partial u^{(n)}}{\partial y} + \frac{\partial v^{(n)}}{\partial x}] \end{aligned}$$

$$N_x^{(mn)} = N_x^{(nm)} = \frac{Eh}{2(1-\mu^2)}(\frac{\partial w^{(m)}}{\partial x}\frac{\partial w^{(n)}}{\partial x} + \mu\frac{\partial w^{(m)}}{\partial y}\frac{\partial w^{(n)}}{\partial y})$$

$$N_y^{(mn)} = N_y^{(nm)} = \frac{Eh}{2(1-\mu^2)}(\frac{\partial w^{(m)}}{\partial y}\frac{\partial w^{(n)}}{\partial y} + \mu\frac{\partial w^{(m)}}{\partial x}\frac{\partial w^{(n)}}{\partial x})$$

$$N_{xy}^{(mn)} = \frac{Eh}{2(1+\mu)}[\frac{\partial w^{(m)}}{\partial x} + \frac{\partial w^{(n)}}{\partial y}] \tag{2.46}$$

This allows the Von Kármán large-deflection equations to be rewritten in power terms as

$$\frac{\partial N_x^{(0)}}{\partial x} + \frac{\partial N_{xy}^{(0)}}{\partial y} = 0$$

$$\frac{\partial N_{xy}^{(0)}}{\partial x} + \frac{\partial N_y^{(0)}}{\partial y} = 0$$

$$D\nabla^4 w^{(1)} - N_x^{(0)}\frac{\partial^2 w^{(1)}}{\partial x^2} + 2N_{xy}^{(0)}\frac{\partial^2 w^{(1)}}{\partial x \partial y} + N_y^{(0)}\frac{\partial^2 w^{(1)}}{\partial y^2} = 0 \tag{2.47}$$

$$\frac{\partial N_x^{(2)}}{\partial x} + \frac{\partial N_{xy}^{(2)}}{\partial y} = -(\frac{\partial N_x^{(11)}}{\partial x} + \frac{\partial N_{xy}^{(11)}}{\partial y})$$

$$\frac{\partial N_{xy}^{(2)}}{\partial x} + \frac{\partial N_y^{(2)}}{\partial y} = -(\frac{\partial N_y^{(11)}}{\partial y} + \frac{\partial N_{xy}^{(11)}}{\partial x})$$

$$\begin{aligned} &D\nabla^4 w^{(3)} - N_x^{(0)}\frac{\partial^2 w^{(3)}}{\partial x^2} + 2N_{xy}^{(0)}\frac{\partial^2 w^{(3)}}{\partial x \partial y} + N_y^{(0)}\frac{\partial^2 w^{(3)}}{\partial y^2} \\ &= (N_x^{(2)} + N_x^{(11)})\frac{\partial^2 w^{(1)}}{\partial x^2} + (N_y^{(2)} + N_y^{(11)})\frac{\partial^2 w^{(1)}}{\partial y^2} + 2(N_{xy}^{(2)} + N_{xy}^{(11)})\frac{\partial^2 w^{(1)}}{\partial x \partial y} \end{aligned} \tag{2.48}$$

$$\frac{\partial N_x^{(4)}}{\partial x} + \frac{\partial N_{xy}^{(4)}}{\partial y} = -(2\frac{\partial N_x^{(13)}}{\partial x} + \frac{\partial N_{xy}^{(13)}}{\partial y} + \frac{\partial N_{xy}^{(31)}}{\partial y})$$

$$\frac{\partial N_{xy}^{(4)}}{\partial x} + \frac{\partial N_y^{(4)}}{\partial y} = -(2\frac{\partial N_y^{(13)}}{\partial y} + \frac{\partial N_{xy}^{(13)}}{\partial x} + \frac{\partial N_{xy}^{(31)}}{\partial x})$$

$$
\begin{aligned}
&D\nabla^4 w^{(5)} - N_x^{(0)}\frac{\partial^2 w^{(5)}}{\partial x^2} + 2N_{xy}^{(0)}\frac{\partial^2 w^{(5)}}{\partial x \partial y} + N_y^{(0)}\frac{\partial^2 w^{(5)}}{\partial y^2} \\
&\quad = (N_x^{(2)} + N_x^{(11)})\frac{\partial^2 w^{(3)}}{\partial x^2} + (N_y^{(2)} + N_y^{(11)})\frac{\partial^2 w^{(3)}}{\partial y^2} + 2(N_{xy}^{(2)} + N_{xy}^{(11)})\frac{\partial^2 w^{(3)}}{\partial x \partial y} \\
&+ (N_x^{(4)} + N_x^{(13)})\frac{\partial^2 w^{(1)}}{\partial x^2} + (N_y^{(4)} + N_y^{(13)})\frac{\partial^2 w^{(1)}}{\partial y^2} + 2(N_{xy}^{(4)} + N_{xy}^{(13)})\frac{\partial^2 w^{(1)}}{\partial x \partial y} \quad (2.49)
\end{aligned}
$$

To obtain the linear differential equations, the power series terms in the arbitrary parameter ϵ have to vanish which requires each coefficient of the power series to vanish. The odd powers in the series for u and v and the even powers in the series for w can form a set of homogeneous differential equations with homogeneous boundary conditions. Thus equations (2.47) can be regarded as the linear small-deflection equations, where the forces $N^{(0)}$ are independent of out-of-plane displacement w. Solutions of the first equations enables resolving of succeeding equations terms, therefore the behaviour of plate beyond buckling can be examined. Stein also provided another approximation using exactly the same procedure as discussed above except that the perturbation parameter ϵ^2 is defined as a function of buckling load, as $\epsilon^2 = (P - P_{cr})/P_{cr}$. Results for both theory and experiments are given for a plate under longitudinal compression for comparison. Figure 2.8 from Stein [77] shows load versus end shortening curves under compression and where b, h are width and thickness of plate respectively, and μ is Poisson's ratio. The experimental curve shows mode jumping with m being the number of buckles in the longitudinal direction. The linear set of equations show the advantages of simplicity of solution, which brings efficiency in solving linear partial differential equations instead of nonlinear large-deflection partial differential equations. For the compression problem of a square plate, results of the second approximation shows agreement with exact results. However, there are certain limitations depending on the application desired. Stein indicated that solutions may be unable to converge satisfactorily for certain problems, and the linear equation can not be used for postbuckling problems with eccentricities.

Further work by Stein [3] provided a further analytical approach which is key material for this thesis. In this work, Stein presented an analytical solution for isotropic and orthotropic plates in compression and in shear for postbuckling

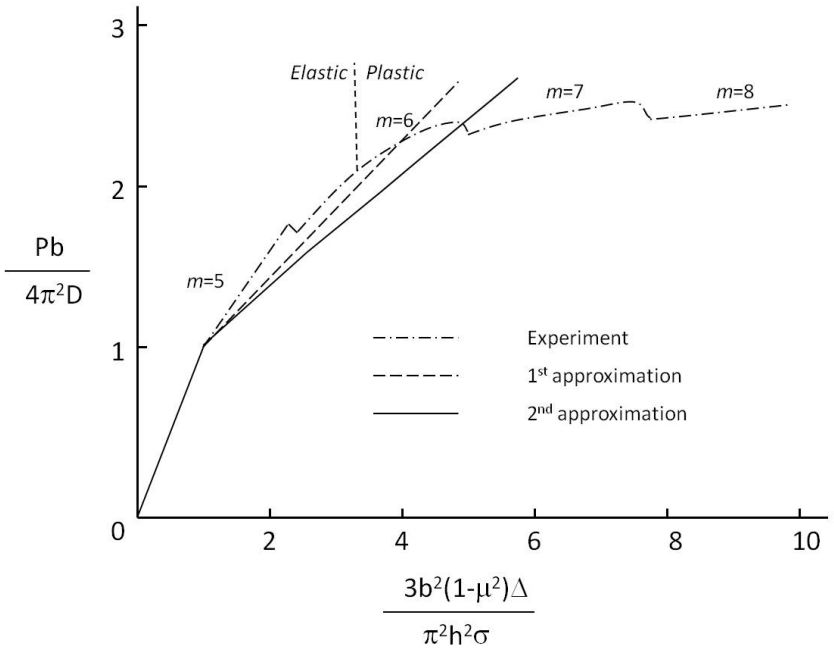

Figure 2.8: Comparison of non-dimensional load versus end shortening curves as given by theory and experiment [3]

analysis. In contrast to his previous work, Von Kármán large-deflection equations are converted into non-linear ordinary differential equations, by assuming trigonometric functions in the longitudinal direction. To obtain non-linear ordinary differential equations, the displacement has first to be derived based on a trigonometric series approximation, which gives

$$u = -\bar{u}_{cn}(\frac{x}{a} - \frac{1}{2}) + u_0(y) + u_s(y)sin\frac{2\pi x}{\lambda} + u_c(y)cos\frac{2\pi x}{\lambda}$$

$$v = v_0(y) + v_s(y)sin\frac{2\pi x}{\lambda} + v_c(y)cos\frac{2\pi x}{\lambda}$$

$$w = w_s(y)sin\frac{\pi x}{\lambda} + w_c(y)cos\frac{\pi x}{\lambda} \tag{2.50}$$

where $\bar{u}_{cn}$ is the applied longitudinal compressive displacement. The out-of-plane displacement w is sinusoidally periodic with half-wavelength λ, and the in-plane displacements u and v are sinusoidally periodic with half-wavelength $\lambda/2$. The

strains and curvatures are then given by applying Von Kármán plate theory with a similar trigonometric form for the stress and moment resultants. Further calculations involving the energy principle give the virtual work of the system in terms of twenty unknown quantities to be solved. By applying the differential equations which have to be satisfied, the stress-strain relations and proper boundary conditions, the first-order ordinary differential equations can be solved. By using an algorithm from Lentini and Pereyra [78] which is based on Newton's method, the equations are solved for certain problems.

To apply the analysis, a long isotropic plate is investigated under compression and shear respectively. The longitudinal edges are forced to keep straight and the in-plane displacements normal to the edges are zero during the investigations. The results from Stein indicated that in a postbuckling analysis: (1) plates with clamped edges are stiffer than those with simply-supported edges, and plates with a zero displacement edge condition are stiffer than those with zero average stress condition; (2) an isotropic plate is slightly stiffer than a $\pm 45°$-laminate for the same loading and boundary conditions; (3) for an isotropic plate, transverse tension builds up in the postbuckling range due to shallow buckles and the zero transverse in-plane deformation condition, while for a $\pm 45°$-laminate, tension does not build up due to the deeper buckles; (4) for a long, isotropic plate loaded in shear, the tensile longitudinal stress reaches about four times its critical value, the shear displacement increases to seven times its critical value and moreover the tensile transverse stress increases to about seventeen times its critical value for the zero-displacement-simply-supported-edge conditions in the postbuckling range, indicating that the longitudinal and transverse stresses can be very large during postbuckling; (5) for a $\pm 45°$-laminate in shear loading, it is indicated that isotropic plates have greater stiffness than the laminate for all cases.

Both of Stein's works provide an analytical concept of investigating the nonlinear behaviour of plates in the postbuckling range. Results are validated by comparing with exact solutions, experiments and other researchers' work. However, there are still limitations in both works which bring possibilities of improving and developing the theory. The earlier work from Stein is shown to be efficient and accurate for certain problems, but the validation of solutions depends on the application desired which brings uncertainty for the general case. The later work

introduces a trigonometric series which better represents displacement for buckling analysis and gives remarkable solutions. A limitation of the theory is that only postbuckling behaviour of isotropic and orthotropic plates are considered in this work which can not used for a mere general case. Furthermore, the twenty unknowns lead to the satisfaction of a number of differential equations and proper choice of boundary conditions, which makes the solution quite difficult to implement. In this thesis, a further improvement has been made to the assumption of displacement which couples the half-wavelengths λ and $\lambda/2$ together to represent a more accurate form for the in-plane displacements u and v.

Chapter 3

Exact finite strip analysis and Wittrick-Williams algorithm

3.1 Exact finite strip analysis

Finite strip analysis is an alternative approach to finite element analysis for buckling and postbuckling analysis of rectangular plates and prismatic plate structures. It provides an efficient procedure for numerical analysis which can reduce the computational costs significantly. For the buckling and postbuckling analysis of plates, classical plate theory, first-order shear deformation and higher-order shear deformation theory can be utilised, while the semi-analytical solution technique ensures reliable and efficient solutions to be obtained.

The finite strip method was first introduced and described by Cheung [79] in 1976. Applications for rectangular plates and plate structures were investigated, dealing with buckling and vibration analysis. Early works based on classical plate theory as a model of plate behaviour also included Cheung and Cheung [80], Babu and Reddy [81], Turvey and Wittrick [82], Dawe [83], and Graves Smith and Sridharan [84]. Most of these works assumed a sinusoidal mode in the longitudinal direction for isotropic and orthotropic plates with no shear loading applied. Wittrick [85, 86] derived explicit expressions for the stiffness properties of long, thin

isotropic plates loaded with longitudinal compression combined with uniform longitudinal shear. Classical plate theory is used and the buckling mode is assumed to vary sinusoidally in the longitudinal direction. The assumptions lead to 'exact' solutions for problems where no shear load or anisotropy are present, and provide accurate solutions for infinitely long plates. Wittrick and Williams [87] later extended the work to anisotropic plate assemblies under combined loads and compiled it into a computer software VIPASA. These analyses from Wittrick [85, 86] and Wittrick and Williams [87] form the basis of so-called 'exact' finite strip analysis.

Buckling and postbuckling behaviour of plate structures using finite strip analysis based on classical plate theory, first-order shear deformation theory and higher-order shear deformation theory has been investigated by many researchers. Kong and Cheung [88] presented finite strip buckling analysis based upon third-order shear deformation plate theory which was used to examine the effects of geometrical non-linearity and initial imperfection. Numerical results demonstrate the performance of the modified finite strip analysis. Dawe and Peshkam [89] and Wang and Dawe [53, 54] provided semi-analytical finite strip analysis based on first-order shear deformation theory with modification on longitudinal displacement. The calculated buckling and postbuckling behaviour of plates demonstrated good agreement with finite element analysis. Later Tan and Dawe [90] presented a general spline finite strip method based upon first-order shear deformation theory and incorporated a sub-structuring technique into the solution process. Numerical results showed the positive effects of the method on flexible matching of boundary conditions. Further extensions of their work [55, 91] concentrated on thermal effects on buckling and postbuckling behaviour of laminated composite plates by using spline finite strip analysis. Bradford and Azahri [92] presented a finite element analysis using different series functions as buckling coefficients which provided an efficient way of examining the buckling behaviour of plates with different load and boundary conditions applied. Ovesy and co-workers contributed several analytical methods based on the finite strip technique to determine the buckling and postbuckling behaviour of plate structures. Ovsey *et al.* [93] and Ovsey and Assaee [94] presented a so-called semi-energy finite strip approach in the context of classical plate theory. The out-of-plane displacement

w is assumed as a function of a properly selected deflection series. This has been substituted into Von Kármán's compatibility equations which are solved exactly to get stresses and displacements. The governing equilibrium equations are then solved by considering minimum potential energy. Numerical results describing postbuckling behaviour are given for laminated composite plates and comparison made with other researchers work and the finite element approach. The semi-energy finite strip analysis is then extended by Ovesy and Assaee [95, 96] by including bending-twisting coupling effects in the postbuckling analysis. Results are given for the postbuckling analysis of laminated composite plates considering coupling and uncoupling effects respectively, and compared with the finite element software ANSYS [97]. The results indicated that the coupling of in-plane bending membrane and out-of-plane twisting curvature should be taken into account for postbuckling analysis. Similar analysis presented by Loughlan [98] makes the same conclusion for anti-symmetric angle-ply laminates. A further extension by Ovesy *et al.* [99] considered the thick plate problem were shear deformation effects need to be considered. The same semi-energy finite strip approach is followed based on first-order shear deformation theory, with results for the postbuckling behaviour of thick symmetric laminated plates demonstrated. Conclusions showed that for certain accuracy requirements, the approach requires fewer degrees of freedom compared to the finite element approach and hence leads to computational efficiency. The other approach proposed by Ovesy *et al.* [100, 101, 102, 103], the so-called full-energy finite strip analysis postulated all displacement by a proper shape function. The displacements are substituted into Von Kármán's compatibility equations, and the equilibrium equations are solved using an energy method. Results are given based on the semi-energy and full-energy approaches for the postbuckling analysis of laminated plates. It is indicated that the full-energy finite strip approach is slightly more accurate for postbuckling analysis than semi-energy approach, however it increases the computation time. This is due to the increasing number of degrees of freedom in the full-energy approach. Suggestions are also made for improving the accuracy of the semi-energy approach, which involve introducing multi-terms into the shape function for displacement w instead of single terms. Further work [104, 105] on the semi-energy and full-energy approaches is carried out to examine the effects

of initial imperfections on laminated composite plates. Most recently, Ovesy and Ghannadpour [106] and Ghannadpour and Ovesy [107] presented an exact strip analysis based on the full-energy approach. The Von Kármán's equilibrium equations are solved exactly and the transcendental stiffness matrix is assembled for the plate strips. Solutions are found by the energy method and convergence of the critical buckling load is secured by introducing a recursive Newton's method from Yuan [108]. Various analytical techniques including, Eccher *et al.* [109, 110] and Yao and Rasmussen [111] have provided isoparametric spline finite strip analyses which use transverse cubic shape functions in the expression of the displacement function. Lui and Lam [112] provided a deep discussion of the effects of initial imperfections on plate buckling. A polynomial expression for imperfections and trigonometric series for deformations are used to better represent the problem.

3.2 Wittrick-Williams algorithm

The Wittrick-Williams algorithm is a numerical technique which can be used to find the critical buckling loads and natural frequencies of a structure for non-linear eigenvalue problems. The algorithm was first presented by W. H. Wittrick and F. W. Williams in 1971 [113] for determining the natural frequencies of vibration problems, however following this it was used to find the critical buckling stresses for plates [87]. The algorithm was not developed to calculate the value of natural frequencies, but enable the number of natural frequencies which lie below a certain frequency to be calculated, allowing convergence on any natural frequency at the accuracy required. The algorithm works is outlined below.

The global stiffness matrix $\mathbf{K}(\omega)$ is first assembled

$$\mathbf{K}(\omega)\mathbf{D} = \mathbf{P} \tag{3.1}$$

where $\mathbf{P}$ is the perturbation forces, $\mathbf{D}$ is the displacement vector and ω is natural frequency or load factor [114]. Since the global stiffness matrix $\mathbf{K}(\omega)$ is transcendental in terms of the non-linear elements ω, the solution of the natural

frequency or load factor can be found by solving the transcendental eigenvalue equation below

$$\mathbf{K}(\omega)\mathbf{D} = 0 \tag{3.2}$$

The Wittrick-Williams algorithm calculates the number of eigenvalues J lying below a trial value ω^*, where J can be calculated as

$$J = J_0 + s\left\{\mathbf{K}(\omega^*)\right\} \tag{3.3}$$

where J_0 is defined as the number of natural frequencies which would still be exceeded by ω^* if constraints were imposed so as to make all the displacements $\mathbf{D}$ zero, and $s\left\{\mathbf{K}(\omega^*)\right\}$ is known as the sign count which is the number of negative diagonal elements of the upper triangular matrix $\mathbf{K}^{\Delta}(\omega^*)$ obtained from Gauss elimination of $\mathbf{K}(\omega^*)$ [87]. J can be also be calculated from the following equation if substructures are not used

$$J_0 = \sum_m J_m \tag{3.4}$$

where J_m is the number of eigenvalue exceeded the trial value ω^* with their ends fully restrained.

Chapter 4

Exact strip analysis software VICONOPT

The exact strip analysis software VICONOPT [6] has been developed as an analysis and optimum design software for aerospace engineering and has been used in both industry and academic for many years. From an analysis perspective, VICONOPT has the capacity to carry out vibration analyses, buckling analyses and postbuckling analyses. In terms of optimisation, VICONOPT provides an efficient optimum design tools from optimum design perspective. This chapter introduces the main features of the earlier programs VIPASA and VICON upon which VICONOPT is based and developments in VICONOPT in recent years.

4.1 Main features of VIPASA analysis

VIPASA analysis uses a stiffness matrix approach based on exact flat plate theory with Winkler foundations. The Wittrick-Williams algorithm is also used to guarantee convergence on the required eigenvalues. Multi-level substructuring is used very concisely and flexibly to reduce solution times, data preparation, and computer memory usage [115]. VIPASA analysis assumes the mode of buckling or vibration varies sinusoidally in the longitudinal direction x, and hence the

amplitudes u, v, w and ψ relating to the axes x, y, z are also sinusoidal. The computation is repeated rotation for a range of user specified half-wavelengths λ and converged to the required eigenvalues with a pre-set accuracy allowance. VIPASA analysis requires the in-plane membrane stiffness matrix **A** and the out-of-plane bending stiffness matrix **D** to be uncoupled, i.e. the coupling stiffness matrix **B** is null in the constitutive equation of plate. If all the component plates are either isotropic or orthotropic with no shear, i.e. $N_S = 0$, the nodal lines of zero displacement are straight and perpendicular to the longitudinal direction x and the simply supported end condition is satisfied with λ divided exactly into plate length ℓ. If anisotropic materials and shear are considered the global stiffness matrix becomes complex and the solution obtained is approximate for such end conditions. In a VIPASA analysis, due to the assumption of a sinusoidal mode in the longitudinal direction with half-wavelength λ, the exact solution can be obtained by taking $\lambda = \ell, \ell/2, \ell/3, ...$ if no shear load and anisotropy exist and simply supported boundary conditions are satisfied. The minimum buckling load can be found by examining all values of λ until the smallest one is smaller than the smallest plate width (i.e. the unsupported width between different plates). The advantages of VIPASA analysis, are that it is based on an 'exact' plate theory in comparison with other approximated methods such as finite element and finite strip methods, and that the solution time can be shown to be 1000 times faster than finite element programs such as STAGS [116]. The limitations of VIPASA analysis is the requirement that shear load and anisotropy are absent for an accurate analysis for simply supported end conditions. To solve a problem with shear load, anisotropy and various end conditions, VICON analysis is recommended to provide a more accurate modeling solution.

4.2 Main features of VICON analysis

To overcome the inaccuracies in VIPASA analysis for shear load and anisotropy, VICON analysis has been developed by researchers at Cardiff University in collaboration with NASA [117]. VICON analysis permits the same assumptions, loading and stiffness matrices as VIPASA analysis. The key difference between

VICON analysis and VIPASA analysis is the introduction of Lagrangian Multipliers which couple the responses of different half-wavelengths λ. VICON analysis uses Lagrangian Multipliers to minimise the total energy of panel so that the a shear loaded panel support can be accurately represented. VICON analysis deals with an infinitely long plate assembly with constraints which represent rigid or elastic point supports repeating at interval of ℓ. The mode of buckling or vibration repeats n times over an interval $L = M\ell$, where M and n are integers, as shown in Figure 4.1. The boundary conditions can be expressed explicitly to give accurate results. Meanwhile, accurate buckling and vibration modes are achieved by providing different half-wavelength λ which are coupled together. VICON analysis assumes that the buckling and vibration modes repeat over a length $L = 2\ell/\xi$, where $0 \leq \xi \leq 1$. The half-wavelengths required in VICON analysis is governed by the expression

$$\lambda_m = \frac{\ell}{(\xi + 2m)}, (m = 0, \pm 1, \pm 2, ... \pm q) \tag{4.1}$$

where m and q are integers having different meanings. To determine the minimum buckling load, ξ and m are determined by users and appropriate values of ξ which can be given as $\xi = 2n/M(0 \leq \xi \leq 1)$ are examined to ensure the lowest buckling load can be found. As the mode of buckling or vibration is repeated n times over M lengthwise bays of length ℓ, L can be written as

$$L = \frac{2n\ell}{\xi} \tag{4.2}$$

Eigenvalues of problems (i.e. buckling load factors and natural frequencies of vibration) are found in a similar way to that using in VIPASA analysis. The slight difference is that the Wittrick-Williams algorithm has been extended to allow for introducing Lagrangian Multipliers, i.e. to couple the 'exact' stiffness matrices for different half-wavelengths [118]. VICON analysis improves the accuracy for more general buckling problems and also ensures the advantage of time reduction, which as stated previously has been shown to be 159 times faster than finite element program STAGS [116].

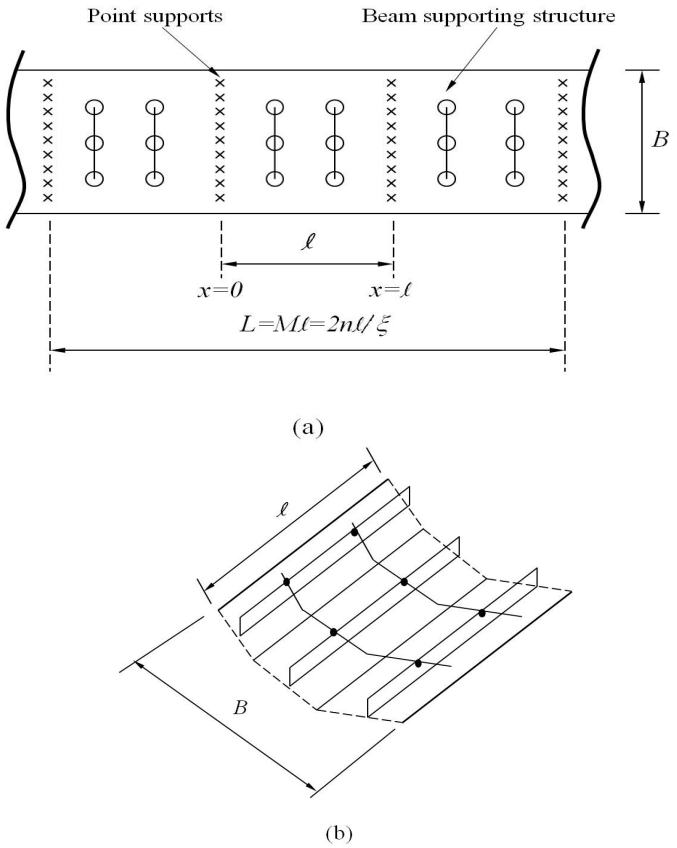

Figure 4.1: Illustration of the infinitely long structure with constraints. (a) plan view (b) isometric view

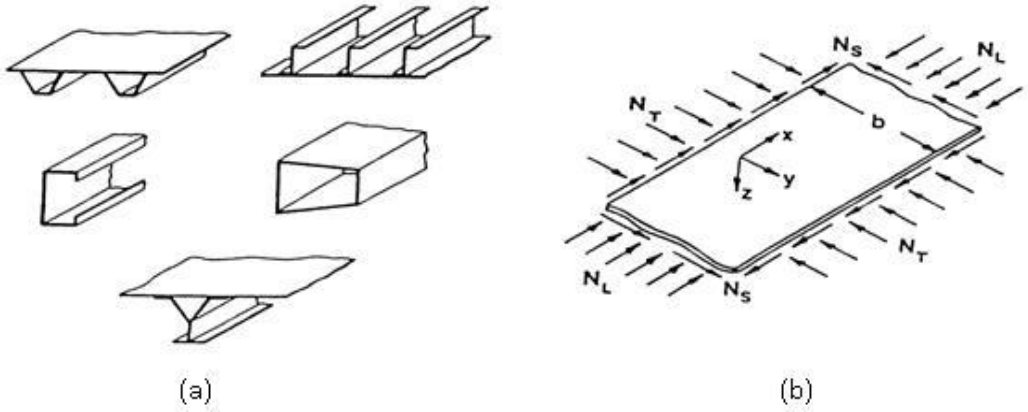

Figure 4.2: (a) Prismatic plate assemblies (b) Component plate, showing in-plate loading and coordinates

4.3 VICONOPT

VICONOPT is a FORTRAN 77 computer program which has over 50000 lines of code. It incorporates the earlier programs VIPASA (Vibration and Instability of Plate Assemblies including Shear and Anisotropy) [87] and VICON (VIPASA with CONstraints) [117]. It covers the prismatic assemblies of anisotropic plate structures with a combination of longitudinal invariant in-plane stresses [119]. Typical panel sections that can be analysed by VICONOPT and a typical plate component with in-plate loading are shown in Figure 4.2. In the following section the main features of the optimisation program VICONOPT will be introduced in detail, including a critical assessment of postbuckling capability.

VICONOPT analysis was first presented by Williams *et al.* [6] at the SDM conference, then in 1993 a further release by Williams *et al.* [120] applied material strength constraints and also included bending and pressure loading, approximations for curved and tapered members and allowance for the effects of transverse shear deformation. In 1996, a new release from Williams *et al.* [121] included multi-level substructuring and local postbuckling analysis, as well as cost optimisation, simultaneous analysis and/or design of multiple structures, the ability to study wave propagation along the plate assembly and the ability to attach three-dimensional supporting frames. To provide an optimum design capability

to VICONOPT, the well know linear optimiser CONMIN [122] was introduced in 1990, which led to the first release of the program VICONOPT. Postbuckling analysis capability was added by Powell *et al.* [123], which extensively modified the buckling analysis of VICONOPT to include local postbuckling capacity, and in 2002 Fischer *et al.* [124, 125, 126] presented the development of VICONOPT MLO (Multi-Level Optimisation), which is a Visual C++ program providing a multilevel optimisation interface between VICONOPT and the finite element software MSC/NASTRAN [127]. These developments were reviewed by Kennedy *et al.* [114] in 2007. In 2008, an improvement to the postbuckling capacity was implemented by Anderson and Kennedy [128] with convergence by Newton iteration. This provided an accurate convergence on the critical buckling load and associated postbuckling mode. Research done by Qu [129] applied postbuckling effects in VICONOPT MLO creating the new multilevel optimisation interface VICONOPT MLOP (VICONOPT MLO with Postbuckling) [130]. Most recently analysis carried out by the author [131] of this thesis provided an analytical approach for VICONOPT postbuckling capacity, which improved the mode shape and prediction of stress and strain for a postbuckled plate.

4.4 Main features of VICONOPT design optimisation

VICONOPT's optimum design capacity was developed by introducing the linear optimiser CONMIN [122]. VICONOPT currently has different design capabilities, including continuous optimisation [132], discrete optimisation [132], discontinuous cost functions [132] and vibration constraints [133, 134, 135]. Two main objectives of VICONOPT optimum design are minimising the mass of structural components and therefore achieving reduction in cost. In this section, an overview of the main features and procedures of continuous optimisation are introduced while the theory and details will not be further discussed in this thesis.

In the design problem formulated in VICONOPT, a number of different design variables (e.g. plate widths, layer thicknesses and layer ply angles) can be

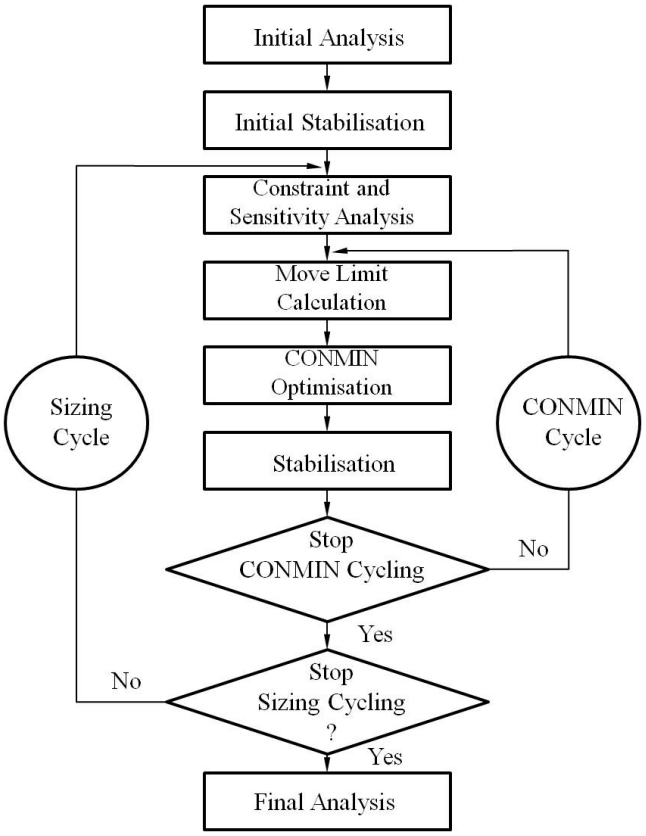

Figure 4.3: Continuous design procedure of VICONOPT using sizing strategy

specified and then optimised. The continuous design phase in VICONOPT is based on the sizing strategy and the main procedures are illustrated in Fig 4.3.

Initial analysis is firstly carried out in a design problem which determines the critical buckling load. The initial stabilisation [116] process follows which modifies the unstable or over-stable initial design to a just stable configuration. At the beginning of the sizing cycle, a constraint and sensitivity analysis is carried out to determine the buckling load factor. Later on in the move limit calculation the proper upper and lower limits of the design variables are determined. In the following CONMIN optimisation, results obtained in the constraint and sensitivity analysis are re-used to tailor the linear optimisation of CONMIN by adjusting the move limits for subsequent CONMIN cycles. After CONMIN optimisation, a stabilisation process which is similar to the initial stabilisation process is carried

out to adjust the design variables to achieve a just stable configuration for the next CONMIN cycle. The final analysis verifies the buckling results for the design problem before the end of the design problem.

4.5 Postbuckling analysis in VICONOPT

VICONOPT was first extended to enable postbuckling analysis by Powell *et al.* [123] in 1998. The method is presented for geometrically non-linear postbuckling analysis of perfect or imperfect longitudinally compressed prismatic plate assemblies with local modes. It uses the efficient exact stiffness calculation based on the Wittrick-Williams algorithm to find the critical buckling load and postbuckling mode shape of a structure at the very beginning of the iterative procedures. The applied load is then found for the first iteration of the first cycle based on the ratio of postbuckling to prebucklng axial stiffness. A number of iterations are then carried out to find the longitudinal strain, flexural shortening strain, initial buckling load and stress resultants. This postbuckling analysis was implemented in VIPASA analysis for postbuckling analysis capacity, however, difficulty was experienced in converging when investigating a stiffened panel with regularly spaced stiffeners which was believed to be due to the accuracy of the mode shape which caused mode jumping in postbuckling [136].

An alternative type of postbuckling analysis which is also the one currently being used in VICONOPT was developed by Anderson and Kennedy [128] and further discussed by Kennedy and Featherston [137]. In this method, instead of using the Wittrick-Williams algorithm to determine the critical buckling load and associated mode, the so-called Newton method is used to perform Newton iterations for accurate convergence on the postbuckling modes and stress distributions. At the start of each cycle, the increment of longitudinal strain has to be determined to ensure the total applied load, the stress and strain distribution and the postbuckling mode shape can be found after convergence.

Postbuckling analysis has also been extended to the optimum design capacity of VICONOPT. Qu *et al.* [130] presented the multilevel optimisation of aircraft wing structures using VICONOPT MLO with the effects of postbuckling. The

new method, the improved exact strip postbuckling analysis presented in this thesis is expected to improve some analysis features of VICONOPT postbuckling analysis.

Chapter 5

Improved exact strip postbuckling analysis

5.1 Introduction

Exact strip analysis of a prismatic plate provides a reliable efficient approach to the preliminary design stage of aerospace wing and fuselage panels. In addition, it reduces the computational and modeling time incurred by discretisation in finite element (FE) analysis. In the postbuckling range however, assumptions concerning the longitudinal invariance of stress and the sinusoidal variation of buckling modes in the longitudinal direction result in errors in the prediction of stress and strain.

This chapter outlines the major contribution of this thesis - the improved exact strip postbuckling analysis which provides greater accuracy of mode shape and stress and strain distribution prediction in postbuckling analysis. The improved analysis is based on an existing approach created by Stein [3], from which analytical results for the postbuckling of isotropic and orthotropic plates are obtained. Furthermore it uses the work of Kennedy [7] from which the prediction of stress and strain in postbuckling analysis are derived. In the improved analysis, more accurate governing equations are derived and solved for different combina-

tions of edge conditions and load cases. Implementation of the improved analysis in VICONOPT is validated to enhance the accuracy of postbuckling mode shape and postbuckling distribution of stress and strain.

The work begins by first examining the strip level at which the in-plane displacements, out-of-plane displacements, strains and curvatures are expressed. In-plane equilibrium conditions are necessarily assembled to find these quantities. However out-of-plane displacements from VICONOPT which will be utilised in the consequent calculation of in-plane displacements are expressed at the edge of each strip, namely at node level. To ensure the out-of-plane displacements are usable for the following analysis, the quantities and equilibrium conditions are converted from strip level to node level by introducing finite difference approximations and linear interpolations. The disadvantage of this approach is that too many quantities are converted to approximate forms, which brings the risk of losing accuracy in the final results. For the sake of ensuring the accuracy of the results, the previous analysis at the strip level is terminated and the same analysis procedures are investigated at node level instead. The analysis at node level requires all the quantities and equilibrium equations to be expressed at node level. This reduces the approximations introduced in the entire analysis but leads to higher order derivatives of the finite difference approximations in the stress-strain relationships. However, the results of analysis at node level tend to be more accurate than those at strip level, and the latter will not be discussed further in this thesis.

Before starting the entire procedure of calculations, Figure 5.1 provides a flow chart which demonstrates all the calculations described in the following sections. The red arrow represents the beginning of each analysis cycle while the green arrow represents the ending of the cycle. The main purpose of the calculations is actually finding the effective uniform stresses which will be used in VICONOPT for calculation of the postbuckling mode shape for the next cycle. The calculation starts from assumed expressions of in-plane displacements $\mathbf{u_i}$ and out-of-plane displacements $\mathbf{w_i}$. However, the improved analysis utilises $\mathbf{w_i}$ from VICONOPT directly at the very beginning of analysis. Then strains, stresses and effective uniform stresses which are obtained by an energy approach are calculated in terms of known variables $\mathbf{w_i}$ and unknown variables $\mathbf{u_i}$. To calculate $\mathbf{u_i}$,

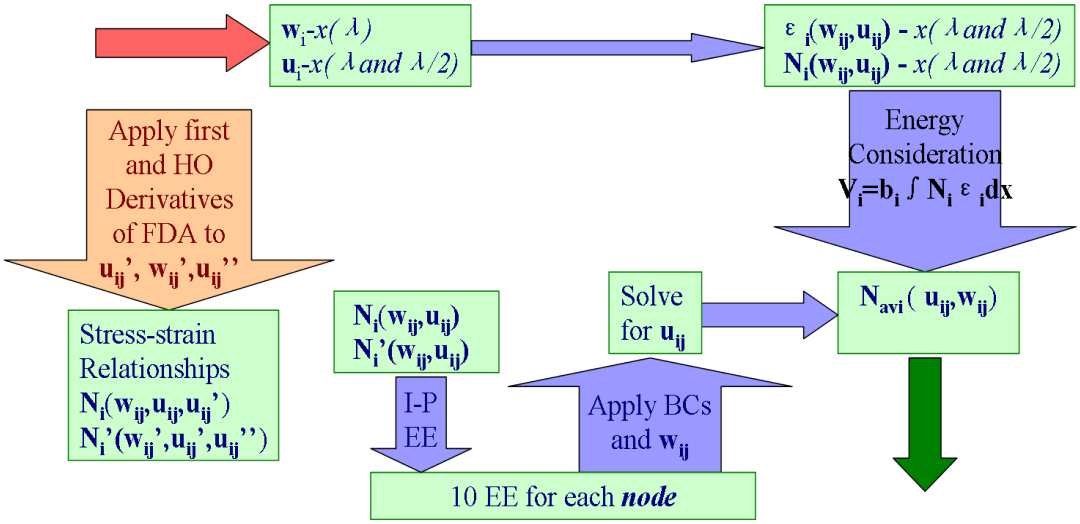

Figure 5.1: Flow chart of entire procedure of calculations

first and higher order derivatives of finite different approximations are applied to stress and strain relationships. By considering in-plane equilibrium and boundary conditions, ten equilibrium equations are given at each edge of the strips. Substituting the known variables $\mathbf{w_i}$ into the equilibrium equations, the unknown variables $\mathbf{w_i}$ can be calculated. The detailed instructions and calculations for each stage of the procedure will be given in following sections.

5.2 Descriptions and assumptions of the analysis

The following improved exact strip postbuckling analysis assumes classical plate theory (CPT), there is no allowance for transverse shear deformation. Initial imperfections are not allowed at present while in-plane anisotropy and curvature effects (i.e. general **A**, **B** and **D** matrices) are permitted. The analysis allows variation of in-plane displacements within the plates, so that the internal displacements are no longer governed entirely by the boundary conditions. The in-plane displacements, strains and stress resultants are combinations of sinusoidal responses with half-wavelengths λ and $\lambda/2$ to allow for curvature effects

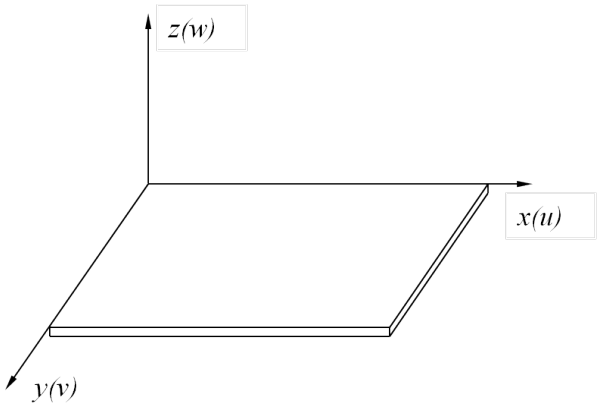

Figure 5.2: Typical coordinates with displacements

in coupled problems. The analysis finds the longitudinal, transverse and shear stress resultants on the edges of each strip, i.e. all resultants are at node level.

5.3 Displacements

In the trial mode, the typical flat plate is divided into *n-1* strips which gives n nodes at the strip edges. Figure 5.2 shows the typical coordinates of a plate with displacement vectors. The out-of-plane deflection w_{ij} and rotation ψ_{ij} are assumed to vary sinusoidally in the longitudinal x direction with half-wavelength λ, written in the form as

$$w_i = w_{ic} \cos \frac{\pi x}{\lambda} + w_{is} \sin \frac{\pi x}{\lambda} \tag{5.1}$$

$$\psi_i = \psi_{ic} \cos \frac{\pi x}{\lambda} + \psi_{is} \sin \frac{\pi x}{\lambda} \tag{5.2}$$

The presence of both sine and cosine terms allows for the skewing of the nodal lines which occurs for shear-loaded and anisotropic plates. It is assumed that $\psi_{ij} = w'_{ij}$, where the prime denotes the derivative with respect to the transverse direction y. In the absence of shear and anisotropy, the w_{ic} and ψ_{ic} terms are zero in the above equations. According to Stein's method [3] and allowing for

sine and cosine terms with half-wavelengths λ and $\lambda/2$, the in-plane deflections are assumed to take the form

$$u_i = -\bar{\varepsilon}_x(x-a/2)+u_{i0}+u_{ic}\cos\frac{\pi x}{\lambda}+u_{is}\sin\frac{\pi x}{\lambda}+u_{iC}\cos\frac{2\pi x}{\lambda}+u_{iS}\sin\frac{2\pi x}{\lambda} \quad (5.3)$$

$$v_i = v_{i0}+v_{ic}\cos\frac{\pi x}{\lambda}+v_{is}\sin\frac{\pi x}{\lambda}+v_{iC}\cos\frac{2\pi x}{\lambda}+v_{iS}\sin\frac{2\pi x}{\lambda} \quad (5.4)$$

The sine and cosine terms with half-wavelength λ occur in unsymmetric laminates with $\mathbf{B}_i \neq \mathbf{0}$, and otherwise can be ignored. The linear term in equation (5.3) allows for the application of a uniform longitudinal strain $\bar{\varepsilon}_x$.

5.4 Calculation of strains and curvatures

From Von Kármán's large deflection theory, the neutral surface strains and curvatures are given as

$$\begin{bmatrix}\varepsilon_{xi}\\ \varepsilon_{yi}\\ \varepsilon_{xyi}\\ \kappa_{xi}\\ \kappa_{yi}\\ \kappa_{xyi}\end{bmatrix} = \begin{bmatrix}\frac{\partial u_i}{\partial x}+\frac{1}{2}\left(\frac{\partial w_i}{\partial x}\right)^2\\ \frac{\partial v_i}{\partial y}+\frac{1}{2}\left(\frac{\partial w_i}{\partial y}\right)^2\\ \frac{\partial u_i}{\partial y}+\frac{\partial v_i}{\partial x}+\frac{\partial w_i}{\partial x}\frac{\partial w_i}{\partial y}\\ -\frac{\partial^2 w_i}{\partial x^2}\\ -\frac{\partial^2 w_i}{\partial y^2}\\ -2\frac{\partial^2 w_i}{\partial x \partial y}\end{bmatrix} = \begin{bmatrix}\varepsilon_{xi0} & \varepsilon_{xic} & \varepsilon_{xis} & \varepsilon_{xiC} & \varepsilon_{xiS}\\ \varepsilon_{yi0} & \varepsilon_{yic} & \varepsilon_{yis} & \varepsilon_{yiC} & \varepsilon_{yiS}\\ \varepsilon_{xyi0} & \varepsilon_{xyic} & \varepsilon_{xys} & \varepsilon_{xyiC} & \varepsilon_{xyiS}\\ \kappa_{xi0} & \kappa_{xic} & \kappa_{xis} & \kappa_{xiC} & \kappa_{xiS}\\ \kappa_{yi0} & \kappa_{yic} & \kappa_{yis} & \kappa_{yiC} & \kappa_{yiS}\\ \kappa_{xyi0} & \kappa_{xyic} & \kappa_{xyis} & \kappa_{xyiC} & \kappa_{xyiS}\end{bmatrix} \begin{bmatrix}1\\ \cos\frac{\pi x}{\lambda}\\ \sin\frac{\pi x}{\lambda}\\ \cos\frac{2\pi x}{\lambda}\\ \sin\frac{2\pi x}{\lambda}\end{bmatrix} \quad (5.5)$$

On substitution from equations (5.1-5.4) the following expressions are given

$$\varepsilon_{\mathbf{i}} = \varepsilon_{\mathbf{0}}(\mathbf{w_i}) + \frac{\mathbf{1}}{\mathbf{b}}\varepsilon_{\mathbf{1}}\mathbf{u_i} + \varepsilon_{\mathbf{2}}\mathbf{u_i}' \quad (5.6)$$

$$\kappa_{\mathbf{i}} = \kappa_{\mathbf{0}}(\mathbf{w_i}) \quad (5.7)$$

where

$$\varepsilon_{\mathbf{i}} = \begin{bmatrix} \varepsilon_{xi0} & \varepsilon_{xic} & \varepsilon_{xis} & \varepsilon_{xiC} & \varepsilon_{xiS} \\ \varepsilon_{yi0} & \varepsilon_{yic} & \varepsilon_{yis} & \varepsilon_{yiC} & \varepsilon_{yiS} \\ \varepsilon_{xyi0} & \varepsilon_{xyic} & \varepsilon_{xyis} & \varepsilon_{xyiC} & \varepsilon_{xyiS} \end{bmatrix}$$

$$\kappa_{\mathbf{i}} = \begin{bmatrix} \kappa_{xi0} & \kappa_{xic} & \kappa_{xis} & \kappa_{xiC} & \kappa_{xiS} \\ \kappa_{yi0} & \kappa_{yic} & \kappa_{yis} & \kappa_{yiC} & \kappa_{yiS} \\ \kappa_{xyi0} & \kappa_{xyic} & \kappa_{xyis} & \kappa_{xyiC} & \kappa_{xyiS} \end{bmatrix}$$

$$\mathbf{w_i} = \begin{pmatrix} w_{i0} & w_{ic} & w_{is} & \psi_{i0} & \psi_{ic} & \psi_{is} \end{pmatrix}^T$$

$$\mathbf{u_i} = \begin{pmatrix} u_{i0} & u_{ic} & u_{is} & u_{iC} & u_{iS} & v_{i0} & v_{ic} & v_{is} & v_{iC} & v_{iS} \end{pmatrix}^T$$

$$\mathbf{u'_i} = \begin{pmatrix} u'_{i0} & u'_{ic} & u'_{is} & u'_{iC} & u'_{iS} & v'_{i0} & v'_{ic} & v'_{is} & v'_{iC} & v'_{iS} \end{pmatrix}^T$$

$$\varepsilon_{\mathbf{0}}(\mathbf{w_i}) = \begin{bmatrix} -\bar{\varepsilon}_x + \frac{\pi^2}{4\lambda^2}(w_{ic}^2 + w_{is}^2) \\ 0 \\ 0 \\ \frac{\pi^2}{4\lambda^2}(w_{is}^2 - w_{ic}^2) \\ -\frac{\pi^2}{2\lambda^2} w_{ic} w_{is} \\ \frac{1}{4}(\psi_{ic}^2 + \psi_{is}^2) \\ 0 \\ 0 \\ \frac{1}{4}(\psi_{ic}^2 - \psi_{is}^2) \\ \frac{1}{2}\psi_{ic}\psi_{is} \\ \frac{\pi}{2\lambda}(w_{is}\psi_{ic} - w_{ic}\psi_{is}) \\ 0 \\ 0 \\ \frac{\pi}{2\lambda}(w_{is}\psi_{ic} + w_{ic}\psi_{is}) \\ \frac{\pi}{2\lambda}(w_{is}\psi_{is} - w_{ic}\psi_{ic}) \end{bmatrix} \qquad \kappa_{\mathbf{0}}(\mathbf{w_i}) = \begin{bmatrix} 0 \\ \frac{\pi^2}{\lambda^2} w_{ic} \\ \frac{\pi^2}{\lambda^2} w_{is} \\ 0 \\ 0 \\ 0 \\ -\psi'_{ic} \\ -\psi'_{is} \\ 0 \\ 0 \\ 0 \\ -\frac{2\pi}{\lambda}\psi_{is} \\ \frac{2\pi}{\lambda}\psi_{ic} \\ 0 \\ 0 \end{bmatrix}$$

$$\varepsilon_{\mathbf{1}} = \begin{bmatrix} \mathbf{J} & \mathbf{O} \\ \mathbf{O} & \mathbf{O} \\ \mathbf{O} & \mathbf{J} \end{bmatrix} \qquad \varepsilon_{\mathbf{2}} = \begin{bmatrix} \mathbf{O} & \mathbf{O} \\ \mathbf{O} & \mathbf{I} \\ \mathbf{I} & \mathbf{O} \end{bmatrix}$$

$$\mathbf{I} = \begin{bmatrix} 1 & 0 & 0 & 0 & 0 \\ 0 & 1 & 0 & 0 & 0 \\ 0 & 0 & 1 & 0 & 0 \\ 0 & 0 & 0 & 1 & 0 \\ 0 & 0 & 0 & 0 & 1 \end{bmatrix} \qquad \mathbf{O} = \begin{bmatrix} 0 & 0 & 0 & 0 & 0 \\ 0 & 0 & 0 & 0 & 0 \\ 0 & 0 & 0 & 0 & 0 \\ 0 & 0 & 0 & 0 & 0 \\ 0 & 0 & 0 & 0 & 0 \end{bmatrix}$$

$$\mathbf{J} = \begin{bmatrix} 0 & 0 & 0 & 0 & 0 \\ 0 & 0 & \omega_i & 0 & 0 \\ 0 & -\omega_i & 0 & 0 & 0 \\ 0 & 0 & 0 & 0 & 2\omega_i \\ 0 & 0 & 0 & -2\omega_i & 0 \end{bmatrix} \qquad \omega_i = \frac{\pi b_i}{\lambda} \tag{5.8}$$

5.5 Stress-strain relationships

Following the calculation of strains and curvatures, the stress-strain relationships are consequently obtained in order to derive the equilibrium equations. For a general anisotropic plate, the stress-strain relationships are written as

$$N_{xi} = (A_i)_{11}\varepsilon_{xi} + (A_i)_{12}\varepsilon_{yi} + (A_i)_{16}\gamma_{xyi} + (B_i)_{11}\kappa_{xi} + (B_i)_{12}\kappa_{yi} + (B_i)_{16}\kappa_{xyi} \tag{5.9}$$

$$N_{yi} = (A_i)_{12}\varepsilon_{xi} + (A_i)_{22}\varepsilon_{yi} + (A_i)_{26}\gamma_{xyi} + (B_i)_{12}\kappa_{xi} + (B_i)_{22}\kappa_{yi} + (B_i)_{26}\kappa_{xyi} \tag{5.10}$$

$$N_{xyi} = (A_i)_{16}\varepsilon_{xi} + (A_i)_{26}\varepsilon_{yi} + (A_i)_{66}\gamma_{xyi} + (B_i)_{16}\kappa_{xi} + (B_i)_{26}\kappa_{yi} + (B_i)_{66}\kappa_{xyi} \tag{5.11}$$

$$M_{xi} = (B_i)_{11}\varepsilon_{xi} + (B_i)_{12}\varepsilon_{yi} + (B_i)_{16}\gamma_{xyi} + (D_i)_{11}\kappa_{xi} + (D_i)_{12}\kappa_{yi} + (D_i)_{16}\kappa_{xyi} \tag{5.12}$$

$$M_{yi} = (B_i)_{12}\varepsilon_{xi} + (B_i)_{22}\varepsilon_{yi} + (B_i)_{26}\gamma_{xyi} + (D_i)_{12}\kappa_{xi} + (D_i)_{22}\kappa_{yi} + (D_i)_{26}\kappa_{xyi} \quad (5.13)$$

$$M_{xyi} = (B_i)_{16}\varepsilon_{xi} + (B_i)_{26}\varepsilon_{yi} + (B_i)_{66}\gamma_{xyi} + (D_i)_{16}\kappa_{xi} + (D_i)_{26}\kappa_{yi} + (D_i)_{66}\kappa_{xyi} \quad (5.14)$$

In the subsequent analysis, the moment resultants are not essential so that only the in-plane stress-strain relationships are analyzed. The stress resultants and their first derivatives at node i can therefore be rewritten in matrix form as

$$\mathbf{N_i} = \bar{\mathbf{A}}_\mathbf{i}\varepsilon_\mathbf{0}\left(\mathbf{w_i}\right) + \bar{\mathbf{B}}_\mathbf{i}\kappa_\mathbf{0}\left(\mathbf{w_i}\right) + \frac{\mathbf{1}}{\mathbf{b}}\bar{\mathbf{A}}_\mathbf{i}\varepsilon_\mathbf{1}\mathbf{u_i} + \bar{\mathbf{A}}_\mathbf{i}\varepsilon_\mathbf{2}\mathbf{u_i}' \quad (5.15)$$

$$\mathbf{N_i}' = \bar{\mathbf{A}}_\mathbf{i}\varepsilon_\mathbf{0}'\left(\mathbf{w_i}\right) + \bar{\mathbf{B}}_\mathbf{i}\kappa_\mathbf{0}'\left(\mathbf{w_i}\right) + \frac{\mathbf{1}}{\mathbf{b}}\bar{\mathbf{A}}_\mathbf{i}\varepsilon_\mathbf{1}\mathbf{u_i}' + \bar{\mathbf{A}}_\mathbf{i}\varepsilon_\mathbf{2}\mathbf{u_i}'' \quad (5.16)$$

where

$$\mathbf{N_i} = \begin{bmatrix} N_{xi0} & N_{xic} & N_{xis} & N_{xiC} & N_{xiS} \\ N_{yi0} & N_{yic} & N_{yis} & N_{yiC} & N_{yiS} \\ N_{xyi0} & N_{xyic} & N_{xyis} & N_{xyiC} & N_{xyiS} \end{bmatrix}$$

$$\mathbf{N_i'} = \begin{bmatrix} N'_{xi0} & N'_{xic} & N'_{xis} & N'_{xiC} & N'_{xiS} \\ N'_{yi0} & N'_{yic} & N'_{yis} & N'_{yiC} & N'_{yiS} \\ N'_{xyi0} & N'_{xyic} & N'_{xyis} & N'_{xyiC} & N'_{xyiS} \end{bmatrix}$$

$$\bar{\mathbf{A}}_\mathbf{i} = \begin{bmatrix} (A_i)_{11}\mathbf{I} & (A_i)_{12}\mathbf{I} & (A_i)_{16}\mathbf{I} \\ (A_i)_{12}\mathbf{I} & (A_i)_{22}\mathbf{I} & (A_i)_{26}\mathbf{I} \\ (A_i)_{16}\mathbf{I} & (A_i)_{26}\mathbf{I} & (A_i)_{66}\mathbf{I} \end{bmatrix} \qquad \bar{\mathbf{B}}_\mathbf{i} = \begin{bmatrix} (B_i)_{11}\mathbf{I} & (B_i)_{12}\mathbf{I} & (B_i)_{16}\mathbf{I} \\ (B_i)_{12}\mathbf{I} & (B_i)_{22}\mathbf{I} & (B_i)_{26}\mathbf{I} \\ (B_i)_{16}\mathbf{I} & (B_i)_{26}\mathbf{I} & (B_i)_{66}\mathbf{I} \end{bmatrix}$$

$$\mathbf{u_i'} = \begin{pmatrix} u'_{i0} & u'_{ic} & u'_{is} & u'_{iC} & u'_{iS} & v'_{i0} & v'_{ic} & v'_{is} & v'_{iC} & v'_{iS} \end{pmatrix}$$

$$\mathbf{u_i''} = \begin{pmatrix} u''_{i0} & u''_{ic} & u''_{is} & u''_{iC} & u''_{iS} & v''_{i0} & v''_{ic} & v''_{is} & v''_{iC} & v''_{iS} \end{pmatrix}$$

$$\varepsilon'_{\mathbf{0}}(\mathbf{w_i}) = \begin{bmatrix} \frac{\pi^2}{2\lambda^2}(w_{ic}\psi_{ic} + w_{is}\psi_{is}) \\ 0 \\ 0 \\ \frac{\pi^2}{2\lambda^2}(w_{is}\psi_{is} - w_{ic}\psi_{ic}) \\ -\frac{\pi^2}{2\lambda^2}(w_{ic}\psi_{is} + w_{is}\psi_{ic}) \\ \frac{1}{2}(\psi_{ic}\psi'_{ic} + \psi_{is}\psi'_{is}) \\ 0 \\ 0 \\ \frac{1}{2}(\psi_{ic}\psi'_{ic} - \psi_{is}\psi'_{is}) \\ \frac{1}{2}(\psi_{is}\psi'_{ic} + \psi_{ic}\psi'_{is}) \\ \frac{\pi}{2\lambda}(w_{is}\psi'_{ic} + w'_{is}\psi_{ic} - w_{ic}\psi'_{is} - w_{ic}\psi_{is}) \\ 0 \\ 0 \\ \frac{\pi}{2\lambda}(w_{is}\psi'_{ic} + w'_{is}\psi_{ic} + w_{ic}\psi'_{is} + w_{ic}\psi_{is}) \\ \frac{\pi}{2\lambda}(w_{is}\psi'_{is} + \psi^2_{is} - w_{ic}\psi'_{ic} - \psi^2_{ic}) \end{bmatrix} \quad \kappa'_{\mathbf{0}}(\mathbf{w_i}) = \begin{bmatrix} 0 \\ \frac{\pi^2}{\lambda^2}\psi_{ic} \\ \frac{\pi^2}{\lambda^2}\psi_{is} \\ 0 \\ 0 \\ 0 \\ -\psi''_{ic} \\ -\psi''_{is} \\ 0 \\ 0 \\ 0 \\ -\frac{2\pi}{\lambda}\psi'_{is} \\ \frac{2\pi}{\lambda}\psi'_{ic} \\ 0 \\ 0 \end{bmatrix} \tag{5.17}$$

The derivatives $\mathbf{u'_i}$, $\mathbf{u''_i}$ are obtained by introducing finite difference approximations with adjustments by parabolic interpolation at the plate edges

$$\begin{cases} \mathbf{u'_i} = \frac{1}{2b}(-\mathbf{3u_i} + \mathbf{4u_{i+1}} - \mathbf{u_{i+2}}) & (i = 1) \\ \mathbf{u'_i} = \frac{1}{2b}(\mathbf{u_{i+1}} - \mathbf{u_{i-1}}) & (1 < i < n) \\ \mathbf{u'_i} = \frac{1}{2b}(\mathbf{u_{i-2}} - \mathbf{4u_{i-1}} + \mathbf{3u_i}) & (i = n) \end{cases} \tag{5.18}$$

$$\begin{cases} \mathbf{u''_i} = \frac{1}{b^2}(\mathbf{2u_i} - \mathbf{5u_{i+1}} + \mathbf{4u_{i+2}} - \mathbf{u_{i+3}}) & (i = 1) \\ \mathbf{u''_i} = \frac{1}{b^2}(\mathbf{u_{i+1}} - \mathbf{2u_i} + \mathbf{u_{i-1}}) & (1 < i < n) \\ \mathbf{u''_i} = \frac{1}{b^2}(\mathbf{u_{i-3}} - \mathbf{4u_{i-1}} + \mathbf{5u_{i-1}} - \mathbf{2u_i}) & (i = n) \end{cases} \tag{5.19}$$

substituting equations (5.17) into equations (5.15, 5.16) and applying finite difference approximations in equations (5.18, 5.19) to the derivatives, detailed expressions for $\mathbf{N_i}$ and $\mathbf{N'_i}$ can be obtained.

5.6 Equilibrium equations

To solve for the in-plane displacement $\mathbf{u_i}$, the in-plane equilibrium conditions for node i are given as

$$\frac{\partial \mathbf{N_{yi}}}{\partial y} + \frac{\partial \mathbf{N_{xyi}}}{\partial x} = 0 \tag{5.20}$$

$$\frac{\partial \mathbf{N_{xyi}}}{\partial y} + \frac{\partial \mathbf{N_{xi}}}{\partial x} = 0 \tag{5.21}$$

which can be further extended in the following expressions by rewriting the stress resultants in terms of their components

$$N'_{yi0} = 0$$

$$N'_{yic} + \frac{\pi}{\lambda} N_{xyis} = 0$$

$$N'_{yis} - \frac{\pi}{\lambda} N_{xyic} = 0$$

$$N'_{yiC} + \frac{2\pi}{\lambda} N_{xyiS} = 0$$

$$N'_{yiS} - \frac{2\pi}{\lambda} N_{xyiC} = 0$$

$$N'_{xyi0} = 0$$

$$N'_{xyic} + \frac{\pi}{\lambda} N_{xis} = 0$$

$$N'_{xyis} - \frac{\pi}{\lambda} N_{xic} = 0$$

$$N'_{xyiC} + \frac{2\pi}{\lambda} N_{xiS} = 0$$

$$N'_{xyiS} - \frac{2\pi}{\lambda} N_{xiC} = 0 \tag{5.22}$$

Substituting expressions for $\mathbf{N_i}$ and $\mathbf{N'_i}$ gives ten equilibrium equations for each node, in terms of the unknown in-plane displacement terms u_{i0}, u_{ic}, u_{is}, u_{iC}, u_{iS}, v_{i0}, v_{ic}, v_{is}, v_{iC} and v_{iS} of equations (5.3) and (5.4). The equilibrium equations are formulated in the following forms, where expressions in curly brackets are for the first node (i=1), interior nodes ($1 < i < n$) and the last node (i=n), respectively from top to bottom

$$\begin{aligned}
&\frac{\left(\bar{A}_i\right)_{22}}{4b} \begin{cases} \psi_{ic}\left(-3\psi_{ic} + 4\psi_{i+1,c} - \psi_{i+2,c}\right) + \psi_{is}\left(-3\psi_{is} + 4\psi_{i+1,s} - \psi_{i+2,s}\right) \\ \psi_{ic}\left(\psi_{i+1,c} - \psi_{i-1,c}\right) + \psi_{is}\left(\psi_{i+1,s} - \psi_{i-1,s}\right) \\ \psi_{ic}\left(3\psi_{ic} - 4\psi_{i-1,c} + \psi_{i-2,c}\right) + \psi_{is}\left(3\psi_{is} - 4\psi_{i-1,s} + \psi_{i-2,s}\right) \end{cases} \\
&+ \frac{\left(\bar{A}_i\right)_{12}\pi^2}{2\lambda^2}\left(w_{ic}\psi_{ic} + w_{is}\psi_{is}\right) + \frac{\left(\bar{A}_i\right)_{26}}{b^2} \begin{cases} 2u_{i0} - 5u_{i+1,0} + 4u_{i+2,0} - u_{i+3,0} \\ u_{i+1,0} - 2u_{i0} + u_{i-1,0} \\ 2u_{i0} - 5u_{i-1,0} + 4u_{i-2,0} - u_{i-3,0} \end{cases} \\
&+ \frac{\left(\bar{A}_i\right)_{26}\pi}{4\lambda b} \begin{cases} \psi_{ic}\left(-3w_{is} + 4w_{i+1,s} - w_{i+2,s}\right) + w_{is}\left(-3\psi_{ic} + 4\psi_{i+1,c} - \psi_{i+2,c}\right) \\ \psi_{ic}\left(w_{i+1,s} - w_{i-1,s}\right) + w_{is}\left(\psi_{i+1,c} - \psi_{i-1,c}\right) \\ \psi_{ic}\left(3w_{is} - 4w_{i-1,s} + w_{i-2,s}\right) + w_{is}\left(3\psi_{ic} - 4\psi_{i-1,c} + \psi_{i-2,c}\right) \end{cases} \\
&+ \frac{\left(\bar{A}_i\right)_{26}\pi}{4\lambda b} \begin{cases} -w_{ic}\left(-3\psi_{is} + 4\psi_{i+1,s} - \psi_{i+2,s}\right) - \psi_{is}\left(-3w_{ic} + 4w_{i+1,c} - w_{i+2,c}\right) \\ -w_{ic}\left(\psi_{i+1,s} - \psi_{i-1,s}\right) - \psi_{is}\left(w_{i+1,c} - w_{i-1,c}\right) \\ -w_{ic}\left(3\psi_{is} - 4\psi_{i-1,s} + \psi_{i-2,s}\right) - \psi_{is}\left(3w_{ic} - 4w_{i-1,c} + w_{i-2,c}\right) \end{cases} \\
&+ \frac{\left(\bar{A}_i\right)_{22}}{b^2} \begin{cases} 2v_{i0} - 5v_{i+1,0} + 4v_{i+2,0} - v_{i+3,0} \\ v_{i+1,0} - 2v_{i0} + v_{i-1,0} \\ 2v_{i0} - 5v_{i-1,0} + 4v_{i-2,0} - v_{i-3,0} \end{cases} = 0
\end{aligned} \tag{5.23}$$

$$
\begin{aligned}
&- \frac{\left(\bar{B}_i\right)_{22}}{b^2} \begin{cases} 2\psi_{ic} - 5\psi_{i+1,c} + 4\psi_{i+2,c} - \psi_{i+3,c} \\ \psi_{i+1,c} - 2\psi_{ic} + \psi_{i-1,c} \\ 2\psi_{ic} - 5\psi_{i-1,c} + \psi_4 i - 2, c - \psi_{i-3,c} \end{cases} + \frac{2\pi^2 \left(\bar{B}_i\right)_{66}}{\lambda^2} \psi_{ic} \\
&+ \frac{\left(\bar{A}_i\right)_{22}}{b^2} \begin{cases} 2v_{ic} - 5v_{i+1,c} + 4v_{i+2,c} - v_{i+3,c} \\ v_{i+1,c} - 2v_{ic} + v_{i-1,c} \\ 2v_{ic} - 5v_{i-1,c} + 4v_{i-2,c} - v_{i-3,c} \end{cases} + \frac{\left(\bar{A}_i\right)_{12} \omega_i}{2b^2} \begin{cases} -3u_{is} + 4u_{i+1,s} - u_{i+2,s} \\ u_{i+1,s} - u_{i-1,s} \\ 3u_{is} - 4u_{i-1,s} + u_{i-2,s} \end{cases} \\
&+ \frac{\left(\bar{A}_i\right)_{26} \omega_i}{2b^2} \begin{cases} -3v_{is} + 4v_{i+1,s} - v_{i+2,s} \\ v_{i+1,s} - v_{i-1,s} \\ 3v_{is} - 4v_{i-1,s} + v_{i-2,s} \end{cases} - \frac{\left(\bar{B}_i\right)_{26} \pi}{\lambda b} \begin{cases} -3\psi_{is} + 4\psi_{i+1,s} - \psi_{i+2s} \\ \psi_{i+1,s} - \psi_{i-1,s} \\ 3\psi_{is} - 4\psi_{i-1,s} + \psi_{i-2,s} \end{cases} \\
&- \frac{\left(B_i\right)_{26} \pi}{2\lambda b} \begin{cases} -3\psi_{is} + 4\psi_{i+1,s} - \psi_{i+2,s} \\ \psi_{i+1,s} - \psi_{i-1,s} \\ 3\psi_{is} - 4\psi_{i-1,s} + \psi_{i-2,s} \end{cases} + \frac{\left(B_i\right)_{12} \pi^2}{\lambda^2} \psi_{ic} + \frac{\left(B_i\right)_{16} \pi^3}{\lambda^3} w_{is} \\
&+ \frac{\left(A_i\right)_{26} \pi}{2\lambda b} \begin{cases} -3v_{is} + 4v_{i+1,s} - v_{i+2,s} \\ v_{i+1,s} - v_{i-1,s} \\ 3v_{is} - 4v_{i-1,s} + v_{i-2,s} \end{cases} + \frac{\left(A_i\right)_{66} \pi}{2\lambda b} \begin{cases} -3u_{is} + 4u_{i+1,s} - u_{i+2,s} \\ u_{i+1,s} - u_{i-1,s} \\ 3u_{is} - 4u_{i-1,s} + u_{i-2,s} \end{cases} \\
&+ \frac{\left(\bar{A}_i\right)_{26}}{b^2} \begin{cases} 2u_{ic} - 5u_{i+1,c} + 4u_{i+2,c} - u_{i+3,c} \\ u_{i+1,c} - 2u_{ic} + u_{i-1,c} \\ 2u_{ic} - 5u_{i-1,c} + 4u_{i-2,c} - u_{i-3,c} \end{cases} - \frac{\left(\bar{A}_i\right)_{16} \omega_i \pi}{\lambda b} u_{ic} - \frac{\left(\bar{A}_i\right)_{66} \omega_i \pi}{\lambda b} v_{ic} = 0
\end{aligned}
\tag{5.24}
$$

$$
\begin{aligned}
&- \frac{\left(\bar{B}_i\right)_{22}}{b^2} \begin{cases} 2\psi_{is} - 5\psi_{i+1,s} + 4\psi_{i+2,s} - \psi_{i+3,s} \\ \psi_{i+1,s} - 2\psi_{is} + \psi_{i-1,s} \\ 2\psi_{is} - 5\psi_{i-1,s} + \psi_4 i - 2, s - \psi_{i-3,s} \end{cases} + \frac{2\pi^2 \left(\bar{B}_i\right)_{66}}{\lambda^2} \psi_{is} \\
&+ \frac{\left(\bar{A}_i\right)_{22}}{b^2} \begin{cases} 2v_{is} - 5v_{i+1,s} + 4v_{i+2,s} - v_{i+3,s} \\ v_{i+1,s} - 2v_{is} + v_{i-1,s} \\ 2v_{is} - 5v_{i-1,s} + 4v_{i-2,s} - v_{i-3,s} \end{cases} - \frac{\left(\bar{A}_i\right)_{12} \omega_i}{2b^2} \begin{cases} -3u_{ic} + 4u_{i+1,c} - u_{i+2,c} \\ u_{i+1,c} - u_{i-1,c} \\ 3u_{ic} - 4u_{i-1,c} + u_{i-2,c} \end{cases} \\
&- \frac{\left(\bar{A}_i\right)_{26} \omega_i}{2b^2} \begin{cases} -3v_{ic} + 4v_{i+1,c} - v_{i+2,c} \\ v_{i+1,c} - v_{i-1,c} \\ 3v_{ic} - 4v_{i-1,c} + v_{i-2,c} \end{cases} + \frac{\left(\bar{B}_i\right)_{26} \pi}{\lambda b} \begin{cases} -3\psi_{ic} + 4\psi_{i+1,c} - \psi_{i+2c} \\ \psi_{i+1,c} - \psi_{i-1,c} \\ 3\psi_{ic} - 4\psi_{i-1,c} + \psi_{i-2,c} \end{cases} \\
&- \frac{\left(B_i\right)_{26} \pi}{2\lambda b} \begin{cases} -3\psi_{ic} + 4\psi_{i+1,c} - \psi_{i+2,c} \\ \psi_{i+1,c} - \psi_{i-1,c} \\ 3\psi_{ic} - 4\psi_{i-1,c} + \psi_{i-2,c} \end{cases} + \frac{\left(B_i\right)_{12} \pi^2}{\lambda^2} \psi_{is} - \frac{\left(B_i\right)_{16} \omega_i \pi^3}{\lambda^3} w_{ic} \\
&- \frac{\left(A_i\right)_{26} \pi}{2\lambda b} \begin{cases} -3v_{ic} + 4v_{i+1,c} - v_{i+2,c} \\ v_{i+1,c} - v_{i-1,c} \\ 3v_{ic} - 4v_{i-1,c} + v_{i-2,c} \end{cases} - \frac{\left(A_i\right)_{66} \pi}{2\lambda b} \begin{cases} -3u_{ic} + 4u_{i+1,c} - u_{i+2,c} \\ u_{i+1,c} - u_{i-1,c} \\ 3u_{ic} - 4u_{i-1,c} + u_{i-2,c} \end{cases} \\
&+ \frac{\left(\bar{A}_i\right)_{26}}{b^2} \begin{cases} 2u_{is} - 5u_{i+1,s} + 4u_{i+2,s} - u_{i+3,s} \\ u_{i+1,s} - 2u_{is} + u_{i-1,s} \\ 2u_{is} - 5u_{i-1,s} + 4u_{i-2,s} - u_{i-3,s} \end{cases} - \frac{\left(\bar{A}_i\right)_{16} \omega_i \pi}{\lambda b} u_{is} - \frac{\left(\bar{A}_i\right)_{66} \omega_i \pi}{\lambda b} v_{is} = 0
\end{aligned}
\tag{5.25}
$$

$$
\begin{aligned}
&\frac{(\bar{A}_i)_{22}}{4b}\begin{cases}\psi_{ic}(-3\psi_{ic}+4\psi_{i+1,c}-\psi_{i+2,c})-\psi_{is}(-3\psi_{is}+4\psi_{i+1,s}-\psi_{i+2,s})\\ \psi_{ic}(\psi_{i+1,c}-\psi_{i-1,c})-\psi_{is}(\psi_{i+1,s}-\psi_{i-1,s})\\ \psi_{ic}(3\psi_{ic}-4\psi_{i-1,c}+\psi_{i-2,c})-\psi_{is}(3\psi_{is}-4\psi_{i-1,s}+\psi_{i-2,s})\end{cases}\\
&+\frac{\pi^2(\bar{A}_i)_{12}}{2\lambda^2}(w_{is}\psi_{is}-w_{ic}\psi_{ic})-\frac{(\bar{A}_i)_{16}\pi^3}{\lambda^3}w_{ic}w_{is}+(\bar{A}_i)_{26}\frac{\pi}{\lambda}\psi_{ic}\psi_{is}\\
&+\frac{(\bar{A}_i)_{66}\pi^2}{\lambda^2}(w_{is}\psi_{is}-w_{ic}\psi_{ic})-(\bar{A}_i)_{16}\frac{4\omega_i\pi}{\lambda b}u_{iC}+(\bar{A}_i)_{66}\frac{4\omega_i\pi}{\lambda b}v_{iC}\\
&\frac{(\bar{A}_i)_{26}\,\pi}{4\lambda b}\begin{cases}\psi_{ic}(-3w_{is}+4w_{i+1,s}-w_{i+2,s})+w_{is}(-3\psi_{ic}+4\psi_{i+1,c}-\psi_{i+2,c})\\ \psi_{ic}(w_{i+1,s}-w_{i-1,s})+w_{is}(\psi_{i+1,c}-\psi_{i-1,c})\\ \psi_{ic}(3w_{is}-4w_{i-1,s}+w_{i-2,s})+w_{is}(3\psi_{ic}-4\psi_{i-1,c}+\psi_{i-2,c})\end{cases}\\
&\frac{(\bar{A}_i)_{26}\,\pi}{4\lambda b}\begin{cases}w_{ic}(-3\psi_{is}+4\psi_{i+1,s}-\psi_{i+2,s})+\psi_{is}(-3w_{ic}+4w_{i+1,c}-w_{i+2,c})\\ w_{ic}(\psi_{i+1,s}-\psi_{i-1,s})+\psi_{is}(w_{i+1,c}-w_{i-1,c})\\ w_{ic}(3\psi_{is}-4\psi_{i-1,s}+\psi_{i-2,s})+\psi_{is}(3w_{ic}-4w_{i-1,c}+w_{i-2,c})\end{cases}\\
&+\frac{(\bar{A}_i)_{22}}{b^2}\begin{cases}2v_{iC}-5v_{i+1,C}+4v_{i+2,C}-v_{i+3,C}\\ v_{i+1,C}-2v_{iC}+v_{i-1,C}\\ 2v_{iC}-5v_{i-1,C}+4v_{i-2,C}-v_{i-3,C}\end{cases}+\frac{(\bar{A}_i)_{12}\omega_i}{b^2}\begin{cases}-3u_{iS}+4u_{i+1,S}-u_{i+2,S}\\ u_{i+1,S}-u_{i-1,S}\\ 3u_{iS}-4u_{i-1,S}+u_{i-2,S}\end{cases}\\
&+\frac{(\bar{A}_i)_{26}\omega_i}{b^2}\begin{cases}-3v_{iS}+4v_{i+1,S}-v_{i+2,S}\\ v_{i+1,S}-v_{i-1,S}\\ 3v_{iS}-4v_{i-1,S}+v_{i-2,S}\end{cases}+\frac{(\bar{A}_i)_{26}}{b^2}\begin{cases}2u_{iC}-5u_{i+1,C}+4u_{i+2,C}-u_{i+3,C}\\ u_{i+1,C}-2u_{iC}+u_{i-1,C}\\ 2u_{iC}-5u_{i-1,C}+4u_{i-2,C}-u_{i-3,C}\end{cases}\\
&+\frac{(\bar{A}_i)_{66}\pi}{\lambda b}\begin{cases}-3u_{iS}+4u_{i+1,S}-u_{i+2,S}\\ u_{i+1,S}-u_{i-1,S}\\ 3u_{iS}-4u_{i-1,S}+u_{i-2,S}\end{cases}+\frac{(\bar{A}_i)_{26}\pi}{\lambda b}\begin{cases}-3v_{iS}+4v_{i+1,S}-v_{i+2,S}\\ v_{i+1,S}-v_{i-1,S}\\ 3v_{iS}-4v_{i-1,S}+v_{i-2,S}\end{cases}=0
\end{aligned}
\tag{5.26}
$$

$$
\begin{aligned}
&\frac{(\bar{A}_i)_{22}}{4b}\begin{cases}\psi_{is}(-3\psi_{ic}+4\psi_{i+1,c}-\psi_{i+2,c})+\psi_{ic}(-3\psi_{is}+4\psi_{i+1,s}-\psi_{i+2,s})\\ \psi_{is}(\psi_{i+1,c}-\psi_{i-1,c})+\psi_{ic}(\psi_{i+1,s}-\psi_{i-1,s})\\ \psi_{is}(3\psi_{ic}-4\psi_{i-1,c}+\psi_{i-2,c})+\psi_{ic}(3\psi_{is}-4\psi_{i-1,s}+\psi_{i-2,s})\end{cases}\\
&\frac{(\bar{A}_i)_{26}\,\pi}{4\lambda b}\begin{cases}w_{is}(-3\psi_{is}+4\psi_{i+1,s}-\psi_{i+2,s})-w_{is}(-3\psi_{ic}+4\psi_{i+1,c}-\psi_{i+2,c})\\ w_{is}(\psi_{i+1,s}-\psi_{i-1,s})-w_{is}(\psi_{i+1,c}-\psi_{i-1,c})\\ w_{is}(3\psi_{is}-4\psi_{i-1,s}+\psi_{i-2,s})-w_{is}(3\psi_{ic}-4\psi_{i-1,c}+\psi_{i-2,c})\end{cases}\\
&-\frac{\pi^2(\bar{A}_i)_{12}}{2\lambda^2}(w_{is}\psi_{ic}+w_{ic}\psi_{is})+(\bar{A}_i)_{26}\frac{\pi}{2\lambda}(\psi_{is}^2-\psi_{ic}^2)-(\bar{A}_i)_{16}\frac{\pi^3}{2\lambda^3}(w_{is}^2-w_{ic}^2)\\
&-\frac{(\bar{A}_i)_{26}\pi}{2\lambda}(\psi_{ic}^2-\psi_{is}^2)-\frac{(\bar{A}_i)_{66}\pi^2}{\lambda^2}(w_{is}\psi_{ic}+w_{ic}\psi_{is})-(\bar{A}_i)_{16}\frac{4\omega_i\pi}{\lambda b}u_{iS}-(\bar{A}_i)_{66}\frac{4\omega_i\pi}{\lambda b}v_{iS}\\
&-\frac{(\bar{A}_i)_{66}\pi}{\lambda b}\begin{cases}-3u_{iC}+4u_{i+1,C}-u_{i+2,C}\\ u_{i+1,C}-u_{i-1,C}\\ 3u_{iC}-4u_{i-1,C}+u_{i-2,C}\end{cases}-\frac{(\bar{A}_i)_{26}\pi}{\lambda b}\begin{cases}-3v_{iC}+4v_{i+1,C}-v_{i+2,C}\\ v_{i+1,C}-v_{i-1,C}\\ 3v_{iC}-4v_{i-1,C}+v_{i-2,C}\end{cases}\\
&+\frac{(\bar{A}_i)_{22}}{b^2}\begin{cases}2v_{is}-5v_{i+1,s}+4v_{i+2,s}-v_{i+3,s}\\ v_{i+1,s}-2v_{is}+v_{i-1,s}\\ 2v_{is}-5v_{i-1,s}+4v_{i-2,s}-v_{i-3,s}\end{cases}+\frac{(\bar{A}_i)_{26}}{b^2}\begin{cases}2u_{is}-5u_{i+1,s}+4u_{i+2,s}-u_{i+3,s}\\ u_{i+1,s}-2u_{is}+u_{i-1,s}\\ 2u_{is}-5u_{i-1,s}+4u_{i-2,s}-u_{i-3,s}\end{cases}\\
&-\frac{(\bar{A}_i)_{12}\omega_i}{b^2}\begin{cases}-3u_{iC}+4u_{i+1,C}-u_{i+2,C}\\ u_{i+1,C}-u_{i-1,C}\\ 3u_{iC}-4u_{i-1,C}+u_{i-2,C}\end{cases}-\frac{(\bar{A}_i)_{16}\omega_i}{b^2}\begin{cases}-3v_{iC}+4v_{i+1,C}-v_{i+2,C}\\ v_{i+1,C}-v_{i-1,C}\\ 3v_{iC}-4v_{i-1,C}+v_{i-2,C}\end{cases}=0
\end{aligned}
\tag{5.27}
$$

$$
\begin{aligned}
&\frac{(\bar{A}_i)_{66}\pi}{4\lambda b}\begin{cases}w_{is}(-3\psi_{ic}+4\psi_{i+1,c}-\psi_{i+2,c})-w_{ic}(-3\psi_{is}+4\psi_{i+1,s}-\psi_{i+2,s})\\ w_{is}(\psi_{i+1,c}-\psi_{i-1,c})-w_{ic}(\psi_{i+1,s}-\psi_{i-1,s})\\ w_{is}(3\psi_{ic}-4\psi_{i-1,c}+\psi_{i-2,c})-w_{ic}(3\psi_{is}-4\psi_{i-1,s}+\psi_{i-2,s})\end{cases}\\
&\frac{(\bar{A}_i)_{66}\pi}{4\lambda b}\begin{cases}\psi_{ic}(-3w_{ic}+4w_{i+1,c}-w_{i+2,c})-\psi_{is}(-3w_{is}+4w_{i+1,s}-w_{i+2,s})\\ \psi_{ic}(w_{i+1,c}-w_{i-1,c})-\psi_{is}(w_{i+1,s}-w_{i-1,s})\\ \psi_{ic}(3w_{ic}-4w_{i-1,c}+w_{i-2,c})-\psi_{is}(3w_{is}-4w_{i-1,s}+w_{i-2,s})\end{cases}\\
&\frac{(\bar{A}_i)_{66}}{b^2}\begin{cases}2u_{i0}-5u_{i+1,0}+4u_{i+2,0}-u_{i+3,0}\\ u_{i+1,0}-2u_{i0}+u_{i-1,0}\\ 2u_{i0}-5u_{i-1,0}+4u_{i-2,0}-u_{i-3,0}\end{cases}+\frac{(\bar{A}_i)_{26}}{b^2}\begin{cases}2v_{i0}-5v_{i+1,0}+4v_{i+2,0}-v_{i+3,0}\\ v_{i+1,0}-2v_{i0}+v_{i-1,0}\\ 2v_{i0}-5v_{i-1,0}+4v_{i-2,0}-v_{i-3,0}\end{cases}\\
&+\frac{(\bar{A}_i)_{16}\pi^2}{2\lambda^2}(w_{ic}\psi_{ic}+w_{is}\psi_{is})\\
&\frac{(\bar{A}_i)_{26}}{4b}\begin{cases}\psi_{is}(-3\psi_{is}+4\psi_{i+1,s}-\psi_{i+2,s})+\psi_{ic}(-3\psi_{ic}+4\psi_{i+1,c}-\psi_{i+2,c})\\ \psi_{is}(\psi_{i+1,s}-\psi_{i-1,s})+\psi_{ic}(\psi_{i+1,c}-\psi_{i-1,c})\\ \psi_{is}(3\psi_{is}-4\psi_{i-1,s}+\psi_{i-2,s})+\psi_{ic}(3\psi_{ic}-4\psi_{i-1,c}+\psi_{i-2,c})\end{cases}=0
\end{aligned}
\tag{5.28}
$$

$$
\begin{aligned}
&- \frac{(\bar{B}_i)_{66}\pi}{\lambda b}\begin{cases} -3\psi_{is} + 4\psi_{i+1,s} - \psi_{i+2,s} \\ \psi_{i+1,s} - \psi_{i-1,s} \\ 3\psi_{is} - 4\psi_{i-1,s} + \psi_{i-2,s} \end{cases} + \frac{(\bar{A}_i)_{66}\omega_i}{2b^2}\begin{cases} -3v_{is} + 4v_{i+1,s} - v_{i+2,s} \\ v_{i+1,s} - v_{i-1,s} \\ 3v_{is} - 4v_{i-1,s} + v_{i-2,s} \end{cases} \\
&+ \frac{(\bar{A}_i)_{16}\omega_i}{2b^2}\begin{cases} -3u_{is} + 4u_{i+1,s} - u_{i+2,s} \\ u_{i+1,s} - u_{i-1,s} \\ 3u_{is} - 4u_{i-1,s} + u_{i-2,s} \end{cases} - \frac{(\bar{B}_i)_{26}}{b^2}\begin{cases} 2\psi_{ic} - 5\psi_{i+1,c} + 4\psi_{i+2,c} - \psi_{i+3,c} \\ \psi_{i+1,c} - 2\psi_{ic} + \psi_{i-1,c} \\ 2\psi_{ic} - 5\psi_{i-1,c} + 4\psi_{i-2,c} - \psi_{i-3,c} \end{cases} \\
&+ \frac{(\bar{A}_i)_{26}}{b^2}\begin{cases} 2v_{ic} - 5v_{i+1,c} + 4v_{i+2,c} - v_{i+3,c} \\ v_{i+1,c} - 2v_{ic} + v_{i-1,c} \\ 2v_{ic} - 5v_{i-1,c} + 4v_{i-2,c} - v_{i-3,c} \end{cases} + \frac{(\bar{A}_i)_{66}}{b^2}\begin{cases} 2u_{ic} - 5u_{i+1,c} + 4u_{i+2,c} - u_{i+3,c} \\ u_{i+1,c} - 2u_{ic} + u_{i-1,c} \\ 2u_{ic} - 5u_{i-1,c} + 4u_{i-2,c} - u_{i-3,c} \end{cases} \\
&+ \frac{(\bar{B}_i)_{11}\pi^3}{\lambda^3}w_{is} + (\bar{B}_i)_{16}\frac{\pi^2}{\lambda^2}\psi_{ic} - \frac{(\bar{B}_i)_{12}\pi}{2\lambda b}\begin{cases} -3\psi_{is} + 4\psi_{i+1,s} - \psi_{i+2,s} \\ \psi_{i+1,s} - \psi_{i-1,s} \\ 3\psi_{is} - 4\psi_{i-1,s} + \psi_{i-2,s} \end{cases} \\
&+ (\bar{B}_i)_{16}\frac{2\pi^2}{\lambda^2}\psi_{ic} - (\bar{A}_i)_{11}\frac{\omega_i\pi}{\lambda b}u_{ic} - (\bar{A}_i)_{16}\frac{\omega_i\pi}{\lambda b}v_{ic} - \frac{(\bar{B}_i)_{66}\pi}{\lambda b}\begin{cases} -3\psi_{is} + 4\psi_{i+1,s} - \psi_{i+2,s} \\ \psi_{i+1,s} - \psi_{i-1,s} \\ 3\psi_{is} - 4\psi_{i-1,s} + \psi_{i-2,s} \end{cases} \\
&+ \frac{(\bar{A}_{12})\pi}{2\lambda b}\begin{cases} -3v_{is} + 4v_{i+1,s} - v_{i+2,s} \\ v_{i+1,s} - v_{i-1,s} \\ 3v_{is} - 4v_{i-1,s} + v_{i-2,s} \end{cases} + \frac{(\bar{A}_{16})\pi}{2\lambda b}\begin{cases} -3u_{is} + 4u_{i+1,s} - u_{i+2,s} \\ u_{i+1,s} - u_{i-1,s} \\ 3u_{is} - 4u_{i-1,s} + u_{i-2,s} \end{cases} = 0
\end{aligned}
\tag{5.29}
$$

$$
\begin{aligned}
&\frac{(\bar{B}_i)_{12}\pi}{2\lambda b}\begin{cases} -3\psi_{ic}+4\psi_{i+1,c}-\psi_{i+2,c} \\ \psi_{i+1,c}-\psi_{i-1,c} \\ 3\psi_{ic}-4\psi_{i-1,c}+\psi_{i-2,c} \end{cases} + \frac{(\bar{A}_i)_{16}\pi}{2\lambda b}\begin{cases} -3u_{ic}+4u_{i+1,c}-u_{i+2,c} \\ u_{i+1,c}-u_{i-1,c} \\ 3u_{ic}-4u_{i-1,c}+u_{i-2,c} \end{cases} \\
&+ (\bar{B}_i)_{16}\frac{2\pi^2}{\lambda^2}\psi_{is} + (\bar{B}_i)_{16}\frac{\pi^2}{\lambda^2}\psi_{is} - (\bar{B}_i)_{11}\frac{\pi^3}{\lambda^3}w_{ic} \\
&- \frac{(\bar{A}_i)_{66}\omega_i}{2b^2}\begin{cases} -3v_{ic}+4v_{i+1,c}-v_{i+2,c} \\ v_{i+1,c}-v_{i-1,c} \\ 3v_{ic}-4v_{i-1,c}+v_{i-2,c} \end{cases} - \frac{(\bar{B}_i)_{26}}{b^2}\begin{cases} 2\psi_{is}-5\psi_{i+1,s}+4\psi_{i+2,s}-\psi_{i+3,s} \\ \psi_{i+1,s}-2\psi_{is}+\psi_{i-1,s} \\ 2\psi_{is}-5\psi_{i-1,s}+4\psi_{i-2,s}-\psi_{i-3,s} \end{cases} \\
&- \frac{(\bar{A}_i)_{12}\pi}{2\lambda b}\begin{cases} -3v_{ic}+4v_{i+1,c}-v_{i+2,c} \\ v_{i+1,c}-v_{i-1,c} \\ 3v_{ic}-4v_{i-1,c}+v_{i-2,c} \end{cases} + \frac{(\bar{B}_i)_{66}\pi}{\lambda b}\begin{cases} -3\psi_{ic}+4\psi_{i+1,c}-\psi_{i+2,c} \\ \psi_{i+1,c}-\psi_{i-1,c} \\ 3\psi_{ic}-4\psi_{i-1,c}+\psi_{i-2,c} \end{cases} \\
&- \frac{(\bar{A}_i)_{16}\omega_i}{2b^2}\begin{cases} -3u_{ic}+4u_{i+1,c}-u_{i+2,c} \\ u_{i+1,c}-u_{i-1,c} \\ 3u_{ic}-4u_{i-1,c}+u_{i-2,c} \end{cases} + \frac{(\bar{A}_i)_{66}}{b^2}\begin{cases} 2u_{is}-5u_{i+1,s}+4u_{i+2,s}-u_{i+3,s} \\ u_{i+1,s}-2u_{is}+u_{i-1,s} \\ 2u_{is}-5u_{i-1,s}+4u_{i-2,s}-u_{i-3,s} \end{cases} \\
&+ \frac{(\bar{A}_i)_{26}}{b^2}\begin{cases} 2v_{is}-5v_{i+1,s}+4v_{i+2,s}-v_{i+3,s} \\ v_{i+1,s}-2v_{is}+v_{i-1,s} \\ 2v_{is}-5v_{i-1,s}+4v_{i-2,s}-v_{i-3,s} \end{cases} - (\bar{A}_i)_{11}\frac{\omega_i\pi}{\lambda b}u_{is} - (\bar{A}_i)_{16}\frac{\omega_i\pi}{\lambda b}v_{is} = 0
\end{aligned}
\tag{5.30}
$$

$$
\begin{aligned}
&\frac{(\bar{A}_i)_{26}}{4b}\begin{cases}\psi_{ic}(-3\psi_{ic}+4\psi_{i+1,c}-\psi_{i+2,c})-\psi_{is}(-3\psi_{is}+4\psi_{i+1,s}-\psi_{i+2,s})\\ \psi_{ic}(\psi_{i+1,c}-\psi_{i-1,c})-\psi_{is}(\psi_{i+1,s}-\psi_{i-1,s})\\ \psi_{ic}(3\psi_{ic}-4\psi_{i-1,c}+\psi_{i-2,c})-\psi_{is}(3\psi_{is}-4\psi_{i-1,s}+\psi_{i-2,s})\end{cases}\\
&\frac{(\bar{A}_i)_{66}\pi}{4\lambda b}\begin{cases}w_{is}(-3\psi_{ic}+4\psi_{i+1,c}-\psi_{i+2,c})+w_{ic}(-3\psi_{is}+4\psi_{i+1,s}-\psi_{i+2,s})\\ w_{is}(\psi_{i+1,c}-\psi_{i-1,c})+w_{ic}(\psi_{i+1,s}-\psi_{i-1,s})\\ w_{is}(3\psi_{ic}-4\psi_{i-1,c}+\psi_{i-2,c})+w_{ic}(3\psi_{is}-4\psi_{i-1,s}+\psi_{i-2,s})\end{cases}\\
&\frac{(\bar{A}_i)_{66}\pi}{4\lambda b}\begin{cases}\psi_{is}(-3w_{ic}+4w_{i+1,c}-w_{i+2,c})+\psi_{ic}(-3w_{is}+4w_{i+1,s}-w_{i+2,s})\\ \psi_{is}(w_{i+1,c}-w_{i-1,c})+\psi_{ic}(w_{i+1,s}-w_{i-1,s})\\ \psi_{is}(3w_{ic}-4w_{i-1,c}+w_{i-2,c})+\psi_{ic}(3w_{is}-4w_{i-1,s}+w_{i-2,s})\end{cases}\\
&+\frac{(\bar{A}_i)_{66}\omega_i}{b^2}\begin{cases}-3v_{iS}+4v_{i+1,S}-v_{i+2,S}\\ v_{i+1,S}-v_{i-1,S}\\ 3v_{iS}-4v_{i-1,S}+v_{i-2,S}\end{cases}+\frac{(\bar{A}_i)_{26}}{b^2}\begin{cases}2v_{iC}-5v_{i+1,C}+4v_{i+2,C}-v_{i+3,C}\\ v_{i+1,C}-2v_{iC}+v_{i-1,C}\\ 2v_{iC}-5v_{i-1,C}+4v_{i-2,C}-v_{i-3,C}\end{cases}\\
&+\frac{(\bar{A}_i)_{16}\omega_i}{b^2}\begin{cases}-3u_{iS}+4u_{i+1,S}-u_{i+2,S}\\ u_{i+1,S}-u_{i-1,S}\\ 3u_{iS}-4u_{i-1,S}+u_{i-2,S}\end{cases}+\frac{(\bar{A}_i)_{66}}{b^2}\begin{cases}2u_{iC}-5u_{i+1,C}+4u_{i+2,C}-u_{i+3,C}\\ u_{i+1,C}-2u_{iC}+u_{i-1,C}\\ 2u_{iC}-5u_{i-1,C}+4u_{i-2,C}-u_{i-3,C}\end{cases}\\
&-(A_i)_{11}\frac{4\omega_i\pi}{\lambda b}u_{iC}-(\bar{A}_i)_{16}\frac{4\omega_i\pi}{\lambda b}v_{iC}+(\bar{A}_i)_{16}\frac{\pi^2}{2\lambda^2}(w_{is}\psi_{is}-w_{ic}\psi_{ic})\\
&-(A_i)_{11}\frac{\pi^3}{\lambda^3}w_{ic}w_{is}-(\bar{A}_i)_{12}\frac{\pi}{\lambda}\psi_{ic}\psi_{is}+(\bar{A}_i)_{16}\frac{\pi^2}{\lambda^2}(w_{is}\psi_{is}-w_{ic}\psi_{ic})\\
&+\frac{(\bar{A}_i)_{16}\pi}{\lambda b}\begin{cases}-3u_{iS}+4u_{i+1,S}-u_{i+2,S}\\ u_{i+1,S}-u_{i-1,S}\\ 3u_{iS}-4u_{i-1,S}+u_{i-2,S}\end{cases}+\frac{(\bar{A}_i)_{12}\pi}{\lambda b}\begin{cases}-3v_{iS}+4v_{i+1,S}-v_{i+2,S}\\ v_{i+1,S}-v_{i-1,S}\\ 3v_{iS}-4v_{i-1,S}+v_{i-2,S}\end{cases}=0
\end{aligned}
\tag{5.31}
$$

$$
\begin{aligned}
&-\frac{(\bar{A}_i)_{66}\omega_i}{b^2}\begin{cases} -3v_{iC}+4v_{i+1,C}-v_{i+2,C} \\ v_{i+1,C}-v_{i-1,C} \\ 3v_{iC}-4v_{i-1,C}+v_{i-2,C}\end{cases}+\frac{(\bar{A}_i)_{26}}{b^2}\begin{cases} 2v_{iS}-5v_{i+1,S}+4v_{i+2,S}-v_{i+3,S} \\ v_{i+1,S}-2v_{iS}+v_{i-1,S} \\ 2v_{iS}-5v_{i-1,S}+4v_{i-2,S}-v_{i-3,S}\end{cases} \\
&-\frac{(\bar{A}_i)_{16}\pi}{\lambda b}\begin{cases} -3u_{iC}+4u_{i+1,C}-u_{i+2,C} \\ u_{i+1,C}-u_{i-1,C} \\ 3u_{iC}-4u_{i-1,C}+u_{i-2,C}\end{cases}+\frac{(\bar{A}_i)_{66}}{b^2}\begin{cases} 2u_{iS}-5u_{i+1,S}+4u_{i+2,S}-u_{i+3,S} \\ u_{i+1,S}-2u_{iS}+u_{i-1,S} \\ 2u_{iS}-5u_{i-1,S}+4u_{i-2,S}-u_{i-3,S}\end{cases} \\
&-(\bar{A}_i)_{16}\frac{\pi^2}{2\lambda^2}(w_{is}\psi_{ic}+w_{ic}\psi_{is})+(\bar{A}_i)_{66}\frac{\pi}{2\lambda}(\psi_{is}^2-\psi_{ic}^2)-(\bar{A}_i)_{16}\frac{\pi^2}{\lambda^2}(w_{is}\psi_{ic}+w_{ic}\psi_{is}) \\
&\frac{(\bar{A}_i)_{26}}{4b}\begin{cases} \psi_{is}(-3\psi_{ic}+4\psi_{i+1,c}-\psi_{i+2,c})+\psi_{is}(-3\psi_{is}+4\psi_{i+1,s}-\psi_{i+2,s}) \\ \psi_{is}(\psi_{i+1,c}-\psi_{i-1,c})+\psi_{is}(\psi_{i+1,s}-\psi_{i-1,s}) \\ \psi_{is}(3\psi_{ic}-4\psi_{i-1,c}+\psi_{i-2,c})+\psi_{is}(3\psi_{is}-4\psi_{i-1,s}+\psi_{i-2,s})\end{cases} \\
&\frac{(\bar{A}_i)_{66}\pi}{4\lambda b}\begin{cases} w_{is}(-3\psi_{is}+4\psi_{i+1,s}-\psi_{i+2,s})-w_{ic}(-3\psi_{ic}+4\psi_{i+1,c}-\psi_{i+2,c}) \\ w_{is}(\psi_{i+1,s}-\psi_{i-1,s})-w_{ic}(\psi_{i+1,c}-\psi_{i-1,c}) \\ w_{is}(3\psi_{is}-4\psi_{i-1,s}+\psi_{i-2,s})-w_{ic}(3\psi_{ic}-4\psi_{i-1,c}+\psi_{i-2,c})\end{cases} \\
&-(\bar{A}_i)_{11}\frac{4\omega_i\pi}{\lambda b}u_{iS}-(\bar{A}_i)_{16}\frac{4\omega_i\pi}{\lambda b}v_{iS}-(\bar{A}_i)_{11}\frac{\pi^3}{2\lambda^3}(w_{is}^2-w_{ic}^2)-(\bar{A}_i)_{12}\frac{\pi}{2\lambda}(\psi_{ic}^2-\psi_{is}^2) \\
&-\frac{(\bar{A}_i)_{12}\pi}{\lambda b}\begin{cases} -3v_{iC}+4v_{i+1,C}-v_{i+2,C} \\ v_{i+1,C}-v_{i-1,C} \\ 3v_{iC}-4v_{i-1,C}+v_{i-2,C}\end{cases}-\frac{(\bar{A}_i)_{16}\omega_i}{b^2}\begin{cases} -3u_{iC}+4u_{i+1,C}-u_{i+2,C} \\ u_{i+1,C}-u_{i-1,C} \\ 3u_{iC}-4u_{i-1,C}+u_{i-2,C}\end{cases}=0
\end{aligned}
\tag{5.32}
$$

To solve the in-plane displacements $\mathbf{u_i}$, ten equilibrium equations for each node are assembled into the global equilibrium equations which can be written in matrix form as

$$\mathbf{Hu} = \mathbf{G}(\mathbf{w}) \tag{5.33}$$

where $\mathbf{u}$ includes the unknown in-plane displacements $\mathbf{u_i}$ for all the nodes of the structure, $\mathbf{H}$ is a square matrix with constant coefficients and $\mathbf{G}(\mathbf{w})$ is a non-linear function of the out-of-plane displacements $\mathbf{w}$ which are known from the VICONOPT analysis. Equation (5.33) can be therefore solved to give the in-plane displacements as

$$\mathbf{u} = \mathbf{H^{-1}G}(\mathbf{w}) \tag{5.34}$$

from which the components of stress resultants N_{xij}, N_{yij} and N_{xyij} can be obtained and then the uniform effective stress resultants can then be calculated.

5.7 Calculation of effective uniform stress resultants

For the next iteration of VICONOPT, equivalent uniform stress resultants are needed. In buckling analyses, the work done by the applied loading at node i is calculated by

$$V = V_{xi} + V_{yi} + V_{xyi} \tag{5.35}$$

where

$$V_{xi} = b_i \int_0^\lambda N_{xi}\varepsilon_{xi}dx \tag{5.36}$$

$$V_{yi} = b_i \int_0^\lambda N_{yi}\varepsilon_{yi}dx \tag{5.37}$$

$$V_{xyi} = b_i \int_0^\lambda N_{xyi}\varepsilon_{xyi}dx \tag{5.38}$$

Writing the general expressions for the stress resultants as

$$N_{xi} = N_{xi0} + N_{xic}\cos\frac{\pi x}{\lambda} + N_{xis}\sin\frac{\pi x}{\lambda} + N_{xiC}\cos\frac{2\pi x}{\lambda} + N_{xiS}\sin\frac{2\pi x}{\lambda} \tag{5.39}$$

$$N_{yi} = N_{yi0} + N_{yic}\cos\frac{\pi x}{\lambda} + N_{yis}\sin\frac{\pi x}{\lambda} + N_{yiC}\cos\frac{2\pi x}{\lambda} + N_{yiS}\sin\frac{2\pi x}{\lambda} \tag{5.40}$$

$$N_{xyi} = N_{xyi0} + N_{xyic}\cos\frac{\pi x}{\lambda} + N_{xyis}\sin\frac{\pi x}{\lambda} + N_{xyiC}\cos\frac{2\pi x}{\lambda} + N_{xyiS}\sin\frac{2\pi x}{\lambda} \tag{5.41}$$

and substituting equations (5.8) and equations (5.39-5.41) into equations (5.36-5.38), the work done can be written as

$$V_{xi} = b_i(N_{xi0}\eta_{xi0} + N_{xic}\eta_{xic} + N_{xis}\eta_{xis} + N_{xiC}\eta_{xiC} + N_{xiS}\eta_{xiS}) \tag{5.42}$$

$$V_{yi} = b_i(N_{yi0}\eta_{yi0} + N_{yic}\eta_{yic} + N_{yis}\eta_{yis} + N_{yiC}\eta_{yiC} + N_{yiS}\eta_{yiS}) \tag{5.43}$$

$$V_{xyi} = b_i(N_{xyi0}\eta_{xyi0} + N_{xyic}\eta_{xyic} + N_{xyis}\eta_{xyis} + N_{xyiC}\eta_{xyiC} + N_{xyiS}\eta_{xyiS}) \tag{5.44}$$

where η_i are coefficients expressed in terms of known variables ε, $\mathbf{u_i}$ and $\mathbf{w_i}$

$$\eta_{xi0} = -\lambda\bar{\varepsilon}_x - 2u_{ic} + \frac{\pi^2}{4\lambda}\left(w_{ic}^2 + w_{is}^2\right)$$

$$\eta_{xic} = \frac{\pi}{2}u_{is} - \frac{8}{3}u_{iC} - \frac{2\pi}{3\lambda}w_{ic}w_{is}$$

$$\eta_{xis} = -\frac{2\lambda}{\pi}\bar{\varepsilon}_x - \frac{\pi}{2}u_{ic} - \frac{4}{3}u_{iS} + \frac{\pi}{3\lambda}\left(w_{is}^2 + w_{ic}^2\right)$$

$$\eta_{xiC} = \frac{2}{3}u_{ic} + \pi u_{iS} + \frac{\pi^2}{8\lambda}\left(w_{is}^2 - w_{ic}^2\right)$$

$$\eta_{xiS} = \frac{4}{3}u_{is} - \pi u_{iC} - \frac{\pi^2}{4\lambda}w_{is}w_{ic}$$

$$\eta_{yi0} = \lambda v'_{i0} + \frac{2\lambda}{\pi}v'_{is} + \frac{\lambda}{4}\left(\psi_{ic}^2 + \psi_{is}^2\right)$$

$$\eta_{yic} = \frac{\lambda}{2}v'_{i0} + \frac{4\lambda}{3\pi}v'_{iS} + \frac{2\lambda}{3\pi}\psi_{ic}\psi_{is}$$

$$\eta_{yis} = \frac{2\lambda}{\pi}v'_{i0} + \frac{\lambda}{2}v'_{is} - \frac{2\lambda}{3\pi}v'_{iC} + \frac{\lambda}{3\pi}\left(\psi_{ic}^2 + 2\psi_{is}^2\right)$$

$$\eta_{yiC} = -\frac{2\lambda}{3\pi}v'_{is} + \frac{\lambda}{2}v'_{iC} + \frac{\lambda}{8}\left(\psi_{ic}^2 - \psi_{is}^2\right)$$

$$\eta_{yiS} = \frac{4\lambda}{3\pi}v'_{ic} + \frac{\lambda}{2}v'_{iS} + \frac{\lambda}{4}\psi_{ic}\psi_{is}$$

$$\eta_{xyi0} = \lambda u'_{i0} + \frac{2\lambda}{\pi}u'_{is} - 2v_{ic} + \frac{\pi}{2}\left(w_{is}\psi_{ic} - w_{ic}\psi_{is}\right)$$

$$\eta_{xyic} = \frac{\lambda}{2}u'_{ic} + \frac{4\lambda}{3\pi}u'_{iS} + \frac{\pi}{2}v_{is} - \frac{8}{3}v_{iC} + \frac{2}{3}\left(w_{is}\psi_{is} - w_{ic}\psi_{ic}\right)$$

$$\eta_{xyis} = \frac{2\lambda}{\pi}u'_{i0} + \frac{\lambda}{2}u'_{is} - \frac{2\lambda}{3\pi}u'_{iC} - \frac{\pi}{2}v_{ic} - \frac{4}{3}v_{iS} - \frac{1}{3}\left(w_{is}\psi_{ic} + 7w_{ic}\psi_{is}\right)$$

$$\eta_{xyiC} = \frac{\lambda}{2}u'_{iC} + \frac{2}{3}v_{ic} + \frac{\pi}{4}v_{iS} + \pi\left(w_{ic}\psi_{is} + w_{is}\psi_{ic}\right) - \frac{2\lambda}{3\pi}u'_{is}$$

$$\eta_{xyiS} = \frac{4\lambda}{3\pi}u'_{ic} + \frac{\lambda}{2}u'_{iS} + \frac{4}{3}v_{is} - \pi v_{iC} + \frac{\pi}{4}\left(w_{is}\psi_{is} - w_{ic}\psi_{ic}\right) \tag{5.45}$$

Comparing with the corresponding expressions for uniform loading yields the following expressions for equivalent uniform stress resultants, which are used in the strip stiffness calculations.

$$N_{xi} = N_{xi0} + \frac{1}{\eta_{xi0}}\left(N_{xic}\eta_{xic} + N_{xis}\eta_{xis} + N_{xiC}\eta_{xiC} + N_{xiS}\eta_{xiS}\right) \tag{5.46}$$

$$N_{yi} = N_{yi0} + \frac{1}{\eta_{yi0}}\left(N_{yic}\eta_{yic} + N_{yis}\eta_{yis} + N_{yiC}\eta_{yiC} + N_{yiS}\eta_{yiS}\right) \tag{5.47}$$

$$N_{xyi} = N_{xyi0} + \frac{1}{\eta_{xyi0}}\left(N_{xyic}\eta_{xyic} + N_{xyis}\eta_{xyis} + N_{xyiC}\eta_{xyiC} + N_{xyiS}\eta_{xyiS}\right) \tag{5.48}$$

To calculate the effective uniform stress resultants, the components of stress resultants N_{xij}, N_{yij} and N_{xyij} are needed.

5.8 Calculation of components N_{xij}, N_{yij} and N_{xyij}

Using the stress-strain relationships for the force resultants for node i in equations (5.9-5.11)

$$N_{xi} = (A_i)_{11}\varepsilon_{xi} + (A_i)_{12}\varepsilon_{yi} + (A_i)_{16}\gamma_{xyi} + (B_i)_{11}\kappa_{xi} + (B_i)_{12}\kappa_{yi} + (B_i)_{16}\kappa_{xyi} \tag{5.49}$$

$$N_{yi} = (A_i)_{12}\varepsilon_{xi} + (A_i)_{22}\varepsilon_{yi} + (A_i)_{26}\gamma_{xyi} + (B_i)_{12}\kappa_{xi} + (B_i)_{22}\kappa_{yi} + (B_i)_{26}\kappa_{xyi} \tag{5.50}$$

$$N_{xyi} = (A_i)_{16}\varepsilon_{xi} + (A_i)_{26}\varepsilon_{yi} + (A_i)_{66}\gamma_{xyi} + (B_i)_{16}\kappa_{xi} + (B_i)_{26}\kappa_{yi} + (B_i)_{66}\kappa_{xyi} \quad (5.51)$$

Substituting equation (5.5) into the formulas above, the following expressions can be written

$$\begin{aligned} N_{xi} =& [(A_i)_{11}\varepsilon_{xi0} + (A_i)_{12}\varepsilon_{yi0} + (A_i)_{16}\gamma_{xyi0}] \\ &+ [(A_i)_{11}\varepsilon_{xic} + (A_i)_{12}\varepsilon_{yic} + (A_i)_{16}\gamma_{xyic} \\ &+ (B_i)_{11}\kappa_{xic} + (B_i)_{12}\kappa_{yic} + (B_i)_{16}\kappa_{xyic}] \cos\frac{\pi x}{\lambda} \\ &+ [(A_i)_{11}\varepsilon_{xis} + (A_i)_{12}\varepsilon_{yis} + (A_i)_{16}\gamma_{xyis} \\ &+ (B_i)_{11}\kappa_{xis} + (B_i)_{12}\kappa_{yis} + (B_i)_{16}\kappa_{xyis}] \sin\frac{\pi x}{\lambda} \\ &+ [(A_i)_{11}\varepsilon_{xiC} + (A_i)_{12}\varepsilon_{yiC} + (A_i)_{16}\gamma_{xyiC}] \cos\frac{2\pi x}{\lambda} \\ &+ [(A_i)_{11}\varepsilon_{xiS} + (A_i)_{12}\varepsilon_{yiS} + (A_i)_{16}\gamma_{xyiS}] \sin\frac{2\pi x}{\lambda} \end{aligned} \quad (5.52)$$

$$\begin{aligned} N_{yi} =& [(A_i)_{12}\varepsilon_{xi0} + (A_i)_{22}\varepsilon_{yi0} + (A_i)_{26}\gamma_{xyi0}] \\ &+ [(A_i)_{12}\varepsilon_{xic} + (A_i)_{22}\varepsilon_{yic} + (A_i)_{26}\gamma_{xyic} \\ &+ (B_i)_{12}\kappa_{xic} + (B_i)_{22}\kappa_{yic} + (B_i)_{26}\kappa_{xyic}] \cos\frac{\pi x}{\lambda} \\ &+ [(A_i)_{12}\varepsilon_{xis} + (A_i)_{22}\varepsilon_{yis} + (A_i)_{26}\gamma_{xyis} \\ &+ (B_i)_{12}\kappa_{xis} + (B_i)_{22}\kappa_{yis} + (B_i)_{26}\kappa_{xyis}] \sin\frac{\pi x}{\lambda} \\ &+ [(A_i)_{12}\varepsilon_{xiC} + (A_i)_{22}\varepsilon_{yiC} + (A_i)_{26}\gamma_{xyiC}] \cos\frac{2\pi x}{\lambda} \\ &+ [(A_i)_{12}\varepsilon_{xiS} + (A_i)_{22}\varepsilon_{yiS} + (A_i)_{26}\gamma_{xyiS}] \sin\frac{2\pi x}{\lambda} \end{aligned} \quad (5.53)$$

$$\begin{aligned}
N_{xi} =&[(A_i)_{16}\varepsilon_{xi0} + (A_i)_{26}\varepsilon_{yi0} + (A_i)_{66}\gamma_{xyi0}] \\
&+ [(A_i)_{16}\varepsilon_{xic} + (A_i)_{26}\varepsilon_{yic} + (A_i)_{66}\gamma_{xyic} \\
&+ (B_i)_{16}\kappa_{xic} + (B_i)_{26}\kappa_{yic} + (B_i)_{66}\kappa_{xyic}] \cos\frac{\pi x}{\lambda} \\
&+ [(A_i)_{16}\varepsilon_{xis} + (A_i)_{26}\varepsilon_{yis} + (A_i)_{66}\gamma_{xyis} \\
&+ (B_i)_{16}\kappa_{xis} + (B_i)_{26}\kappa_{yis} + (B_i)_{66}\kappa_{xyis}] \sin\frac{\pi x}{\lambda} \\
&+ [(A_i)_{16}\varepsilon_{xiC} + (A_i)_{26}\varepsilon_{yiC} + (A_i)_{66}\gamma_{xyiC}] \cos\frac{2\pi x}{\lambda} \\
&+ [(A_i)_{16}\varepsilon_{xiS} + (A_i)_{26}\varepsilon_{yiS} + (A_i)_{66}\gamma_{xyiS}] \sin\frac{2\pi x}{\lambda}
\end{aligned} \tag{5.54}$$

From which

$$N_{xi0} = (A_i)_{11}\varepsilon_{xi0} + (A_i)_{12}\varepsilon_{yi0} + (A_i)_{16}\gamma_{xyi0}$$

$$N_{xic} = (A_i)_{11}\varepsilon_{xic} + (A_i)_{12}\varepsilon_{yic} + (A_i)_{16}\gamma_{xyic} + (B_i)_{11}\kappa_{xic} + (B_i)_{12}\kappa_{yic} + (B_i)_{16}\kappa_{xyic}$$

$$N_{xis} = (A_i)_{11}\varepsilon_{xis} + (A_i)_{12}\varepsilon_{yis} + (A_i)_{16}\gamma_{xyis} + (B_i)_{11}\kappa_{xis} + (B_i)_{12}\kappa_{yis} + (B_i)_{16}\kappa_{xyis}$$

$$N_{xiC} = (A_i)_{11}\varepsilon_{xiC} + (A_i)_{12}\varepsilon_{yiC} + (A_i)_{16}\gamma_{xyiC}$$

$$N_{xiS} = (A_i)_{11}\varepsilon_{xiS} + (A_i)_{12}\varepsilon_{yiS} + (A_i)_{16}\gamma_{xyiS}$$

$$N_{yi0} = (A_i)_{12}\varepsilon_{xi0} + (A_i)_{22}\varepsilon_{yi0} + (A_i)_{26}\gamma_{xyi0}$$

$$N_{yic} = (A_i)_{12}\varepsilon_{xic} + (A_i)_{22}\varepsilon_{yic} + (A_i)_{26}\gamma_{xyic} + (B_i)_{12}\kappa_{xic} + (B_i)_{22}\kappa_{yic} + (B_i)_{26}\kappa_{xyic}$$

$$N_{yis} = (A_i)_{12}\varepsilon_{xis} + (A_i)_{22}\varepsilon_{yis} + (A_i)_{26}\gamma_{xyis} + (B_i)_{12}\kappa_{xis} + (B_i)_{22}\kappa_{yis} + (B_i)_{26}\kappa_{xyis}$$

$$N_{yiC} = (A_i)_{12}\varepsilon_{xiC} + (A_i)_{22}\varepsilon_{yiC} + (A_i)_{26}\gamma_{xyiC}$$

$$N_{yiS} = (A_i)_{12}\varepsilon_{xiS} + (A_i)_{22}\varepsilon_{yiS} + (A_i)_{26}\gamma_{xyiS}$$

$$N_{xyi0} = (A_i)_{16}\varepsilon_{xi0} + (A_i)_{26}\varepsilon_{yi0} + (A_i)_{66}\gamma_{xyi0}$$

$$N_{xyic} = (A_i)_{16}\varepsilon_{xic} + (A_i)_{26}\varepsilon_{yic} + (A_i)_{66}\gamma_{xyic} + (B_i)_{16}\kappa_{xic} + (B_i)_{26}\kappa_{yic} + (B_i)_{66}\kappa_{xyic}$$

$$N_{xyis} = (A_i)_{16}\varepsilon_{xis} + (A_i)_{26}\varepsilon_{yis} + (A_i)_{66}\gamma_{xyis} + (B_i)_{16}\kappa_{xis} + (B_i)_{26}\kappa_{yis} + (B_i)_{66}\kappa_{xyis}$$

$$N_{xyiC} = (A_i)_{16}\varepsilon_{xiC} + (A_i)_{26}\varepsilon_{yiC} + (A_i)_{66}\gamma_{xyiC}$$

$$N_{xyiS} = (A_i)_{16}\varepsilon_{xiS} + (A_i)_{26}\varepsilon_{yiS} + (A_i)_{66}\gamma_{xyiS} \tag{5.55}$$

5.9 Calculation of derivatives

The above calculations provide an explicit solution procedure for the effective uniform stresses for the next iteration in VICONOPT. However for Newton iterations in VICONOPT, the derivatives of stresses at each node with respect to all the components of out-of-plane displacement w at each node are also required.

In reference [137], Kennedy and Featherston describe the detailed process of Newton iterations in VICONOPT. The mode vector $\mathbf{D} = \{D_j; j = 1, ...n\}$ includes displacements and rotations both at the longitudinal plate edges and strip edges of each plate. $\mathbf{K} = \{K_{ij}; i, j = 1, ...n\}$ is the corresponding exact stiffness matrix, which is a transcendental function of the stress resultants in each strip. Suppose

$$\mathbf{D} = \mathbf{D}^* + \mathbf{d} \tag{5.56}$$

where $\mathbf{D}^*$ is a trial mode vector and $\mathbf{d} = \{d_j; j = 1, ...n\}$ is the adjustments of $\mathbf{D}^*$. The Newton iteration is therefore written as matrix form

$$\left(\mathbf{K}* + \sum_{j=1}^{n} \frac{\partial \mathbf{K}^*}{\partial D_j} d_j\right)(\mathbf{K}^* + \mathbf{d}) = 0 \tag{5.57}$$

where $\mathbf{K}^* = \mathbf{K}(\mathbf{D}^*)$. Neglecting higher order terms then write equation (5.57) as

$$\sum_{j=1}^{n} \left(K_{ij}^* + \sum_{k=1}^{n} \frac{\partial K_{ik}^*}{\partial D_j} D_k*\right) d_j = -\sum_{j=1}^{n} K_{ij}^* D_j^* \tag{5.58}$$

To solve the equation and obtain $\mathbf{d}$, the terms $\partial \mathbf{K}_{ik}^* / \partial \mathbf{D}_j$ are required to be calculated. Stiffness matrix $\mathbf{K}$ is in terms of stress resultants which are calculated by the above sections and the derivatives $\partial \mathbf{K}_{ik}^* / \partial \mathbf{D}_j$ are calculated in Appendix A. After $\mathbf{d}$ is obtained, equation (5.56) gives a new trial mode vector $\mathbf{D}$ which is used as $\mathbf{D}^*$ in the next iteration.

Chapter 6

Illustrative results and discussion for isotropic plates

This chapter introduces the framework of the program written based on the improved exact strip postbuckling analysis. The entire process by which the improved postbuckling analysis works with VICONOPT to enable the postbuckling analysis capacity is demonstrated. Illustrative results of isotropic plates with different load and edge conditions are then shown. The results are compared with old VICONOPT results to present the improvements, while are also compared with FE (ABAQUS) results for validation.

6.1 Introduction

The program based on the improved exact strip postbuckling analysis utilises out-of-plane displacements **w** from VICONOPT to calculate unknown in-plane displacements **u** and **v**. Then the strains ε and curvatures κ which depend on displacements **u** and **v** can then be obtained. Finally the uniform stress resultants and their derivatives with respect to each component of **w** can be calculated. For the next cycle in VICONOPT, the uniform stress resultants and their derivatives are used to obtain the new postbuckling mode shape which provides the out-of-

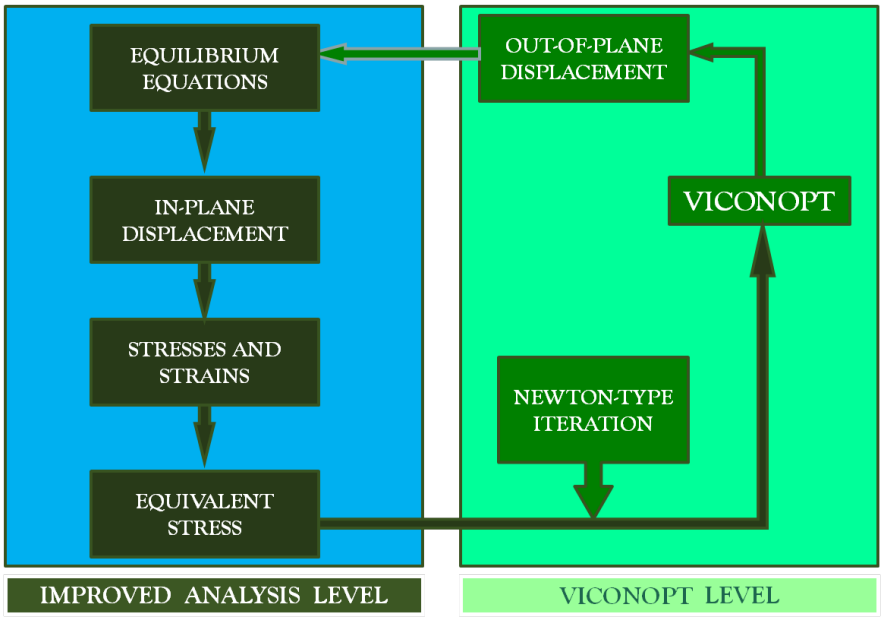

Figure 6.1: Improved postbuckling analysis before being implemented into VICONOPT

plane displacements for the new cycle. Therefore, improved postbuckling analysis finds the uniform stress resultants and their derivatives for each cycle only. It cannot automatically move on to the next cycle because the new postbuckling mode shape which is calculated by VICONOPT is necessary. Hence it is efficient and essential to implement the improved postbuckling analysis into VICONOPT so that it is able to work with VICONOPT as a whole program. Figures 6.1 and 6.2 show two flow charts which illustrate how the improved postbuckling analysis works before and after being implemented into VICONOPT. Implementation of the improved postbuckling analysis into VICONOPT enables achievement of more accurate postbuckling analysis in VICONOPT. To start a complete VICONOPT postbuckling analysis, the pre-processing stages including spatial modelling, assigning material properties and applying load must be completed in VICONOPT. Then VICONOPT provides the critical buckling load, critical longitudinal strain and mode shape after initial buckling analysis has done. The out-of-plane displacements are then utilised by the improved postbuckling analysis to calculate in-plane displacements, strains, curvatures, uniform stress resultants and their

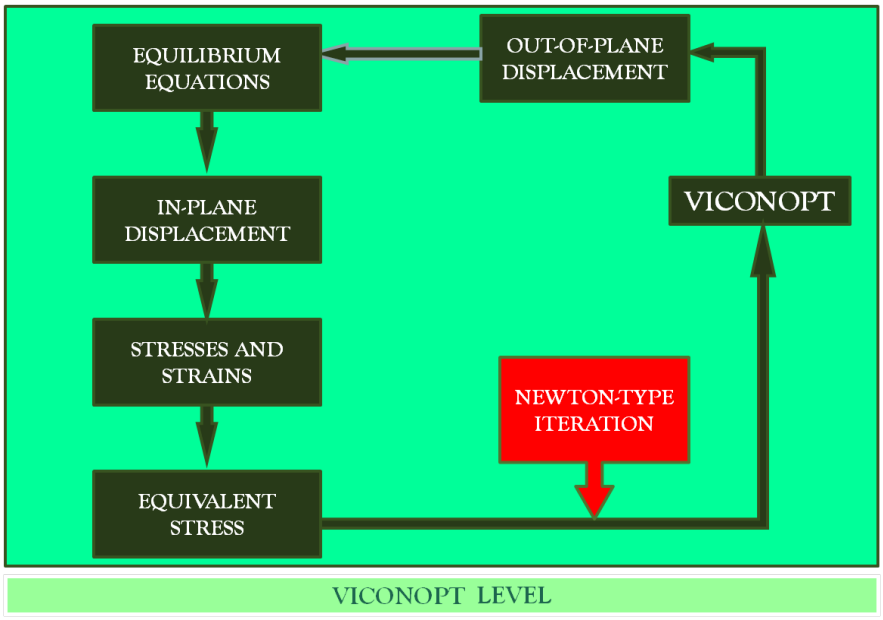

Figure 6.2: Improved postbuckling analysis after being implemented into VICONOPT

derivatives for each cycle. This process is achieved by an iterative procedure where the increment for each cycle is defined by the user and the above quantities are required to converge in each cycle. The post-processing stage for improved postbuckling analysis including creation of figures and contour plots shown in the following sections are completed in a spreadsheet. By using in-plane and out-of-plane displacement and stress resultants and their components, the spreadsheet is able to calculate the stresses and strains at a particular point on the plate and create the contour plot for stresses and strains in the postbuckling stage.

6.1.1 Isotropic square plate model

The model used in the postbuckling analysis is an isotropic square thin plate. The plate has length and width 0.3m, thickness 0.001m, Young's modulus is 110kNmm^{-2} and Poisson's ratio 0.3. Various edge conditions including a fixed edge condition, a free edge condition and a straight edge condition are applied on the top and bottom edges symmetrically. Symmetric uniform compression

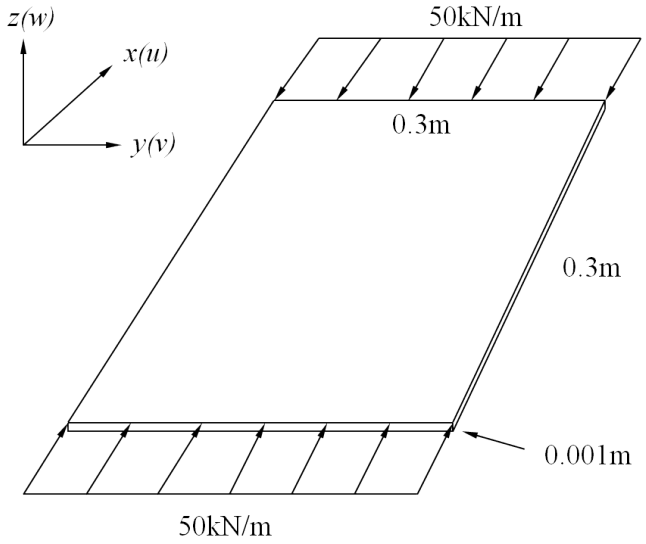

Figure 6.3: Dimension of the plate and axes

is applied on the left and right edges which are simply supported respectively and the amount of load is 50kN/m. The plate is divided into 10 strips of equal width for the VICONOPT analysis and improved postbuckling analysis, and it is divided into 900 elements (30×30) in the ABAQUS analysis. Figure 6.3 shows the dimensions and axes of the plate, and Figure 6.4 shows the load and edge assignments.

6.1.2 In-plane edge conditions

All edges are simply supported against out-of-plane displacement **w** in the model, while the uniform compressions are applied on the left and right edges as shown in Figure 6.4. Various in-plane edge conditions are applied on the unloaded top and bottom edges respectively. The edge conditions analysed in this study include the fixed edge condition, free edge condition and straight edge condition. The fixed edge condition requires the longitudinal top and bottom edges are fixed in-plane, i.e. in the solution of equation (5.33) all components of $\mathbf{u}_i$ are forced to zero at nodes $i = 1$ and $i = n$ which represent the top and bottom edges respectively. The free edge condition releases the constraints of v_i, i.e. all components on u_i

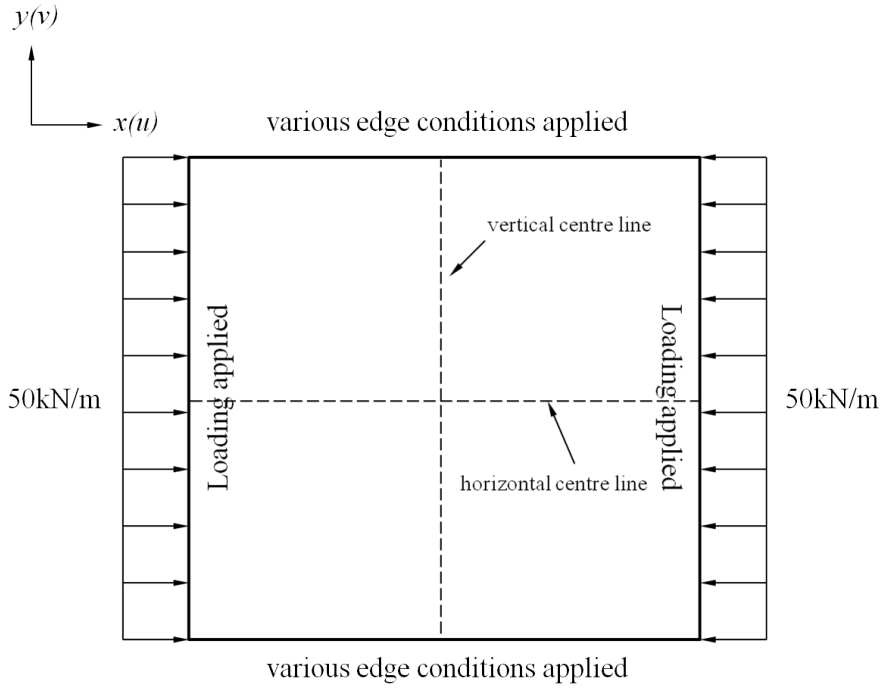

Figure 6.4: Loads and edge assignments

are required to be zero at nodes $i = 1$ and $i = n$. The straight edge condition requires the top and bottom edges are kept straight therefore whilst v_{i0} at node $i = 1$, $i = n$ could be non-zero, the remaining components of $\mathbf{u}_i$ are forced to zero at the top and bottom edges. However in the actual analysis using the improved postbuckling analysis, to avoid the rigid body movement one more constraint is applied for the free edge condition and the straight edge condition, which is, the component v_{i0} at the middle nodes of the plate are forced to zero.

6.2 Numerical study and contour plots of stress distributions

VICONOPT assumes longitudinal invariance of stress and a sinusoidal postbuckling mode which is believed to reduce the accuracy of stress and strain distributions in the postbuckling range. Therefore, one of the objectives of the improved postbuckling analysis is to improve the prediction of stress distributions in the postbuckling analysis. Illustrative results in this section show the numerical study and contour plots of longitudinal and transverse stress (N_x and N_y) distributions at different stages of the postbuckling analysis. The contour plots indicate the distribution of longitudinal stress N_x and transverse stress N_y, while the numerical study compares the stresses on both the horizontal and vertical centre lines of the plate (as shown in Figure 6.4) between the improved postbuckling analysis and ABAQUS analysis. The stresses are compared by plotting the stress distribution along the horizontal and vertical centre lines respectively. A correlation study has been carried out between the improved postbuckling analysis and ABAQUS analysis for three edge conditions, then the error evaluation and discussion has been given. To avoid excessive duplication of figures, the numerical study compares the stresses on the top surface of the plate only since the bottom surface shows similar curves and trends as the top surface but in the opposite direction.

Three stages (i.e. cycle 1, cycle 5 and cycle 10) are chosen to represent the entire postbuckling process. The comparison between improved postbuckling analysis and VICONOPT results shows the improvement and development of

this new analysis, then the comparison between the improved postbuckling analysis and ABAQUS results validates the accuracy of the analysis. The contour plots for the improved postbuckling analysis and old VICONOPT results are obtained by a set of spreadsheets. The mode shape for a particular cycle enables the corresponding stresses distributions to be plotted. The contour plots of stress distribution are shown for both top surface and bottom surface of plate respectively. Three different edge conditions including fixed edge condition, free edge condition and straight edge condition are also illustrated in this section. To provide an overall evaluation of the accuracy of the improved postbuckling analysis, figures of total longitudinal load against longitudinal strain are plotted and compared with those from ABAQUS analysis and old VICONOPT analysis for three different edge conditions before the onset of investigation for particular cycles. The dots on the curves denote the values for analysis cycle 1, 5 and 10 from right to left. Figure 6.5 shows a plot of the total longitudinal load against longitudinal strain and indicates that the improved postbuckling analysis shows close agreement with ABAQUS analysis while old VICONOPT results loses some accuracy.

6.2.1 Stress distributions in cycle 1

The stress distributions of cycle 1 which represents the very beginning of postbuckling behaviour are shown. When the longitudinal strain of cycle 1 in the improved postbuckling analysis (4.0274×10^{-5}) and ABAQUS (4.0266×10^{-5}) exceeded the critical buckling strain (4.0169×10^{-5}) by 0.26% and 0.24%, the out-of-plane displacement **w** and effective uniform stresses were saved and used as input to the procedure described in Chapter 5. In the contour plots, blue shading denotes increasing compression while red indicates decreasing compression (which usually results in regions of tension on the bottom surface). The units of stresses in all contour plots in this chapter are in N/m. The contour plots of N_x and N_y distributions across the top surface of the plate for fixed edge conditions are shown in Figures 6.6 and 6.7 for comparison. Figures 6.8 and 6.9 show the numerical comparison of stress N_x and N_y on both horizontal and vertical centre line of plate. The error evaluation has been given in the tables in Figures 6.8 and

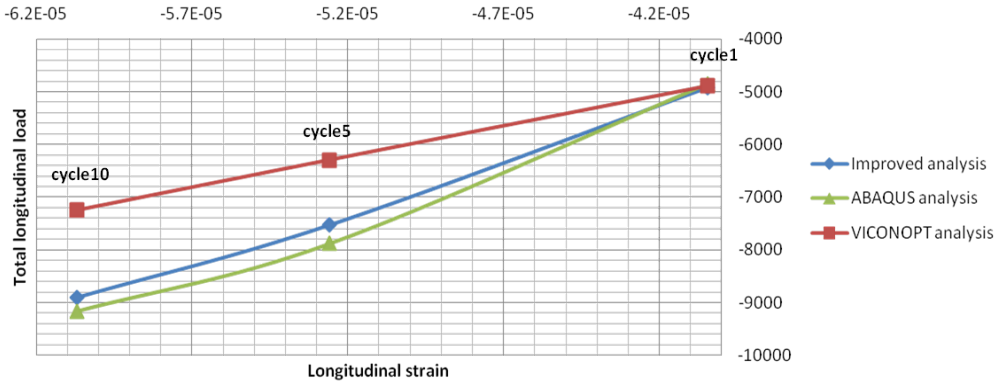

(a)

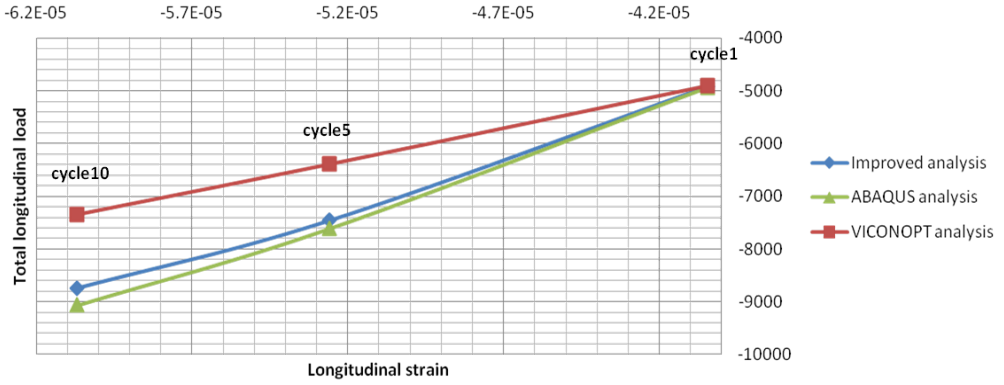

(b)

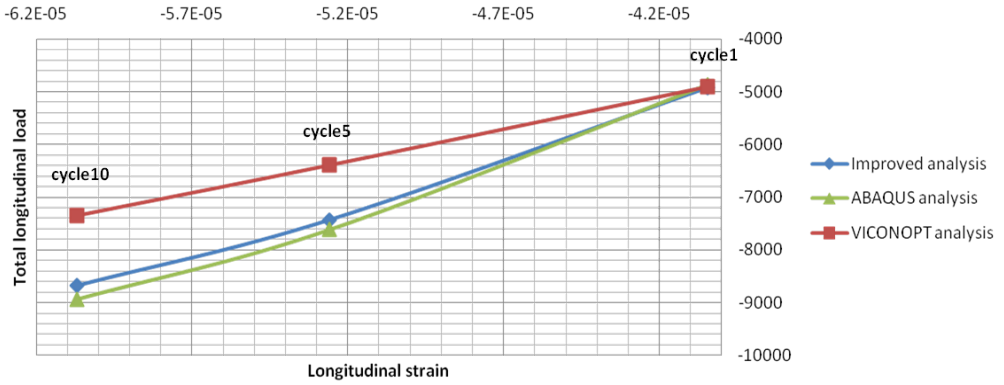

(c)

Figure 6.5: Total longitudinal load (N) against longitudinal strain for (a) fixed edge, (b) free edge and (c) straight edge.

6.9, where the mean error and root mean square (RMS) error have been calculated for comparison between improved postbuckling analysis, ABAQUS analysis and VICONOPT analysis. Figures 6.10 and 6.11 show contour plots of the N_x and N_y distributions across the bottom surface of the plate.

It is seen that the improved postbuckling analysis gives closer prediction of stresses N_x and N_y to the ABAQUS results than VICONOPT results does, which validates the improved postbuckling analysis. For the distribution of stress N_x and N_y in cycle 1, improved postbuckling analysis does show improvement over old VICONOPT although it is not apparent enough. It is believed that the improvement would become apparent in the following cycle 5 and cycle 10. Owing to the fixed edge condition applied on top and bottom edges, the stresses do not vary much on these two edges. In Figure 6.8, the mean error and RMS error of stress N_x across horizontal centre line and vertical centre line between improved postbuckling analysis and ABAQUS analysis are 1.39% and 1.55%, and 2.41% and 3.02% respectively, while for stress N_y the mean error and RMS error are 4.12% and 4.99%, and 3.52% and 4.33% respectively. Figure 6.8 also shows the mean error and RMS error of N_x and N_y between ABAQUS analysis and old VICONOPT analysis. The improved postbuckling analysis achieves good agreement with ABAQUS analysis in prediction of stresses distribution hence validates the accuracy of the analysis, while VICONOPT analysis also gives good comparison due to it is currently cycle 1 in this stage. However, the improved postbuckling analysis provides more accurate results in distribution of N_y than VICONOPT analysis which starts to lose accuracy in N_y.

Figures 6.12 to 6.17 show the prediction of stresses N_x and N_y distributions for free edge conditions. The mean error and RMS error of N_x across the horizontal centre line and vertical centre line are 0.50% and 0.56%, and 0.20% and 0.22% respectively which are small enough to validate the accuracy of the improved postbuckling analysis. While for the mean error and RMS error of N_y, the errors increase up to 4.25% and 5.11%, and 5.02% and 5.87%. The improved postbuckling analysis shows good agreement with the ABAQUS results for this edge condition. Owing to the free edge condition which releases the constraints on all components in $\mathbf{v}_i$, the stresses vary much more than those having fixed edge condition.

Figures 6.18 to 6.23 show the prediction of stresses N_x and N_y distributions for straight edge conditions. The mean error and RMS error for stress N_x across the horizontal centre line and vertical centre line are 1.88% and 2.38%, and 1.47% and 1.70% respectively, and for stress N_y are 4.96% and 5.41%, and 2.95% and 3.58% respectively. The improved postbuckling analysis shows good agreement with the ABAQUS results except for very small differences in the patterns near the four corners of plate. The differences are caused by the slight differences in the left and right edge conditions applied in improved postbuckling analysis and ABAQUS analysis. In improved postbuckling analysis, the left and right edges which are loaded by uniform compression are free to move. However, in ABAQUS analysis both edges are forced to keep straight.

The improved postbuckling analysis shows very good comparison on distribution of longitudinal stress N_x and transverse stress N_y. It has been validated by both contour plots of stress distributions and also a numerical study on particular nodes of the plate. Although improved postbuckling analysis gives good outcomes for cycle 1, the results in this section represent the very beginning of postbuckling analysis. Therefore, it is essential to investigate the stresses distribution far beyond the onset of postbuckling behaviour.

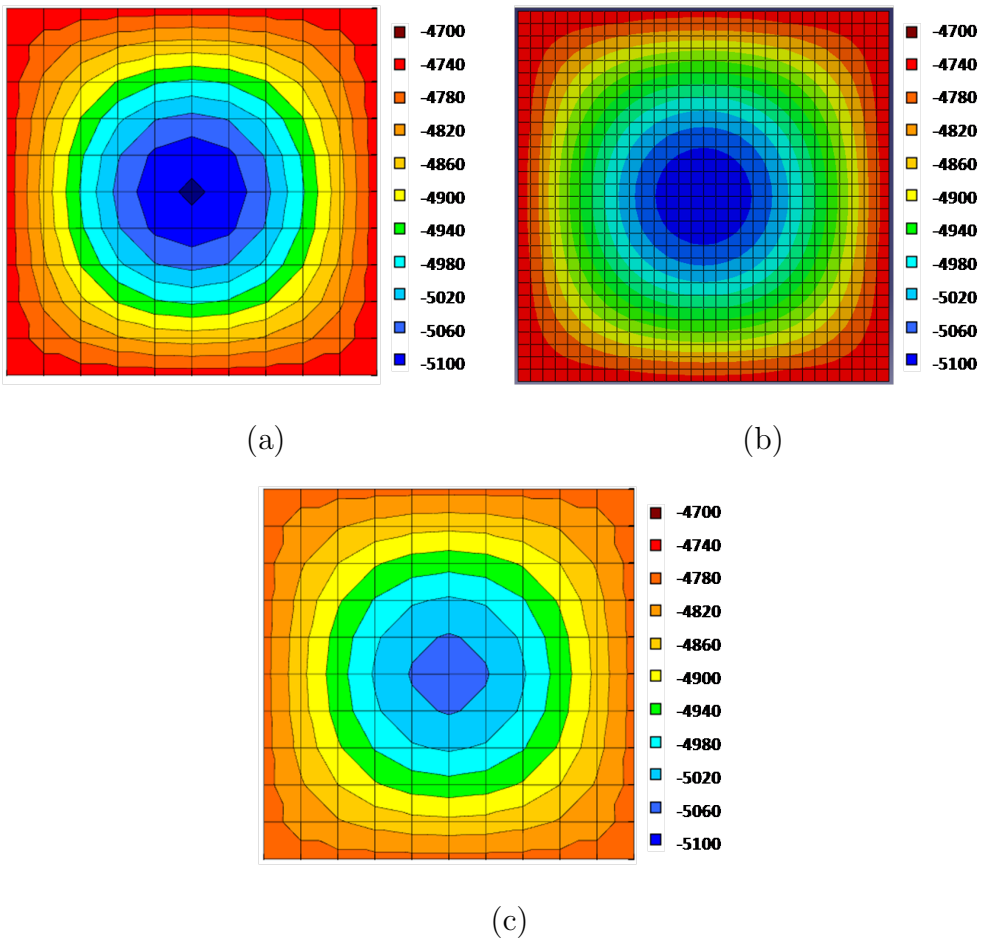

Figure 6.6: Variation of stress N_x across the top surface of plate for cycle 1 in (a) improved postbuckling analysis, (b) ABAQUS analysis and (c) old VICONOPT analysis, with all edges simply supported against out-of-plane deflection and the longitudinal edges fixed in-plane.

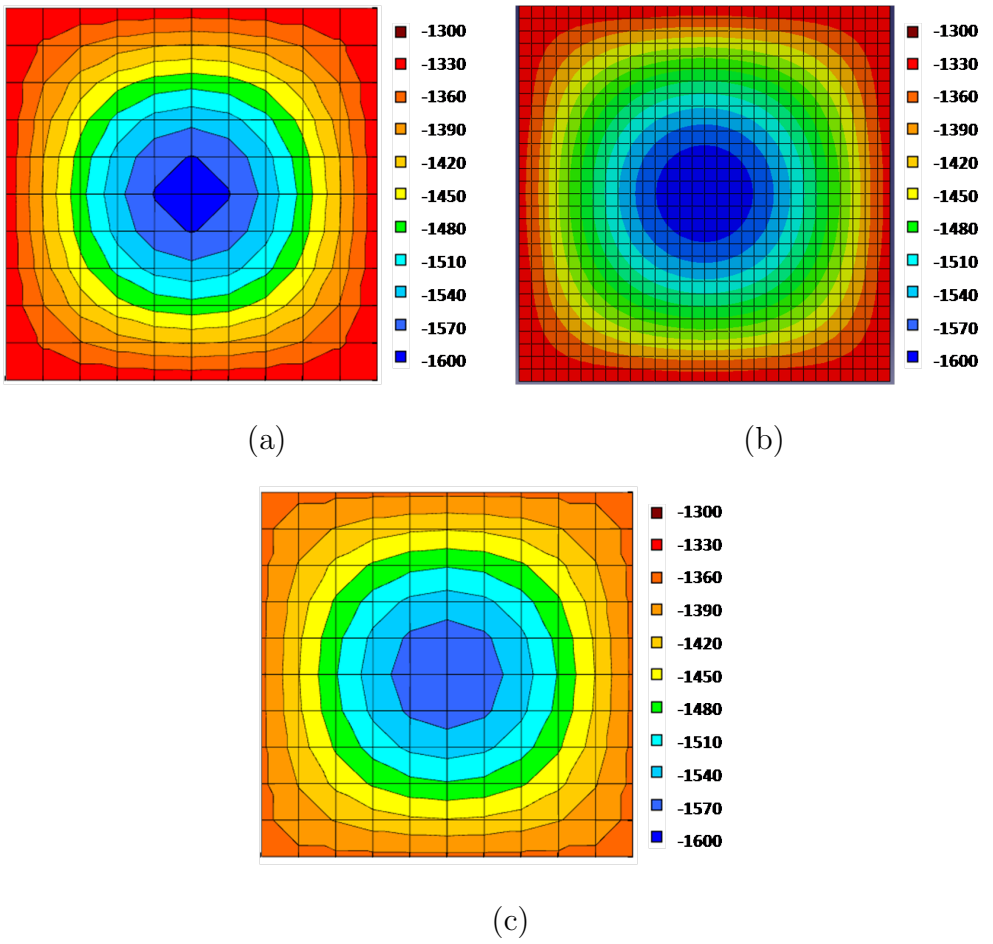

Figure 6.7: Variation of stress N_y across the top surface of plate for cycle 1 in (a) improved postbuckling analysis, (b) ABAQUS analysis and (c) old VICONOPT analysis, with all edges simply supported against out-of-plane deflection and the longitudinal edges fixed in-plane.

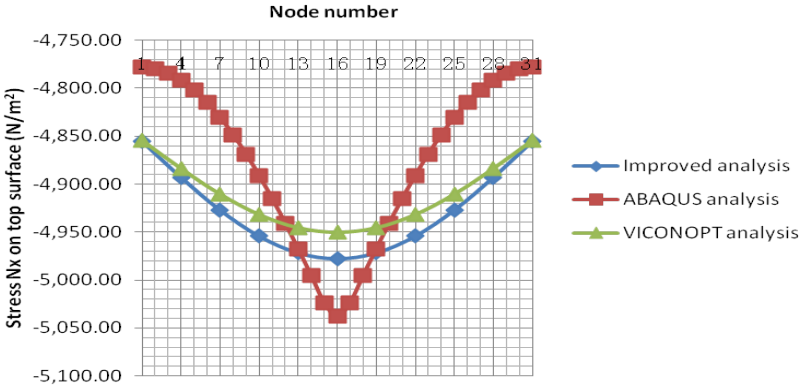

Node number	1	4	7	10	13	16	19	22	25	28	31		Mean	RMS % error
Improved analysis	-4855.11	-4892.81	-4926.92	-4954.05	-4971.51	-4977.53	-4971.51	-4954.05	-4926.91	-4892.80	-4855.11		-4925.30	
ABAQUS analysis	-4778.39	-4791.75	-4830.57	-4891.10	-4967.46	-5037.83	-4967.46	-4891.10	-4830.57	-4791.75	-4778.39		-4868.76	
VICONOPT analysis	-4854.89	-4884.07	-4910.58	-4931.75	-4945.41	-4950.12	-4945.41	-4931.75	-4910.58	-4884.07	-4854.89		-4909.41	
ABS(A-I)	76.72	101.06	96.35	62.95	4.05	60.30	4.05	62.95	96.34	101.05	76.72		67.50	
% error(A-I)	1.61	2.11	1.99	1.29	0.08	1.20	0.08	1.29	1.99	2.11	1.61		**1.39**	
(A-I)^2	5885.40	10212.21	9282.44	3963.15	16.39	3636.15	16.39	3963.08	9282.30	10212.03	5885.26		5668.62	**1.55**
ABS(A-V)	76.50	92.32	80.01	40.65	22.05	87.71	22.05	40.65	80.01	92.32	76.50		64.62	
% error(A-V)	1.60	1.93	1.66	0.83	0.44	1.74	0.44	0.83	1.66	1.93	1.60		**1.33**	
(A-V)^2	5852.85	8522.97	6401.99	1652.64	486.40	7692.91	486.41	1652.61	6401.89	8522.85	5852.75		4866.03	**1.43**

(a)

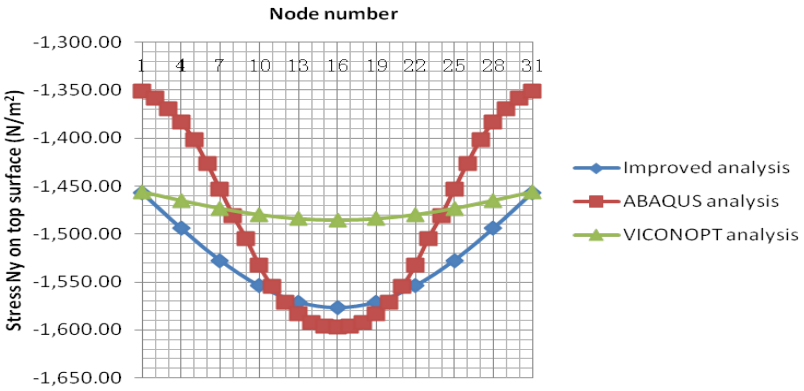

Node number	1	4	7	10	13	16	19	22	25	28	31		Mean	RMS % error
Improved analysis	-1456.52	-1493.81	-1527.42	-1554.06	-1571.16	-1577.05	-1571.16	-1554.06	-1527.42	-1493.81	-1456.52		-1525.73	
ABAQUS analysis	-1351.04	-1383.10	-1453.42	-1532.61	-1583.40	-1596.68	-1583.40	-1532.61	-1453.42	-1383.10	-1351.04		-1473.07	
VICONOPT analysis	-1456.47	-1465.22	-1473.17	-1479.53	-1483.62	-1485.04	-1483.62	-1479.53	-1473.17	-1465.22	-1456.47		-1472.82	
ABS(A-I)	105.48	110.71	74.00	21.45	12.24	19.63	12.24	21.45	74.00	110.71	105.48		60.67	
% error(A-I)	7.81	8.00	5.09	1.40	0.77	1.23	0.77	1.40	5.09	8.00	7.81		**4.12**	
(A-I)^2	11126.53	12256.80	5475.42	460.27	149.75	385.24	149.76	460.25	5475.32	12256.61	11126.35		5392.94	**4.99**
ABS(A-V)	105.43	82.12	19.75	53.08	99.78	111.64	99.78	53.08	19.75	82.12	105.43		75.63	
% error(A-V)	7.80	5.94	1.36	3.46	6.30	6.99	6.30	3.46	1.36	5.94	7.80		**5.13**	
(A-V)^2	11115.10	6743.86	390.25	2817.93	9955.72	12464.33	9955.73	2817.94	390.24	6743.82	11115.06		6773.64	**5.59**

(b)

Figure 6.8: Comparison of stress (a) N_x and (b) N_y across the horizontal centre line of top surface of plate for cycle 1 in improved postbuckling analysis, ABAQUS analysis and VICONOPT analysis, with longitudinal edges fixed in-plane.

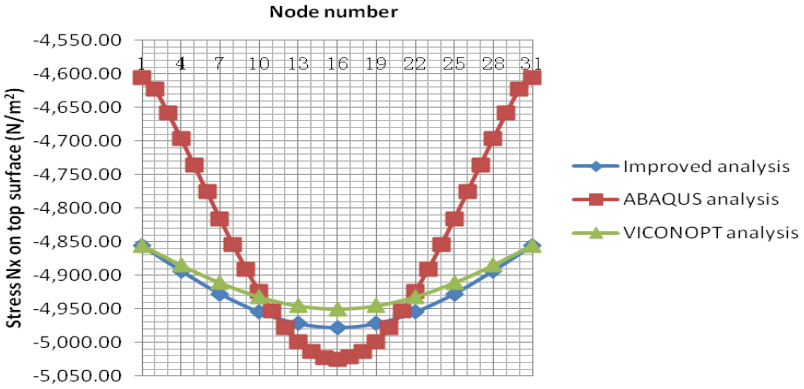

Node number	1	4	7	10	13	16	19	22	25	28	31		Mean	RMS % error
Improved analysis	-4856.14	-4893.66	-4927.56	-4954.40	-4971.60	-4977.53	-4971.60	-4954.40	-4927.56	-4893.66	-4856.14		-4925.84	
ABAQUS analysis	-4606.41	-4696.05	-4815.79	-4924.06	-4998.67	-5025.21	-4998.67	-4924.06	-4815.79	-4696.05	-4606.41		-4827.92	
VICONOPT analysis	-4856.15	-4885.36	-4911.51	-4932.19	-4945.45	-4950.12	-4945.45	-4932.19	-4911.51	-4885.36	-4856.15		-4910.13	
ABS(A-I)	249.73	197.61	111.77	30.34	27.07	47.68	27.07	30.34	111.77	197.61	249.73		116.43	
% error(A-I)	5.42	4.21	2.32	0.62	0.54	0.95	0.54	0.62	2.32	4.21	5.42		**2.41**	
(A-I)^2	62364.48	39050.05	12492.13	920.34	732.55	2273.43	732.55	920.34	12492.13	39050.05	62364.48		21217.50	**3.02**
ABS(A-V)	249.74	189.31	95.72	8.13	53.22	75.09	53.22	8.13	95.72	189.31	249.74		115.21	
% error(A-V)	5.42	4.03	1.99	0.17	1.06	1.49	1.06	0.17	1.99	4.03	5.42		**2.39**	
(A-V)^2	62369.32	35839.75	9162.75	66.02	2832.02	5638.39	2832.02	66.02	9162.75	35839.75	62369.32		20561.64	**2.97**

(a)

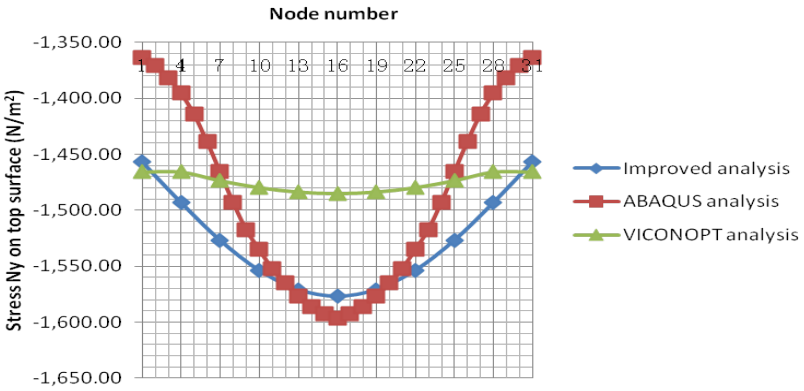

Node number	1	4	7	10	13	16	19	22	25	28	31		Mean	RMS % error
Improved analysis	-1456.81	-1493.34	-1527.06	-1553.87	-1571.11	-1577.05	-1571.11	-1553.87	-1527.06	-1493.34	-1456.81		-1525.59	
ABAQUS analysis	-1363.59	-1395.65	-1465.97	-1535.16	-1576.95	-1596.68	-1576.95	-1535.16	-1465.97	-1395.65	-1363.59		-1479.21	
VICONOPT analysis	-1465.61	-1465.61	-1473.45	-1479.66	-1483.64	-1485.04	-1483.64	-1479.66	-1473.45	-1465.61	-1465.61		-1474.63	
ABS(A-I)	93.22	97.70	61.09	18.72	5.84	19.63	5.84	18.72	61.09	97.70	93.22		52.07	
% error(A-I)	6.84	7.00	4.17	1.22	0.37	1.23	0.37	1.22	4.17	7.00	6.84		**3.52**	
(A-I)^2	8690.57	9544.42	3732.39	350.29	34.09	385.24	34.09	350.29	3732.39	9544.42	8690.57		4098.98	**4.33**
ABS(A-V)	102.02	69.96	7.48	55.50	93.31	111.64	93.31	55.50	7.48	69.96	102.02		69.84	
% error(A-V)	7.48	5.01	0.51	3.62	5.92	6.99	5.92	3.62	0.51	5.01	7.48		**4.72**	
(A-V)^2	10408.11	4894.42	56.02	3080.64	8707.32	12464.33	8707.32	3080.64	56.02	4894.42	10408.11		6068.85	**5.27**

(b)

Figure 6.9: Comparison of stress (a) N_x and (b) N_y across the vertical centre line of top surface of plate for cycle 1 in improved postbuckling analysis, ABAQUS analysis and VICONOPT analysis, with longitudinal edges fixed in-plane.

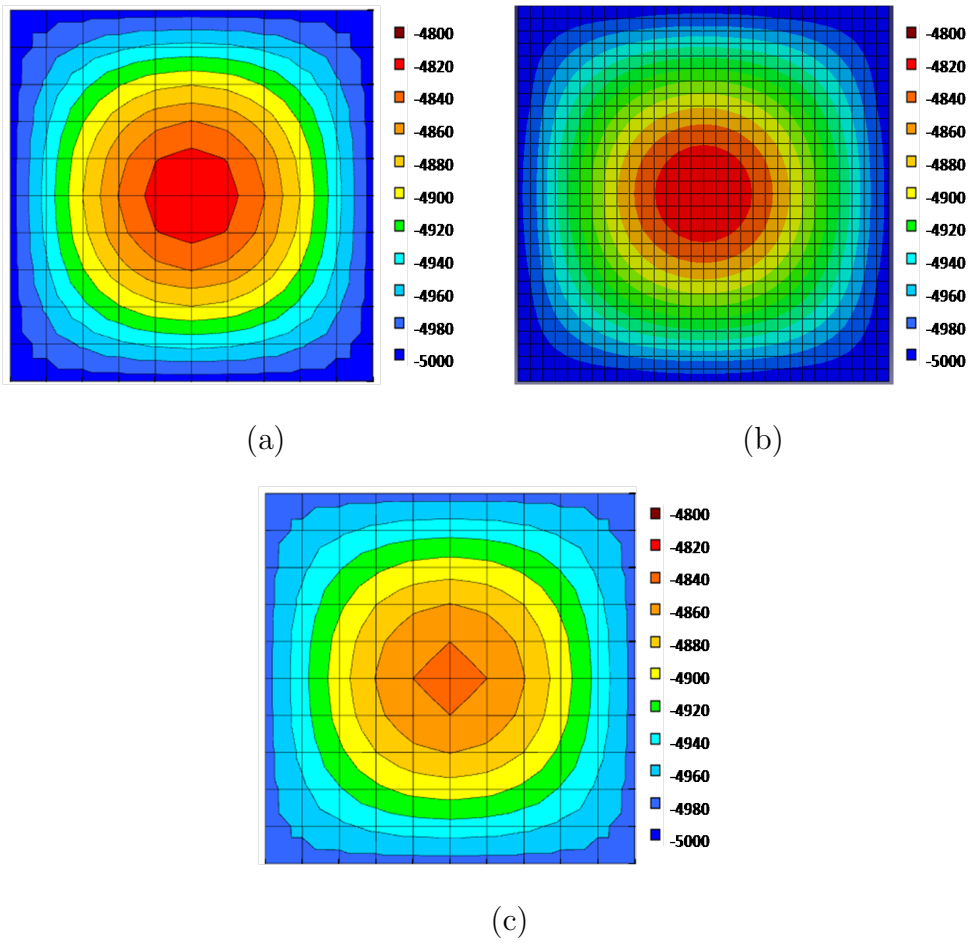

Figure 6.10: Variation of stress N_x across the bottom surface of plate for cycle 1 in (a) improved postbuckling analysis, (b) ABAQUS analysis and (c) old VICONOPT analysis, with all edges simply supported against out-of-plane deflection and the longitudinal edges fixed in-plane.

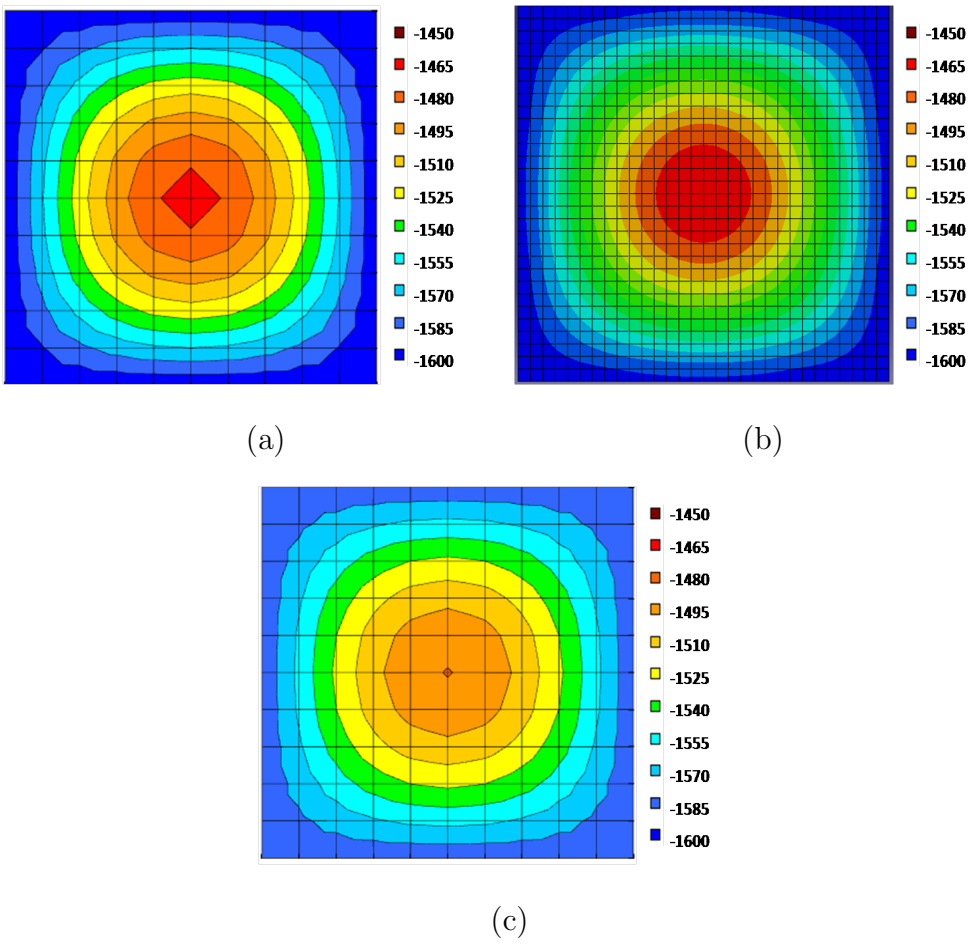

Figure 6.11: Variation of stress N_y across the bottom surface of plate for cycle 1 in (a) improved postbuckling analysis, (b) ABAQUS analysis and (c) old VICONOPT analysis, with all edges simply supported against out-of-plane deflection and the longitudinal edges fixed in-plane.

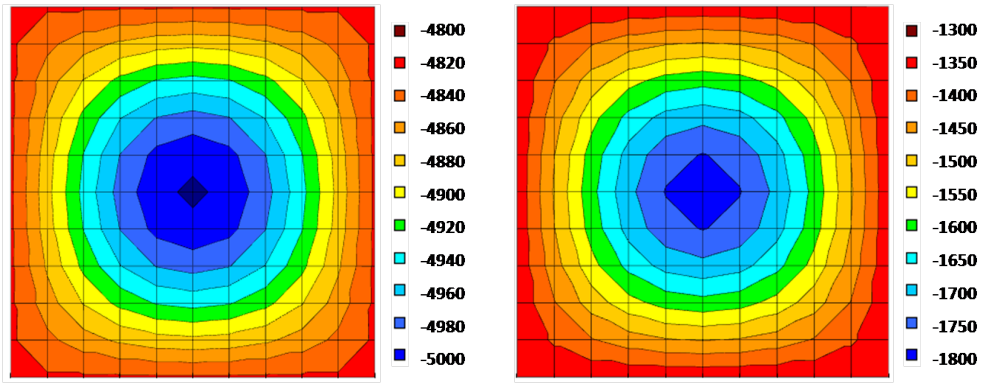

(a) (b)

Figure 6.12: Variation of stress (a) N_x and (b) N_y across the top surface of plate for cycle 1 in improved postbuckling analysis, with all edges simply supported against out-of-plane deflection and the longitudinal edges free in-plane.

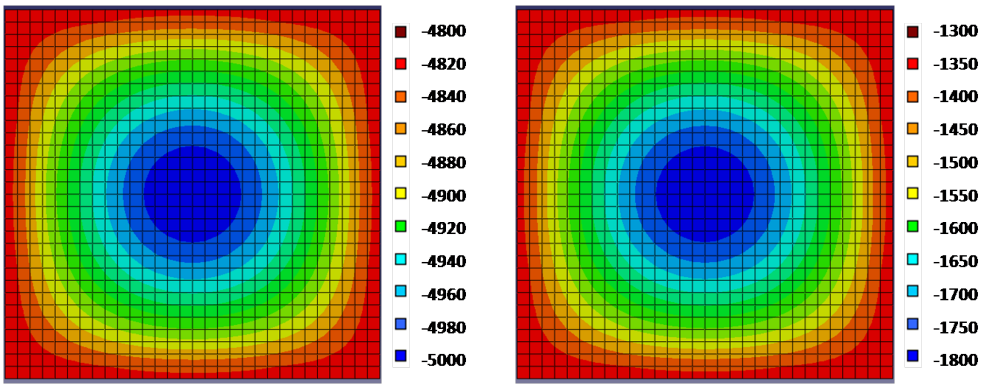

(a) (b)

Figure 6.13: Variation of stress (a) N_x and (b) N_y across the top surface of plate for cycle 1 in ABAQUS analysis, with all edges simply supported against out-of-plane deflection and the longitudinal edges free in-plane.

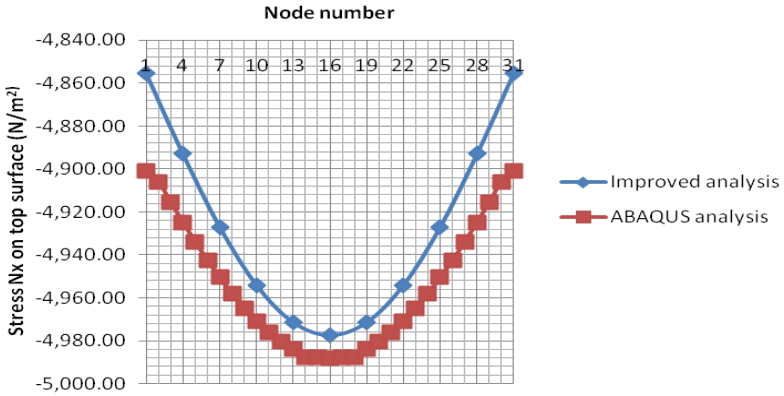

Node number	1	4	7	10	13	16	19	22	25	28	31		Mean	RMS % error
Improved analysis	-4855.22	-4892.90	-4926.94	-4954.00	-4971.40	-4977.39	-4971.40	-4954.00	-4926.94	-4892.90	-4855.22		-4925.30	
ABAQUS analysis	-4901.03	-4924.81	-4950.54	-4970.87	-4983.86	-4988.32	-4983.86	-4970.87	-4950.54	-4924.81	-4901.03		-4950.05	
ABS(A-I)	45.81	31.91	23.60	16.87	12.46	10.93	12.46	16.87	23.60	31.91	45.81		24.75	
% error	0.93	0.65	0.48	0.34	0.25	0.22	0.25	0.34	0.48	0.65	0.93		**0.50**	
(A-I)^2	2098.47	1018.50	556.81	284.47	155.34	119.40	155.35	284.49	556.84	1018.56	2098.55		7.59E+02	**0.56**

(a)

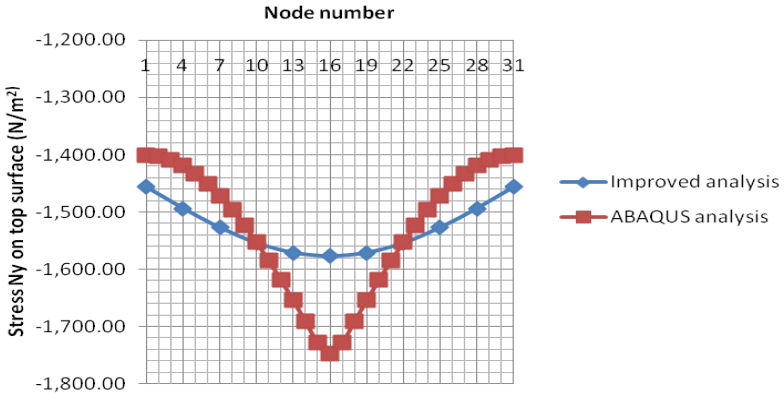

Node number	1	4	7	10	13	16	19	22	25	28	31		Mean	RMS % error
Improved analysis	-1456.52	-1493.80	-1527.39	-1554.02	-1571.10	-1576.98	-1571.09	-1554.01	-1527.39	-1493.80	-1456.52		-1525.69	
ABAQUS analysis	-1401.04	-1419.10	-1471.42	-1552.61	-1654.40	-1747.52	-1654.40	-1552.61	-1471.42	-1419.10	-1401.04		-1522.24	
ABS(A-I)	55.48	74.70	55.97	1.41	83.30	170.54	83.31	1.40	55.97	74.70	55.48		64.75	
% error	3.96	5.26	3.80	0.09	5.04	9.76	5.04	0.09	3.80	5.26	3.96		**4.25**	
(A-I)^2	3078.44	5580.75	3132.77	1.98	6939.71	29084.69	6939.76	1.97	3132.69	5580.63	3078.34		6.05E+03	**5.11**

(b)

Figure 6.14: Comparison of stress (a) N_x and (b) N_y across the horizontal centre line of top surface of plate for cycle 1 in improved postbuckling analysis and ABAQUS analysis, with longitudinal edges free in-plane.

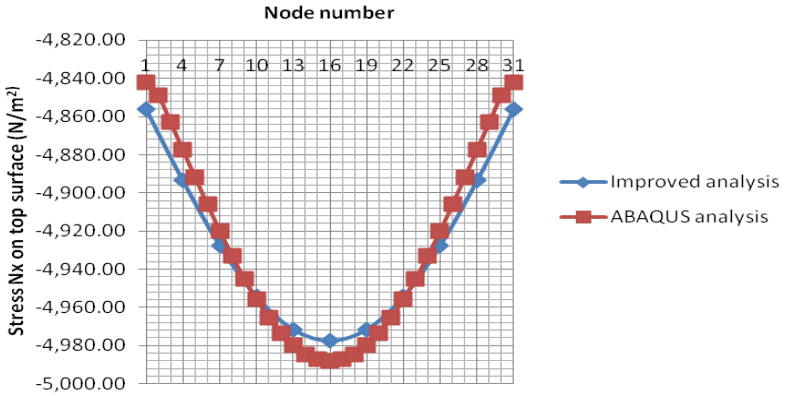

Node number	1	4	7	10	13	16	19	22	25	28	31		Mean	RMS % error
Improved analysis	-4856.10	-4893.59	-4927.47	-4954.29	-4971.48	-4977.39	-4971.48	-4954.29	-4927.47	-4893.59	-4856.10		-4925.75	
ABAQUS analysis	-4841.90	-4877.31	-4919.83	-4955.89	-4979.91	-4988.32	-4979.91	-4955.89	-4919.83	-4877.31	-4841.90		-4921.64	
ABS(A-I)	14.20	16.28	7.64	1.60	8.43	10.93	8.43	1.60	7.64	16.28	14.20		9.75	
% error	0.29	0.33	0.16	0.03	0.17	0.22	0.17	0.03	0.16	0.33	0.29		**0.20**	
(A-I)^2	201.60	265.01	58.44	2.56	71.12	119.40	71.12	2.56	58.44	265.01	201.60		1.20E+02	**0.22**

(a)

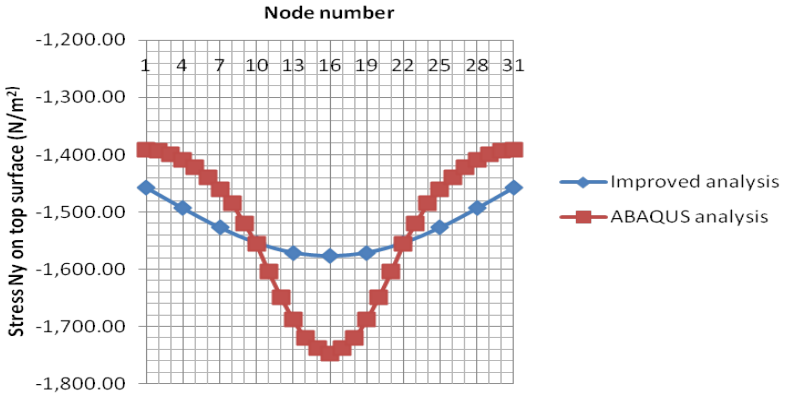

Node number	1	4	7	10	13	16	19	22	25	28	31		Mean	RMS % error
Improved analysis	-1456.68	-1493.23	-1526.97	-1553.79	-1571.03	-1576.98	-1571.03	-1553.79	-1526.97	-1493.23	-1456.68		-1525.49	
ABAQUS analysis	-1390.79	-1408.85	-1461.17	-1556.36	-1688.15	-1747.52	-1688.15	-1556.36	-1461.17	-1408.85	-1390.79		-1523.47	
ABS(A-I)	65.89	84.38	65.79	2.57	117.12	170.54	117.12	2.57	65.79	84.38	65.89		76.55	
% error	4.74	5.99	4.50	0.17	6.94	9.76	6.94	0.17	4.50	5.99	4.74		**5.02**	
(A-I)^2	4341.03	7119.94	4328.94	6.63	13717.26	29084.69	13717.26	6.63	4328.94	7119.94	4341.03		8.01E+03	**5.87**

(b)

Figure 6.15: Comparison of stress (a) N_x and (b) N_y across the vertical centre line of top surface of plate for cycle 1 in improved postbuckling analysis and ABAQUS analysis, with longitudinal edges free in-plane.

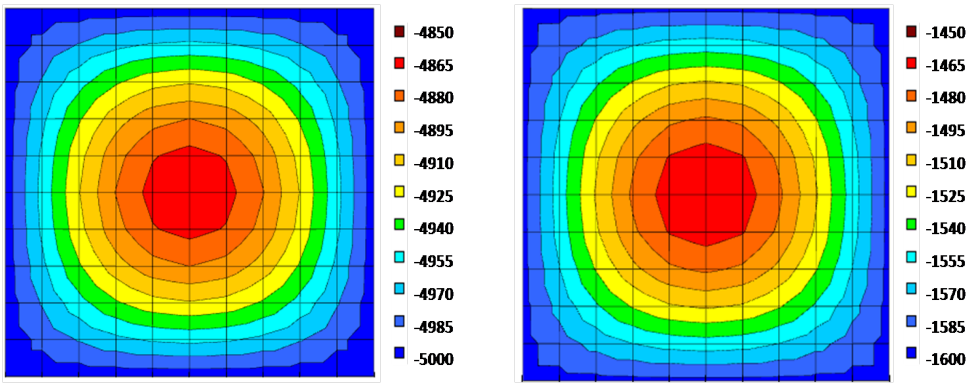

(a) (b)

Figure 6.16: Variation of stress (a) N_x and (b) N_y across the bottom surface of plate for cycle 1 in improved postbuckling analysis, with all edges simply supported against out-of-plane deflection and the longitudinal edges free in-plane.

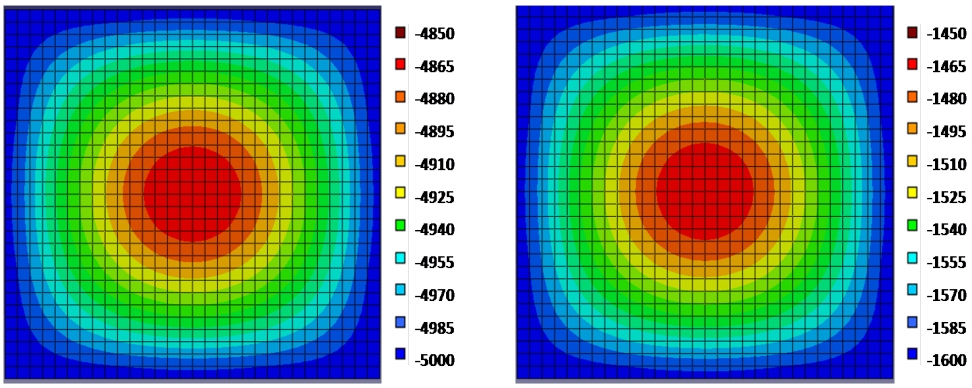

(a) (b)

Figure 6.17: Variation of stress (a) N_x and (b) N_y across the bottom surface of plate for cycle 1 in ABAQUS analysis, with all edges simply supported against out-of-plane deflection and the longitudinal edges free in-plane.

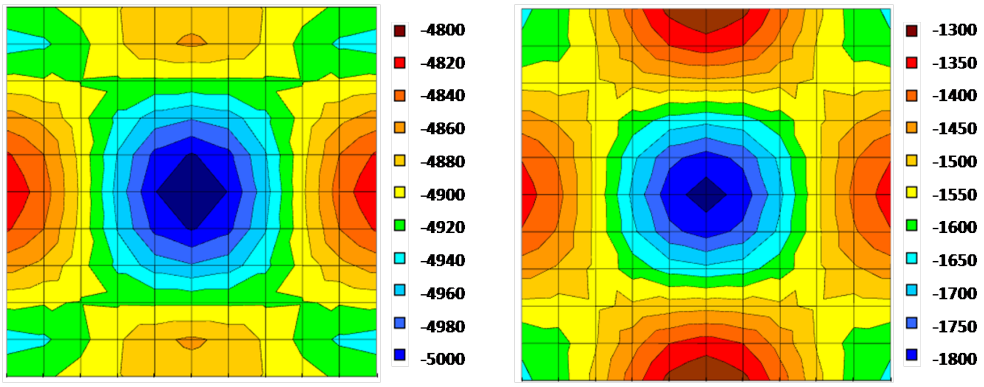

(a) (b)

Figure 6.18: Variation of stress (a) N_x and (b) N_y across the top surface of plate for cycle 1 in improved postbuckling analysis, with all edges simply supported against out-of-plane deflection and the longitudinal edges straight in-plane.

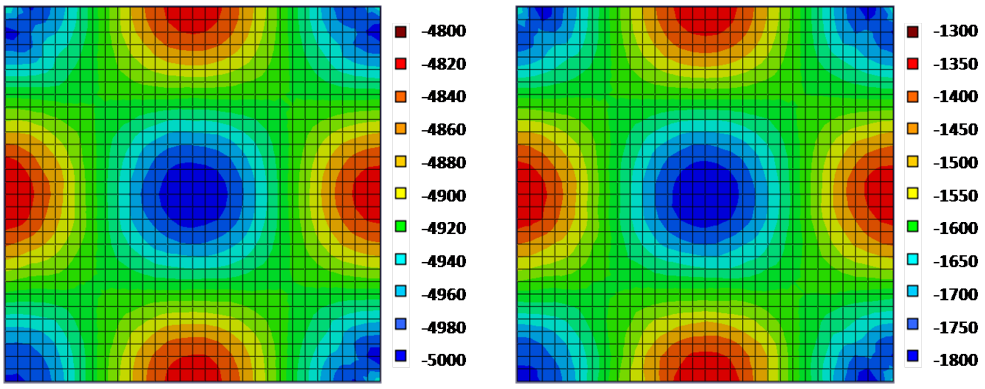

(a) (b)

Figure 6.19: Variation of stress (a) N_x and (b) N_y across the top surface of plate for cycle 1 in ABAQUS analysis, with all edges simply supported against out-of-plane deflection and the longitudinal edges straight in-plane.

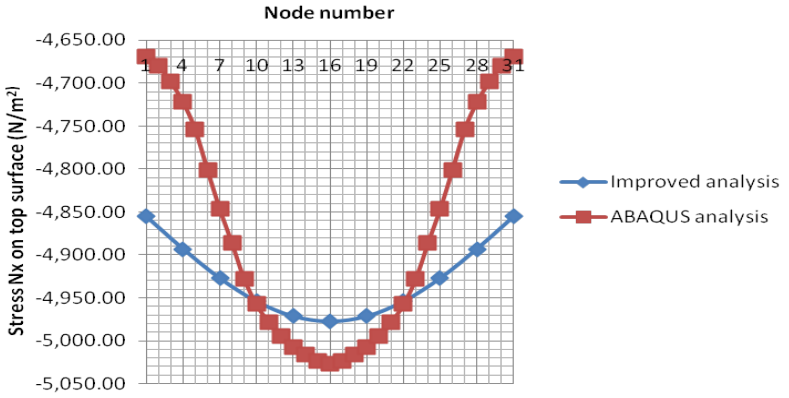

Node number	1	4	7	10	13	16	19	22	25	28	31	Mean	RMS % error
Improved analysis	-4.86E+03	-4.89E+03	-4.93E+03	-4.95E+03	-4.97E+03	-4.98E+03	-4.97E+03	-4.95E+03	-4.93E+03	-4.89E+03	-4.86E+03	-4925.33	
ABAQUS analysis	-4.67E+03	-4.72E+03	-4.85E+03	-4.96E+03	-5.01E+03	-5.03E+03	-5.01E+03	-4.96E+03	-4.85E+03	-4.72E+03	-4.67E+03	-4857.27	
ABS(A-I)	186.52	171.27	80.87	3.41	36.17	49.42	36.17	3.41	80.86	171.27	186.52	91.44	
% error	3.99	3.63	1.67	0.07	0.72	0.98	0.72	0.07	1.67	3.63	3.99	**1.88**	
(A-I)^2	3.48E+04	2.93E+04	6.54E+03	1.16E+01	1.31E+03	2.44E+03	1.31E+03	1.16E+01	6.54E+03	2.93E+04	3.48E+04	1.33E+04	**2.38**

(a)

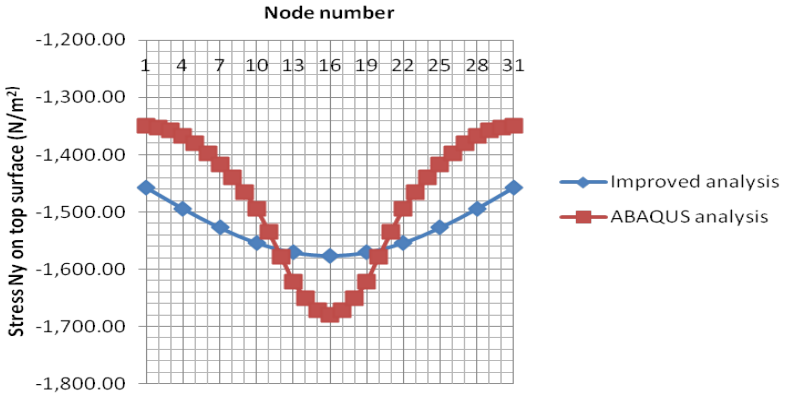

Node number	1	4	7	10	13	16	19	22	25	28	31	Mean	RMS % error
Improved analysis	-1.35E+03	-1.37E+03	-1.42E+03	-1.49E+03	-1.62E+03	-1.68E+03	-1.62E+03	-1.49E+03	-1.42E+03	-1.37E+03	-1.35E+03	-1470.98	
ABAQUS analysis	-1.44E+03	-1.46E+03	-1.51E+03	-1.60E+03	-1.66E+03	-1.68E+03	-1.66E+03	-1.60E+03	-1.51E+03	-1.46E+03	-1.44E+03	-1547.75	
ABS(A-I)	91.41	92.26	94.72	106.53	37.32	0.00	37.32	106.53	94.72	92.26	91.41	76.77	
% error	6.34	6.32	6.27	6.65	2.25	0.00	2.25	6.65	6.27	6.32	6.34	**4.96**	
(A-I)^2	8.36E+03	8.51E+03	8.97E+03	1.13E+04	1.39E+03	0.00E+00	1.39E+03	1.13E+04	8.97E+03	8.51E+03	8.36E+03	7.01E+03	**5.41**

(b)

Figure 6.20: Comparison of stress (a) N_x and (b) N_y across the horizontal centre line of top surface of plate for cycle 1 in improved postbuckling analysis and ABAQUS analysis, with longitudinal edges straight in-plane.

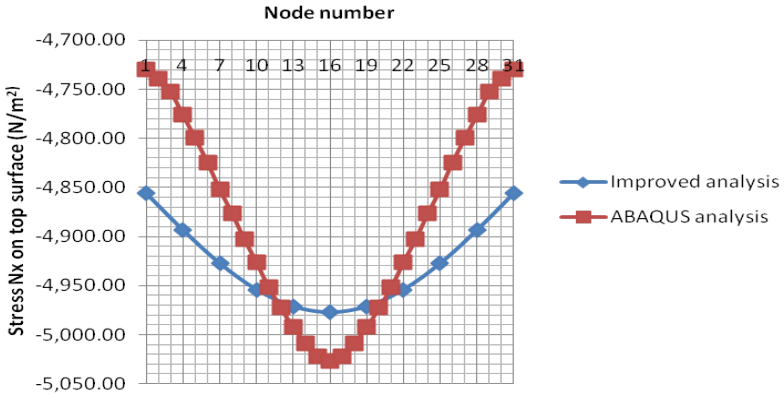

Node number	1	4	7	10	13	16	19	22	25	28	31	Mean	RMS % error
Improved analysis	-4.86E+03	-4.89E+03	-4.93E+03	-4.95E+03	-4.97E+03	-4.98E+03	-4.97E+03	-4.95E+03	-4.93E+03	-4.89E+03	-4.86E+03	-4925.68	
ABAQUS analysis	-4.73E+03	-4.78E+03	-4.85E+03	-4.93E+03	-4.99E+03	-5.03E+03	-4.99E+03	-4.93E+03	-4.85E+03	-4.78E+03	-4.73E+03	-4870.88	
ABS(A-I)	126.29	117.36	75.59	28.06	21.21	49.42	21.21	28.06	75.59	117.36	126.29	71.49	
% error	2.67	2.46	1.56	0.57	0.42	0.98	0.42	0.57	1.56	2.46	2.67	**1.47**	
(A-I)^2	1.60E+04	1.38E+04	5.71E+03	7.87E+02	4.50E+02	2.44E+03	4.50E+02	7.87E+02	5.71E+03	1.38E+04	1.60E+04	6.89E+03	**1.70**

(a)

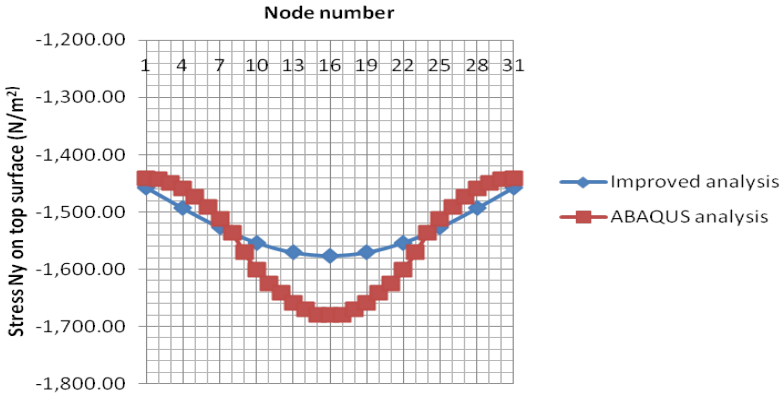

Node number	1	4	7	10	13	16	19	22	25	28	31	Mean	RMS % error
Improved analysis	-1.46E+03	-1.49E+03	-1.53E+03	-1.55E+03	-1.57E+03	-1.58E+03	-1.57E+03	-1.55E+03	-1.53E+03	-1.49E+03	-1.46E+03	-1525.56	
ABAQUS analysis	-1.44E+03	-1.46E+03	-1.51E+03	-1.60E+03	-1.66E+03	-1.68E+03	-1.66E+03	-1.60E+03	-1.51E+03	-1.46E+03	-1.44E+03	-1547.75	
ABS(A-I)	15.50	33.92	15.26	47.21	87.84	103.35	87.84	47.21	15.26	33.92	15.50	45.71	
% error	1.08	2.32	1.01	2.95	5.30	6.15	5.30	2.95	1.01	2.32	1.08	**2.95**	
(A-I)^2	2.40E+02	1.15E+03	2.33E+02	2.23E+03	7.72E+03	1.07E+04	7.72E+03	2.23E+03	2.33E+02	1.15E+03	2.40E+02	3.07E+03	**3.58**

(b)

Figure 6.21: Comparison of stress (a) N_x and (b) N_y across the vertical centre line of top surface of plate for cycle 1 in improved postbuckling analysis and ABAQUS analysis, with longitudinal edges straight in-plane.

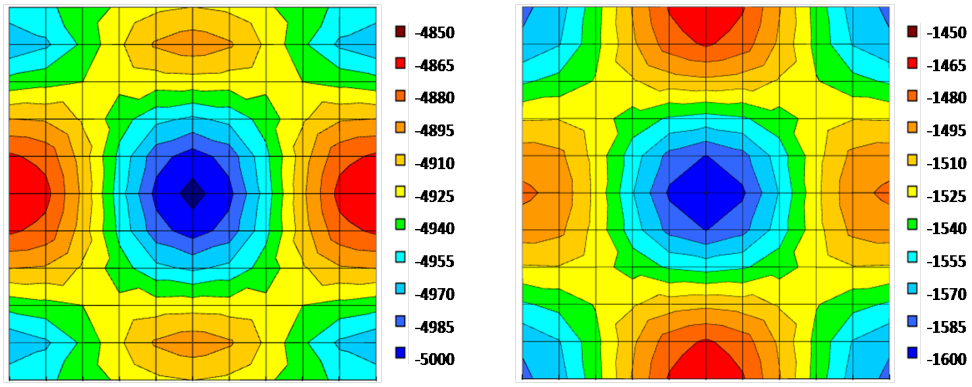

(a) (b)

Figure 6.22: Variation of stress (a) N_x and (b) N_y across the bottom surface of plate for cycle 1 in improved postbuckling analysis, with all edges simply supported against out-of-plane deflection and the longitudinal edges straight in-plane.

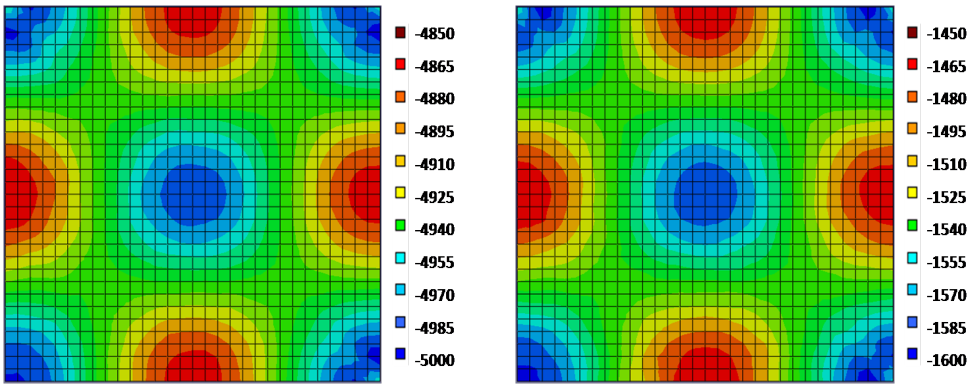

(a) (b)

Figure 6.23: Variation of stress (a) N_x and (b) N_y across the bottom surface of plate for cycle 1 in ABAQUS analysis, with all edges simply supported against out-of-plane deflection and the longitudinal edges straight in-plane.

6.2.2 Stress distributions in cycle 5

The stress distribution of cycle 5 has been selected to represent the state of the panel further into the postbuckling analysis. To find the stress distribution at a particular stage (e.g. cycle 5), the improved postbuckling analysis needs ideally work with VICONOPT continuously to find the new mode shape in cycle 5. However this will require full integration of the improved postbuckling analysis into the VICONOPT code by others (which is not finished yet) to find the new mode shape at each cycle, the old mode shape calculated by old VICONOPT will be used in the following sections instead for presentation of cycles 5 and 10. The new stress calculations in the improved postbuckling analysis will be used to calculate the stresses and corresponding contour plots using the spreadsheets. A comparison of stress distributions between the improved postbuckling analysis, ABAQUS analysis and the old VICONOPT analysis is made to show the improvement of the improved postbuckling analysis. Although the results of improved postbuckling analysis for cycle 5 do not provide a truly complete presentation of the new analysis, the difference between the old mode shape in VICONOPT and new mode shape in improved postbuckling analysis is small enough to give a good indication of the improvement to be made using the new method. Reference [131] shows that the maximum difference in mode shape between improved postbuckling analysis and old VICONOPT is 0.09779% for cycle 5 in postbuckling analysis. When the longitudinal strain of cycle 5 in the improved postbuckling analysis (4.6199×10^{-5}) and ABAQUS (4.6212×10^{-5}) exceeded the critical buckling strain (4.0169×10^{-5}) by 15.01% and 15.04%, the out-of-plane displacement **w** and effective uniform stresses were saved and used as input to the procedure described in Chapter 5. In the contour plots, blue shading denotes increasing compression while red indicates decreasing compression (which usually results in regions of tension on the bottom surface). The contour plots of N_x and N_y distributions for fixed edge conditions are shown in Figures 6.24 and 6.25 for comparison. Numerical comparison of both N_x and N_y are given in Figures 6.26 and 6.27 to show the differences between improved postbuckling analysis and ABAQUS analysis. Figure 6.28 and 6.29 show contour plots of the N_x and N_y distributions across the bottom surface of the plate.

The plots in Figures 6.24 to 6.29 are shown for the improved postbuckling analysis, ABAQUS analysis and old VICONOPT analysis for comparison. The value of stresses for both N_x and N_y across horizontal and vertical centre line of plate are also given. The improved postbuckling analysis shows good agreement with ABAQUS results, but the old VICONOPT results start to lose accuracy in the prediction of stress distribution especially in N_y. Owing to the assumption of longitudinal stress invariance in old VICONOPT results for simplification in postbuckling analysis, the distribution of transverse stress N_y loses accuracy and shows similar prediction with longitudinal stress N_x.

Figures 6.30 to 6.35 show the distribution of longitudinal stress N_x and transverse stress N_y for both top surface and bottom surface of the plate in postbuckling cycle 5, with in-plane longitudinal edges free. The stress distribution for the free edge condition shows more stress variation than the fixed edge condition. Moreover, the stress distribution of the free edge condition in the ABAQUS results shows more stress variation than that of the improved postbuckling analysis along the longitudinal edges.

Figures 6.36 to 6.41 show the distribution of longitudinal stress N_x and transverse stress N_y for both top surface and bottom surface of the plate in postbuckling cycle 5, with in-plane longitudinal edges straight. The improved postbuckling analysis shows good agreement with ABAQUS results for both longitudinal and transverse stress on both top surface and bottom surface. The small difference in pattern is believed to be due to the slightly different transverse edge conditions between improved postbuckling analysis and ABAQUS analysis.

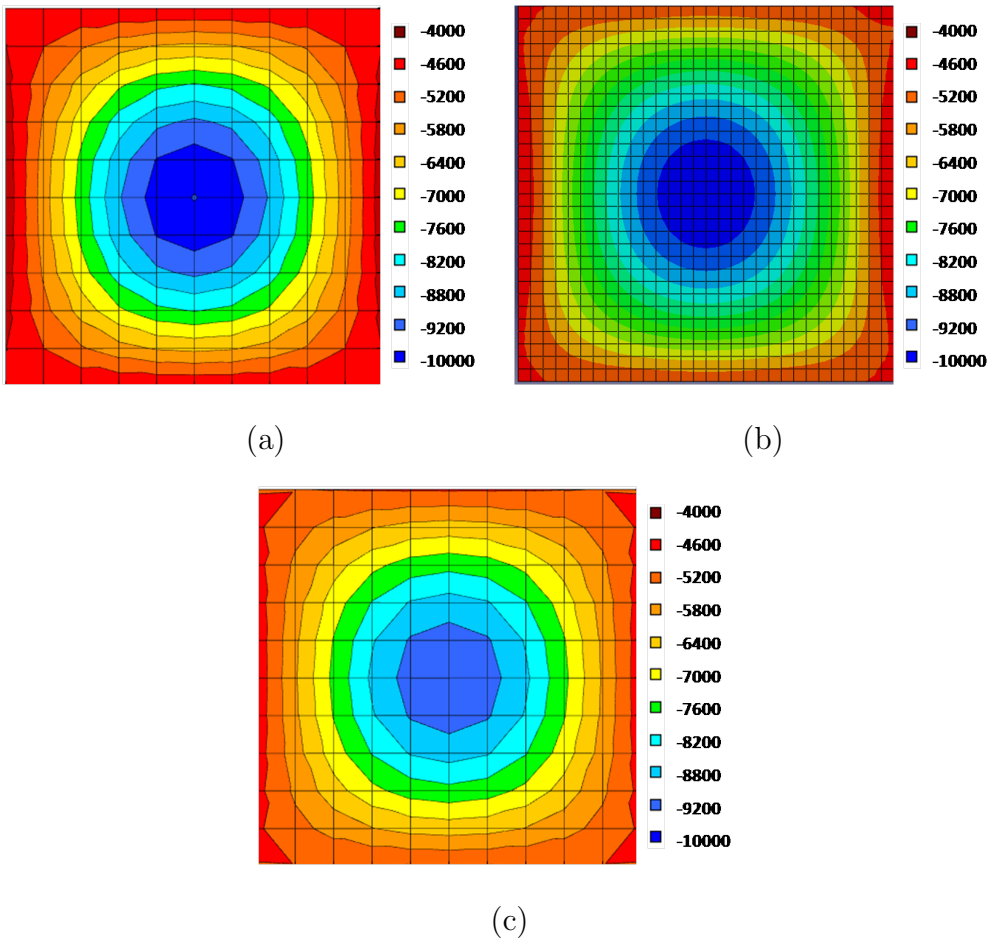

Figure 6.24: Variation of stress N_x across the top surface of plate for cycle 5 in (a) improved postbuckling analysis, (b) ABAQUS analysis and (c) old VICONOPT analysis, with all edges simply supported against out-of-plane deflection and the longitudinal edges fixed in-plane.

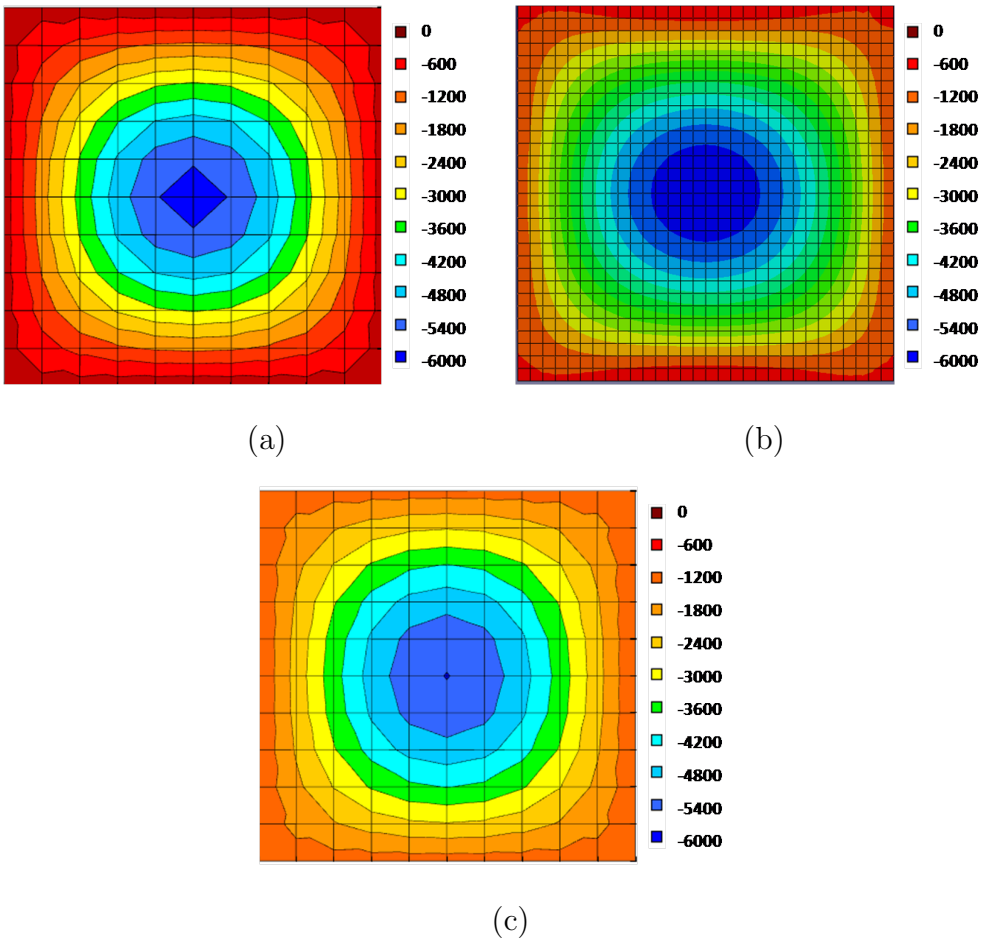

Figure 6.25: Variation of stress N_y across the top surface of plate for cycle 5 in (a) improved postbuckling analysis, (b) ABAQUS analysis and (c) old VICONOPT analysis, with all edges simply supported against out-of-plane deflection and the longitudinal edges fixed in-plane.

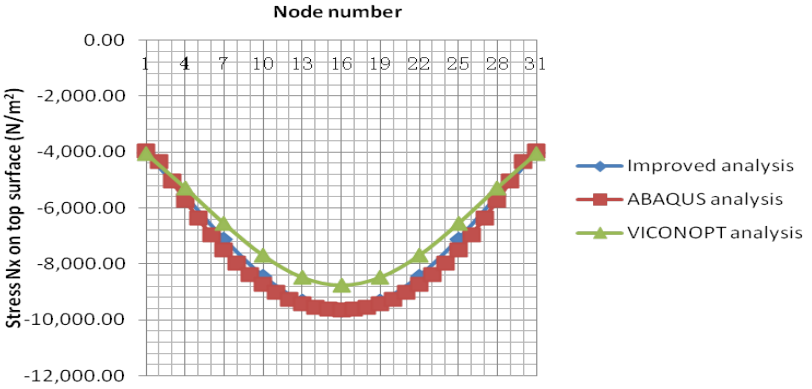

Node number	1	4	7	10	13	16	19	22	25	28	31		Mean	RMS % error
Improved analysis	-4022.43	-5562.80	-7104.07	-8429.62	-9328.43	-9646.79	-9328.42	-8429.59	-7104.04	-5562.77	-4022.39		-7140.12	
ABAQUS analysis	-3967.20	-5724.84	-7503.47	-8741.43	-9426.50	-9640.67	-9426.50	-8741.43	-7503.47	-5724.84	-3967.20		-7306.14	
VICONOPT analysis	-4068.76	-5282.22	-6554.76	-7684.72	-8466.21	-8745.64	-8466.20	-7684.70	-6554.73	-5282.19	-4068.73		-6623.53	
ABS(A-I)	55.23	162.04	399.40	311.81	98.07	6.12	98.08	311.84	399.43	162.07	55.19		187.21	
% error(A-I)	1.39	2.83	5.32	3.57	1.04	0.06	1.04	3.57	5.32	2.83	1.39		**2.56**	
(A-I)^2	3049.87	26255.34	1.60E+05	97225.14	9617.04	37.46	9619.92	97241.82	1.60E+05	26267.28	3046.06		53765.70	**3.17**
ABS(A-V)	101.56	442.62	948.71	1056.71	960.29	895.03	960.30	1056.73	948.74	442.65	101.53		719.53	
% error(A-V)	2.56	7.73	12.64	12.09	10.19	9.28	10.19	12.09	12.64	7.73	2.56		**9.85**	
(A-V)^2	10313.69	1.96E+05	9.00E+05	1.12E+06	9.22E+05	8.01E+05	9.22E+05	1.12E+06	9.00E+05	1.96E+05	10308.33		644668.76	**10.99**

(a)

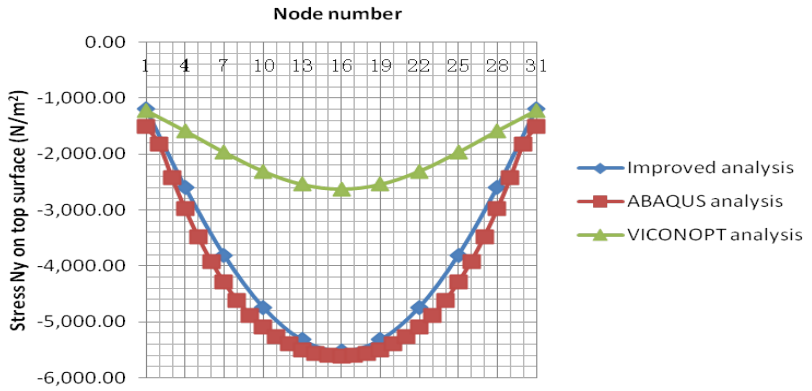

Node number	1	4	7	10	13	16	19	22	25	28	31		Mean	RMS % error
Improved analysis	-1190.96	-2590.82	-3805.07	-4735.91	-5318.24	-5516.13	-5318.23	-4735.89	-3805.05	-2590.79	-1190.93		-3708.91	
ABAQUS analysis	-1509.32	-2981.81	-4292.12	-5094.58	-5494.26	-5610.84	-5494.26	-5094.58	-4292.12	-2981.81	-1509.32		-4032.27	
VICONOPT analysis	-1220.63	-1584.67	-1966.43	-2305.42	-2539.86	-2623.69	-2539.86	-2305.41	-1966.42	-1584.66	-1220.62		-1987.06	
ABS(A-I)	318.36	390.99	487.05	358.67	176.02	94.71	176.03	358.69	487.07	391.02	318.39		323.36	
% error(A-I)	21.09	13.11	11.35	7.04	3.20	1.69	3.20	7.04	11.35	13.11	21.09		**8.02**	
(A-I)^2	1.01E+05	1.53E+05	2.37E+05	1.29E+05	3.10E+04	8.97E+03	3.10E+04	1.29E+05	2.37E+05	1.53E+05	1.01E+05		119199.00	**8.56**
ABS(A-V)	288.69	1397.14	2325.69	2789.16	2954.40	2987.15	2954.40	2789.17	2325.70	1397.15	288.70		2045.21	
% error(A-V)	19.13	46.86	54.19	54.75	53.77	53.24	53.77	54.75	54.19	46.86	19.13		**50.72**	
(A-V)^2	83343.71	1.95E+06	5.41E+06	7.78E+06	8.73E+06	8.92E+06	8.73E+06	7.78E+06	5.41E+06	1.95E+06	83348.28		5166124.35	**56.37**

(b)

Figure 6.26: Comparison of stress (a) N_x and (b) N_y across the horizontal centre line of top surface of plate for cycle 5 in improved postbuckling analysis, ABAQUS analysis and VICONOPT analysis, with longitudinal edges fixed in-plane.

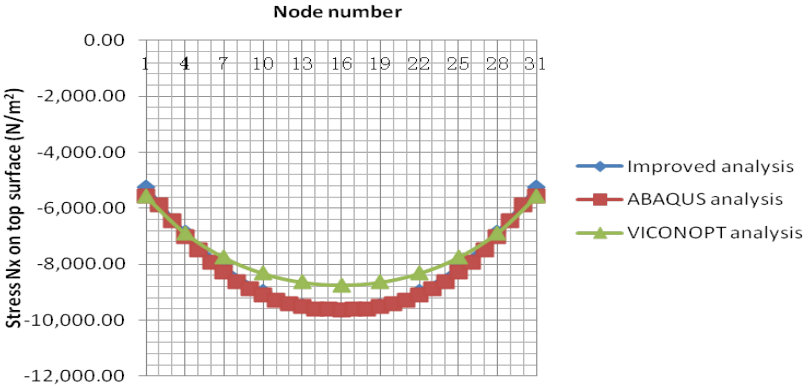

Node number	1	4	7	10	13	16	19	22	25	28	31		Mean	RMS % error
Improved analysis	-5258.13	-6870.40	-8101.43	-8968.39	-9478.95	-9646.79	-9478.95	-8968.39	-8101.43	-6870.40	-5258.13		-7909.22	
ABAQUS analysis	-5572.28	-7010.03	-8300.55	-9106.14	-9517.93	-9640.67	-9517.93	-9106.14	-8300.55	-7010.03	-5572.28		-8059.50	
VICONOPT analysis	-5584.50	-6886.56	-7763.41	-8330.27	-8645.20	-8745.64	-8645.20	-8330.27	-7763.41	-6886.56	-5584.50		-7560.50	
ABS(A-I)	314.15	139.63	199.12	137.75	38.98	6.12	38.98	137.75	199.12	139.63	314.15		151.40	
% error(A-I)	5.64	1.99	2.40	1.51	0.41	0.06	0.41	1.51	2.40	1.99	5.64		**1.88**	
(A-I)^2	98691.83	19495.29	39648.64	18974.12	1519.17	37.46	1519.17	18974.12	39648.64	19495.29	98691.83		32426.87	**2.23**
ABS(A-V)	12.22	123.47	537.14	775.87	872.73	895.03	872.73	775.87	537.14	123.47	12.22		503.45	
% error(A-V)	0.22	1.76	6.47	8.52	9.17	9.28	9.17	8.52	6.47	1.76	0.22		**6.25**	
(A-V)^2	149.30	15245.06	2.89E+05	6.02E+05	7.62E+05	8.01E+05	7.62E+05	6.02E+05	2.89E+05	15245.06	149.30		376018.24	**7.61**

(a)

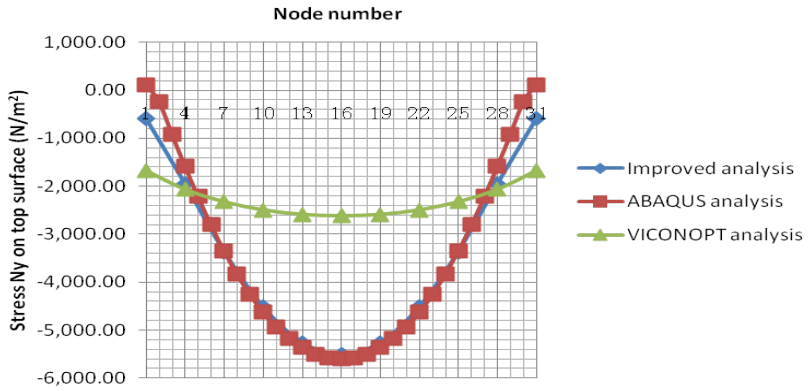

Node number	1	4	7	10	13	16	19	22	25	28	31		Mean	RMS % error
Improved analysis	-587.44	-1951.53	-3364.59	-4521.00	-5262.46	-5516.13	-5262.46	-4521.00	-3364.59	-1951.53	-587.44		-3353.65	
ABAQUS analysis	116.54	-1586.87	-3347.54	-4625.25	-5369.36	-5610.84	-5369.36	-4625.25	-3347.54	-1586.87	116.54		-3203.25	
VICONOPT analysis	-1675.35	-2065.97	-2329.02	-2499.08	-2593.56	-2623.69	-2593.56	-2499.08	-2329.02	-2065.97	-1675.35		-2268.15	
ABS(A-I)	703.98	364.66	17.05	104.25	106.90	94.71	106.90	104.25	17.05	364.66	703.98		244.40	
% error(A-I)	604.08	22.98	0.51	2.25	1.99	1.69	1.99	2.25	0.51	22.98	604.08		**7.63**	
(A-I)^2	4.96E+05	1.33E+05	290.63	10868.25	11426.80	8970.51	11426.80	10868.25	290.63	1.33E+05	4.96E+05		119207.42	**10.78**
ABS(A-V)	1791.89	479.10	1018.52	2126.17	2775.80	2987.15	2775.80	2126.17	1018.52	479.10	1791.89		1760.92	
% error(A-V)	1537.59	30.19	30.43	45.97	51.70	53.24	51.70	45.97	30.43	30.19	1537.59		**54.97**	
(A-V)^2	3.21E+06	2.30E+05	1.04E+06	4.52E+06	7.71E+06	8.92E+06	7.71E+06	4.52E+06	1.04E+06	2.30E+05	3.21E+06		3848177.35	**61.24**

(b)

Figure 6.27: Comparison of stress (a) N_x and (b) N_y across the vertical centre line of top surface of plate for cycle 5 in improved postbuckling analysis, ABAQUS analysis and VICONOPT analysis, with longitudinal edges fixed in-plane.

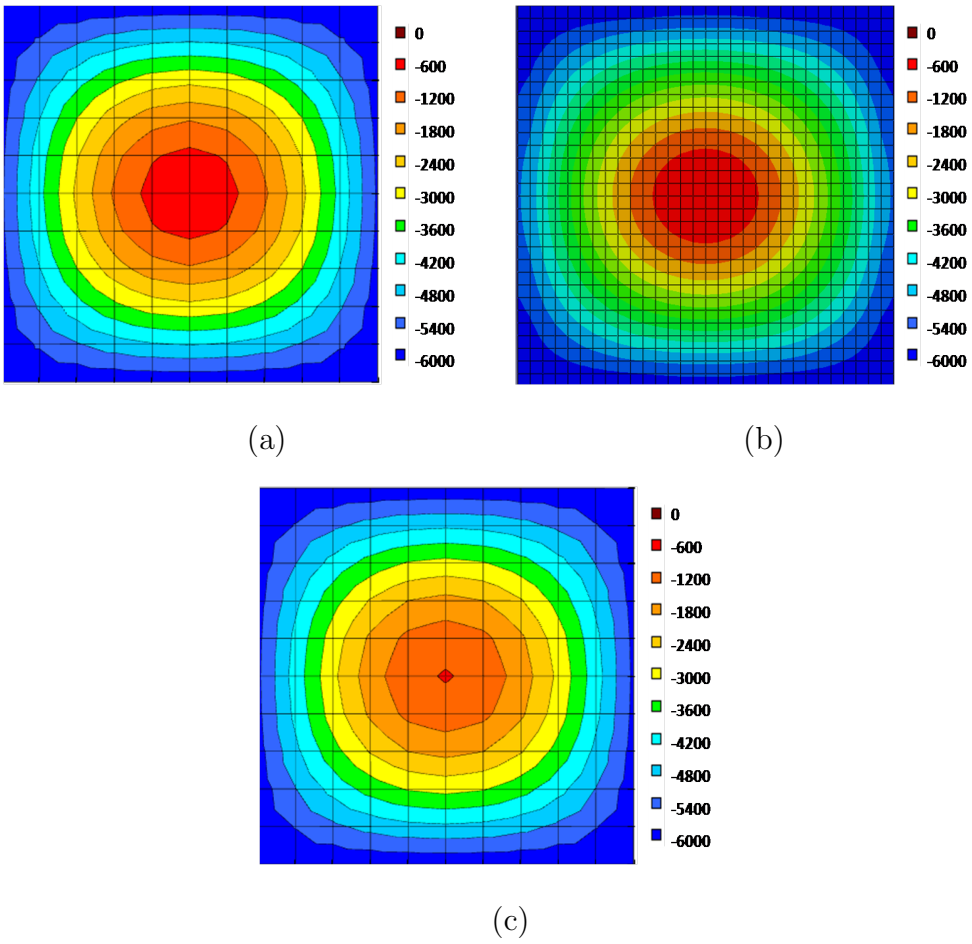

Figure 6.28: Variation of stress N_x across the bottom surface of plate for cycle 5 in (a) improved postbuckling analysis, (b) ABAQUS analysis and (c) old VICONOPT analysis, with all edges simply supported against out-of-plane deflection and the longitudinal edges fixed in-plane.

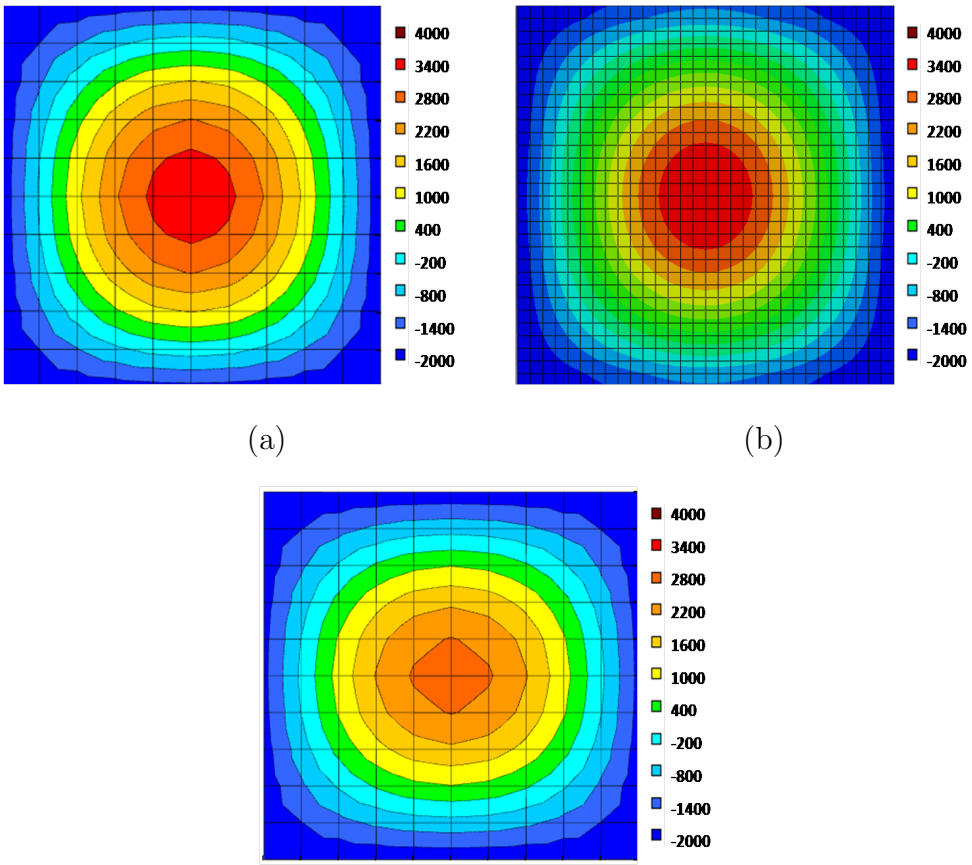

Figure 6.29: Variation of stress N_y across the bottom surface of plate for cycle 5 in (a) improved postbuckling analysis, (b) ABAQUS analysis and (c) old VICONOPT analysis, with all edges simply supported against out-of-plane deflection and the longitudinal edges fixed in-plane.

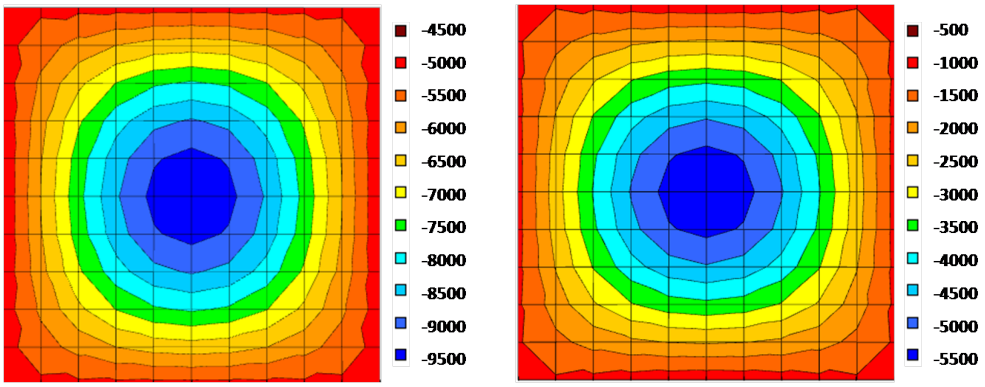

(a) (b)

Figure 6.30: Variation of stress (a) N_x and (b) N_y across the top surface of plate for cycle 5 in improved postbuckling analysis, with all edges simply supported against out-of-plane deflection and the longitudinal edges free in-plane.

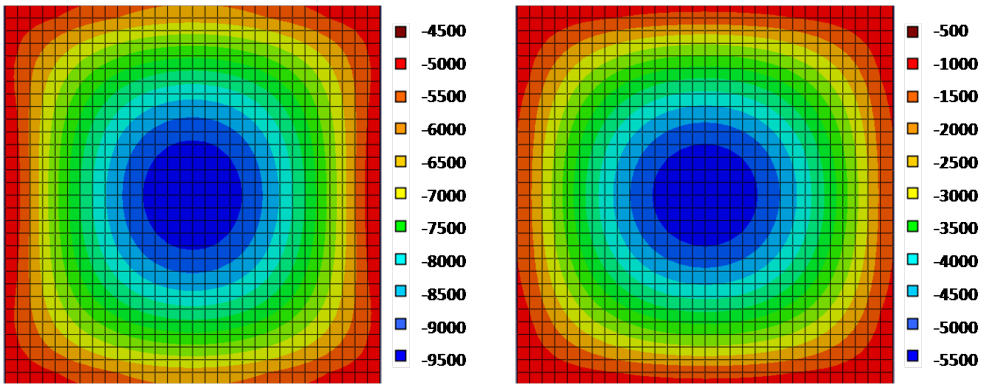

(a) (b)

Figure 6.31: Variation of stress (a) N_x and (b) N_y across the top surface of plate for cycle 5 in ABAQUS analysis, with all edges simply supported against out-of-plane deflection and the longitudinal edges free in-plane.

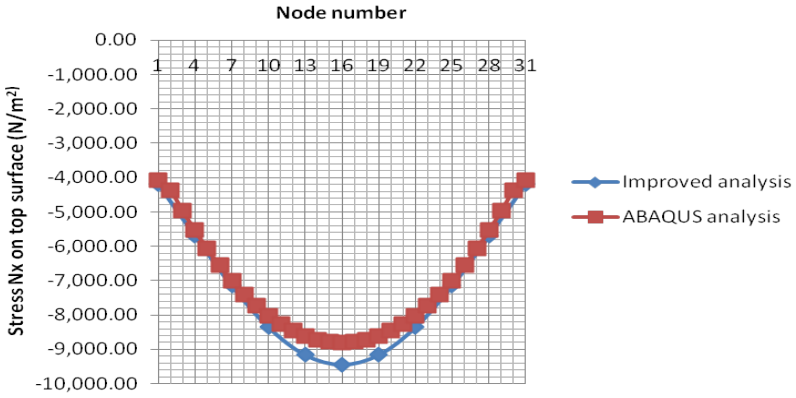

Node number	1	4	7	10	13	16	19	22	25	28	31	Mean	RMS % error
Improved analysis	-4194.79	-5698.99	-7145.54	-8354.02	-9158.12	-9440.30	-9158.11	-8354.00	-7145.51	-5698.95	-4194.75	-7140.28	
ABAQUS analysis	-4078.11	-5536.79	-7004.18	-8032.65	-8611.17	-8793.95	-8611.17	-8032.65	-7004.18	-5536.79	-4078.11	-6847.25	
ABS(A-I)	116.68	162.20	141.36	321.37	546.95	646.35	546.94	321.35	141.33	162.16	116.64	293.03	
% error	2.86	2.93	2.02	4.00	6.35	7.35	6.35	4.00	2.02	2.93	2.86	**4.28**	
(A-I)^2	1.36E+04	2.63E+04	2.00E+04	1.03E+05	2.99E+05	4.18E+05	2.99E+05	1.03E+05	2.00E+04	2.63E+04	1.36E+04	1.22E+05	**5.10**

(a)

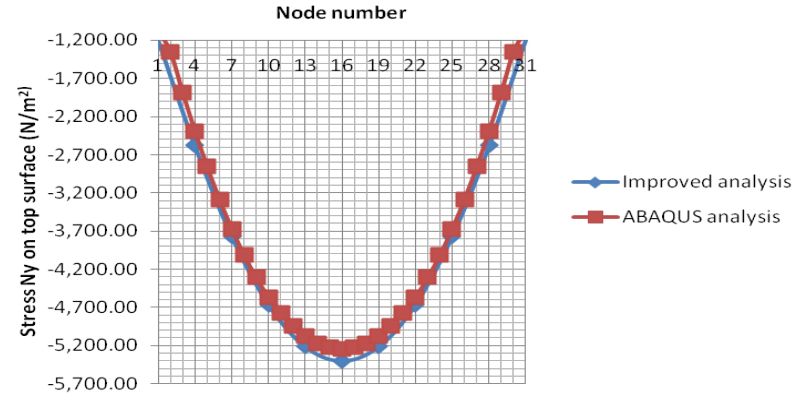

Node number	1	4	7	10	13	16	19	22	25	28	31	Mean	RMS % error
Improved analysis	-1191.50	-2580.39	-3765.93	-4661.29	-5214.92	-5401.84	-5214.91	-4661.27	-3765.91	-2580.36	-1191.46	-3657.25	
ABAQUS analysis	-1079.16	-2389.77	-3669.07	-4563.45	-5078.18	-5244.58	-5078.18	-4563.45	-3669.07	-2389.77	-1079.16	-3527.62	
ABS(A-I)	112.34	190.62	96.86	97.84	136.74	157.26	136.73	97.82	96.84	190.59	112.31	129.63	
% error	10.41	7.98	2.64	2.14	2.69	3.00	2.69	2.14	2.64	7.98	10.41	**3.67**	
(A-I)^2	1.26E+04	3.63E+04	9.38E+03	9.57E+03	1.87E+04	2.47E+04	1.87E+04	9.57E+03	9.38E+03	3.63E+04	1.26E+04	1.80E+04	**3.80**

(b)

Figure 6.32: Comparison of stress (a) N_x and (b) N_y across the horizontal centre line of top surface of plate for cycle 5 in improved postbuckling analysis and ABAQUS analysis, with longitudinal edges free in-plane.

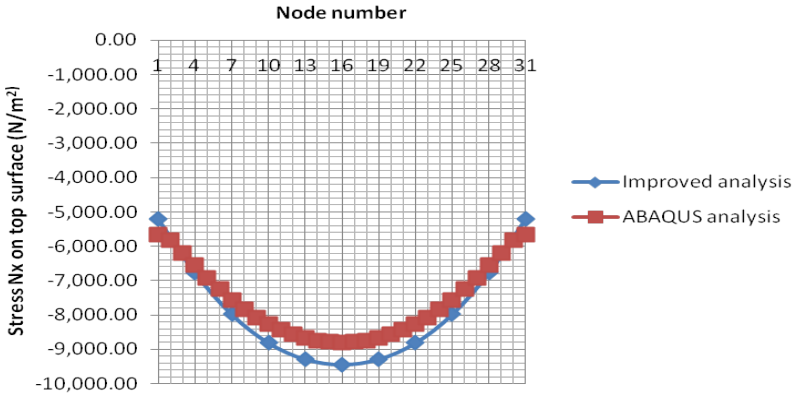

Node number	1	4	7	10	13	16	19	22	25	28	31		Mean	RMS % error
Improved analysis	-5196.72	-6762.05	-7976.95	-8810.06	-9286.58	-9440.30	-9286.58	-8810.06	-7976.95	-6762.05	-5196.72		-7773.18	
ABAQUS analysis	-5657.37	-6559.49	-7555.65	-8267.36	-8667.64	-8793.95	-8667.64	-8267.36	-7555.65	-6559.49	-5657.37		-7473.54	
ABS(A-I)	460.65	202.56	421.30	542.70	618.94	646.35	618.94	542.70	421.30	202.56	460.65		467.15	
% error	8.14	3.09	5.58	6.56	7.14	7.35	7.14	6.56	5.58	3.09	8.14		**6.25**	
(A-I)^2	2.12E+05	4.10E+04	1.77E+05	2.95E+05	3.83E+05	4.18E+05	3.83E+05	2.95E+05	1.77E+05	4.10E+04	2.12E+05		2.39E+05	**6.55**

(a)

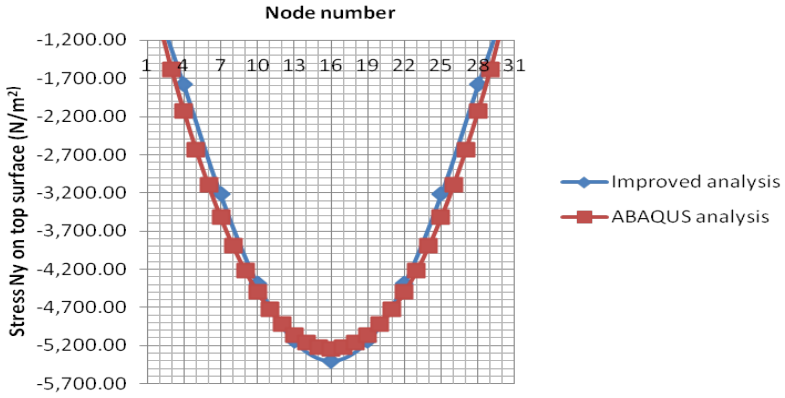

Node number	1	4	7	10	13	16	19	22	25	28	31		Mean	RMS % error
Improved analysis	-382.77	-1778.30	-3217.81	-4386.75	-5141.46	-5401.84	-5141.46	-4386.75	-3217.81	-1778.30	-382.77		-3201.46	
ABAQUS analysis	-707.71	-2128.76	-3518.90	-4497.80	-5062.29	-5244.58	-5062.29	-4497.80	-3518.90	-2128.76	-707.71		-3370.50	
ABS(A-I)	324.94	350.46	301.09	111.05	79.17	157.26	79.17	111.05	301.09	350.46	324.94		226.43	
% error	45.91	16.46	8.56	2.47	1.56	3.00	1.56	2.47	8.56	16.46	45.91		**6.72**	
(A-I)^2	1.06E+05	1.23E+05	9.07E+04	1.23E+04	6.27E+03	2.47E+04	6.27E+03	1.23E+04	9.07E+04	1.23E+05	1.06E+05		6.36E+04	**7.48**

(b)

Figure 6.33: Comparison of stress (a) N_x and (b) N_y across the vertical centre line of top surface of plate for cycle 5 in improved postbuckling analysis and ABAQUS analysis, with longitudinal edges free in-plane.

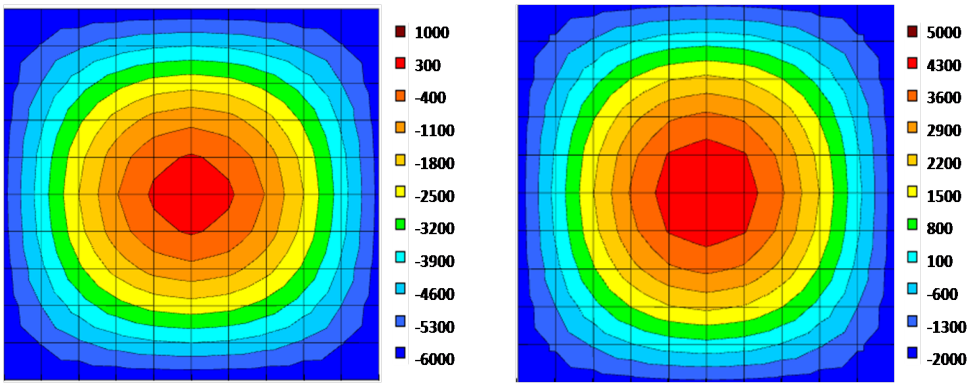

(a) (b)

Figure 6.34: Variation of stress (a) N_x and (b) N_y across the bottom surface of plate for cycle 5 in improved postbuckling analysis, with all edges simply supported against out-of-plane deflection and the longitudinal edges free in-plane.

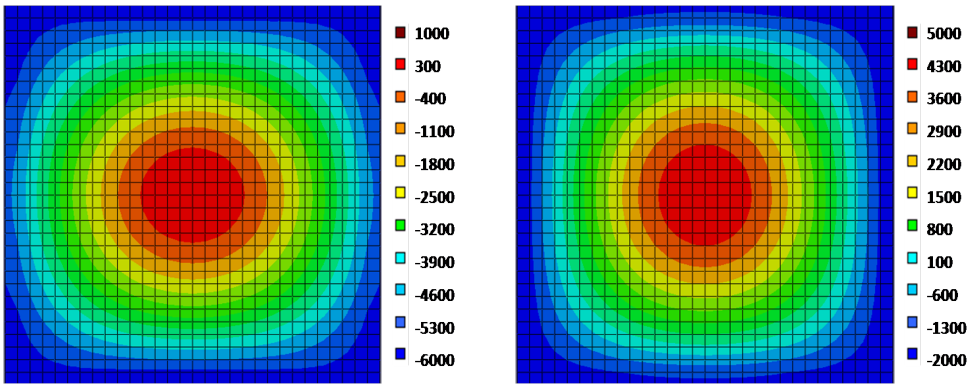

(a) (b)

Figure 6.35: Variation of stress (a) N_x and (b) N_y across the bottom surface of plate for cycle 5 in ABAQUS analysis, with all edges simply supported against out-of-plane deflection and the longitudinal edges free in-plane.

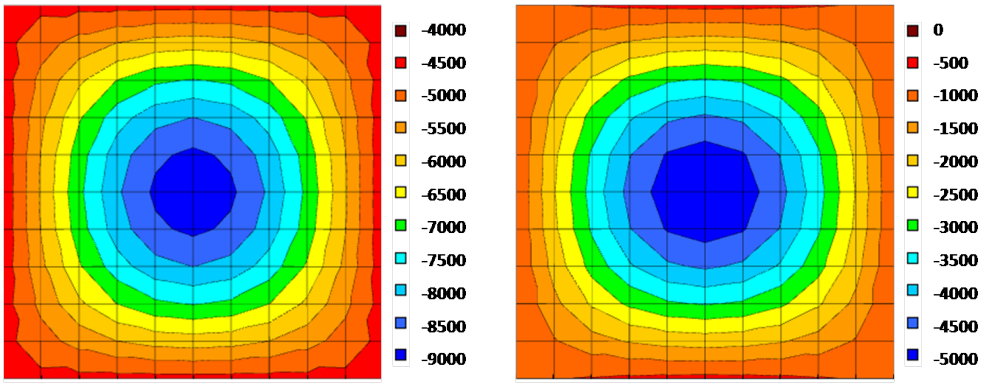

(a) (b)

Figure 6.36: Variation of stress (a) N_x and (b) N_y across the top surface of plate for cycle 5 in improved postbuckling analysis, with all edges simply supported against out-of-plane deflection and the longitudinal edges straight in-plane.

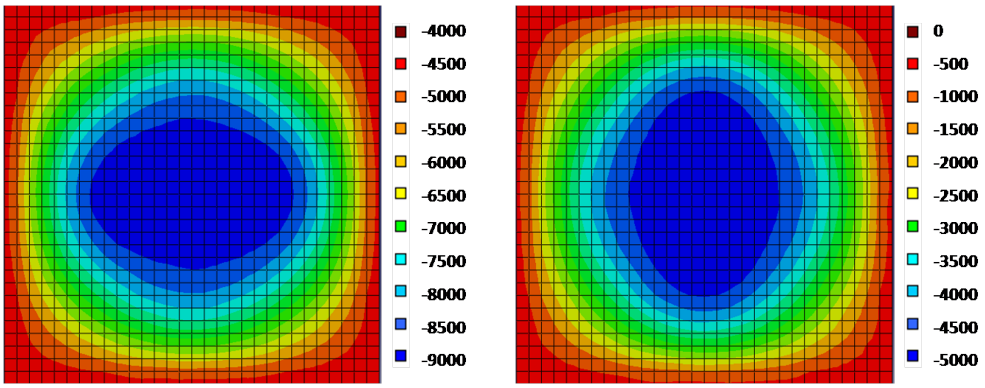

(a) (b)

Figure 6.37: Variation of stress (a) N_x and (b) N_y across the top surface of plate for cycle 5 in ABAQUS analysis, with all edges simply supported against out-of-plane deflection and the longitudinal edges straight in-plane.

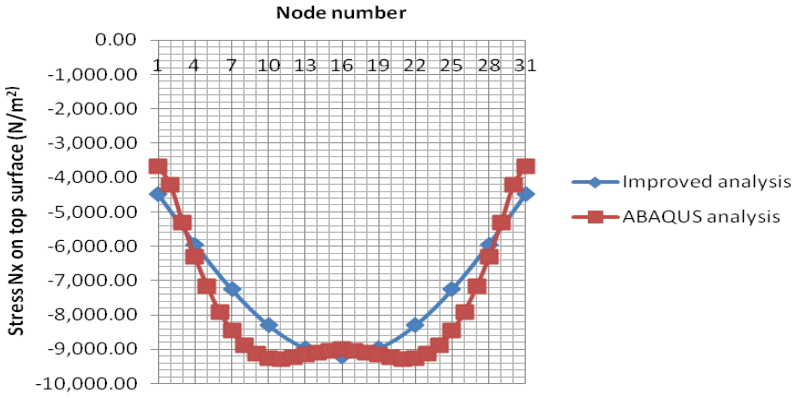

Node number	1	4	7	10	13	16	19	22	25	28	31	Mean	RMS % error
Improved analysis	-4.49E+03	-5.94E+03	-7.25E+03	-8.29E+03	-8.96E+03	-9.19E+03	-8.96E+03	-8.29E+03	-7.25E+03	-5.94E+03	-4.49E+03	-7189.53	
ABAQUS analysis	-3.67E+03	-6.31E+03	-8.46E+03	-9.25E+03	-9.15E+03	-9.00E+03	-9.15E+03	-9.25E+03	-8.46E+03	-6.31E+03	-3.67E+03	-7518.46	
ABS(A-I)	817.99	367.11	1206.27	958.72	191.52	193.11	191.53	958.74	1206.29	367.14	817.96	661.49	
% error	22.27	5.82	14.26	10.36	2.09	2.15	2.09	10.36	14.26	5.82	22.27	**8.80**	
(A-I)^2	6.69E+05	1.35E+05	1.46E+06	9.19E+05	3.67E+04	3.73E+04	3.67E+04	9.19E+05	1.46E+06	1.35E+05	6.69E+05	5.88E+05	**10.20**

(a)

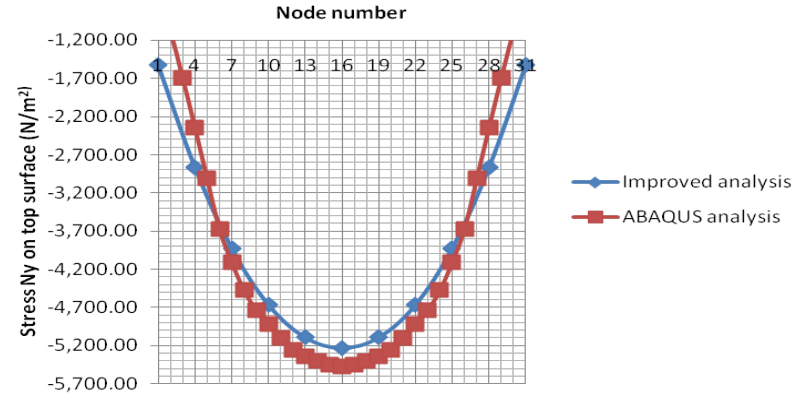

Node number	1	4	7	10	13	16	19	22	25	28	31	Mean	RMS % error
Improved analysis	-1.52E+03	-2.86E+03	-3.92E+03	-4.67E+03	-5.09E+03	-5.23E+03	-5.09E+03	-4.67E+03	-3.92E+03	-2.86E+03	-1.52E+03	-3761.73	
ABAQUS analysis	-7.38E+02	-2.34E+03	-4.11E+03	-4.92E+03	-5.35E+03	-5.48E+03	-5.35E+03	-4.92E+03	-4.11E+03	-2.34E+03	-7.38E+02	-3670.89	
ABS(A-I)	785.12	522.02	181.31	254.25	251.14	241.57	251.14	254.26	181.33	521.99	785.09	384.47	
% error	106.37	22.29	4.42	5.17	4.70	4.41	4.70	5.17	4.42	22.28	106.37	**10.47**	
(A-I)^2	6.16E+05	2.73E+05	3.29E+04	6.46E+04	6.31E+04	5.84E+04	6.31E+04	6.46E+04	3.29E+04	2.72E+05	6.16E+05	1.96E+05	**12.06**

(b)

Figure 6.38: Comparison of stress (a) N_x and (b) N_y across the horizontal centre line of top surface of plate for cycle 5 in improved postbuckling analysis and ABAQUS analysis, with longitudinal edges straight in-plane.

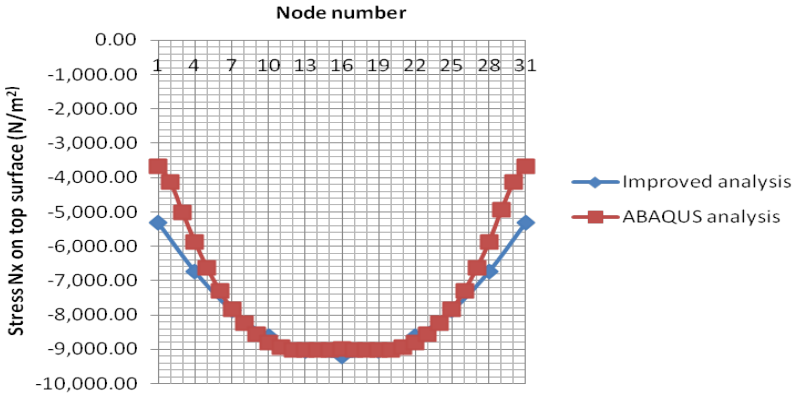

Node number	1	4	7	10	13	16	19	22	25	28	31	Mean	RMS % error
Improved analysis	-5.31E+03	-6.73E+03	-7.86E+03	-8.62E+03	-9.06E+03	-9.19E+03	-9.06E+03	-8.62E+03	-7.86E+03	-6.73E+03	-5.31E+03	-7667.96	
ABAQUS analysis	-3.67E+03	-5.87E+03	-7.83E+03	-8.79E+03	-9.03E+03	-9.00E+03	-9.03E+03	-8.79E+03	-7.83E+03	-5.87E+03	-3.67E+03	-7214.25	
ABS(A-I)	1645.94	859.15	30.38	166.52	29.87	193.11	29.87	166.52	30.38	859.15	1645.94	514.26	
% error	44.89	14.64	0.39	1.89	0.33	2.15	0.33	1.89	0.39	14.64	44.89	**7.13**	
(A-I)^2	2.71E+06	7.38E+05	9.23E+02	2.77E+04	8.92E+02	3.73E+04	8.92E+02	2.77E+04	9.23E+02	7.38E+05	2.71E+06	6.36E+05	**11.05**

(a)

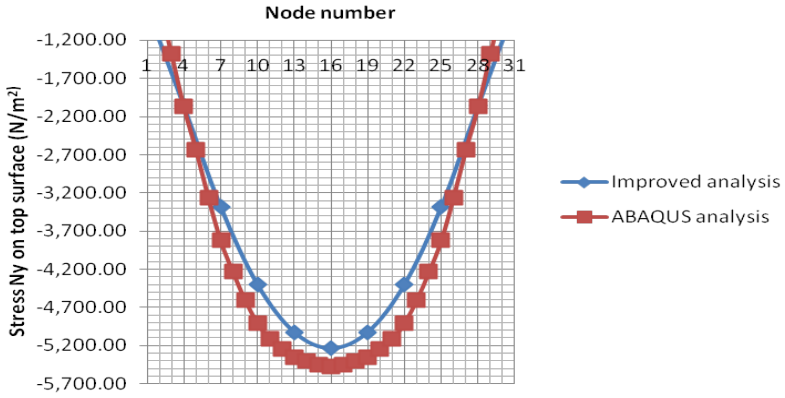

Node number	1	4	7	10	13	16	19	22	25	28	31	Mean	RMS % error
Improved analysis	-7.70E+02	-2.06E+03	-3.38E+03	-4.40E+03	-5.02E+03	-5.23E+03	-5.02E+03	-4.40E+03	-3.38E+03	-2.06E+03	-7.70E+02	-3317.69	
ABAQUS analysis	-1.59E+02	-2.07E+03	-3.82E+03	-4.91E+03	-5.35E+03	-5.48E+03	-5.35E+03	-4.91E+03	-3.82E+03	-2.07E+03	-1.59E+02	-3463.80	
ABS(A-I)	611.38	11.78	443.52	509.74	329.19	241.57	329.19	509.74	443.52	11.78	611.38	368.44	
% error	385.12	0.57	11.60	10.39	6.15	4.41	6.15	10.39	11.60	0.57	385.12	**10.64**	
(A-I)^2	3.74E+05	1.39E+02	1.97E+05	2.60E+05	1.08E+05	5.84E+04	1.08E+05	2.60E+05	1.97E+05	1.39E+02	3.74E+05	1.76E+05	**12.11**

(b)

Figure 6.39: Comparison of stress (a) N_x and (b) N_y across the vertical centre line of top surface of plate for cycle 5 in improved postbuckling analysis and ABAQUS analysis, with longitudinal edges straight in-plane.

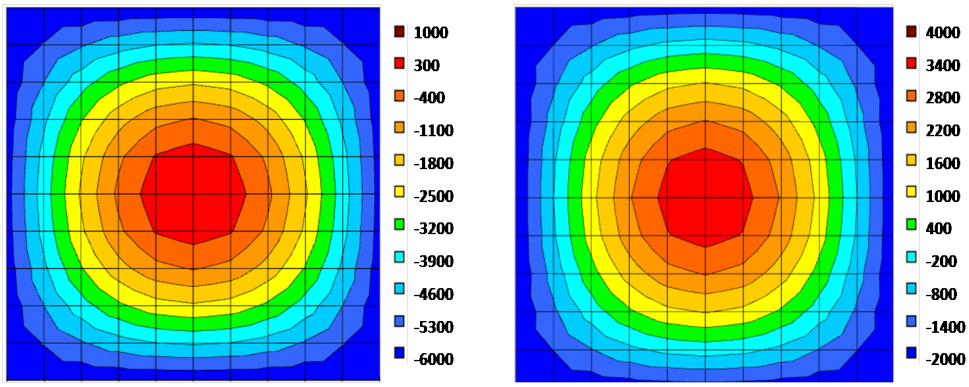

(a) (b)

Figure 6.40: Variation of stress (a) N_x and (b) N_y across the bottom surface of plate for cycle 5 in improved postbuckling analysis, with all edges simply supported against out-of-plane deflection and the longitudinal edges straight in-plane.

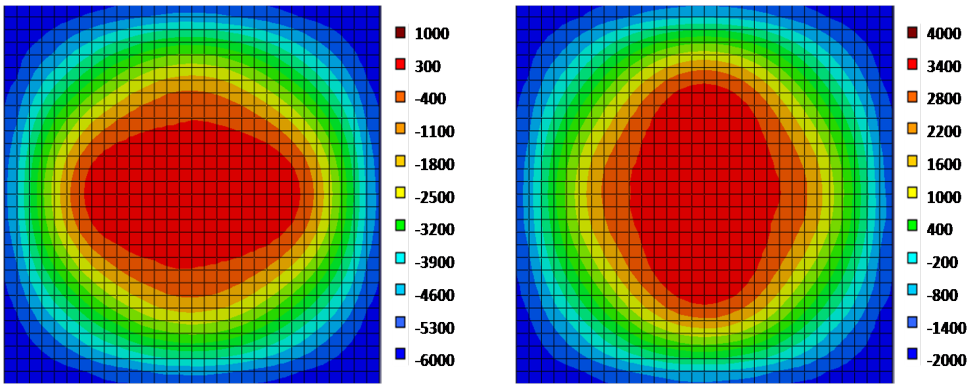

(a) (b)

Figure 6.41: Variation of stress (a) N_x and (b) N_y across the bottom surface of plate for cycle 5 in ABAQUS analysis, with all edges simply supported against out-of-plane deflection and the longitudinal edges straight in-plane.

6.2.3 Stress distributions in cycle 10

The stress distributions at cycle 10 have been selected to represent the state at a point much further into postbuckling stage. When the longitudinal strain of cycle 10 in the improved postbuckling analysis (5.4232×10^{-5}) and ABAQUS (5.3218×10^{-5}) exceeded the critical buckling strain (4.0169×10^{-5}) by 35.01% and 32.49%, the out-of-plane displacement **w** and effective uniform stresses were saved and the stress distribution calculated and plotted in the spreadsheet. In the contour plots, blue shading denotes increasing compression while red indicates decreasing compression (which usually results in regions of tension on the bottom surface). Numerical comparisons are also given for stresses across both the horizontal centre line and the vertical centre line to validate the improved postbuckling analysis numerically. The contour plots of N_x and N_y distributions and numerical comparisons (Figures 6.42 to 6.47) for fixed edge conditions for both top and bottom surfaces in three different analyses are shown for comparison.

The improved postbuckling analysis shows good agreement with ABAQUS results in the distribution of longitudinal stress N_x and transverse stress N_y for both top surface and bottom surface. However, it loses some accuracy in mean error and RMS error of N_y across both horizontal centre line and vertical centre line. Old VICONOPT also shows good agreement with ABAQUS results for distribution of longitudinal stress N_x although it is less accurate than improved postbuckling analysis. For prediction of transverse stress N_y, old VICONOPT shows an inaccurate distribution which is improved by the improved postbuckling analysis. It is believed, as mentioned in section 6.2.2 that this is due to the assumption of longitudinal stress invariance in the old VICONOPT analysis. The improved postbuckling analysis improves the accuracy of the stress distributions and shows good agreement with FE analysis.

Figures 6.48 to 6.53 show distribution of longitudinal stress N_x and transverse stress N_y for both top surface and bottom surface of the plate in postbuckling cycle 10, with in-plane longitudinal edges free. Improved postbuckling analysis shows a very small stress variation along the longitudinal edges in the prediction of longitudinal stress N_x, while ABAQUS analysis shows more obvious stress variation. Improved postbuckling analysis shows small tension at the middle

of the longitudinal edges in the prediction of longitudinal stress N_y, but the ABAQUS results show no tension at this stage.

Figures 6.54 to 6.59 show the distribution of longitudinal stress N_x and transverse stress N_y for both top surface and bottom surface of the plate in postbuckling cycle 10, with in-plane longitudinal edges straight. The improved postbuckling analysis shows good agreement with ABAQUS results for both longitudinal and transverse stress on both top surface and bottom surface. The improved postbuckling analysis shows small tension on both transverse edges and only tiny tension on both longitudinal edges for distribution of N_x. ABAQUS results show small tension on all four edges and a more symmetric pattern for distribution of N_x. This is due to the tiny difference between the 'straight edge condition' in improved postbuckling analysis and ABAQUS analysis. In ABAQUS analysis, all four edges are kept straight and therefore the pattern of stress distribution is more symmetric. However, in improved postbuckling analysis, the transverse edges are simply supported and the longitudinal edges are kept straight.

This section demonstrates one of the improvements achieved by improved postbuckling analysis, which is enhancing the accuracy of stress distribution in postbuckling analysis. Improved postbuckling analysis shows good agreement with ABAQUS analysis for distribution of longitudinal stress N_x and transverse stress N_y on both top and bottom surface. Improved postbuckling analysis has been validated in the sense that it gives close prediction with FE results for longitudinal stress distribution. Moreover, it corrects the inaccurate prediction in old VICONOPT for transverse stress distribution. However, improved postbuckling analysis loses some numerical accuracy (e.g. prediction of transverse stresses N_y across both horizontal and vertical centre line in cycle 10). Therefore, the errors have been evaluated in the following section to discuss possible reasons for errors and to propose further improvements in future work.

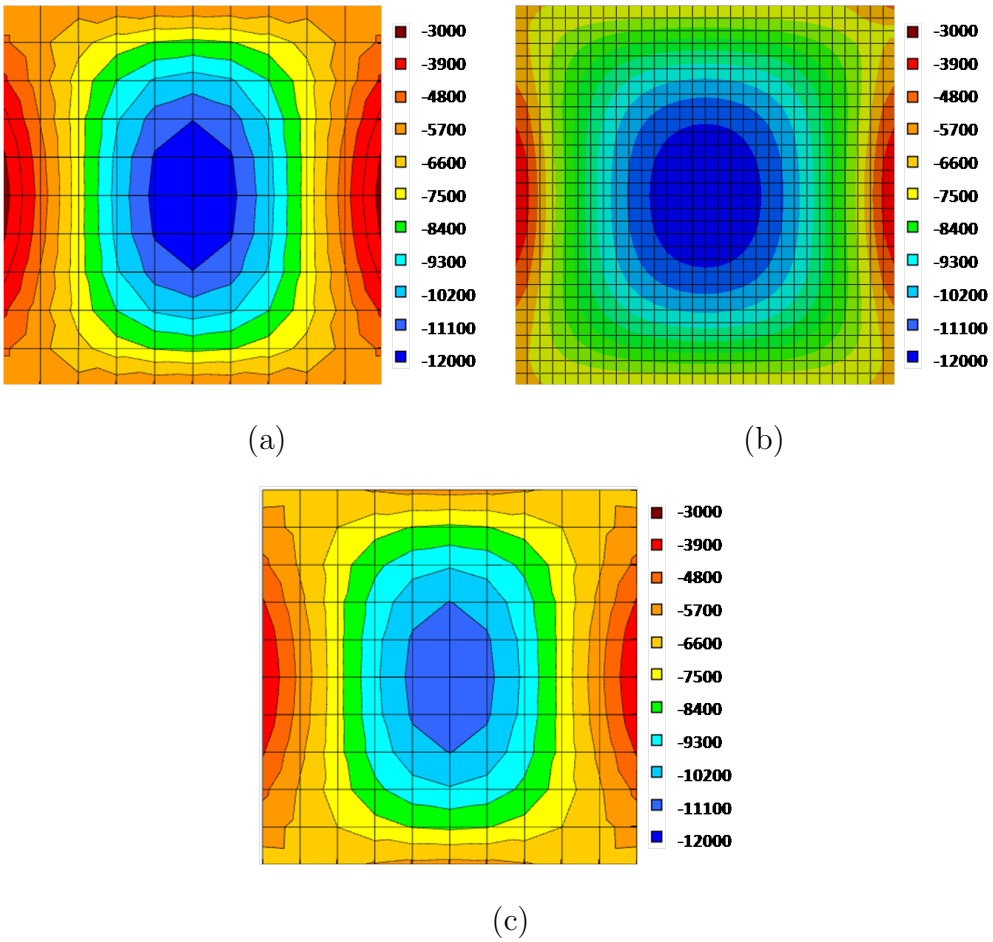

Figure 6.42: Variation of stress N_x across the top surface of plate for cycle 10 in (a) improved postbuckling analysis, (b) ABAQUS analysis and (c) old VICONOPT analysis, with all edges simply supported against out-of-plane deflection and the longitudinal edges fixed in-plane.

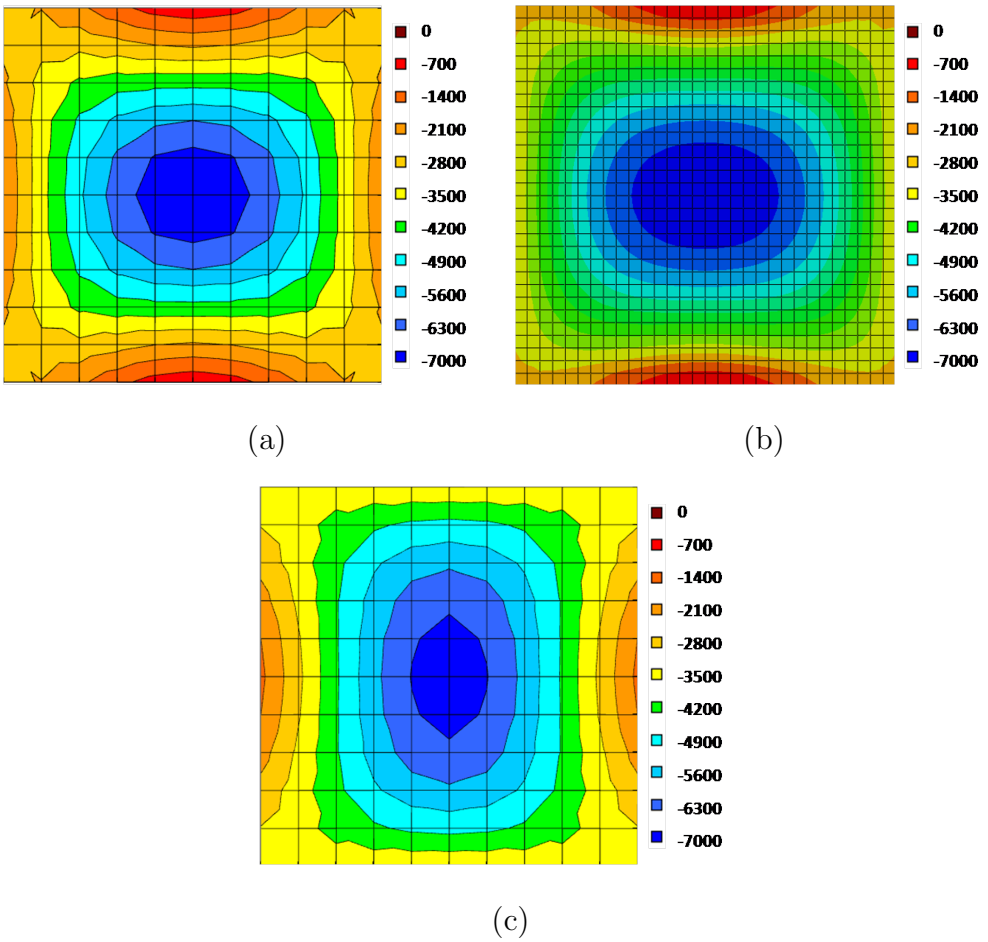

Figure 6.43: Variation of stress N_y across the top surface of plate for cycle 10 in (a) improved postbuckling analysis, (b) ABAQUS analysis and (c) old VICONOPT analysis, with all edges simply supported against out-of-plane deflection and the longitudinal edges fixed in-plane.

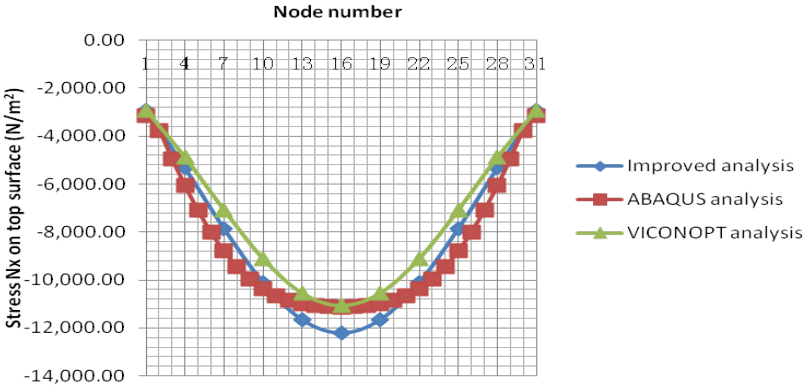

Node number	1	4	7	10	13	16	19	22	25	28	31		Mean	RMS % error
Improved analysis	-2918.95	-5329.63	-7857.59	-1.01E+04	-1.17E+04	-1.22E+04	-1.17E+04	-1.01E+04	-7857.54	-5329.57	-2918.89		-7994.16	
ABAQUS analysis	-3145.47	-6068.99	-8791.90	-1.04E+04	-1.10E+04	-1.11E+04	-1.10E+04	-1.04E+04	-8791.90	-6068.99	-3145.47		-8167.33	
VICONOPT analysis	-2932.56	-4895.87	-7092.66	-9123.39	-1.06E+04	-1.11E+04	-1.06E+04	-9123.35	-7092.61	-4895.82	-2932.52		-7299.29	
ABS(A-I)	226.52	739.36	934.31	253.83	664.58	1074.25	664.56	253.87	934.36	739.42	226.58		610.15	
% error(A-I)	7.20	12.18	10.63	2.45	6.05	9.65	6.05	2.45	10.63	12.18	7.20		**7.47**	
(A-I)^2	5.13E+04	5.47E+05	8.73E+05	64428.20	4.42E+05	1.15E+06	4.42E+05	64451.49	8.73E+05	5.47E+05	5.13E+04		464383.42	**8.34**
ABS(A-V)	212.91	1173.12	1699.24	1232.71	428.87	54.55	428.89	1232.75	1699.29	1173.17	212.95		868.04	
% error(A-V)	6.77	19.33	19.33	11.90	3.90	0.49	3.90	11.90	19.33	19.33	6.77		**10.63**	
(A-V)^2	4.53E+04	1.38E+06	2.89E+06	1.52E+06	1.84E+05	2.98E+03	1.84E+05	1.52E+06	2.89E+06	1.38E+06	4.53E+04		1093481.63	**12.80**

(a)

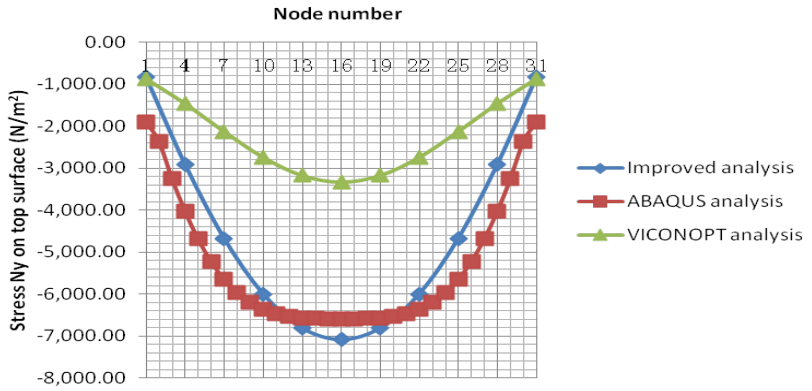

Node number	1	4	7	10	13	16	19	22	25	28	31		Mean	RMS % error
Improved analysis	-834.39	-2914.61	-4677.57	-5999.96	-6813.20	-7086.94	-6813.19	-5999.94	-4677.54	-2914.56	-834.34		-4506.02	
ABAQUS analysis	-1898.80	-4028.03	-5647.62	-6369.73	-6568.19	-6589.50	-6568.19	-6369.73	-5647.62	-4028.03	-1898.80		-5055.84	
VICONOPT analysis	-879.77	-1468.76	-2127.80	-2737.02	-3168.37	-3324.29	-3168.36	-2737.00	-2127.78	-1468.75	-879.76		-2189.79	
ABS(A-I)	1064.41	1113.42	970.05	369.77	245.01	497.44	245.00	369.79	970.08	1113.47	1064.46		729.36	
% error(A-I)	56.06	27.64	17.18	5.81	3.73	7.55	3.73	5.81	17.18	27.64	56.06		**14.43**	
(A-I)^2	1.13E+06	1.24E+06	9.41E+05	1.37E+05	60031.29	2.47E+05	60025.03	1.37E+05	9.41E+05	1.24E+06	1.13E+06		660782.79	**16.08**
ABS(A-V)	1019.03	2559.27	3519.82	3632.71	3399.82	3265.21	3399.83	3632.73	3519.84	2559.28	1019.04		2866.05	
% error(A-V)	53.67	63.54	62.32	57.03	51.76	49.55	51.76	57.03	62.32	63.54	53.67		**56.69**	
(A-V)^2	1.04E+06	6.55E+06	1.24E+07	1.32E+07	1.16E+07	1.07E+07	1.16E+07	1.32E+07	1.24E+07	6.55E+06	1.04E+06		9102506.66	**59.67**

(b)

Figure 6.44: Comparison of stress (a) N_x and (b) N_y across the horizontal centre line of top surface of plate for cycle 10 in improved postbuckling analysis, ABAQUS analysis and VICONOPT analysis, with longitudinal edges fixed in-plane.

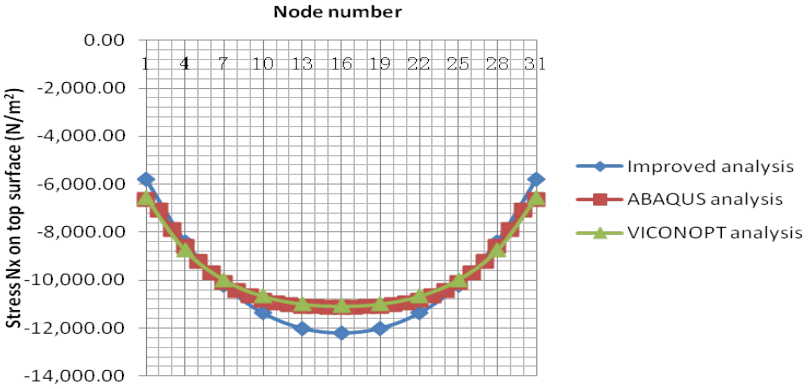

Node number	1	4	7	10	13	16	19	22	25	28	31		Mean	RMS % error
Improved analysis	-5789.75	-8402.26	-1.02E+04	-1.14E+04	-1.20E+04	-1.22E+04	-1.20E+04	-1.14E+04	-1.02E+04	-8402.26	-5789.75		-9800.54	
ABAQUS analysis	-6641.39	-8598.70	-1.01E+04	-1.08E+04	-1.11E+04	-1.11E+04	-1.11E+04	-1.08E+04	-1.01E+04	-8598.70	-6641.39		-9612.12	
VICONOPT analysis	-6555.64	-8742.82	-9984.79	-1.07E+04	-1.10E+04	-1.11E+04	-1.10E+04	-1.07E+04	-9984.79	-8742.82	-6555.64		-9540.40	
ABS(A-I)	851.64	196.44	95.57	531.20	920.53	1074.25	920.53	531.20	95.57	196.44	851.64		569.54	
% error(A-I)	12.82	2.28	0.94	4.90	8.30	9.65	8.30	4.90	0.94	2.28	12.82		**5.93**	
(A-I)^2	7.25E+05	3.86E+04	9.13E+03	2.82E+05	8.47E+05	1.15E+06	8.47E+05	2.82E+05	9.13E+03	3.86E+04	7.25E+05		450829.75	**6.99**
ABS(A-V)	85.75	144.12	134.81	185.93	104.82	54.55	104.82	185.93	134.81	144.12	85.75		124.13	
% error(A-V)	1.29	1.68	1.33	1.71	0.95	0.49	0.95	1.71	1.33	1.68	1.29		**1.29**	
(A-V)^2	7.35E+03	2.08E+04	1.82E+04	3.46E+04	1.10E+04	2.98E+03	1.10E+04	3.46E+04	1.82E+04	2.08E+04	7.35E+03		16970.77	**1.36**

(a)

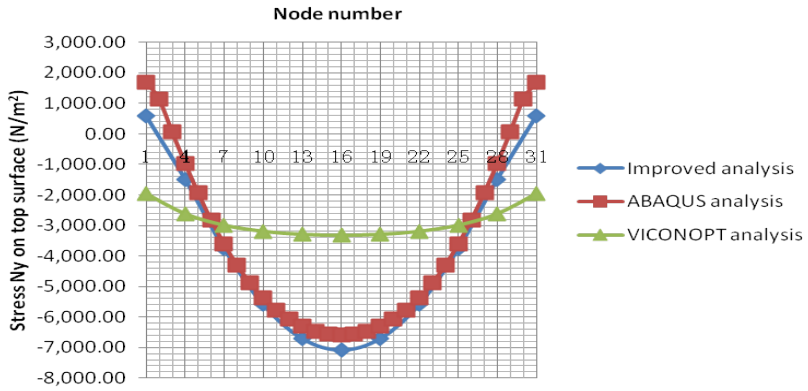

Node number	1	4	7	10	13	16	19	22	25	28	31		Mean	RMS % error
Improved analysis	586.26	-1487.67	-3.76E+03	-5.59E+03	-6.71E+03	-7.09E+03	-6.71E+03	-5.59E+03	-3.76E+03	-1487.67	586.26		-3729.28	
ABAQUS analysis	1680.32	-972.15	-3.61E+03	-5.38E+03	-6.31E+03	-6.59E+03	-6.31E+03	-5.38E+03	-3.61E+03	-972.15	1680.32		-3252.57	
VICONOPT analysis	-1966.69	-2622.85	-2995.44	-3.20E+03	-3.30E+03	-3.32E+03	-3.30E+03	-3.20E+03	-2995.44	-2622.85	-1966.69		-2862.12	
ABS(A-I)	1094.06	515.52	151.41	208.27	403.91	497.44	403.91	208.27	151.41	515.52	1094.06		476.71	
% error(A-I)	65.11	53.03	4.19	3.87	6.40	7.55	6.40	3.87	4.19	53.03	65.11		**14.66**	
(A-I)^2	1.20E+06	2.66E+05	2.29E+04	4.34E+04	1.63E+05	2.47E+05	1.63E+05	4.34E+04	2.29E+04	2.66E+05	1.20E+06		330164.56	**17.67**
ABS(A-V)	3647.01	1650.70	616.50	2182.16	3013.90	3265.21	3013.90	2182.16	616.50	1650.70	3647.01		2316.89	
% error(A-V)	217.04	169.80	17.07	40.55	47.77	49.55	47.77	40.55	17.07	169.80	217.04		**71.23**	
(A-V)^2	1.33E+07	2.72E+06	3.80E+05	4.76E+06	9.08E+06	1.07E+07	9.08E+06	4.76E+06	3.80E+05	2.72E+06	1.33E+07		6469419.11	**78.20**

(b)

Figure 6.45: Comparison of stress (a) N_x and (b) N_y across the vertical centre line of top surface of plate for cycle 10 in improved postbuckling analysis, ABAQUS analysis and VICONOPT analysis, with longitudinal edges fixed in-plane.

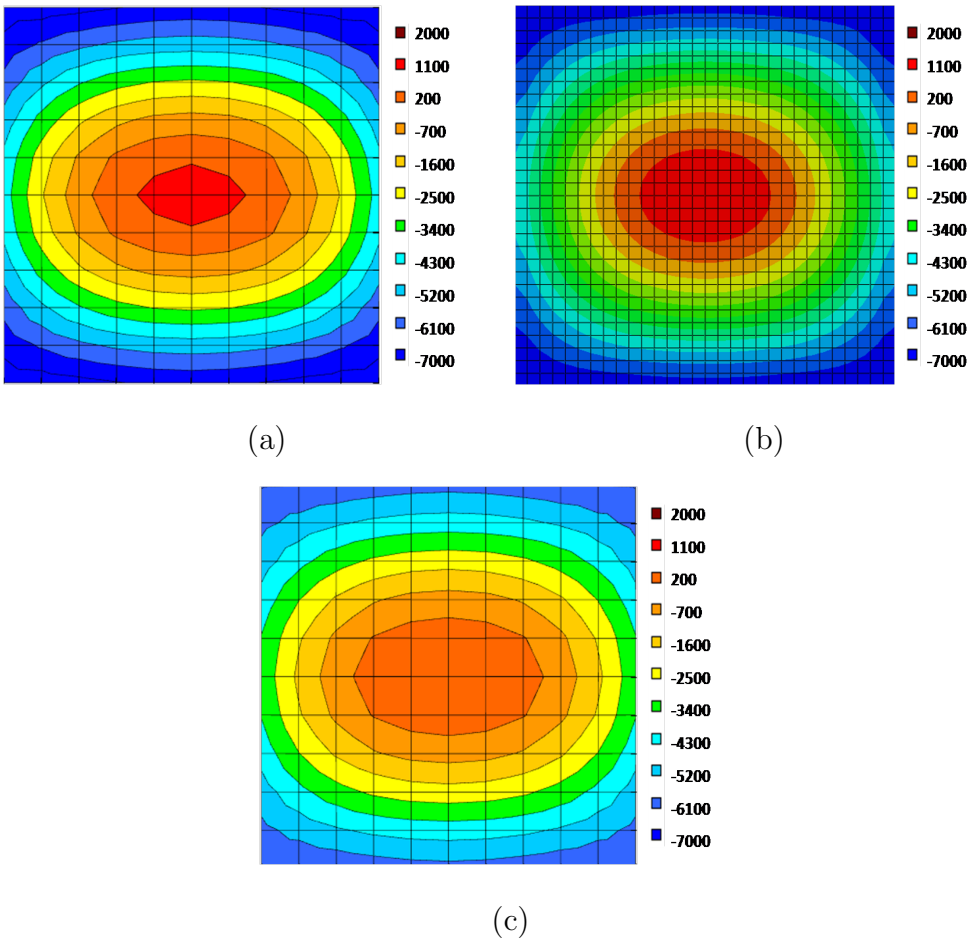

Figure 6.46: Variation of stress N_x across the bottom surface of plate for cycle 10 in (a) improved postbuckling analysis, (b) ABAQUS analysis and (c) old VICONOPT analysis, with all edges simply supported against out-of-plane deflection and the longitudinal edges fixed in-plane.

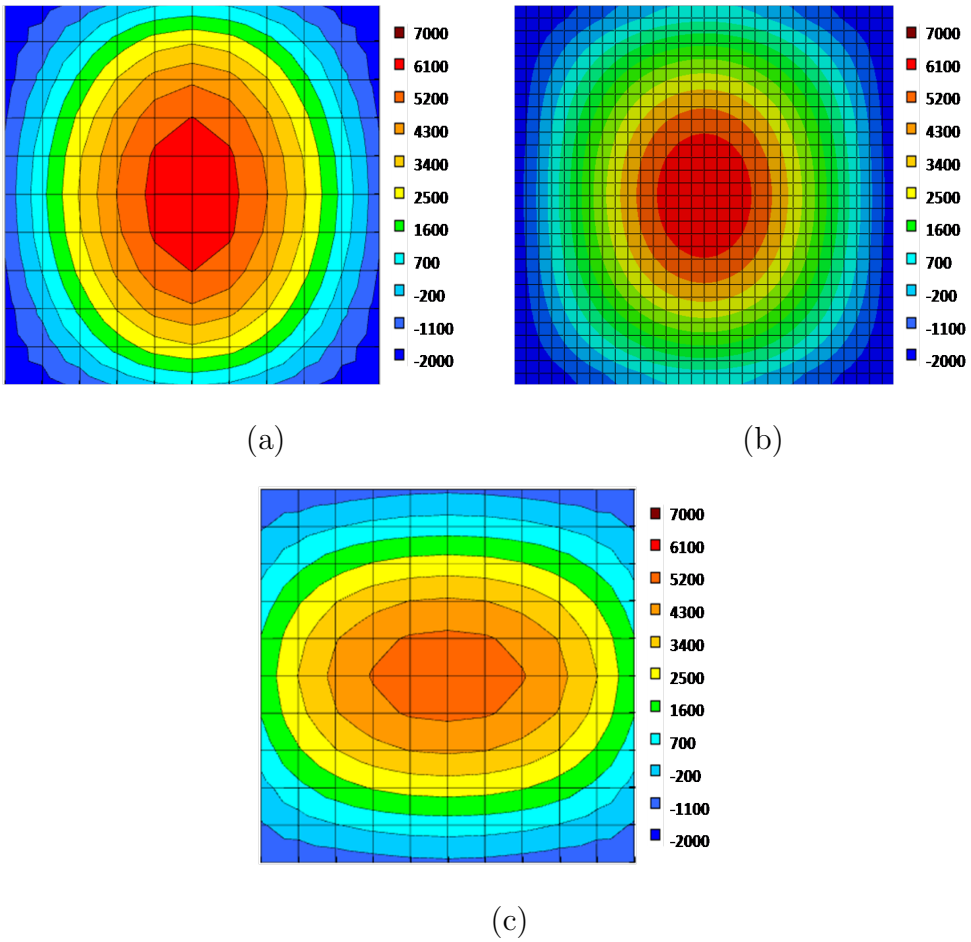

Figure 6.47: Variation of stress N_y across the bottom surface of plate for cycle 10 in (a) improved postbuckling analysis, (b) ABAQUS analysis and (c) old VICONOPT analysis, with all edges simply supported against out-of-plane deflection and the longitudinal edges fixed in-plane.

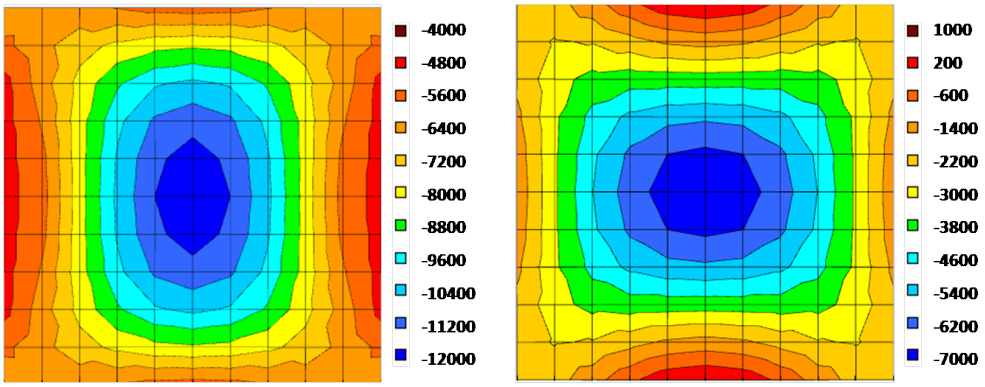

(a) (b)

Figure 6.48: Variation of stress (a) N_x and (b) N_y across the top surface of plate for cycle 10 in improved postbuckling analysis, with all edges simply supported against out-of-plane deflection and the longitudinal edges free in-plane.

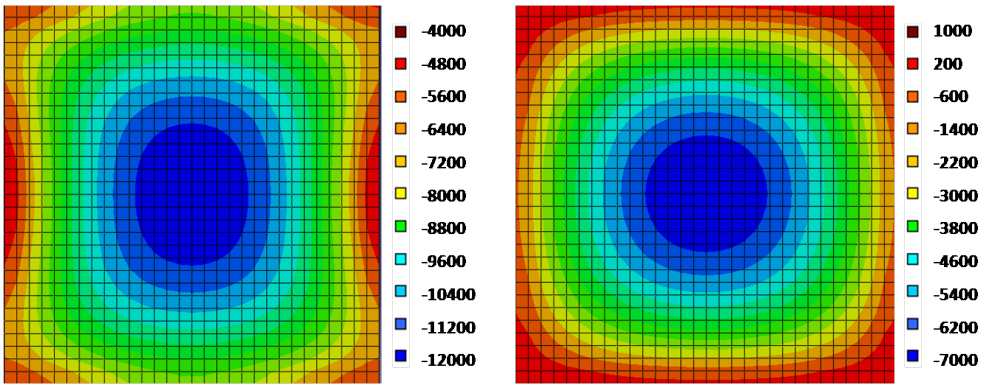

(a) (b)

Figure 6.49: Variation of stress (a) N_x and (b) N_y across the top surface of plate for cycle 10 in ABAQUS analysis, with all edges simply supported against out-of-plane deflection and the longitudinal edges free in-plane.

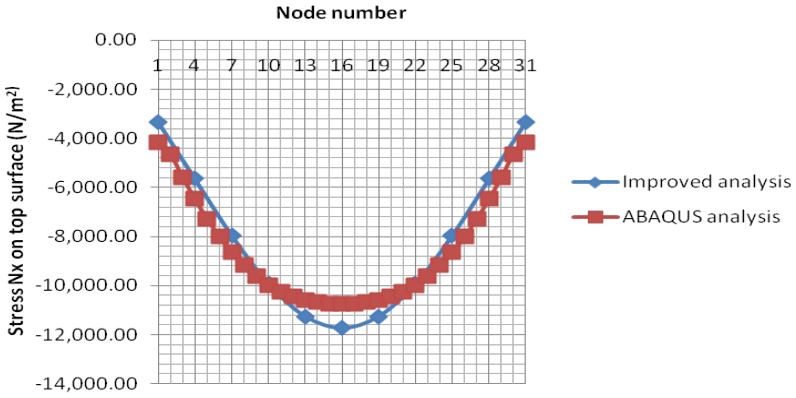

Node number	1	4	7	10	13	16	19	22	25	28	31	Mean	RMS % error
Improved analysis	-3.32E+03	-5.65E+03	-7.95E+03	-9.92E+03	-1.13E+04	-1.17E+04	-1.13E+04	-9.92E+03	-7.95E+03	-5.65E+03	-3.32E+03	-7993.19	
ABAQUS analysis	-4.16E+03	-6.47E+03	-8.65E+03	-9.97E+03	-1.06E+04	-1.08E+04	-1.06E+04	-9.97E+03	-8.65E+03	-6.47E+03	-4.16E+03	-8221.10	
ABS(A-I)	838.86	823.82	692.91	50.11	666.10	972.36	666.08	50.15	692.96	823.88	838.91	646.92	
% error	20.16	12.73	8.01	0.50	6.29	9.04	6.29	0.50	8.01	12.73	20.16	**7.87**	
(A-I)^2	7.04E+05	6.79E+05	4.80E+05	2.51E+03	4.44E+05	9.45E+05	4.44E+05	2.51E+03	4.80E+05	6.79E+05	7.04E+05	5.06E+05	**8.65**

(a)

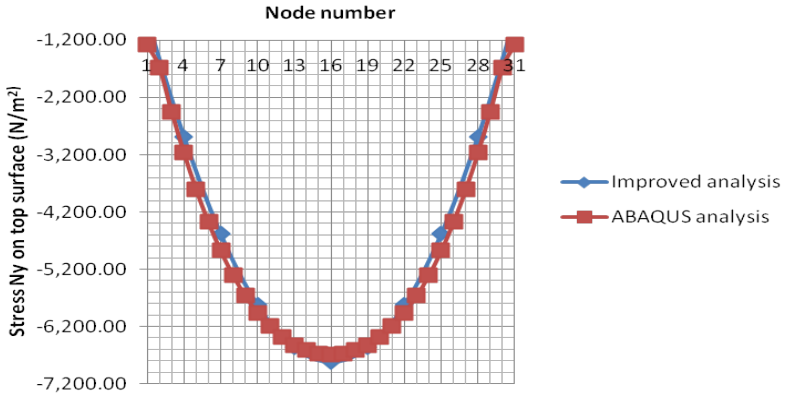

Node number	1	4	7	10	13	16	19	22	25	28	31	Mean	RMS % error
Improved analysis	-8.31E+02	-2.89E+03	-4.58E+03	-5.82E+03	-6.57E+03	-6.81E+03	-6.57E+03	-5.82E+03	-4.58E+03	-2.89E+03	-8.31E+02	-4380.31	
ABAQUS analysis	-1.27E+03	-3.16E+03	-4.88E+03	-5.96E+03	-6.52E+03	-6.69E+03	-6.52E+03	-5.96E+03	-4.88E+03	-3.16E+03	-1.27E+03	-4570.43	
ABS(A-I)	439.87	275.82	295.88	139.27	44.20	122.01	44.19	139.29	295.91	275.86	439.92	228.38	
% error	34.61	8.72	6.07	2.34	0.68	1.82	0.68	2.34	6.07	8.73	34.61	**5.00**	
(A-I)^2	1.93E+05	7.61E+04	8.75E+04	1.94E+04	1.95E+03	1.49E+04	1.95E+03	1.94E+04	8.76E+04	7.61E+04	1.94E+05	7.02E+04	**5.80**

(b)

Figure 6.50: Comparison of stress (a) N_x and (b) N_y across the horizontal centre line of top surface of plate for cycle 10 in improved postbuckling analysis and ABAQUS analysis, with longitudinal edges free in-plane.

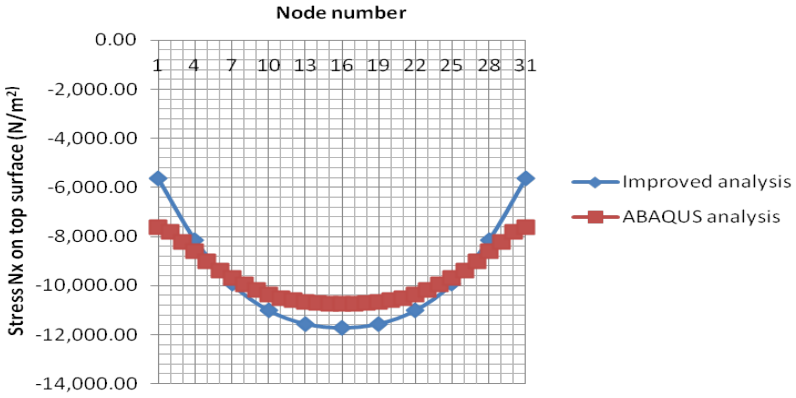

Node number	1	4	7	10	13	16	19	22	25	28	31		Mean	RMS % error
Improved analysis	-5.64E+03	-8.15E+03	-9.93E+03	-1.10E+04	-1.16E+04	-1.17E+04	-1.16E+04	-1.10E+04	-9.93E+03	-8.15E+03	-5.64E+03		-9483.01	
ABAQUS analysis	-7.64E+03	-8.62E+03	-9.70E+03	-1.04E+04	-1.07E+04	-1.08E+04	-1.07E+04	-1.04E+04	-9.70E+03	-8.62E+03	-7.64E+03		-9520.64	
ABS(A-I)	1992.15	472.36	231.92	648.46	891.00	972.36	891.00	648.46	231.92	472.36	1992.15		858.56	
% error	26.09	5.48	2.39	6.26	8.35	9.04	8.35	6.26	2.39	5.48	26.09		**9.02**	
(A-I)^2	3.97E+06	2.23E+05	5.38E+04	4.21E+05	7.94E+05	9.45E+05	7.94E+05	4.21E+05	5.38E+04	2.23E+05	3.97E+06		1.08E+06	**10.91**

(a)

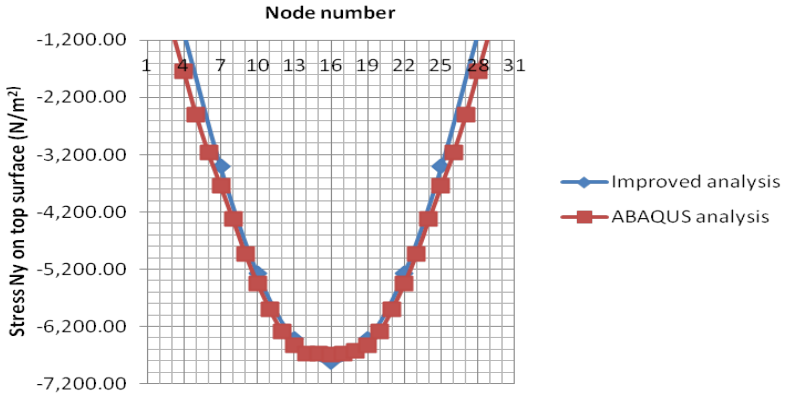

Node number	1	4	7	10	13	16	19	22	25	28	31		Mean	RMS % error
Improved analysis	1.08E+03	-1.07E+03	-3.41E+03	-5.27E+03	-6.42E+03	-6.81E+03	-6.42E+03	-5.27E+03	-3.41E+03	-1.07E+03	1.08E+03		-3364.27	
ABAQUS analysis	4.99E+02	-1.74E+03	-3.74E+03	-5.45E+03	-6.53E+03	-6.69E+03	-6.53E+03	-5.45E+03	-3.74E+03	-1.74E+03	4.99E+02		-3692.54	
ABS(A-I)	576.38	671.20	331.30	182.15	105.43	122.01	105.43	182.15	331.30	671.20	576.38		350.45	
% error	115.39	38.51	8.85	3.34	1.61	1.82	1.61	3.34	8.85	38.51	115.39		**9.49**	
(A-I)^2	3.32E+05	4.51E+05	1.10E+05	3.32E+04	1.11E+04	1.49E+04	1.11E+04	3.32E+04	1.10E+05	4.51E+05	3.32E+05		1.72E+05	**11.22**

(b)

Figure 6.51: Comparison of stress (a) N_x and (b) N_y across the vertical centre line of top surface of plate for cycle 10 in improved postbuckling analysis and ABAQUS analysis, with longitudinal edges free in-plane.

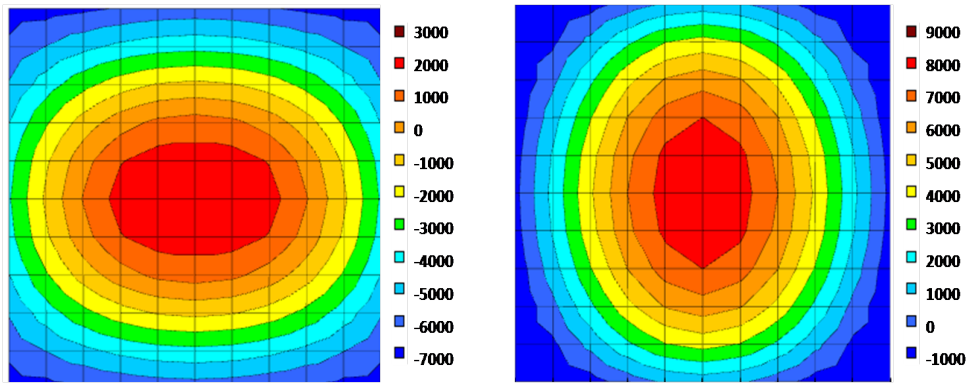

(a) (b)

Figure 6.52: Variation of stress (a) N_x and (b) N_y across the bottom surface of plate for cycle 10 in improved postbuckling analysis, with all edges simply supported against out-of-plane deflection and the longitudinal edges free in-plane.

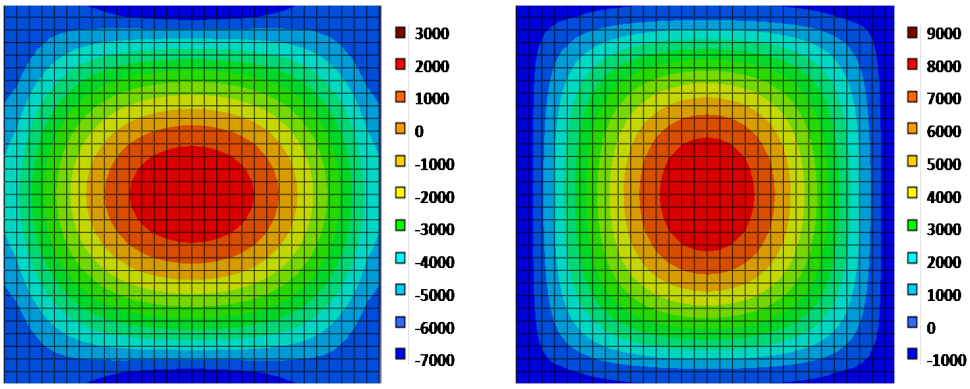

(a) (b)

Figure 6.53: Variation of stress (a) N_x and (b) N_y across the bottom surface of plate for cycle 10 in ABAQUS analysis, with all edges simply supported against out-of-plane deflection and the longitudinal edges free in-plane.

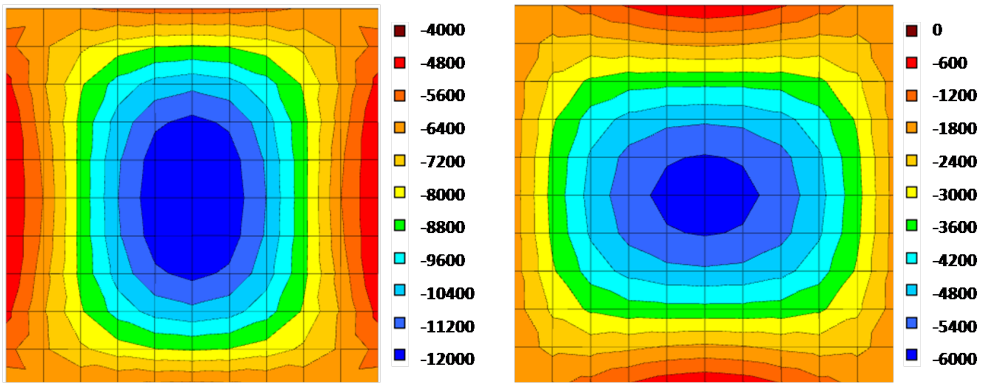

(a) (b)

Figure 6.54: Variation of stress (a) N_x and (b) N_y across the top surface of plate for cycle 10 in improved postbuckling analysis, with all edges simply supported against out-of-plane deflection and the longitudinal edges straight in-plane.

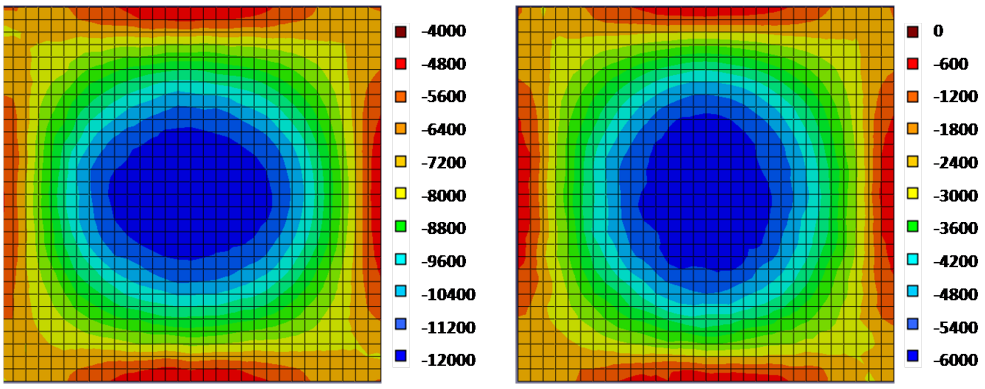

(a) (b)

Figure 6.55: Variation of stress (a) N_x and (b) N_y across the top surface of plate for cycle 10 in ABAQUS analysis, with all edges simply supported against out-of-plane deflection and the longitudinal edges straight in-plane.

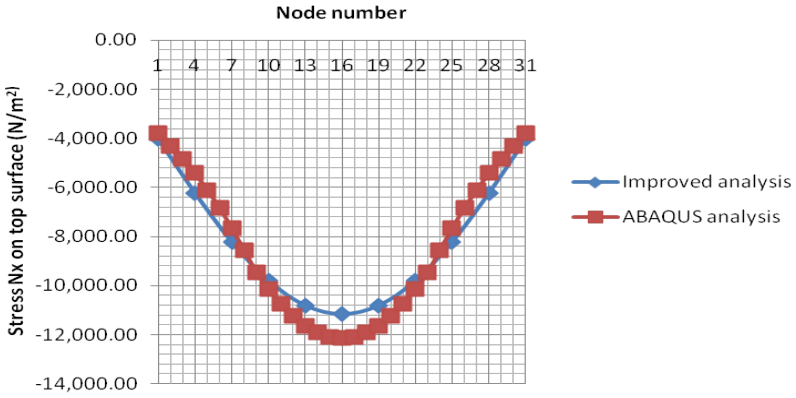

Node number	1	4	7	10	13	16	19	22	25	28	31	Mean	RMS % error
Improved analysis	-4.01E+03	-6.21E+03	-8.21E+03	-9.79E+03	-1.08E+04	-1.12E+04	-1.08E+04	-9.79E+03	-8.21E+03	-6.21E+03	-4.01E+03	-8109.63	
ABAQUS analysis	-3.79E+03	-5.41E+03	-7.67E+03	-1.02E+04	-1.16E+04	-1.22E+04	-1.16E+04	-1.02E+04	-7.67E+03	-5.41E+03	-3.79E+03	-8132.61	
ABS(A-I)	221.26	801.35	536.66	365.82	822.10	995.30	822.11	365.85	536.61	801.30	221.21	589.96	
% error	5.84	14.81	7.00	3.60	7.07	8.19	7.07	3.60	7.00	14.81	5.84	**7.25**	
(A-I)^2	4.90E+04	6.42E+05	2.88E+05	1.34E+05	6.76E+05	9.91E+05	6.76E+05	1.34E+05	2.88E+05	6.42E+05	4.89E+04	4.15E+05	**7.92**

(a)

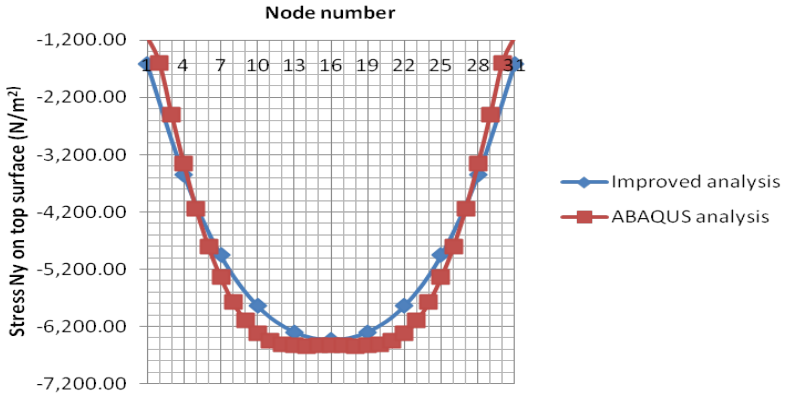

Node number	1	4	7	10	13	16	19	22	25	28	31	Mean	RMS % error
Improved analysis	-1.61E+03	-3.55E+03	-4.96E+03	-5.84E+03	-6.30E+03	-6.44E+03	-6.30E+03	-5.84E+03	-4.96E+03	-3.55E+03	-1.61E+03	-4631.55	
ABAQUS analysis	-1.13E+03	-3.36E+03	-5.34E+03	-6.33E+03	-6.53E+03	-6.52E+03	-6.53E+03	-6.33E+03	-5.34E+03	-3.36E+03	-1.13E+03	-4718.69	
ABS(A-I)	476.03	193.38	383.75	485.30	235.79	87.57	235.79	485.32	383.78	193.34	475.98	330.55	
% error	42.08	5.76	7.18	7.67	3.61	1.34	3.61	7.67	7.18	5.76	42.07	**7.01**	
(A-I)^2	2.27E+05	3.74E+04	1.47E+05	2.36E+05	5.56E+04	7.67E+03	5.56E+04	2.36E+05	1.47E+05	3.74E+04	2.27E+05	1.28E+05	**7.59**

(b)

Figure 6.56: Comparison of stress (a) N_x and (b) N_y across the horizontal centre line of top surface of plate for cycle 10 in improved postbuckling analysis and ABAQUS analysis, with longitudinal edges straight in-plane.

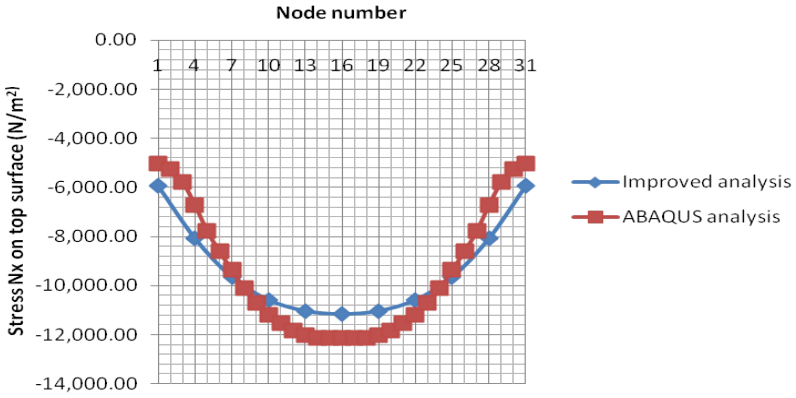

Node number	1	4	7	10	13	16	19	22	25	28	31		Mean	RMS % error
Improved analysis	-5.92E+03	-8.07E+03	-9.64E+03	-1.06E+04	-1.10E+04	-1.12E+04	-1.10E+04	-1.06E+04	-9.64E+03	-8.07E+03	-5.92E+03		-9240.00	
ABAQUS analysis	-5.02E+03	-6.70E+03	-9.37E+03	-1.12E+04	-1.20E+04	-1.22E+04	-1.20E+04	-1.12E+04	-9.37E+03	-6.70E+03	-5.02E+03		-9158.45	
ABS(A-I)	901.58	1363.66	276.23	605.21	990.09	995.30	990.09	605.21	276.23	1363.66	901.58		842.62	
% error	17.97	20.34	2.95	5.41	8.24	8.19	8.24	5.41	2.95	20.34	17.97		**9.20**	
(A-I)^2	8.13E+05	1.86E+06	7.63E+04	3.66E+05	9.80E+05	9.91E+05	9.80E+05	3.66E+05	7.63E+04	1.86E+06	8.13E+05		8.35E+05	**9.98**

(a)

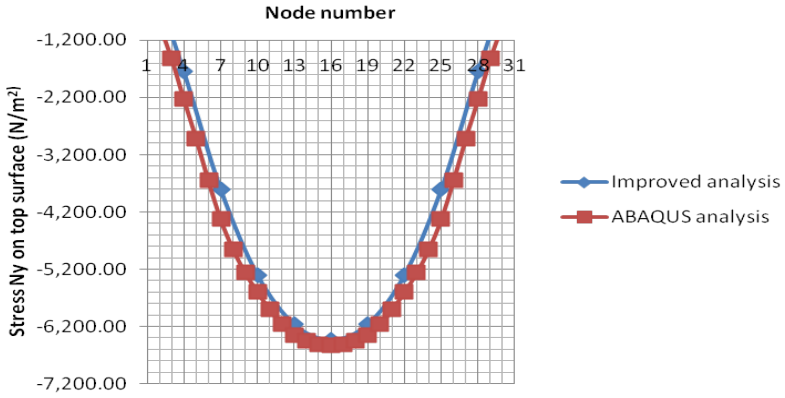

Node number	1	4	7	10	13	16	19	22	25	28	31		Mean	RMS % error
Improved analysis	1.52E+02	-1.74E+03	-3.80E+03	-5.30E+03	-6.16E+03	-6.44E+03	-6.16E+03	-5.30E+03	-3.80E+03	-1.74E+03	1.52E+02		-3649.16	
ABAQUS analysis	-3.66E+02	-2.23E+03	-4.33E+03	-5.60E+03	-6.35E+03	-6.52E+03	-6.35E+03	-5.60E+03	-4.33E+03	-2.23E+03	-3.66E+02		-4023.93	
ABS(A-I)	517.95	488.75	526.38	295.51	188.89	87.57	188.89	295.51	526.38	488.75	517.95		374.77	
% error	141.53	21.91	12.17	5.28	2.97	1.34	2.97	5.28	12.17	21.91	141.53		**9.31**	
(A-I)^2	2.68E+05	2.39E+05	2.77E+05	8.73E+04	3.57E+04	7.67E+03	3.57E+04	8.73E+04	2.77E+05	2.39E+05	2.68E+05		1.66E+05	**10.11**

(b)

Figure 6.57: Comparison of stress (a) N_x and (b) N_y across the vertical centre line of top surface of plate for cycle 10 in improved postbuckling analysis and ABAQUS analysis, with longitudinal edges straight in-plane.

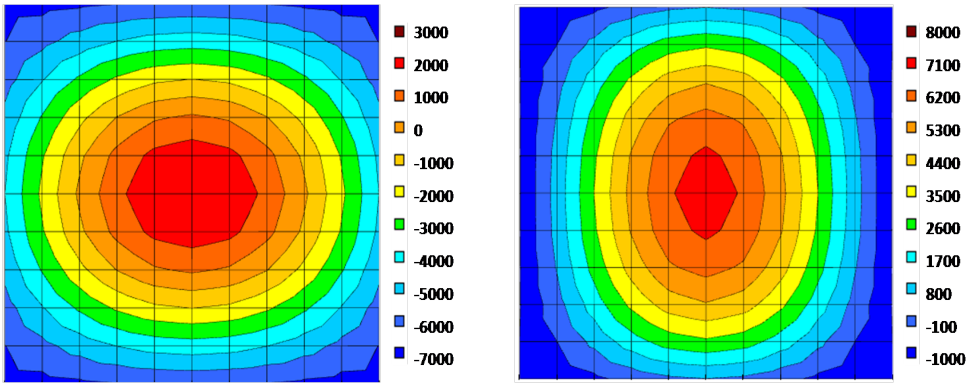

(a) (b)

Figure 6.58: Variation of stress (a) N_x and (b) N_y across the bottom surface of plate for cycle 10 in improved postbuckling analysis, with all edges simply supported against out-of-plane deflection and the longitudinal edges straight in-plane.

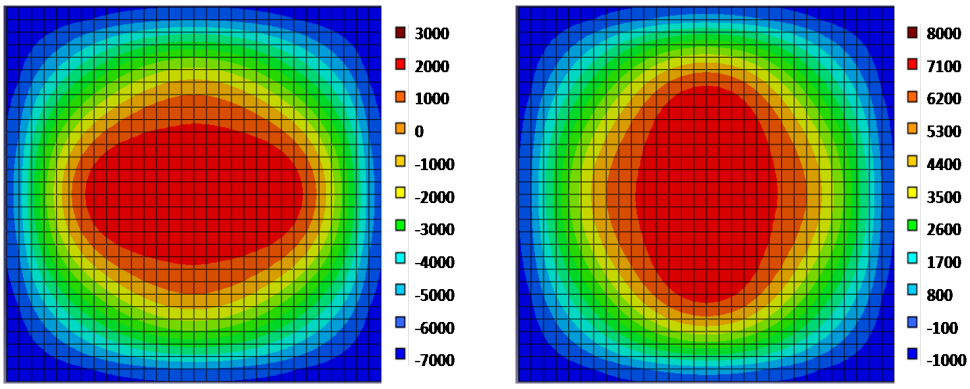

(a) (b)

Figure 6.59: Variation of stress (a) N_x and (b) N_y across the bottom surface of plate for cycle 10 in ABAQUS analysis, with all edges simply supported against out-of-plane deflection and the longitudinal edges straight in-plane.

6.3 Error evaluation and discussion

The illustrative results shown in this chapter provide plenty of evidence which validates the improvement made by the improved postbuckling analysis. The improved postbuckling analysis shows very good comparison with ABAQUS results in the majority of cases. However, it does lose some accuracy in some particular cases. In this section, the possible reason for the inaccuracy in some cases will be discussed and further improvement will also be proposed.

First of all, the errors (both mean error and RMS error) between improved postbuckling analysis and ABAQUS analysis in cycle 1 are basically tiny. The errors are almost less than 5% and in some particular cases the errors are even less than 1%. However, in cycle 10 the errors grow up to around 7% for most cases but are greater than 10% in some particular cases. This is believed to be due to the number of strips used in improved postbuckling analysis. In all cases, the plate has been divided into 10 strips for analysis while in ABAQUS each edge of plate has been divided into 30 elements in the transverse direction. The reduced number of strips therefore is believed to be a possible reason which may reduce the accuracy of the improved postbuckling analysis especially in cycle 10 rather than cycle 1. To show evidence, the distribution of longitudinal stress N_x across the horizontal centre line of plate with fixed edge condition in cycle 5 has been chosen for testing. Figure 6.60 shows curves of N_x for ABAQUS analysis and improved postbuckling analysis with 10 strips and 30 strips respectively. Moreover, the quantitative comparison of stress N_x between improved postbuckling analysis with 30 strips and ABAQUS analysis gives the mean error and the RMS error 1.24% and 1.37% respectively, which is smaller than those of improved postbuckling analysis with 10 strips (1.39% and 1.55%).

Secondly, the errors for free edge condition are generally less than those of the other two edge conditions. Owing to the limitation in old VICONOPT that no fixed edge condition and straight edge condition are available, the initial buckling mode from VICONOPT which is used in improved postbuckling analysis is calculated with longitudinal edges free in-plane. Therefore, the postbuckling analysis for fixed edge condition and straight edge condition actually start from the initial buckling mode of free edge condition. This is believed to be another reason which

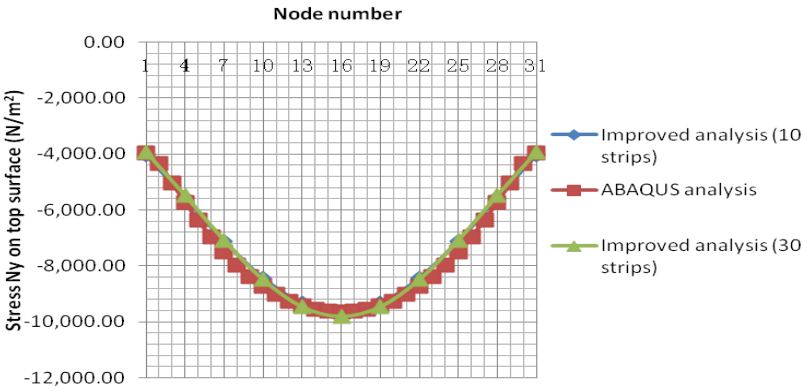

Node number	1	4	7	10	13	16	19	22	25	28	31		Mean	RMS % error
Improved analysis	-4022.43	-5562.80	-7104.07	-8429.62	-9328.43	-9646.79	-9328.42	-8429.59	-7104.04	-5562.77	-4022.39		-7140.12	
ABAQUS analysis	-3922.53	-5474.40	-7078.93	-8490.40	-9461.04	-9807.16	-9461.02	-8490.37	-7078.89	-5474.36	-3922.50		-7151.05	
ABS(A-I)	99.89	88.41	25.14	60.78	132.60	160.37	132.60	60.78	25.14	88.41	99.89		88.55	
% error	2.55	1.61	0.36	0.72	1.40	1.64	1.40	0.72	0.36	1.61	2.55		**1.24**	
(A-I)^2	9978.92	7816.02	632.17	3694.04	17583.50	25718.28	17583.17	3693.80	632.26	7816.19	9978.83		9557.01	**1.37**

Figure 6.60: (a) Curves and (b) quantitative comparison of stress N_x for ABAQUS analysis and improved postbuckling analysis with 10 strips and 30 strips.

increases the overall error for the improved postbuckling analysis of fixed edge condition and straight edge condition.

Thirdly, the biggest errors (e.g. stress N_y across the vertical centre line for fixed edge condition in cycle 10) always appear on the first and last nodes on the vertical centre line (i.e. the middle points of the longitudinal top and bottom edges). This is due to the small differences in the edge conditions applied on longitudinal top and bottom edges between improved postbuckling analysis and ABAQUS analysis. For example, in the fixed edge condition, all components of $\mathbf{u}$ are forced to be zero in the improved postbuckling analysis. However, this cannot be achieved in ABAQUS analysis as $\mathbf{u}$ has been used as a perturbation factor for postbuckling nonlinear analysis. The release of constraint in ABAQUS analysis leads to more free redistribution of stresses than improved postbuckling analysis. Hence the ABAQUS results give a greater peak value at the middle and edge of plate, which is believed to increase the error between improved postbuckling analysis and ABAQUS analysis.

Lastly, the numerical comparison shows that stress N_y loses more accuracy than stress N_x in each case. In section 6.2, the old VICONOPT results have been

proved to be inaccurate in the prediction of the N_y distribution, which is due to the assumption of a sinusoidal buckling mode in the longitudinal direction. Therefore, the enhanced expressions of in-plane displacements and stresses are assumed to provide more accurate analysis. However, stress N_y still loses more accuracy than N_x which is also due to the assumption of a sinusoidal buckling mode in the longitudinal direction.

Chapter 7

Illustrative results and discussion for other cases

In the previous chapter, a quantitative study of longitudinal and transverse stress distributions has been performed in detail for both top and bottom surface of a square isotropic plate with three different edge conditions. The results of the improved analysis have been compared with ABAQUS results and old VICONOPT results. The improved analysis largely shows good agreement with ABAQUS analysis and demonstrates considerable improvement on the existing technique. Hence the improved analysis has been validated to be able to provide more accurate results for the distribution of stresses in the postbuckling range. In this chapter, more cases including a rectangular isotropic plate, a plate under pure shear load and an anisotropic composite plate will be investigated to validate the improved analysis in more general cases. To avoid duplicating plots and results in this chapter, only stress distributions at the top surface of the plate for the fixed edge condition in cycle 5 will be analyzed and discussed. Quantitative analysis of stresses is also carried out across both the horizontal centre line and vertical centre line of the plate. Similarly to previous chapter, blue shading denotes increasing compression while red indicates decreasing compression (which usually results in regions of tension on the bottom surface). The units of stresses in all contour plots in this chapter are in N/m.

7.1 Investigation of isotropic plate with different aspect ratios

7.1.1 Introduction

In this section, a rectangular isotropic plate with different aspect ratios 0.5 and 1.5 will be investigated to compare with a square isotropic plate. For better comparison with a square plate, the material properties and applied compressive load have been defined exactly as the square isotropic model in the previous chapter. The width of the plate will also be kept and the only change will be the different length of the plate. The plate had width 0.3m, thickness 0.001m, Young's modulus 110kNmm^{-2} and Poisson's ratio 0.3. For the model with aspect ratio 0.5 the length of plate is 0.15m, while for the other one with aspect ratio 1.5 the length of the plate is 0.45m.

7.1.2 Results and discussion for isotropic plate with aspect ratio 0.5

Figure 7.1 shows the distribution of longitudinal stress N_x and transverse stress N_y on the top surface of the plate in postbuckling cycle 5. In contrast to the square plate which has a square pattern in the contour plot of stress distribution, Figure 7.1 shows a rectangular pattern which is basically due to the shortening of the length of the plate. Figures 7.2 and 7.3 show the quantitative evaluation of stresses N_x and N_y across the horizontal centre line and vertical centre line respectively. The contour plots in Figure 7.1 show good agreement of stress distribution in the postbuckling range between improved postbuckling analysis and ABAQUS analysis. The mean errors and square root mean errors in Figures 7.2 and 7.3 are basically lower than 10% and some are even lower than 5%, which validates the accuracy of improved postbuckling analysis for a rectangular plate with aspect ratio 0.5.

For the rectangular plate with aspect ratio 0.5 which is 'shorter' than the square plate, the critical buckling load (2071.2N/m) is much higher than that of

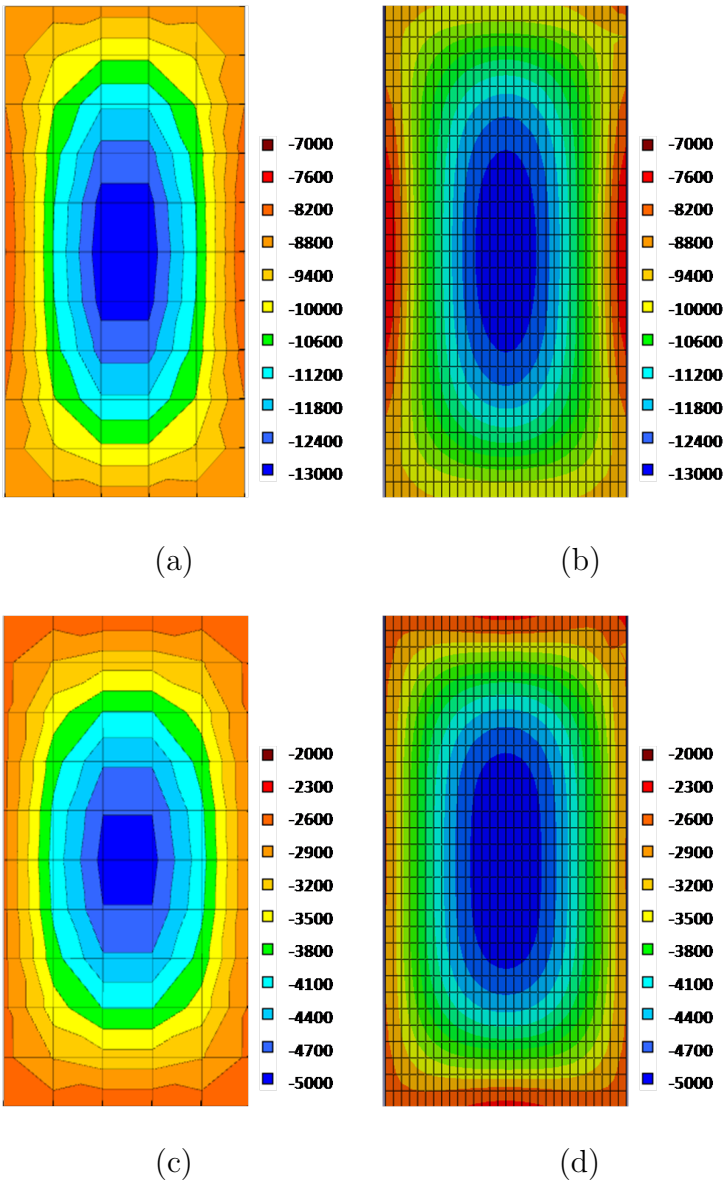

Figure 7.1: Variation of stress N_x across the top surface of plate in (a) N_x in improved postbuckling analysis, (b) $N_x$in ABAQUS analysis, (c) N_y in improved postbuckling analysis and (d) N_y in ABAQUS analysis, with all edges simply supported against out-of-plane deflection and the longitudinal edges fixed in-plane.

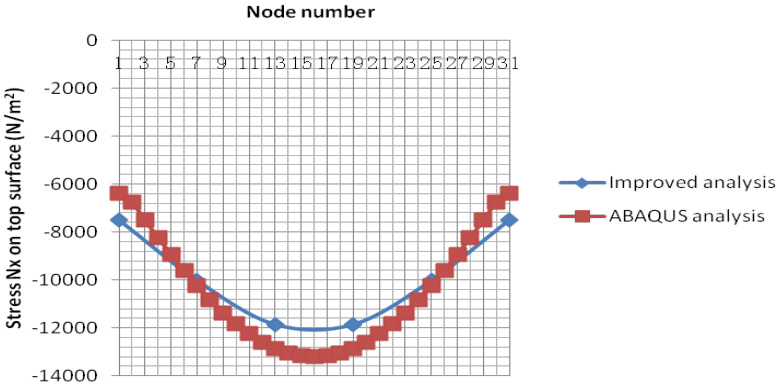

Node numb	1	7	13	19	25	31		Mean	RMS % error
Improved a	-7493.67	-10015.85	-11850.35	-11850.35	-10015.85	-7493.67		-9786.62	
ABAQUS ar	-6385.75	-10246.90	-12861.60	-12861.60	-10246.90	-6385.75		-9831.42	
ABS(A-I)	1107.92	231.05	1011.25	1011.25	231.05	1107.92		783.41	
% error	17.35	2.25	7.86	7.86	2.25	17.35		**7.97**	
(A-I)^2	1.23E+06	5.34E+04	1.02E+06	1.02E+06	5.34E+04	1.23E+06		767831.54	**8.91**

(a)

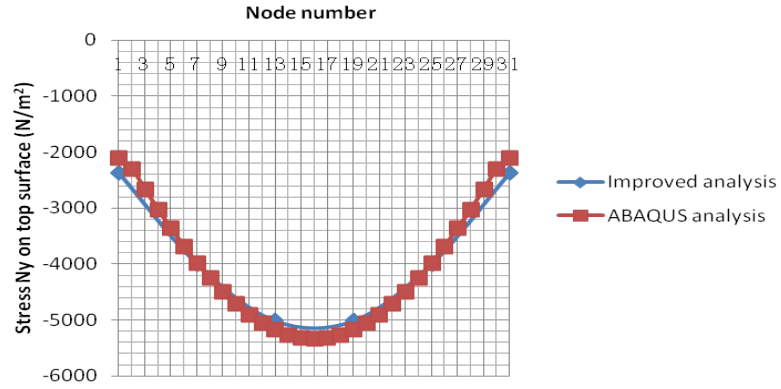

Node numb	1	7	13	19	25	31		Mean	RMS % error
Improved a	-2367.96	-3994.45	-5014.74	-5014.74	-3994.45	-2367.96		-3792.38	
ABAQUS ar	-2113.26	-3979.99	-5179.66	-5179.66	-3979.99	-2113.26		-3757.64	
ABS(A-I)	254.70	14.46	164.92	164.92	14.46	254.70		144.69	
% error	12.05	0.36	3.18	3.18	0.36	12.05		**3.85**	
(A-I)^2	6.49E+04	2.09E+02	2.72E+04	2.72E+04	2.09E+02	6.49E+04		30760.40	**4.67**

(b)

Figure 7.2: Comparison of stress (a) N_x and (b) N_y across the horizontal centre line of top surface of plate in improved postbuckling analysis and ABAQUS analysis, with longitudinal edges fixed in-plane.

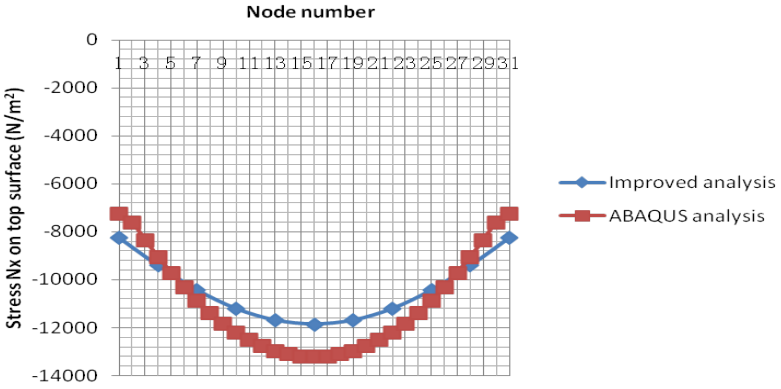

Node number	1	4	7	10	13	16	19	22	25	28	31		Mean	RMS % error
Improved analysis	-8.24E+03	-9.40E+03	-1.04E+04	-1.12E+04	-1.17E+04	-1.19E+04	-1.17E+04	-1.12E+04	-1.04E+04	-9.40E+03	-8.24E+03		-10341.80	
ABAQUS analysis	-7.22E+03	-9.05E+03	-1.09E+04	-1.22E+04	-1.30E+04	-1.32E+04	-1.30E+04	-1.22E+04	-1.09E+04	-9.05E+03	-7.22E+03		-10712.02	
ABS(A-I)	1011.04	344.28	455.13	982.69	1272.15	1363.15	1272.15	982.69	455.13	344.28	1011.04		863.07	
% error	13.99	3.80	4.18	8.06	9.82	10.32	9.82	8.06	4.18	3.80	13.99		**8.06**	
(A-I)^2	1.02E+06	1.19E+05	2.07E+05	9.66E+05	1.62E+06	1.86E+06	1.62E+06	9.66E+05	2.07E+05	1.19E+05	1.02E+06		883822.10	**8.78**

(a)

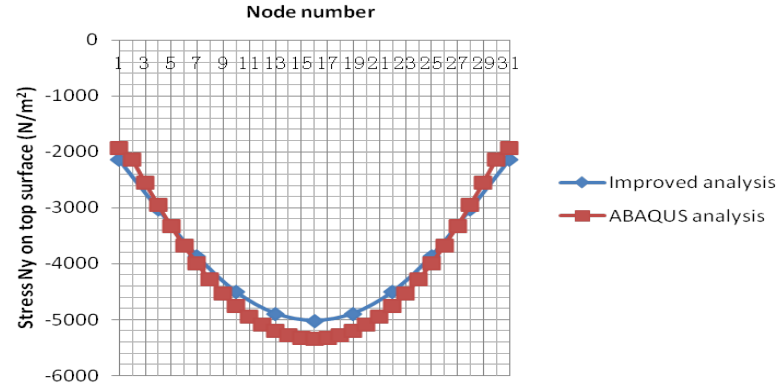

Node number	1	4	7	10	13	16	19	22	25	28	31		Mean	RMS % error
Improved analysis	-2135.61	-3020.19	-3863.74	-4503.94	-4888.47	-5014.74	-4888.47	-4503.94	-3863.74	-3020.19	-2135.61		-3803.51	
ABAQUS analysis	-1931.37	-2947.01	-3993.89	-4752.93	-5194.26	-5337.20	-5194.26	-4752.93	-3993.89	-2947.01	-1931.37		-3906.92	
ABS(A-I)	204.24	73.18	130.15	248.99	305.79	322.46	305.79	248.99	130.15	73.18	204.24		204.29	
% error	10.57	2.48	3.26	5.24	5.89	6.04	5.89	5.24	3.26	2.48	10.57		**5.23**	
(A-I)^2	4.17E+04	5.36E+03	1.69E+04	6.20E+04	9.35E+04	1.04E+05	9.35E+04	6.20E+04	1.69E+04	5.36E+03	4.17E+04		49363.56	**5.69**

(b)

Figure 7.3: Comparison of stress (a) N_x and (b) N_y across the vertical centre line of top surface of plate in improved postbuckling analysis and ABAQUS analysis, with longitudinal edges fixed in-plane.

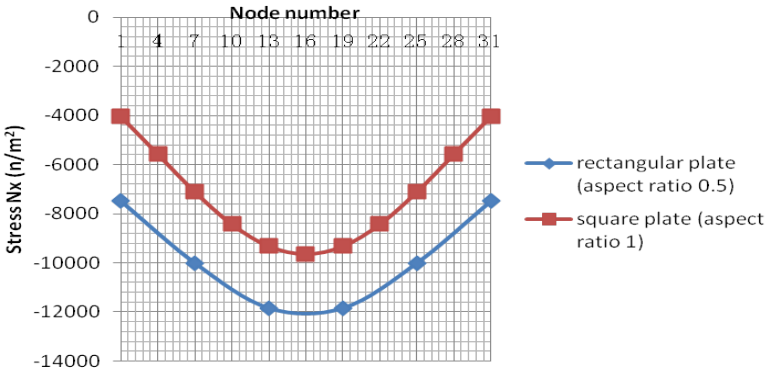

Figure 7.4: Comparison of stress N_x across the horizontal centre line of top surface of plate between square plate and rectangular plate with aspect ratio 0.5 in improved postbuckling analysis

the square plate (1325.6N/m). Therefore, for the plates with the same material properties and applied loading, the 'shorter' rectangular plate has greater in-plane stresses than the square plate (see Figure 7.4).

7.1.3 Results and discussion for isotropic plate with aspect ratio 1.5

Figure 7.5 shows the distribution of longitudinal stress N_x and transverse stress N_y on the top surface of the rectangular plate with aspect ratio 1.5. Figures 7.6 and 7.7 provide a quantitative comparison of stress N_x and stress N_y across the horizontal centre line and vertical centre line. Improved postbuckling analysis gives good agreement with ABAQUS results and the improved postbuckling analysis has therefore been validated for the analysis of a rectangular plate with aspect ratio 1.5.

In contrast to the square plate and the rectangular plate with aspect ratio 0.5, the plate with aspect ratio 1.5 shows two rectangular patterns on the surface. The critical buckling load was found with half-wavelength λ equal to half the length of the plate. For the plate with aspect ratio 1.5, the critical buckling load has been calculated as 1438.4N/m which is greater than that of the square

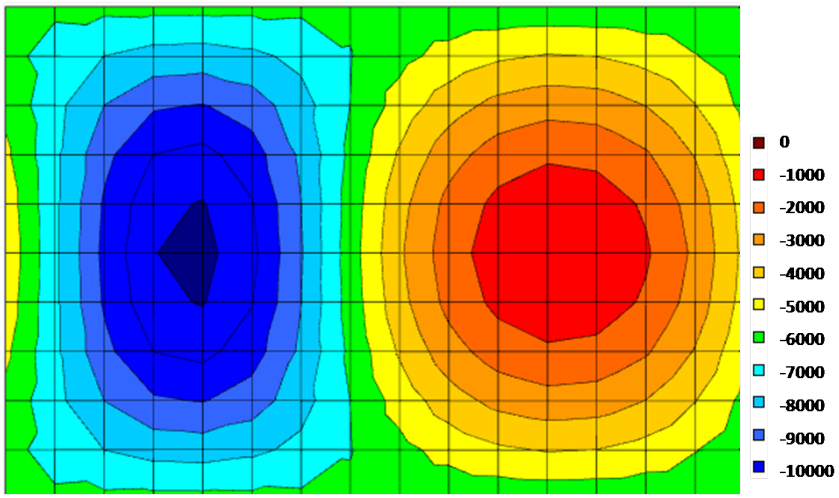
0
-1000
-2000
-3000
-4000
-5000
-6000
-7000
-8000
-9000
-10000

(a)

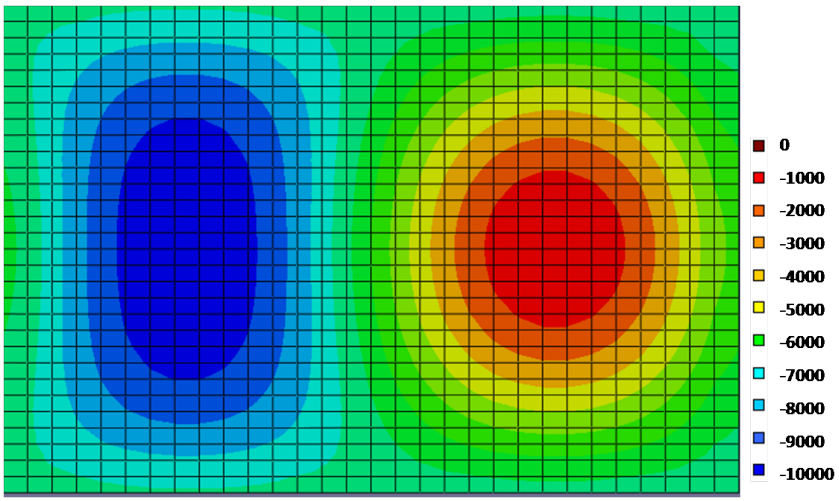
0
-1000
-2000
-3000
-4000
-5000
-6000
-7000
-8000
-9000
-10000

(b)

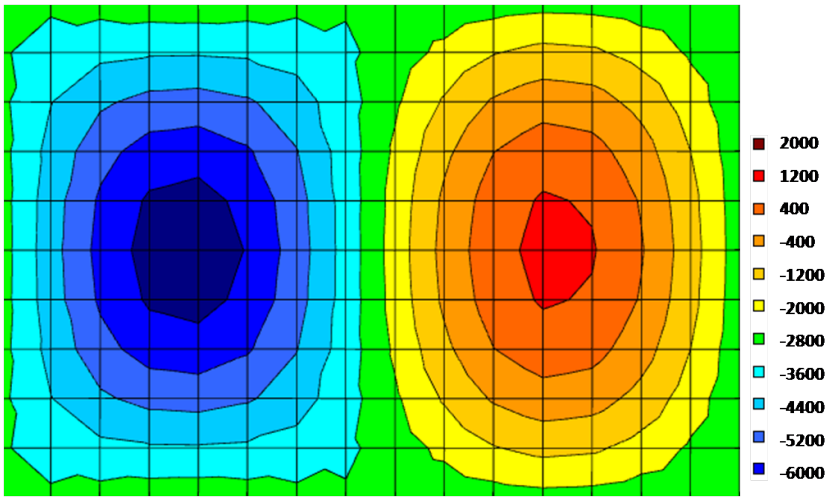

(c)

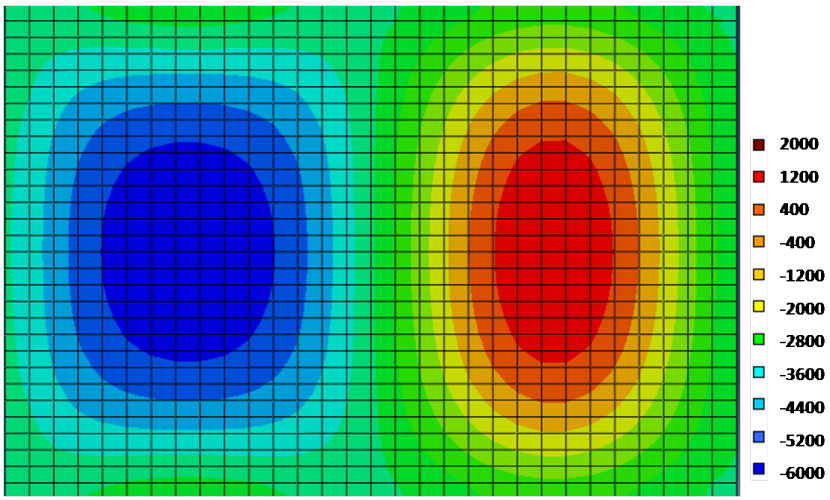

(d)

Figure 7.5: Variation of stress N_x across the top surface of plate in (a) Nx in improved postbuckling analysis, (b) Nx in ABAQUS analysis, (c) Ny in improved postbuckling analysis and (d) Ny in ABAQUS analysis, with all edges simply supported against out-of-plane deflection and the longitudinal edges fixed in-plane.

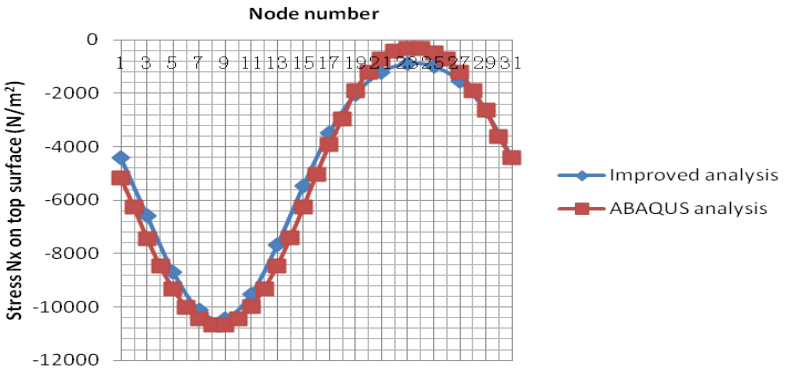

Node number	1	3	5	7	9	11	13	15		Mean	RMS % error
Improved analysis	-4415.43	-6577.21	-8680.58	-1.01E+04	-1.04E+04	-9520.08	-7673.72	-5468.32			
ABAQUS analysis	-5168.43	-7426.91	-9328.00	-1.05E+04	-1.07E+04	-9994.40	-8453.16	-6263.85			
Node number	17	19	21	23	25	27	29	31			
Improved analysis	-3471.61	-2028.84	-1203.09	-887.67	-989.70	-1543.68	-2671.06	-4415.43		-5006.78	
ABAQUS analysis	-3914.03	-1887.69	-702.49	-308.33	-477.60	-1194.05	-2643.59	-4421.73		-5207.56	
ABS(A-I)	753.00	849.70	647.42	331.00	243.70	474.32	779.44	795.53			
	442.42	141.15	500.60	579.34	512.10	349.63	27.47	6.30		464.57	
% error	14.57	11.44	6.94	3.17	2.28	4.75	9.22	12.70			
	11.30	7.48	71.26	187.90	107.22	29.28	1.04	0.14		**8.92**	
(A-I)^2	5.67E+05	7.22E+05	4.19E+05	1.10E+05	5.94E+04	2.25E+05	6.08E+05	6.33E+05			
	1.96E+05	1.99E+04	2.51E+05	3.36E+05	2.62E+05	1.22E+05	7.54E+02	3.97E+01		2.83E+05	**10.22**

(a)

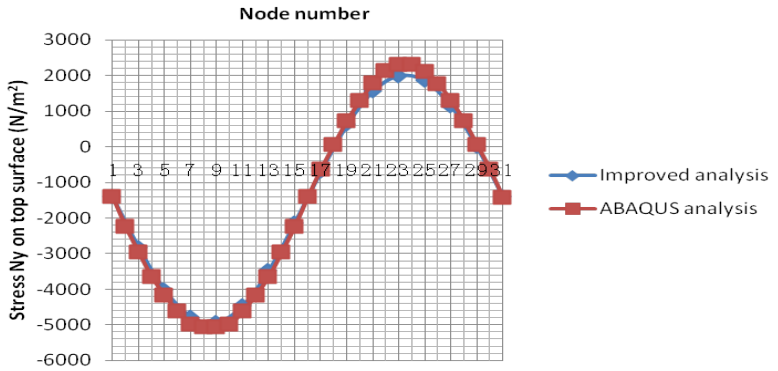

Node number	1	3	5	7	9	11	13	15		Mean	RMS % error
Improved analysis	-1402.57	-2829.98	-4025.33	-4770.76	-4927.25	-4465.28	-3471.63	-2129.78			
ABAQUS analysis	-1389.60	-2953.87	-4162.26	-4974.47	-5056.15	-4606.63	-3635.11	-2226.33			
Node number	17	19	21	23	25	27	29	31			
Improved analysis	-680.46	625.73	1571.65	2005.41	1858.91	1155.02	5.32	-1402.57		-1430.22	
ABAQUS analysis	-628.39	737.66	1783.60	2310.97	2129.26	1303.14	62.56	-1423.08		-1420.54	
ABS(A-I)	12.97	123.89	136.93	203.71	128.90	141.35	163.48	96.55			
	52.07	111.93	211.95	305.56	270.35	148.12	57.24	20.51		136.59	
% error	0.93	4.19	3.29	4.10	2.55	3.07	4.50	4.34			
	8.29	15.17	11.88	13.22	12.70	11.37	91.50	1.44		**9.62**	
(A-I)^2	1.68E+02	1.53E+04	1.88E+04	4.15E+04	1.66E+04	2.00E+04	2.67E+04	9.32E+03			
	2.71E+03	1.25E+04	4.49E+04	9.34E+04	7.31E+04	2.19E+04	3.28E+03	4.20E+02		2.50E+04	**11.14**

(b)

Figure 7.6: Comparison of stress (a) N_x and (b) N_y across the horizontal centre line of top surface of plate in improved postbuckling analysis and ABAQUS analysis, with longitudinal edges fixed in-plane.

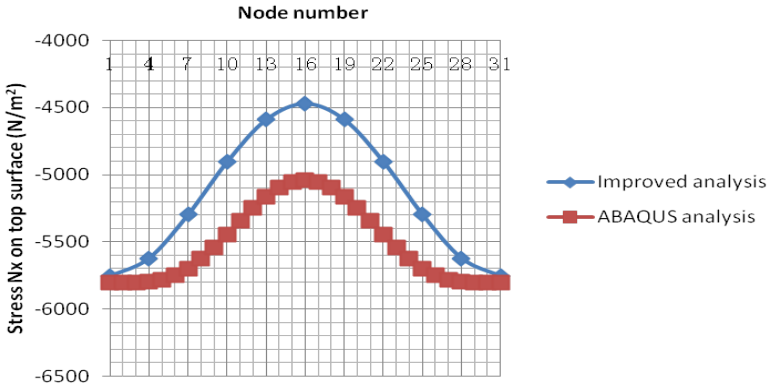

Node number	1	4	7	10	13	16	19	22	25	28	31		Mean	RMS % error
Improved analysis	-1612.14	-1604.76	-1550.44	-1481.66	-1426.21	-1405.12	-1426.21	-1481.66	-1550.44	-1604.76	-1612.14		-1523.23	
ABAQUS analysis	-1643.00	-1631.81	-1600.81	-1558.01	-1519.45	-1503.00	-1519.45	-1558.01	-1600.81	-1631.81	-1643.00		-1582.65	
ABS(A-I)	30.86	27.05	50.37	76.35	93.24	97.88	93.24	76.35	50.37	27.05	30.86		59.42	
% error	1.88	1.66	3.15	4.90	6.14	6.51	6.14	4.90	3.15	1.66	1.88		3.75	
(A-I)^2	952.21	731.72	2536.96	5829.38	8694.32	9579.61	8694.32	5829.38	2536.96	731.72	952.21		4278.98	4.13

(a)

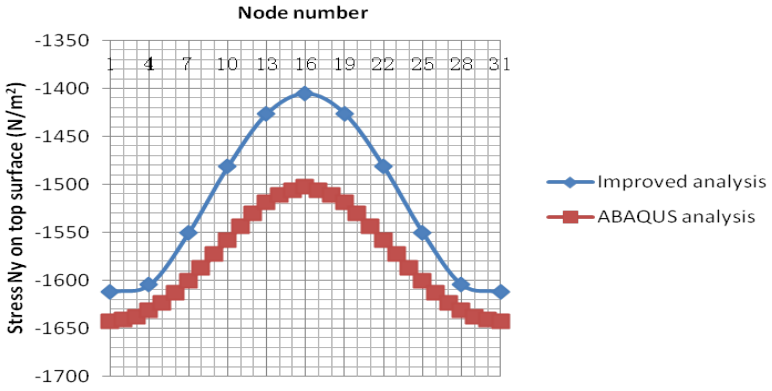

Node number	1	4	7	10	13	16	19	22	25	28	31		Mean	RMS % error
Improved analysis	-5758.13	-5624.03	-5298.95	-4904.86	-4589.63	-4469.96	-4589.63	-4904.86	-5298.95	-5624.03	-5758.13		-5165.56	
ABAQUS analysis	-5802.70	-5800.18	-5698.34	-5444.09	-5163.35	-5041.60	-5163.35	-5444.09	-5698.34	-5800.18	-5802.70		-5532.63	
ABS(A-I)	44.57	176.15	399.39	539.23	573.72	571.64	573.72	539.23	399.39	176.15	44.57		367.07	
% error	0.77	3.04	7.01	9.90	11.11	11.34	11.11	9.90	7.01	3.04	0.77		6.63	
(A-I)^2	1.99E+03	3.10E+04	1.60E+05	2.91E+05	3.29E+05	3.27E+05	3.29E+05	2.91E+05	1.60E+05	3.10E+04	1.99E+03		177423.20	7.61

(b)

Figure 7.7: Comparison of stress (a) N_x and (b) N_y across the vertical centre line of top surface of plate in improved postbuckling analysis and ABAQUS analysis, with longitudinal edges fixed in-plane.

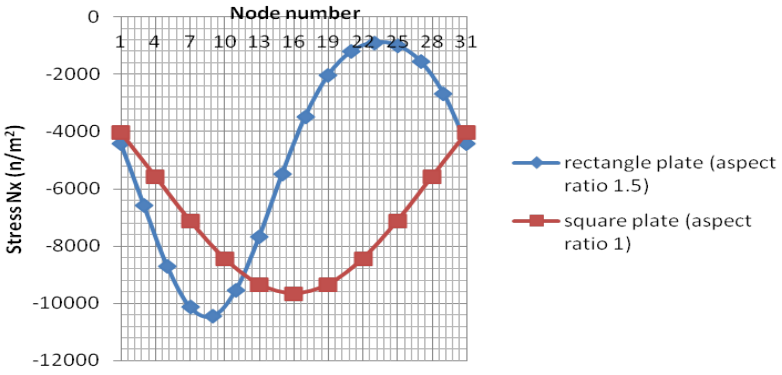

Figure 7.8: Comparison of stress N_x across the horizontal centre line of top surface of plate between square plate and rectangular plate with aspect ratio 1.5 in improved postbuckling analysis

plate (1325.6N/m) but much lower than that of the rectangular plate with aspect ratio 0.5 (2071.2N/m). Figure 7.8 gives the quantitative comparison of stress N_x across the horizontal centre lines of the square plate and the rectangular plate with aspect ratio 1.5. It is apparently seem that for rectangular plate with aspect ratio 1.5, the maximum compressive stress appears at 1/4 of length while the minimum stress appears at 3/4 of length. This is because the stress on the top surface is dominated by the through-thickness effects, which are compressive over the first half of the length and tensile over the remainder. However, for the square plate with whatever edge condition, the maximum compressive stress always appears at the middle of the plate.

7.2 Investigation of anisotropic composite plates

7.2.1 Introduction

In the previous chapter and sections above, the accuracy of the improved postbuckling analysis for a square isotropic square plate with different edge conditions and for a rectangular plate with different aspect ratios has been validated by comparing with ABAQUS results. However, the isotropic plate model leads to the

absence of out-of-plane components w_{ic}, ψ_{ic}, stiffness A_{16}, A_{26} and all stiffness B_{ij}, and all components of ϵ_{xyij} in the stiffness matrix. Therefore, the test of an isotropic plate is only a partial evaluation of the improved postbuckling analysis. To test the improved postbuckling analysis fully, it is necessary to test an anisotropic composite plate which enables these variables to be non-zero in the analysis. In this section, two composite laminates are tested including a symmetric, balanced laminate and an unsymmetric, unbalanced laminate. The first composite model enables involvement of the out-of-plane components w_{ic}, ψ_{ic} and ϵ_{xyiS}, while the second composite model leads to all previously absent variables being non-zero. The composite plates which will be used in this section are square plates under compressive loading with top and bottom edges fixed. The length of the plate is 0.3m and the compressive load (50000N/m) is applied on the left and right edges. For both tests, only the distributions of longitudinal stress N_x and transverse stress N_y on the top surface of the plate in calculation cycle 5 will be evaluated.

7.2.2 Results and discussion for symmetric balanced laminate

A symmetric balanced composite plate is used for analysis in this section. The length of the square plate is 0.3m and the thickness is 0.002m. The composite plate has eight symmetric layers (with equal thickness 0.25mm) which have ply angles [0, 45, -45, 90, 90, -45, 45, 0] respectively. The ply properties of the laminate are given as E_{11}=131kNmm^{-2}, E_{12}=6.41kNmm^{-2}, E_{22}=1.30kNmm^{-2}, G_{13}=6.41kNmm^{-2}, G_{23}=6.41kNmm^{-2} and $\nu_{12} = 0.38$. Uniform compressive stresses are applied on both left and right edges of the plate.

Figures 7.9 and 7.10 show the distribution of longitudinal stresses N_x and transverse stresses N_y on the top surface of the plate. In the ABAQUS results, the distribution pattern is skewed and so the pattern is less symmetric than that of the isotropic plate. However, in improved postbuckling analysis the pattern remains symmetric, like that of the isotropic plate and shows slight skewing which is not apparent from the plot but can only be seen from stress values. Figures

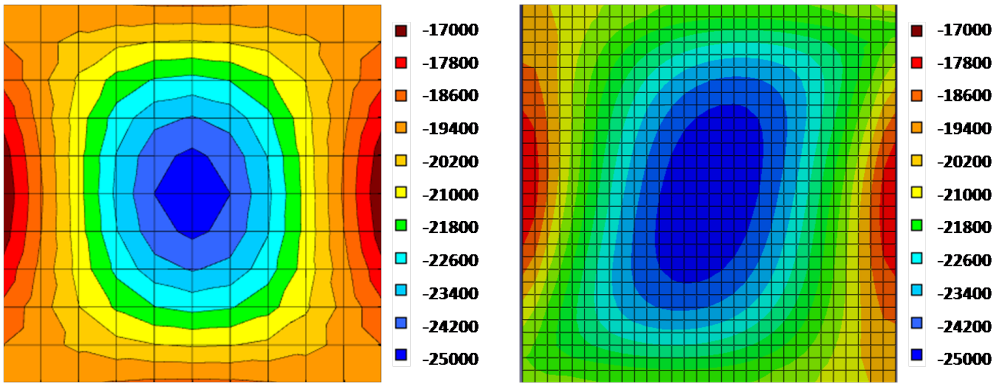

(a) (b)

Figure 7.9: Variation of stress N_x across the top surface of plate in (a) improved postbuckling analysis and (b) ABAQUS analysis, with all edges simply supported against out-of-plane deflection and the longitudinal edges fixed in-plane.

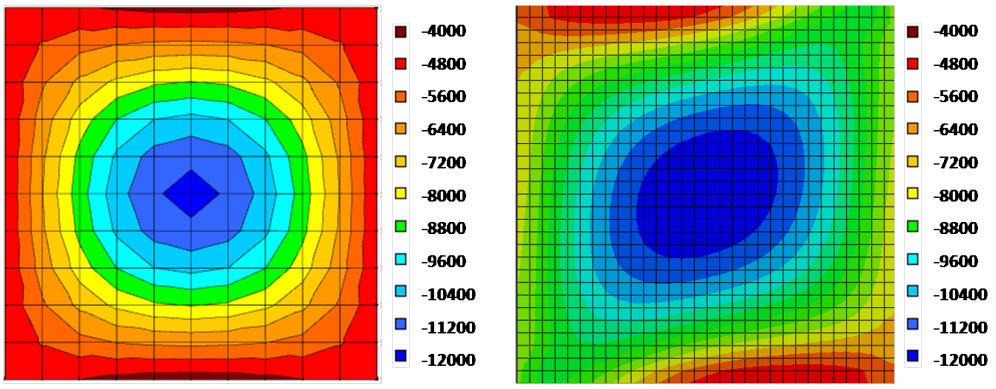

(a) (b)

Figure 7.10: Variation of stress N_y across the top surface of plate in (a) improved postbuckling analysis and (b) ABAQUS analysis, with all edges simply supported against out-of-plane deflection and the longitudinal edges fixed in-plane.

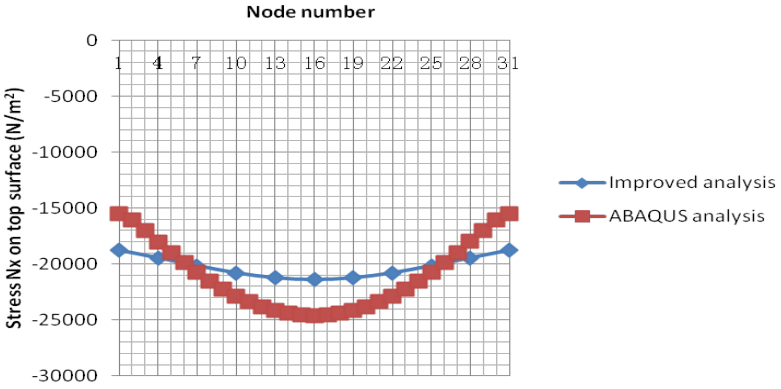

Node number	1	4	7	10	13	16	19	22	25	28	31		Mean	RMS % error
Improved analysis	-1.88E+04	-1.95E+04	-2.02E+04	-2.08E+04	-2.13E+04	-2.14E+04	-2.13E+04	-2.08E+04	-2.02E+04	-1.95E+04	-1.88E+04		-20217.75	
ABAQUS analysis	-1.55E+04	-1.80E+04	-2.07E+04	-2.29E+04	-2.42E+04	-2.46E+04	-2.42E+04	-2.29E+04	-2.07E+04	-1.80E+04	-1.55E+04		-20652.86	
ABS(A-I)	3272.38	1451.17	567.40	2052.47	2917.26	3193.36	2911.46	2042.98	557.71	1457.68	3275.23		2154.47	
% error	21.08	8.06	2.74	8.98	12.07	12.98	12.05	8.94	2.69	8.10	21.10		**10.43**	
(A-I)^2	1.07E+07	2.11E+06	3.22E+05	4.21E+06	8.51E+06	1.02E+07	8.48E+06	4.17E+06	3.11E+05	2.12E+06	1.07E+07		5624572.86	**11.48**

(a)

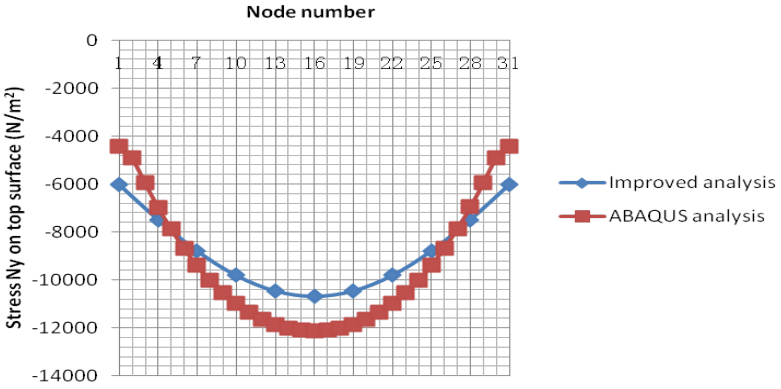

Node number	1	4	7	10	13	16	19	22	25	28	31		Mean	RMS % error
Improved analysis	-6021.44	-7485.44	-8784.78	-9801.52	-1.04E+04	-1.07E+04	-1.04E+04	-9801.52	-8784.78	-7485.44	-6021.44		-8704.59	
ABAQUS analysis	-4.42E+03	-6.96E+03	-9.40E+03	-1.10E+04	-1.18E+04	-1.21E+04	-1.18E+04	-1.10E+04	-9.40E+03	-6.96E+03	-4.42E+03		-9030.53	
ABS(A-I)	1598.29	521.70	613.28	1187.83	1397.31	1440.11	1397.31	1187.18	611.03	525.84	1602.90		1098.43	
% error	36.13	7.49	6.53	10.81	11.80	11.89	11.80	10.80	6.50	7.56	36.28		**12.16**	
(A-I)^2	2.55E+06	2.72E+05	3.76E+05	1.41E+06	1.95E+06	2.07E+06	1.95E+06	1.41E+06	3.73E+05	2.77E+05	2.57E+06		1383738.15	**13.03**

(b)

Figure 7.11: Comparison of stress (a) N_x and (b) N_y across the horizontal centre line of top surface of plate in improved postbuckling analysis and ABAQUS analysis, with longitudinal edges fixed in-plane.

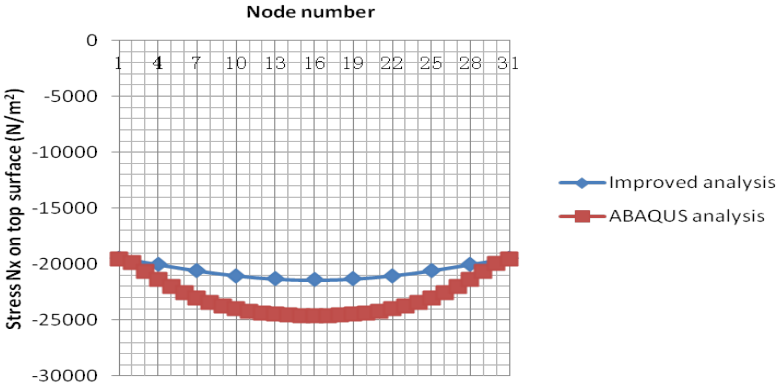

Node number	1	4	7	10	13	16	19	22	25	28	31		Mean	RMS % error
Improved analysis	-1.94E+04	-2.00E+04	-2.06E+04	-2.10E+04	-2.13E+04	-2.14E+04	-2.13E+04	-2.10E+04	-2.06E+04	-2.00E+04	-1.95E+04		-20563.06	
ABAQUS analysis	-1.95E+04	-2.14E+04	-2.31E+04	-2.40E+04	-2.45E+04	-2.46E+04	-2.45E+04	-2.40E+04	-2.31E+04	-2.14E+04	-1.96E+04		-22694.68	
ABS(A-I)	104.93	1374.49	2475.61	2998.06	3165.46	3193.36	3165.98	3002.45	2486.64	1391.03	89.77		2131.62	
% error	0.54	6.42	10.74	12.48	12.93	12.98	12.93	12.50	10.78	6.50	0.46		**9.39**	
(A-I)^2	1.10E+04	1.89E+06	6.13E+06	8.99E+06	1.00E+07	1.02E+07	1.00E+07	9.01E+06	6.18E+06	1.93E+06	8.06E+03		5854501.99	**10.66**

(a)

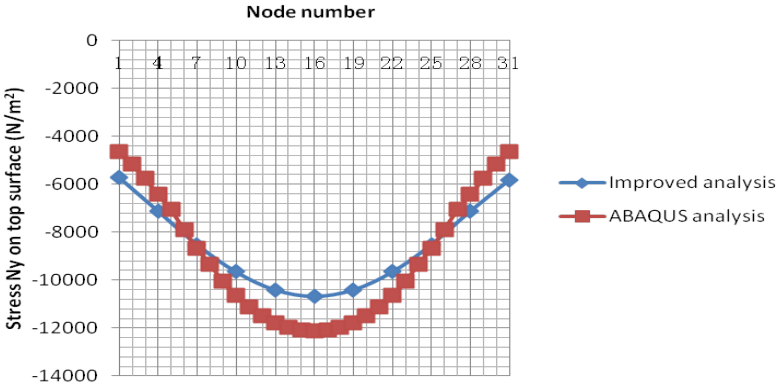

Node number	1	4	7	10	13	16	19	22	25	28	31		Mean	RMS % error
Improved analysis	-5730.99	-7137.44	-8526.51	-9659.96	-1.04E+04	-1.07E+04	-1.04E+04	-9660.65	-8524.88	-7134.83	-5831.95		-8517.55	
ABAQUS analysis	-4.63E+03	-6.42E+03	-8.68E+03	-1.07E+04	-1.18E+04	-1.21E+04	-1.18E+04	-1.07E+04	-8.68E+03	-6.42E+03	-4.63E+03		-8769.02	
ABS(A-I)	1099.89	713.04	156.59	997.46	1368.10	1440.11	1371.73	998.16	158.22	710.43	1200.85		928.60	
% error	23.75	11.10	1.80	9.36	11.62	11.89	11.64	9.36	1.82	11.06	25.93		**10.59**	
(A-I)^2	1.21E+06	5.08E+05	2.45E+04	9.95E+05	1.87E+06	2.07E+06	1.88E+06	9.96E+05	2.50E+04	5.05E+05	1.44E+06		1048455.54	**11.68**

(b)

Figure 7.12: Comparison of stress (a) N_x and (b) N_y across the vertical centre line of top surface of plate in improved postbuckling analysis and ABAQUS analysis, with longitudinal edges fixed in-plane.

7.11 and 7.12 give the quantitative comparison of stresses N_x and N_y which shows good agreement between improved postbuckling analysis and ABAQUS analysis. However these figures show the stress distributions across the horizontal and vertical centre lines and therefore not much skewing is seen in the ABAQUS results. To explore the skewing in ABAQUS analysis, Figure 7.13 plots the distribution of stress N_x along a horizontal line at a quarter width of plate. The curve of stress distribution for ABAQUS analysis shows an apparently unsymmetric pattern while for improved analysis the curve keeps symmetric. This clearly reveals that ABAQUS has some apparent skewing in the stress distributions whereas the improved analysis does not. The reasons for less skewing in improved postbuckling analysis will be analysed and discussed in Section 7.4. Figure 7.12 gives the quantitative comparison of stresses N_x and N_y which shows good agreement between improved postbuckling analysis and ABAQUS analysis.

7.2.3 Results and discussion for unsymmetric unbalanced laminate

To test the accuracy of the improved postbuckling analysis fully, an unsymmetric unbalanced composite plate has been tested in this section. The length and thickness of the square plate are 0.3m and 0.002m respectively, and the plate has eight layers with equal thickness 0.25mm for each one. The compressive stresses are applied on the left and right edges of plate and the amount of stress is 50000N/m which is the same as for the symmetric balanced composite. The ply angles are [0, 45, -45, 90, 90, 0, 0, 45] respectively for each layer from the top to the bottom of plate. The ply properties for this composite plate are given as E_{11}=131kNmm^{-2}, E_{12}=6.41kNmm^{-2}, E_{22}=13kNmm^{-2}, G_{13}=6.41kNmm^{-2}, G_{23}=6.41kNmm^{-2} and $\nu_{12} = 0.38$.

Figures 7.14 and 7.15 shows a comparison of the distribution of stresses N_x and N_y on the top surface of the plate between the improved postbuckling analysis and ABAQUS analysis. The contours of stress distribution from both analyses are similar, and therefore improved postbuckling analysis shows good correlation with ABAQUS results. Figures 7.16 and 7.17 show the quantitative comparison

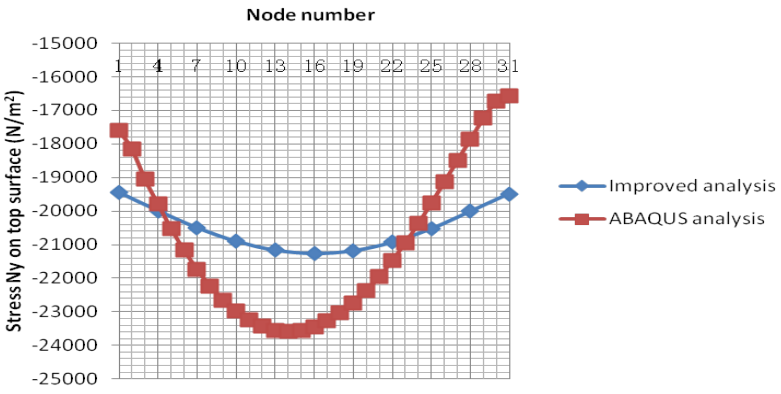

(a)

Node number	1	4	7	10	13	16	19	22	25	28	31	Mean	RMS % error
Improved analysis	-1.95E+04	-2.00E+04	-2.05E+04	-2.09E+04	-2.12E+04	-2.13E+04	-2.12E+04	-2.09E+04	-2.05E+04	-2.00E+04	-1.95E+04	-20485.95	
ABAQUS analysis	-1.76E+04	-1.98E+04	-2.17E+04	-2.30E+04	-2.35E+04	-2.34E+04	-2.27E+04	-2.15E+04	-1.98E+04	-1.79E+04	-1.66E+04	-20682.03	
ABS(A-I)	1852.34	197.44	1239.63	2095.32	2389.27	2193.36	1564.68	548.50	760.80	2141.38	2921.94	1627.70	
% error	10.52	1.00	5.70	9.11	10.15	9.36	6.88	2.55	3.85	11.98	17.64	**7.87**	
(A-I)^2	3.43E+06	3.90E+04	1.54E+06	4.39E+06	5.71E+06	4.81E+06	2.45E+06	3.01E+05	5.79E+05	4.59E+06	8.54E+06	3306162.18	**8.79**

(b)

Figure 7.13: Comparison of stress (a) N_x across the horizontal line at a quarter along the width of top surface of plate in improved postbuckling analysis and ABAQUS analysis, with longitudinal edges fixed in-plane.

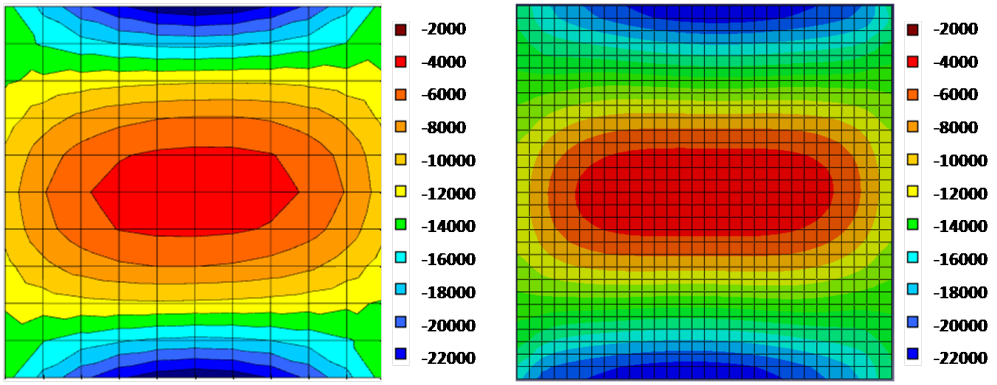

(a) (b)

Figure 7.14: Variation of stress N_x across the top surface of plate in (a) improved postbuckling analysis and (b) ABAQUS analysis, with all edges simply supported against out-of-plane deflection and the longitudinal edges fixed in-plane.

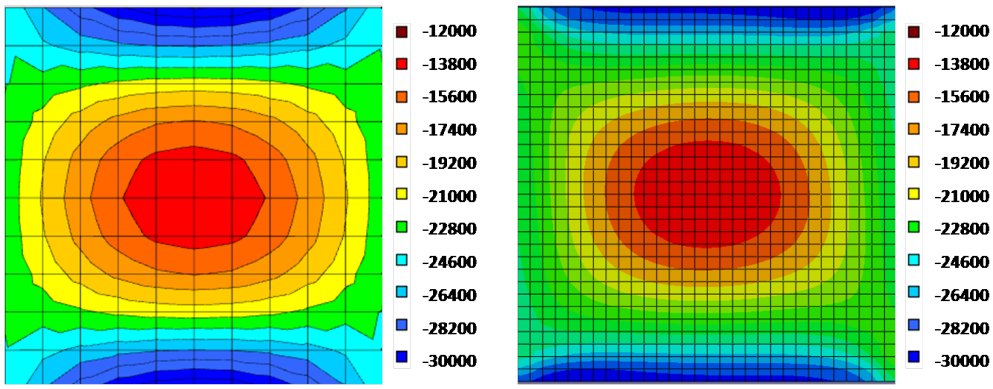

(a) (b)

Figure 7.15: Variation of stress N_y across the top surface of plate in (a) improved postbuckling analysis and (b) ABAQUS analysis, with all edges simply supported against out-of-plane deflection and the longitudinal edges fixed in-plane.

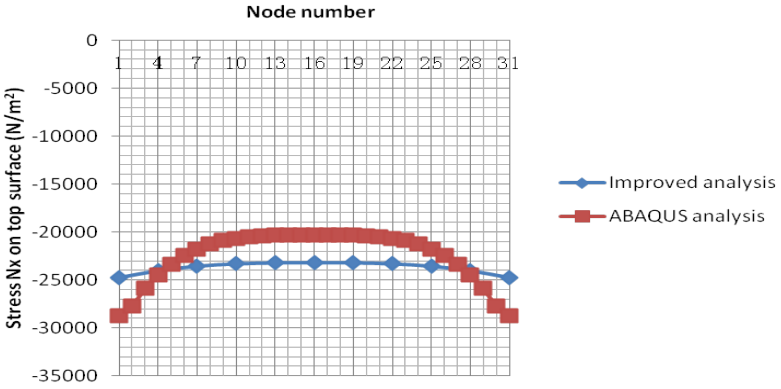

Node number	1	4	7	10	13	16	19	22	25	28	31		Mean	RMS % error
Improved analysis	-2.48E+04	-2.40E+04	-2.36E+04	-2.33E+04	-2.32E+04	-2.32E+04	-2.32E+04	-2.33E+04	-2.36E+04	-2.40E+04	-2.48E+04		-23721.82	
ABAQUS analysis	-2.87E+04	-2.45E+04	-2.17E+04	-2.06E+04	-2.03E+04	-2.03E+04	-2.03E+04	-2.06E+04	-2.18E+04	-2.45E+04	-2.87E+04		-22925.66	
ABS(A-I)	3969.48	441.28	1814.92	2674.15	2869.05	2876.89	2871.83	2672.81	1806.88	449.29	3968.68		2401.39	
% error	13.82	1.80	8.34	12.96	14.10	14.17	14.12	12.95	8.31	1.84	13.82		**10.47**	
(A-I)^2	1.58E+07	1.95E+05	3.29E+06	7.15E+06	8.23E+06	8.28E+06	8.25E+06	7.14E+06	3.26E+06	2.02E+05	1.58E+07		7046626.79	**11.58**

(a)

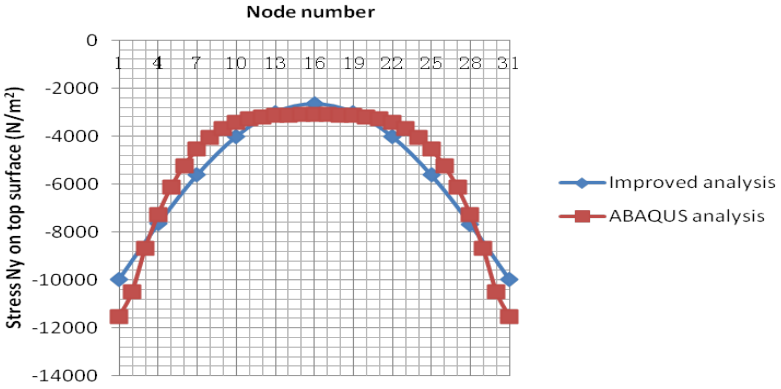

Node number	1	4	7	10	13	16	19	22	25	28	31		Mean	RMS % error
Improved analysis	-9.96E+03	-7.66E+03	-5.62E+03	-4.02E+03	-3.01E+03	-2.66E+03	-3.01E+03	-4.02E+03	-5.62E+03	-7.67E+03	-9.96E+03		-5746.41	
ABAQUS analysis	-1.15E+04	-7.28E+03	-4.55E+03	-3.44E+03	-3.14E+03	-3.11E+03	-3.14E+03	-3.44E+03	-4.56E+03	-7.28E+03	-1.15E+04		-5725.66	
ABS(A-I)	1567.18	386.33	1071.31	581.98	136.18	451.06	131.87	583.65	1067.67	383.84	1560.15		720.11	
% error	13.59	5.31	23.55	16.92	4.34	14.51	4.20	16.97	23.44	5.27	13.54		**12.58**	
(A-I)^2	2.46E+06	1.49E+05	1.15E+06	3.39E+05	1.85E+04	2.03E+05	1.74E+04	3.41E+05	1.14E+06	1.47E+05	2.43E+06		763006.22	**15.26**

(b)

Figure 7.16: Comparison of stress (a) N_x and (b) N_y across the horizontal centre line of top surface of plate in improved postbuckling analysis and ABAQUS analysis, with longitudinal edges fixed in-plane.

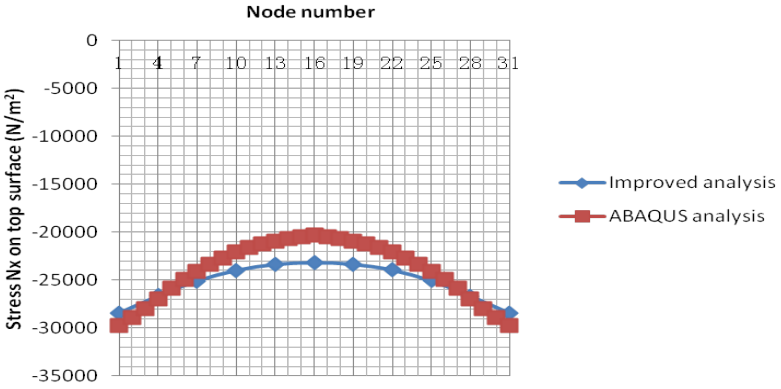

Node number	1	4	7	10	13	16	19	22	25	28	31		Mean	RMS % error
Improved analysis	-2.84E+04	-2.66E+04	-2.51E+04	-2.40E+04	-2.34E+04	-2.32E+04	-2.34E+04	-2.40E+04	-2.51E+04	-2.67E+04	-2.84E+04		-25290.09	
ABAQUS analysis	-2.98E+04	-2.70E+04	-2.41E+04	-2.21E+04	-2.09E+04	-2.03E+04	-2.09E+04	-2.21E+04	-2.41E+04	-2.70E+04	-2.98E+04		-24387.52	
ABS(A-I)	1357.75	375.68	943.59	1903.74	2432.07	2876.89	2424.45	1873.15	931.03	365.45	1357.75		1531.05	
% error	4.56	1.39	3.91	8.62	11.61	14.17	11.58	8.48	3.86	1.35	4.56		**6.28**	
(A-I)^2	1.84E+06	1.41E+05	8.90E+05	3.62E+06	5.91E+06	8.28E+06	5.88E+06	3.51E+06	8.67E+05	1.34E+05	1.84E+06		2992834.94	**7.09**

(a)

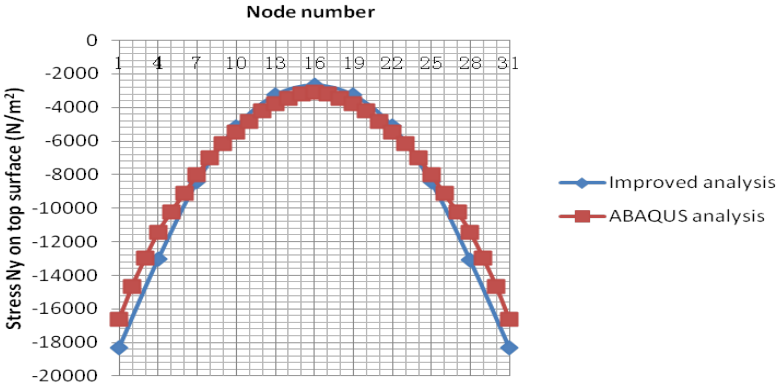

Node number	1	4	7	10	13	16	19	22	25	28	31		Mean	RMS % error
Improved analysis	-1.83E+04	-1.30E+04	-8.42E+03	-5.14E+03	-3.25E+03	-2.66E+03	-3.24E+03	-5.09E+03	-8.45E+03	-1.31E+04	-1.83E+04		-9000.77	
ABAQUS analysis	-1.66E+04	-1.14E+04	-8.01E+03	-5.48E+03	-3.81E+03	-3.11E+03	-3.81E+03	-5.48E+03	-8.01E+03	-1.14E+04	-1.66E+04		-8530.82	
ABS(A-I)	1687.98	1593.01	408.23	347.64	555.94	451.06	562.04	395.17	432.83	1671.36	1687.98		890.29	
% error	10.16	13.92	5.10	6.34	14.60	14.51	14.76	7.21	5.40	14.61	10.16		**10.44**	
(A-I)^2	2.85E+06	2.54E+06	1.67E+05	1.21E+05	3.09E+05	2.03E+05	3.16E+05	1.56E+05	1.87E+05	2.79E+06	2.85E+06		1135368.21	**12.49**

(b)

Figure 7.17: Comparison of stress (a) N_x and (b) N_y across the vertical centre line of top surface of plate in improved postbuckling analysis and ABAQUS analysis, with longitudinal edges fixed in-plane.

of stresses N_x and N_y which validates the accuracy of improved postbuckling analysis for a fully anisotropic plate. Further discussions for the unsymmetric unbalanced composite plate and comparison with analysis of the symmetric balanced composite plate will be made in Section 7.4.

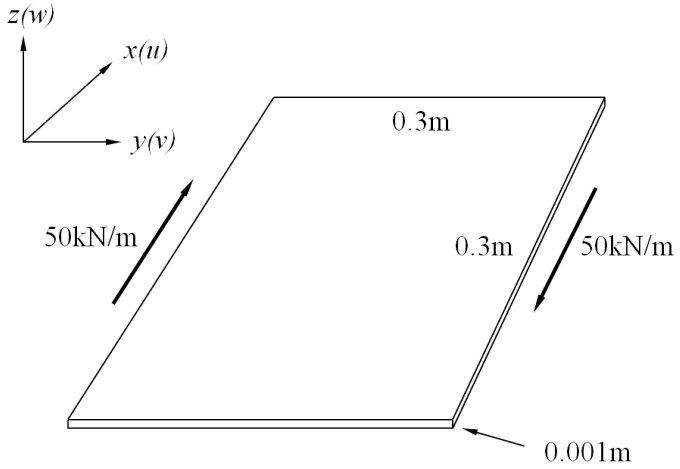

Figure 7.18: Geometry of plate and in-plane shear load assignment

7.3 Investigation of isotropic square plate with shear load

7.3.1 Introduction

To evaluate the postbuckling capacity of improved postbuckling analysis for various load conditions, an isotropic square plate with shear loading on both left and right edges has been tested in this section. Figure 7.18 shows the geometry of the isotropic plate and in-plane shear load on its left and right edges. The plate had width and length 0.3m, thickness 0.001m, Young's modulus 110kNmm^{-2}, Poisson's ratio 0.3 and the amount of shear load is 50kN/m for both edges with opposite directions as shown.

7.3.2 Results and discussions for isotropic square plate with shear load

Figures 7.19 and 7.20 show the distribution of longitudinal stress N_x and transverse stress N_y on the top surface of the plate for both improved postbuckling

analysis and ABAQUS analysis. The contour plots of N_x and N_y show poor agreement between improved postbuckling analysis and ABAQUS analysis. The maximum values of N_x and N_y appear in the middle of the plate in improved postbuckling analysis, however ABAQUS analysis shows a skewed patten in both N_x and N_y and therefore the maximum and minimum values of stress appear on the corner of the diagonals. Figures 7.21 and 7.22 show the quantitative evaluation of stresses between improved postbuckling analysis and ABAQUS analysis. ABAQUS analysis shows more complex variation in both N_x and N_y. In Figure 7.21 which demonstrates the stress distribution across the horizontal centre line, the ABAQUS stresses decrease a small amount then increase from the edge to the middle of the plate. But in the improved postbuckling analysis, the stresses increases monotonically from the edge to the middle of the plate. This is due to the constraints on the left and right edges of plate in ABAQUS that both edges are forced to keep straight throughout the analysis. However, in improved postbuckling analysis these constraints are released. In Figure 7.22 which demonstrates the stress distributions across the vertical centre line, the ABAQUS analysis also shows a more complex variation of stresses than improved postbuckling analysis. Stress N_y reaches its maximum value at around 1/4 and 3/4 width of the plate, then decreases a small amount to the middle. But in improved postbuckling analysis, stress increases from the edge to the middle like the variation of stress N_x. The values of error in Figures 7.21 and 7.22 indicate that improved postbuckling analysis gives acceptable agreement with ABAQUS results in N_x, but poor agreement in N_y. Overall, the comparison of isotropic square plate in shear load is not acceptable and unsatisfied. The evaluation and discussion for the poor agreement for this type of problem will be given in the following section.

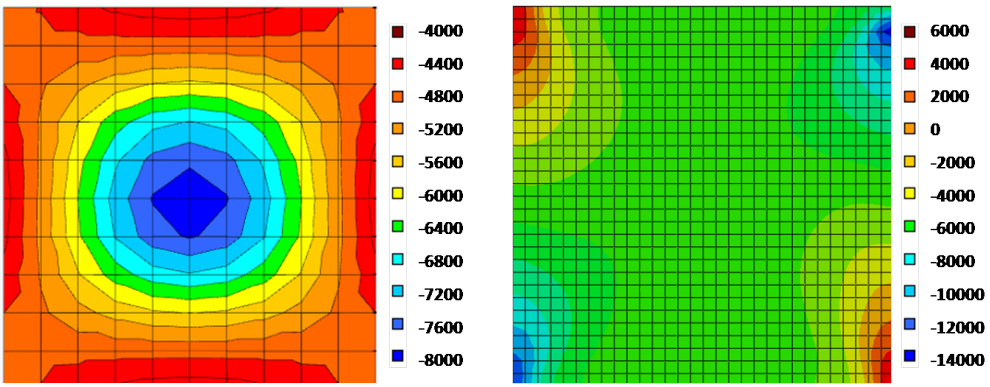

(a) (b)

Figure 7.19: Variation of stress N_x across the top surface of plate with shear loading in (a) improved postbuckling analysis and (b) ABAQUS analysis, with all edges simply supported against out-of-plane deflection and the longitudinal edges fixed in-plane.

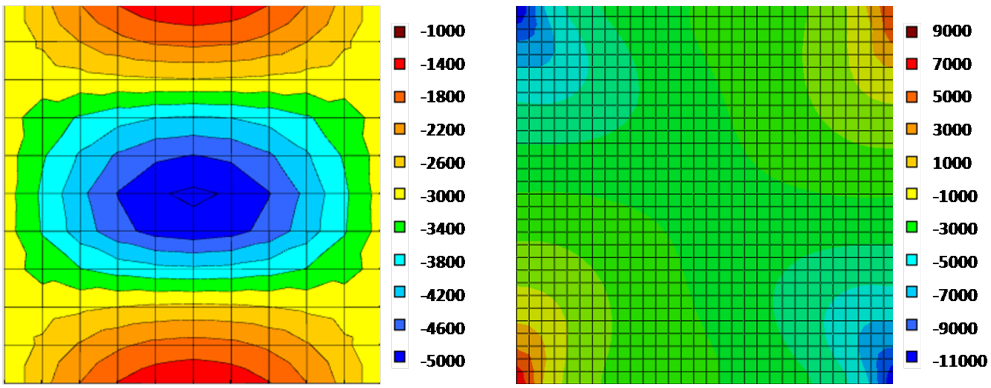

(a) (b)

Figure 7.20: Variation of stress N_y across the top surface of plate with shear loading in (a) improved postbuckling analysis and (b) ABAQUS analysis, with all edges simply supported against out-of-plane deflection and the longitudinal edges fixed in-plane.

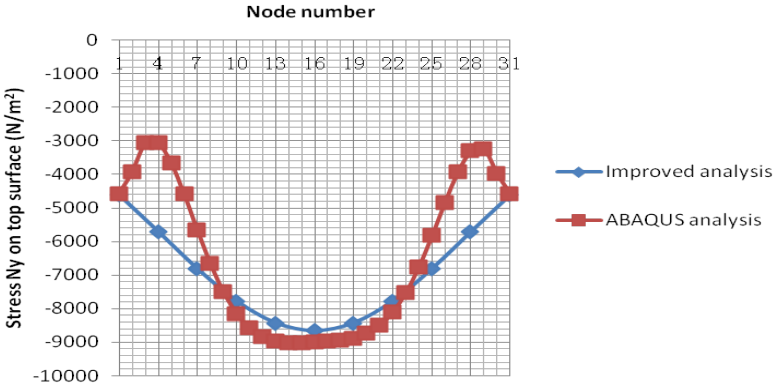

Node number	1	4	7	10	13	16	19	22	25	28	31		Mean	RMS % error
Improved analysis	-4615.80	-5706.38	-6813.03	-7774.19	-8429.97	-8662.94	-8429.97	-7774.19	-6813.03	-5706.38	-4615.80		-6849.25	
ABAQUS analysis	-4568.30	-3056.39	-5646.99	-8143.00	-8977.76	-9002.07	-8874.16	-8102.35	-5824.76	-3299.03	-4571.84		-6369.69	
ABS(A-I)	47.50	2649.99	1166.04	368.81	547.79	339.13	444.19	328.16	988.28	2407.35	43.96		848.29	
% error	1.04	86.70	20.65	4.53	6.10	3.77	5.01	4.05	16.97	72.97	0.96		**13.32**	
(A-I)^2	2.26E+03	7.02E+06	1.36E+06	1.36E+05	3.00E+05	1.15E+05	1.97E+05	1.08E+05	9.77E+05	5.80E+06	1.93E+03		1455856.96	**18.94**

(a)

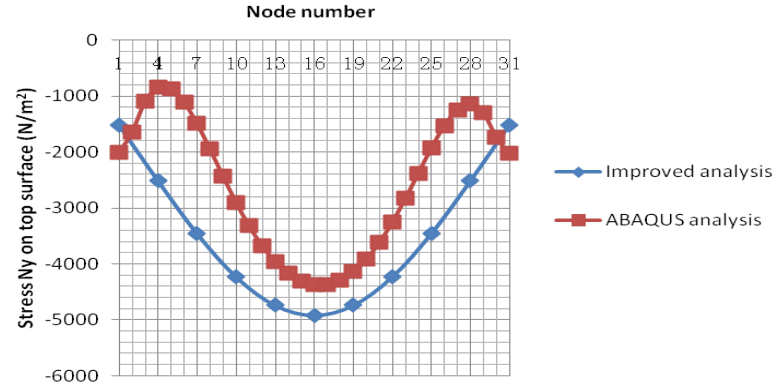

Node number	1	4	7	10	13	16	19	22	25	28	31		Mean	RMS % error
Improved analysis	-1513.99	-2515.02	-3456.65	-4229.98	-4738.64	-4916.12	-4738.64	-4229.98	-3456.65	-2515.02	-1513.99		-3438.61	
ABAQUS analysis	-1999.04	-841.33	-1488.91	-2898.90	-3959.17	-4373.38	-4138.15	-3250.60	-1926.69	-1140.61	-2028.86		-2549.60	
ABS(A-I)	485.05	1673.69	1967.74	1331.08	779.47	542.74	600.49	979.38	1529.96	1374.41	514.87		1070.81	
% error	24.26	198.93	132.16	45.92	19.69	12.41	14.51	30.13	79.41	120.50	25.38		**42.00**	
(A-I)^2	2.35E+05	2.80E+06	3.87E+06	1.77E+06	6.08E+05	2.95E+05	3.61E+05	9.59E+05	2.34E+06	1.89E+06	2.65E+05		1399737.00	**46.40**

(b)

Figure 7.21: Comparison of stress (a) N_x and (b) N_y across the horizontal centre line of top surface of plate in improved postbuckling analysis and ABAQUS analysis, with longitudinal edges fixed in-plane.

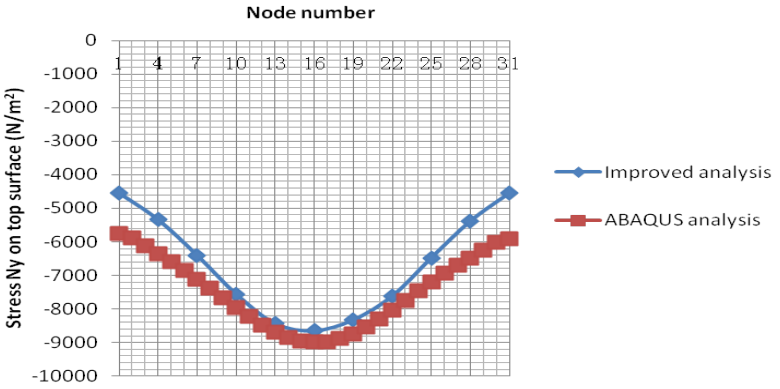

Node number	1	4	7	10	13	16	19	22	25	28	31		Mean	RMS % error
Improved analysis	-4550.25	-5344.63	-6407.13	-7565.62	-8445.33	-8662.94	-8336.15	-7625.35	-6485.54	-5388.96	-4550.25		-6669.29	
ABAQUS analysis	-5770.94	-6366.88	-7122.45	-7969.57	-8692.97	-9002.07	-8752.89	-8048.04	-7206.61	-6483.61	-5910.35		-7393.31	
ABS(A-I)	1220.69	1022.26	715.32	403.95	247.64	339.13	416.74	422.69	721.07	1094.66	1360.10		724.02	
% error	21.15	16.06	10.04	5.07	2.85	3.77	4.76	5.25	10.01	16.88	23.01		**9.79**	
(A-I)^2	1.49E+06	1.05E+06	5.12E+05	1.63E+05	6.13E+04	1.15E+05	1.74E+05	1.79E+05	5.20E+05	1.20E+06	1.85E+06		664245.89	**11.02**

(a)

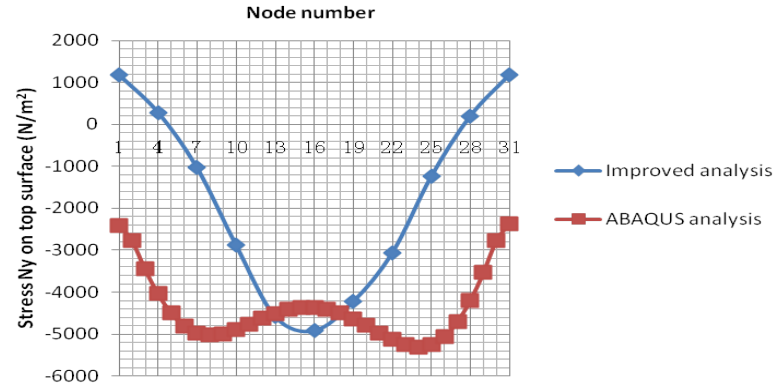

Node number	1	4	7	10	13	16	19	22	25	28	31		Mean	RMS % error
Improved analysis	1170.41	276.06	-1042.77	-2884.63	-4578.63	-4916.12	-4221.62	-3064.47	-1243.02	192.14	1170.41		-1740.20	
ABAQUS analysis	-2409.87	-4043.67	-4981.93	-4898.00	-4514.31	-4373.38	-4641.65	-5139.52	-5257.31	-4201.22	-2367.55		-4257.13	
ABS(A-I)	3580.28	4319.73	3939.16	2013.37	64.32	542.74	420.03	2075.05	4014.29	4393.36	3537.95		2627.30	
% error	148.57	106.83	79.07	41.11	1.42	12.41	9.05	40.37	76.36	104.57	149.44		**61.72**	
(A-I)^2	1.28E+07	1.87E+07	1.55E+07	4.05E+06	4.14E+03	2.95E+05	1.76E+05	4.31E+06	1.61E+07	1.93E+07	1.25E+07		9433022.59	**72.15**

(b)

Figure 7.22: Comparison of stress (a) N_x and (b) N_y across the vertical centre line of top surface of plate in improved postbuckling analysis and ABAQUS analysis, with longitudinal edges fixed in-plane.

7.4 Error evaluation and further discussion of results

In this chapter, other cases including isotropic rectangular plate with different aspect ratios, a symmetric balanced composite plate, an unsymmetric unbalanced composite plate and an isotropic square plate with shear have been tested and analysed. These results and plots provide a full investigation and validation of improved postbuckling analysis. The improved postbuckling analysis shows good agreement in these different cases. However, the quantitative study of these cases also shows some error and inaccuracy of the improved analysis which are now evaluated and discussed.

For an isotropic rectangular plate with different aspect ratios, improved postbuckling analysis shows good agreement with ABAQUS results in both contour plots of stress distribution and quantitative comparison of stresses. In improved postbuckling analysis, the isotropic plate problem leads to non-zero terms w_{is}, $u_{i(0,C)}$, $v_{i(0,C)}$, $N_{xi(0,C)}$ and $N_{yi(0,C)}$. The absence of all the other terms simplifies the governing equilibrium equation (5.22) and gives a symmetric pattern about the horizontal centre line for both stresses N_x and N_y. The results in section 7.1 indicated that for an isotropic plate with the same material properties, edge conditions and applied load, the two rectangular plate give greater critical buckling load than the square plate, particularly in the case of the plate with aspect ratio 0.5. The evidence can be found from classic literature by Timoshenko and Gere [32], who gave the solution of critical buckling load for isotropic plate with uniaxially load in one direction. In the literature, the critical buckling load σ_{cr} has been given as $\sigma_{cr} = \pi^2 D(b/a + a/b)^2/tb^2$, therefore for the plates with the same material properties, thickness and width, the critical buckling load is determined only by aspect ratio. For square plate (a/b=1), rectangular plate with aspect ratio 0.5 and 1.5, the coefficients $(b/a + a/b)^2$=4, 6.25 and 4.69 respectively which shows the agreement with results in this study. Moreover, the results for the square plate show a square pattern in contour plots of stress distribution. However, the results for the plate with aspect ratio 0.5 show a rectangular pattern in contour plots of stress distribution which fit the shape of the plate, while for the plate

with aspect ratio 1.5, the contour plots of stress distribution show two rectangular patterns. One of the patterns indicates the maximum stress distribution and the other indicates the minimum stress distribution.

For anisotropic problems, two composite plates have been tested in this section including a symmetric balanced composite plate and an unsymmetric unbalanced composite plate. For the symmetric balanced problem, improved postbuckling analysis gives non-zero terms $w_{i(c,s)}$, $u_{i(0,C,S)}$, $v_{i(0,C,S)}$, $N_{xi(0,C,S)}$, $N_{yi(0,C,S)}$. In the results for the symmetric balanced composite plate, the improved postbuckling analysis shows slight disagreement with ABAQUS analysis in prediction of stress distribution. From Figures 7.9 and 7.10, ABAQUS analysis shows a skewed pattern in stress distribution for both N_x and N_y, however the improved postbuckling analysis shows less skewing. The contour plots of stress distribution for improved postbuckling analysis are very close to a symmetric pattern which is similar to that of the isotropic plate, and the slight skewing in the improved postbuckling analysis can be only seen in the value of stresses. The ABAQUS analysis is believed to give more convincing results and the improved postbuckling analysis appears to lose some accuracy in stress distribution. The first reason for losing accuracy is the absence of stiffness A_{16} and A_{26} for a symmetric balanced problem, which leads to non-zero terms for only $N_{x(0,C,S)}$ and $N_{y(0,C,S)}$. However, 0 and C terms in N_x and N_y give a symmetric pattern about the horizontal centre line of the plate, and only S terms give a skewed distribution. In the calculation of stresses, the S term is found to be much smaller than the 0 and the C terms which leads to slight skewing because the symmetric distribution 0 and C are dominating. The second, and more significant, reason is believed to be that the out-of-plane mode w used from VICONOPT is not accurate enough. For any problem with skewed mode shape, VIPASA analysis can only give approximate results because the simply supported end conditions are not satisfied. To satisfy the end conditions, VICON analysis would have to be used to give accurate results. However, VICON analysis is currently not available for postbuckling analysis and therefore VIPASA analysis had to be used for postbuckling analysis for anisotropic problems in this section. VIPASA analysis provides an approximate out-of-plane mode w which loses some accuracy and has a lack of skewing. Therefore, the postbuckling analysis of a symmetric balanced composite problem

in improved postbuckling analysis can only be regarded as an approximate alternative to FE analysis. And because lack of skewing in stress distribution does not have much effect on the accuracy of uniform stress resultants, so improved postbuckling analysis can be still believed to be accurate for postbuckling analysis. For the unsymmetric unbalanced problem, improved postbuckling analysis gives non-zero terms for all components of displacements and stresses, i.e. $w_{i(c,s)}$, $u_{i(0,c,s,C,S)}$, $v_{i(0,c,s,C,S)}$, $N_{xi(0,c,s,C,S)}$, $N_{yi(0,c,s,C,S)}$. The results of unsymmetric unbalanced composite plate show good agreement between improved postbuckling analysis and ABAQUS results. The presence of c terms in N_x and N_y provides a more skewed distribution which makes the results skewed enough for more accuracy. The test of an unsymmetric unbalanced problem is actually a full investigation of improved postbuckling analysis because all the components of displacements, strains and stresses are non-zero. The good comparison between improved postbuckling analysis and ABAQUS analysis validates the accuracy of the new postbuckling analysis and hence it is recommended for implementation into VICONOPT as a new capacity.

For the isotropic square plate with shear load, the agreement of both stress distributions and values is poor between improved postbuckling analysis and ABAQUS analysis. The most significant reason for the bad comparison is due to the incorrect mode shape provided by VICONOPT. As mentioned above, for a buckling problem which involves a skewed buckling mode, VIPASA analysis cannot provide an accurate mode shape due to the simply supported edge conditions not being satisfied. To ensure the satisfaction of the edge condition, VICON analysis is necessary for this type of problem. However, the existing postbuckling capacity is not available for VICON analysis and hence it cannot provide the postbuckling mode shape which is needed in improved postbuckling analysis. Therefore, the results of improved postbuckling analysis use the mode shape from VIPASA analysis. From the quantitative comparison in Figures 7.21 and 7.22, the improved postbuckling analysis failed to reveal the skewed pattern in the shear problem which is incorrect. Moreover, the mean value of stresses across the horizontal and vertical centre lines of the plate show a great amount of difference in both N_x and N_y which indicates the inaccuracy in not only stress distribution but also the quantities of stress. The error evaluation in Figures 7.21 and 7.22

shows acceptable agreement in N_x but unacceptable agreement in N_y, but the error is expected to increase a great amount if the stresses along the edges are evaluated. Thus the improved postbuckling analysis for buckling problems of plates under shear loading is unsatisfied at present and is expected to be so until a more accurate postbuckling mode shape can be provided by VICONOPT.

Chapter 8

Conclusions and future work

8.1 Conclusions

Exact strip postbuckling analysis provides an efficient approach to postbuckling analysis of isotropic plate assemblies for industrial and academic purposes in the preliminary design of aircraft structures. This thesis contributes to a theoretical improvement to the existing exact strip postbuckling analysis, which improves the accuracy of mode shape, stress and strain distributions in the postbuckling range. Illustrative results are shown for isotropic and anisotropic plates with combined edge and load cases, improvements are validated by comparing with finite element results. The improved analysis will be implemented into the exact strip analysis software VICONOPT which enables an efficient and accurate procedure for postbuckling analysis of plates and panels.

The improved exact strip postbuckling analysis is inspired by the work done by Stein who provided an analytical solution for isotropic and orthotropic plates in compression and shear. It is assumed that the in-plane and out-of-plane displacements are varying with half-wavelength $\lambda/2$ and λ respectively. However, the improved analysis assumed that the in-plane displacements are varying with half-wavelength λ and $\lambda/2$ which enables the accurate mode shape to be presented. Based on Von Kármán plate theory, the improved governing equilibrium

equations have been derived and solved. Numerical techniques have been applied which ensure three different edge conditions can be assigned to the plate model.

Illustrative numerical results are presented for both isotropic metal plates and anisotropic composite plates respectively with different edge and load conditions. The results of the improved postbuckling analysis are validated by comparing with ABAQUS results and generally show good agreement. The results are also compared with old VICONOPT results in Chapter 6 to show the improvement. The old VICONOPT postbuckling analysis shows good comparison of load versus end shortening in the initial postbuckling range, while accuracy is lost in the postbuckling range for mode shape and stress and strain distribution. The improved analysis derives the improved governing equations and enhances accuracy in mode shape, stress and strain distributions in the postbuckling range, and hence improves the postbuckling mode shape and stress distribution in VICONOPT.

Implementation of the improved analysis into VICONOPT enables a more efficient procedure for postbuckling analysis. The improved analysis utilizes the out-of-plane displacements for initial buckling results from VICONOPT to calculate effective uniform stress resultants and their derivatives, which are used to obtain new out-of-plane displacements for the next cycle of the postbuckling analysis. Implementation of the improved analysis ensures the enhanced postbuckling mode shape and distribution of stress and strain can be obtained and accurate postbuckling analysis can be performed using VICONOPT.

The objective of this thesis has been achieved by introducing the improved exact strip postbuckling analysis which will be implemented into software VICONOPT in the future. The thesis starts with an introduction of the research background of the area and then lists the objectives of this project in Chapter 1. Reviews of buckling and postbuckling phenomena with classic plate theory are introduced in Chapter 2. Moreover, two key papers from Stein on the postbuckling behaviour of plates are briefly reviewed and postbuckling analysis from other researchers in past few decades is also reviewed. In Chapter 3, the exact strip method and Wittrick-Williams algorithm are reviewed as a preparation for a preview of the software VICONOPT. In Chapter 4, the exact strip analysis and optimum design software VICONOPT has been introduced explicitly, and

the theory and analysis of two earlier programs, VIPASA and VICON, have been described. The postbuckling capacity of VICONOPT and its optimum design capacity have also been introduced in this chapter to show the entire analysis properties of this software. Chapter 5 starts to introduce the so called 'improved postbuckling analysis' in detail. The introduction begins with the assumptions that have been made in this analysis, then the in-plane and out-of-plane displacement modes have been given. Then the explicit expression of strain and stress are derived for the equilibrium equation of this analysis. After the expression of the improved governing equilibrium equation has been given, the solution of the equilibrium equations has been obtained at the end of this chapter. In Chapter 6, the illustrative results for an isotropic square plate under compression with three different edge conditions are shown. The improved postbuckling analysis shows good agreement with ABAQUS results which validates the postbuckling analysis capacity for an isotropic square plate. To fully test the new analysis, Chapter 7 provides more cases for testing including an isotropic plate with different aspect ratios, symmetric balanced and unsymmetric unbalanced composite plates and an isotropic square plate with shear load. The results also show good comparison with ABAQUS results except for the isotropic plate with shear load. It is believed that is due to the inaccurate postbuckling mode from VICONOPT. Finally the thesis is summarised and concluded in this chapter.

The improved postbuckling analysis has been demonstrated to be able to provide more accurate postbuckling analysis than the previous version of VICONOPT. The improvement in this analysis may further affect the optimum design capacity in VICONOPT so that more accurate and explicit design work can be achieved. It is believed that further extension of the improved analysis and application on optimum design can provide additional efficient and accurate compatibilities for aircraft engineers and designers.

8.2 Further development

Implementation of the improved exact strip postbuckling analysis provides additional capabilities in VICONOPT for aircraft analysis and design, increasing its

accuracy whilst maintaining the benefits of reduced computational effort when compared to alternatives such as FEA modelling. Further improvements have however been identified throughout the course of this study which may bring additional benefits and which should be considered for implementation in the future. Some recommendations for future development based on the improved analysis are discussed below.

The improved analysis is currently applied to isotropic and anisotropic single plates only, and it is essential to further extend it to the analysis of stiffened panels. This extension would ensure the improved analysis can be used for the postbuckling analysis of complex aircraft structures. To achieve this task, previous experience of stiffened panel assembly in VICONOPT can be referred to. Dealing with the displacements at the junction of different plates is crucial for this task.

From the results of the improved postbuckling analysis, it is suspected that the analysis loses some accuracy due to the assumption of sinusoidal variation of stress with coupling of half-wavelengths λ and $\lambda/2$. It is recommended that the coupling of more different half-wavelengths can provide more accuracy in the analysis. However, the increase of the number of different half-wavelengths will lead to a significant increase in the number of unknown variables, and hence in the number of equilibrium equations for each node and the order of matrix $\mathbf{H}$ in equation (5.33).

A limitation of the improved analysis is concerned with the fact that only three different edge conditions which are fixed edge, straight edge and free edge respectively have been implemented. These can be used directly in an improved analysis, while the flexible edge conditions can not be applied by user. To enable flexible application of edge conditions in improved analysis, rows and columns corresponding to the constraints defined by the user will be eliminated automatically so that the stiffness matrix for the particular edge conditions can be established. Furthermore, unsymmetrical edge conditions can be achieved which may then be helpful for analysis of stiffened panels.

Another limitation is that the old postbuckling capacity in VICONOPT is not available for VICON analysis, which leads to inaccurate postbuckling mode shapes for buckling problems with skewed modes. This is the main reason for

incorrect analysis for isotropic plates with shear load in section 7.4. To enable the accurate postbuckling analysis of shear problems in improved postbuckling analysis, the availability of VICON analysis in postbuckling is necessary.

Since improved analysis brings benefits in terms of efficiency and accuracy in the postbuckling range, it may provide additional advantages to optimum design capacity in VICONOPT. The multi-level optimization of an aircraft wing incorporates postbuckling effects which can be improved by using improved postbuckling analysis.

Appendix A

Derivative calculations in VICONOPT

The implementation of improved exact strip postbuckling analysis into VICONOPT requires derivatives of stresses at each node with respect to all the components of out-of-plane displacement **w** at each node.

In section 5.5, the expression of stress is written as form below

$$\mathbf{N_i}' = \bar{\mathbf{A}}_\mathbf{i}\varepsilon_\mathbf{0}'(\mathbf{w_i}) + \bar{\mathbf{B}}_\mathbf{i}\kappa_\mathbf{0}'(\mathbf{w_i}) + \frac{\mathbf{1}}{\mathbf{b}}\bar{\mathbf{A}}_\mathbf{i}\varepsilon_\mathbf{1}\mathbf{u_i}' + \bar{\mathbf{A}}_\mathbf{i}\varepsilon_\mathbf{2}\mathbf{u_i}'' \tag{A.1}$$

Therefore the derivative with respect to out-of-plane displacement **w** can be written

$$\frac{\partial \mathbf{N_i}}{\partial w_i} = \bar{A}_i\frac{\partial\varepsilon_0(w_i)}{\partial w_i} + \bar{B}_i\frac{\partial\kappa_0(w_i)}{\partial w_i} + \frac{1}{b}\bar{A}_i\varepsilon_1\frac{\partial u_i}{\partial w_i} + \bar{A}_i\varepsilon_2\frac{\partial u_i'}{\partial w_i} \tag{A.2}$$

$$\frac{\partial \varepsilon_0(w_i)}{\partial w_{ic}} = \begin{vmatrix} \frac{\pi^2}{2\lambda^2} w_{ic} \\ 0 \\ 0 \\ -\frac{\pi^2}{2\lambda^2} w_{ic} \\ -\frac{\pi^2}{2\lambda^2} w_{is} \\ 0 \\ 0 \\ 0 \\ 0 \\ 0 \\ -\frac{\pi}{2\lambda}\psi_{is} \\ 0 \\ 0 \\ \frac{\pi}{2\lambda}\psi_{is} \\ -\frac{\pi}{2\lambda}\psi_{ic} \end{vmatrix}, \frac{\partial \varepsilon_0(w_i)}{\partial w_{is}} = \begin{vmatrix} \frac{\pi^2}{2\lambda^2} w_{is} \\ 0 \\ 0 \\ \frac{\pi^2}{2\lambda^2} w_{is} \\ -\frac{\pi^2}{2\lambda^2} w_{ic} \\ 0 \\ 0 \\ 0 \\ 0 \\ \frac{\pi}{2\lambda}\psi_{ic} \\ 0 \\ 0 \\ \frac{\pi}{2\lambda}\psi_{ic} \\ \frac{\pi}{2\lambda}\psi_{is} \end{vmatrix}, \frac{\partial \varepsilon_0(w_i)}{\partial \psi_{ic}} = \begin{vmatrix} 0 \\ 0 \\ 0 \\ 0 \\ 0 \\ \frac{1}{2}\psi_{ic} \\ 0 \\ 0 \\ \frac{1}{2}\psi_{ic} \\ \frac{1}{2}\psi_{is} \\ \frac{\pi}{2\lambda} w_{is} \\ 0 \\ 0 \\ \frac{\pi}{2\lambda} w_{is} \\ -\frac{\pi}{2\lambda} w_{ic} \end{vmatrix}, \frac{\partial \varepsilon_0(w_i)}{\partial \psi_{is}} = \begin{vmatrix} 0 \\ 0 \\ 0 \\ 0 \\ 0 \\ \frac{1}{2}\psi_{is} \\ 0 \\ 0 \\ -\frac{1}{2}\psi_{is} \\ \frac{1}{2}\psi_{ic} \\ -\frac{\pi}{2\lambda} w_{ic} \\ 0 \\ 0 \\ \frac{\pi}{2\lambda} w_{ic} \\ \frac{\pi}{2\lambda} w_{is} \end{vmatrix} \tag{A.3}$$

$$\frac{\partial \kappa_0(w_i)}{\partial w_{ic}} = \begin{vmatrix} 0 \\ \frac{\pi^2}{\lambda^2} \\ 0 \\ 0 \\ 0 \\ 0 \\ 0 \\ 0 \\ 0 \\ 0 \\ 0 \\ 0 \\ 0 \\ 0 \\ 0 \\ 0 \end{vmatrix}, \frac{\partial \kappa_0(w_i)}{\partial w_{is}} = \begin{vmatrix} 0 \\ 0 \\ \frac{\pi^2}{\lambda^2} \\ 0 \\ 0 \\ 0 \\ 0 \\ 0 \\ 0 \\ 0 \\ 0 \\ 0 \\ 0 \\ 0 \\ 0 \\ 0 \end{vmatrix}, \frac{\partial \kappa_0(w_i)}{\partial \psi_{ic}} = \begin{vmatrix} 0 \\ 0 \\ 0 \\ 0 \\ 0 \\ 0 \\ 0 \\ 0 \\ 0 \\ 0 \\ 0 \\ 0 \\ 0 \\ \frac{2\pi}{\lambda} \\ 0 \\ 0 \end{vmatrix}, \frac{\partial \kappa_0(w_i)}{\partial \psi_{is}} = \begin{vmatrix} 0 \\ 0 \\ 0 \\ 0 \\ 0 \\ 0 \\ 0 \\ 0 \\ 0 \\ 0 \\ 0 \\ 0 \\ -\frac{2\pi}{\lambda} \\ 0 \\ 0 \\ 0 \end{vmatrix} \tag{A.4}$$

Equilibrium equation 1:

$$\frac{\partial G(w_i)}{\partial w_{ic}} = -\begin{cases} \frac{A_{12}\pi^2}{2\lambda^2}\psi_{ic} + \frac{A_{26}}{4\lambda b}(6\psi_{is} - 4\psi_{i+1,s} + \psi_{i+2,s}) \\ \frac{A_{12}\pi^2}{2\lambda^2}\psi_{ic} + \frac{A_{26}}{4\lambda b}(-\psi_{i+1,s} + \psi_{i-1,s}) \\ \frac{A_{12}\pi^2}{2\lambda^2}\psi_{ic} + \frac{A_{26}}{4\lambda b}(-6\psi_{is} + 4\psi_{i-1,s} - \psi_{i-2,s}) \end{cases} \tag{A.5}$$

$$\frac{\partial G(w_i)}{\partial w_{is}} = -\begin{cases} \frac{A_{12}\pi^2}{2\lambda^2}\psi_{is} + \frac{A_{26}}{4\lambda b}(-6\psi_{ic} + 4\psi_{i+1,c} - \psi_{i+2,c}) \\ \frac{A_{12}\pi^2}{2\lambda^2}\psi_{is} + \frac{A_{26}}{4\lambda b}(\psi_{i+1,c} - \psi_{i-1,c}) \\ \frac{A_{12}\pi^2}{2\lambda^2}\psi_{is} + \frac{A_{26}}{4\lambda b}(6\psi_{ic} - 4\psi_{i-1,c} + \psi_{i-2,c}) \end{cases} \tag{A.6}$$

$$\begin{aligned} \frac{\partial G(w_i)}{\partial \psi_{ic}} = &-\frac{A_{22}}{4b}\begin{cases} -6\psi_{ic} + 4\psi_{i+1,c} - \psi_{i+2,c} \\ \psi_{i+1,c} - \psi_{i-1,c} \\ 6\psi_{ic} - 4\psi_{i-1,c} + \psi_{i-2,c} \end{cases} - \frac{A_{12}\pi^2}{2\lambda^2}w_{ic} \\ &-\frac{A_{26}}{4\lambda b}\begin{cases} -6w_{is} + 4w_{i+1,s} - w_{i+2,s} \\ w_{i+1,s} - w_{i-1,s} \\ 6w_{is} - 4w_{i-1,s} + w_{i-2,s} \end{cases} \end{aligned} \tag{A.7}$$

$$\begin{aligned} \frac{\partial G(w_i)}{\partial \psi_{is}} = &-\frac{A_{22}}{4b}\begin{cases} -6\psi_{is} + 4\psi_{i+1,s} - \psi_{i+2,s} \\ \psi_{i+1,s} - \psi_{i-1,s} \\ 6\psi_{is} - 4\psi_{i-1,s} + \psi_{i-2,s} \end{cases} - \frac{A_{12}\pi^2}{2\lambda^2}w_{is} \\ &-\frac{A_{26}}{4\lambda b}\begin{cases} 6w_{ic} - 4w_{i+1,c} + w_{i+2,c} \\ -w_{i+1,c} + w_{i-1,c} \\ -6w_{ic} + 4w_{i-1,c} - w_{i-2,c} \end{cases} \end{aligned} \tag{A.8}$$

Equilibrium equation 2:

$$\frac{\partial G(w_i)}{\partial w_{ic}} = 0 \tag{A.9}$$

$$\frac{\partial G(w_i)}{\partial w_{is}} = -\frac{B_{16}\pi^3}{\lambda^3} \tag{A.10}$$

$$\frac{\partial G(w_i)}{\partial \psi_{ic}} = -\frac{2\pi^2 B_{66}}{\lambda^2} + \begin{cases} \frac{2B_{22}}{b^2} \\ \frac{-2B_{22}}{b^2} \\ \frac{2B_{22}}{b^2} \end{cases} - \frac{B_{12}\pi^2}{\lambda^2} \tag{A.11}$$

$$\frac{\partial G(w_i)}{\partial \psi_{is}} = -\begin{cases} \frac{-9B_{26}\pi}{2\lambda b} \\ 0 \\ \frac{9B_{26}\pi}{2\lambda b} \end{cases} \tag{A.12}$$

Equilibrium equation 3:

$$\frac{\partial G(w_i)}{\partial w_{ic}} = \frac{B_{16} w_i \pi^3}{\lambda^3} \tag{A.13}$$

$$\frac{\partial G(w_i)}{\partial w_{is}} = 0 \tag{A.14}$$

$$\frac{\partial G(w_i)}{\partial \psi_{ic}} = -\begin{cases} \frac{-9B_{26}\pi}{2\lambda b} \\ 0 \\ \frac{9B_{26}\pi}{2\lambda b} \end{cases} \tag{A.15}$$

$$\frac{\partial G(w_i)}{\partial \psi_{is}} = -\frac{2\pi^2 B_{66}}{\lambda^2} + \begin{cases} \frac{2B_{22}}{b^2} \\ \frac{-2B_{22}}{b^2} \\ \frac{2B_{22}}{b^2} \end{cases} - \frac{B_{12}\pi^2}{\lambda^2} \tag{A.16}$$

Equilibrium equation 4:

$$\frac{\partial G(w_i)}{\partial w_{ic}} = -\frac{A_{26}\pi}{4\lambda b} \begin{cases} -6\psi_{is} + 4\psi_{i+1,s} - \psi_{i+2,s} \\ \psi_{i+1,s} - \psi_{i-1,s} \\ 6\psi_{is} - 4\psi_{i-1,s} + \psi_{i-2,s} \end{cases} + \frac{\pi^2 A_{12}}{2\lambda^2}\psi_{ic} + \frac{A_{16}\pi^3}{\lambda^3} w_{is} + \frac{A_{66}\pi^2}{\lambda^2}\psi_{ic} \tag{A.17}$$

$$\frac{\partial G(w_i)}{\partial w_{is}} = -\frac{A_{26}\pi}{4\lambda b} \begin{cases} -6\psi_{ic} + 4\psi_{i+1,c} - \psi_{i+2,c} \\ \psi_{i+1,c} - \psi_{i-1,c} \\ 6\psi_{ic} - 4\psi_{i-1,c} + \psi_{i-2,c} \end{cases} + \frac{\pi^2 A_{12}}{2\lambda^2}\psi_{is} + \frac{A_{16}\pi^3}{\lambda^3} w_{ic} + \frac{A_{66}\pi^2}{\lambda^2}\psi_{is} \tag{A.18}$$

$$\frac{\partial G(w_i)}{\partial \psi_{ic}} = -\frac{A_{22}}{4b}\begin{cases} -6\psi_{ic} + 4\psi_{i+1,c} - \psi_{i+2,c} \\ \psi_{i+1,c} - \psi_{i-1,c} \\ 6\psi_{ic} - 4\psi_{i-1,c} + \psi_{i-2,c} \end{cases} + \frac{\pi^2 A_{12}}{2\lambda^2} w_{ic} - \frac{A_{26}\pi}{\lambda}\psi_{is} \tag{A.19}$$

$$+ \frac{A_{66}\pi^2}{\lambda^2} w_{ic} - \frac{A_{26}\pi}{4\lambda b}\begin{cases} -6w_{is} + 4w_{i+1,s} - w_{i+2,s} \\ w_{i+1,s} - w_{i-1,s} \\ 6w_{is} - 4w_{i-1,s} + w_{i-2,s} \end{cases} \tag{A.20}$$

$$\frac{\partial G(w_i)}{\partial \psi_{is}} = \frac{A_{22}}{4b}\begin{cases} -6\psi_{is} + 4\psi_{i+1,s} - \psi_{i+2,s} \\ \psi_{i+1,s} - \psi_{i-1,s} \\ 6\psi_{is} - 4\psi_{i-1,s} + \psi_{i-2,s} \end{cases} - \frac{\pi^2 A_{12}}{2\lambda^2} w_{is} - \frac{A_{26}\pi}{\lambda}\psi_{ic} \tag{A.21}$$

$$- \frac{A_{66}\pi^2}{\lambda^2} w_{is} - \frac{A_{26}\pi}{4\lambda b}\begin{cases} -6w_{ic} + 4w_{i+1,c} - w_{i+2,c} \\ w_{i+1,c} - w_{i-1,c} \\ 6w_{ic} - 4w_{i-1,c} + w_{i-2,c} \end{cases} \tag{A.22}$$

Equilibrium equation 5:

$$\frac{\partial G(w_i)}{\partial w_{ic}} = \frac{A_{26}\pi}{4\pi\lambda}\begin{cases} -3\psi_{ic} + 4\psi_{i+1,c} - \psi_{i+2,c} \\ \psi_{i+1,c} - psi_{i-1,c} \\ 3\psi_{ic} - 4\psi i - 1, c + \psi_{i-2,c} \end{cases} + \frac{\pi^2 A_{12}}{2\lambda^2}\psi_{is} - \frac{A_{16}\pi^3}{\lambda^3} w_{ic} + \frac{A_{66}\pi^2}{\lambda^2}\psi_{is} \tag{A.23}$$

$$\frac{\partial G(w_i)}{\partial w_{is}} = -\frac{A_{26}\pi}{4\pi\lambda}\begin{cases} -3\psi_{is} + 4\psi_{i+1,s} - \psi_{i+2,s} \\ \psi_{i+1,s} - psi_{i-1,s} \\ 3\psi_{is} - 4\psi i - 1, s + \psi_{i-2,s} \end{cases} + \frac{\pi^2 A_{12}}{2\lambda^2}\psi_{ic} + \frac{A_{16}\pi^3}{\lambda^3} w_{is} + \frac{A_{66}\pi^2}{\lambda^2}\psi_{ic} \tag{A.24}$$

$$\frac{\partial G(w_i)}{\partial w_{ic}} = -\frac{A_{22}}{4b}\begin{cases} -6\psi_{is} + 4\psi_{i+1,s} - \psi_{i+2,s} \\ \psi_{i+1,s} - psi_{i-1,s} \\ 6\psi_{is} - 4\psi i - 1, s + \psi_{i-2,s} \end{cases} + \frac{A_{26}\pi}{4\lambda b}\begin{cases} -3w_{ic} \\ 0 \\ 3w_{ic} \end{cases} \tag{A.25}$$

$$+ \frac{\pi^2 A_{12}}{2\lambda^2} w_{is} + 2\frac{A_{26}\pi}{\lambda}\psi_{ic} + \frac{A_{66}\pi^2}{\lambda^2} w_{is} \tag{A.26}$$

$$\frac{\partial G(w_i)}{\partial w_{ic}} = -\frac{A_{22}}{4b}\begin{cases} -6\psi_{ic} + 4\psi_{i+1,c} - \psi_{i+2,c} \\ \psi_{i+1,c} - psi_{i-1,c} \\ 6\psi_{ic} - 4\psi i - 1, c + \psi_{i-2,c} \end{cases} - \frac{A_{26}\pi}{4\lambda b}\begin{cases} -3w_{ic} \\ 0 \\ 3w_{ic} \end{cases} \tag{A.27}$$

$$+ \frac{\pi^2 A_{12}}{2\lambda^2} w_{ic} - 2\frac{A_{26}\pi}{\lambda}\psi_{is} + \frac{A_{66}\pi^2}{\lambda^2} w_{ic} \tag{A.28}$$

Equilibrium equation 6:

$$\frac{\partial G(w_i)}{\partial w_{ic}} = \frac{\pi A_{66}}{4\lambda b}\begin{cases} -3\psi_{is} + 4\psi i + 1, s - \psi_{i+2,s} \\ \psi_{i+1,s} - \psi_{i-1,s} \\ 3\psi_{is} - 4\psi_{i-1,s} + \psi_{i-2,s} \end{cases} - \frac{\pi A_{66}}{4\lambda b}\begin{cases} 3\psi_{is} \\ 0 \\ -3\psi_{is} \end{cases} - \frac{\pi^2 A_{16}}{2\lambda^2}\psi_{ic} \tag{A.29}$$

$$\frac{\partial G(w_i)}{\partial w_{is}} = -\frac{\pi A_{66}}{4\lambda b}\begin{cases} -3\psi_{ic} + 4\psi i + 1, s - \psi_{i+2,c} \\ \psi_{i+1,c} - \psi_{i-1,c} \\ 3\psi_{ic} - 4\psi_{i-1,c} + \psi_{i-2,c} \end{cases} - \frac{\pi A_{66}}{4\lambda b}\begin{cases} 3\psi_{ic} \\ 0 \\ -3\psi_{ic} \end{cases} - \frac{\pi^2 A_{16}}{2\lambda^2}\psi_{is} \tag{A.30}$$

$$\frac{\partial G(w_i)}{\partial \psi_{ic}} = -\frac{\pi A_{66}}{4\lambda b}\begin{cases} -6w_{is} + 4w_{i+1,s} - w_{i+2,s} \\ w_{i+1,s} - w_{i-1,s} \\ 6w_{is} - 4w_{i-1,s} + w_{i-2,s} \end{cases} - \frac{\pi^2 A_{16}}{2\lambda^2} w_{ic} \tag{A.31}$$

$$- \frac{A_{26}}{4b}\begin{cases} -6\psi_{ic} + 4\psi_{i+1,c} - \psi_{i+2,c} \\ \psi_{i+1,c} - \psi_{i-1,c} \\ 6\psi_{ic} - 4\psi_{i-1,c} + \psi_{i-2,c} \end{cases} \tag{A.32}$$

$$\frac{\partial G(w_i)}{\partial \psi_{is}} = \frac{\pi A_{66}}{4\lambda b}\begin{cases} -6w_{ic} + 4w_{i+1,c} - w_{i+2,c} \\ w_{i+1,c} - w_{i-1,c} \\ 6w_{ic} - 4w_{i-1,c} + w_{i-2,c} \end{cases} - \frac{\pi^2 A_{16}}{2\lambda^2} w_{ic} \tag{A.33}$$

$$- \frac{A_{26}}{4b}\begin{cases} -6\psi_{is} + 4\psi_{i+1,s} - \psi_{i+2,s} \\ \psi_{i+1,s} - \psi_{i-1,s} \\ 6\psi_{is} - 4\psi_{i-1,s} + \psi_{i-2,s} \end{cases} \tag{A.34}$$

Equilibrium equation 7:

$$\frac{\partial G(w_i)}{\partial w_{ic}} = 0 \tag{A.35}$$

$$\frac{\partial G(w_i)}{\partial w_{is}} = \frac{\pi^3 B_{11}}{\lambda^3} \tag{A.36}$$

$$\frac{\partial G(w_i)}{\partial \psi_{ic}} = \frac{B_{26}}{b^2} \begin{cases} 2 \\ -2 \\ 2 \end{cases} - \frac{3B_{16}\pi^2}{\lambda^2} \tag{A.37}$$

$$\frac{\partial G(w_i)}{\partial \psi_{is}} = \begin{cases} -3(\frac{\pi B_{66}}{\lambda b} + \frac{B_{12}\pi}{2\lambda b} + \frac{B_{66}\pi}{\lambda b}) \\ 0 \\ 3(\frac{\pi B_{66}}{\lambda b} + \frac{B_{12}\pi}{2\lambda b} + \frac{B_{66}\pi}{\lambda b}) \end{cases} \tag{A.38}$$

Equilibrium equation 8:

$$\frac{\partial G(w_i)}{\partial w_{ic}} = B_{11}\frac{\pi^3}{\lambda^3} \tag{A.39}$$

$$\frac{\partial G(w_i)}{\partial w_{is}} = 0 \tag{A.40}$$

$$\frac{\partial G(w_i)}{\partial \psi_{ic}} = \begin{cases} 3(\frac{B_{12}\pi}{2\lambda b} + \frac{B_{66}\pi}{\lambda b}) \\ 0 \\ -3(\frac{B_{12}\pi}{2\lambda b} + \frac{B_{66}\pi}{\lambda b}) \end{cases} \tag{A.41}$$

$$\frac{\partial G(w_i)}{\partial \psi_{is}} = \frac{B_{26}}{b^2} \begin{cases} 2 \\ -2 \\ 2 \end{cases} - \frac{3B_{16}\pi^2}{\lambda^2} \tag{A.42}$$

Equilibrium equation 9:

$$\frac{\partial G(w_i)}{\partial w_{ic}} = -\frac{A_{66}\pi}{4\lambda b}\begin{cases} -6\psi_{is} + 4\psi_{i+1,s} - \psi_{i+2,s} \\ \psi_{i+1,s} - \psi_{i-1,s} \\ 6\psi_{is} - 4\psi_{i-1,s} + \psi_{i-2,s} \end{cases} + \frac{A_{16}\pi^2}{2\lambda^2} + \frac{A_{16}\pi^2}{\lambda^2}\psi_{ic} + \frac{A_{11}\pi^3}{\lambda^3}w_{is} \tag{A.43}$$

$$\frac{\partial G(w_i)}{\partial w_{is}} = -\frac{A_{66}\pi}{4\lambda b}\begin{cases} -6\psi_{ic} + 4\psi_{i+1,c} - \psi_{i+2,c} \\ \psi_{i+1,c} - \psi_{i-1,c} \\ 6\psi_{ic} - 4\psi_{i-1,c} + \psi_{i-2,c} \end{cases} - \frac{A_{16}\pi^2}{2\lambda^2} - \frac{A_{16}\pi^2}{\lambda^2}\psi_{ic} + \frac{A_{11}\pi^3}{\lambda^3}w_{is} \tag{A.44}$$

$$\frac{\partial G(w_i)}{\partial \psi_{ic}} = -\frac{A_{26}}{4b}\begin{cases} -6\psi_{ic} + 4\psi_{i+1,c} - \psi_{i+2,c} \\ \psi_{i+1,c} - \psi_{i-1,c} \\ 6\psi_{ic} - 4\psi_{i-1,c} + \psi_{i-2,c} \end{cases} - \frac{A_{66}\pi}{4\lambda b}\begin{cases} -6w_{is} + 4w_{i+1,s} - w_{i+2,s} \\ w_{i+1,s} - w_{i-1,s} \\ 6w_{is} - 4w_{i-1,s} + w_{i-2,s} \end{cases} \tag{A.45}$$

$$+ \frac{3A_{16}\pi^2}{2\lambda^2}w_{ic} - \frac{A_{12}\pi}{\lambda}\psi_{is} \tag{A.46}$$

$$\frac{\partial G(w_i)}{\partial \psi_{is}} = \frac{A_{26}}{4b}\begin{cases} -6\psi_{is} + 4\psi_{i+1,s} - \psi_{i+2,s} \\ \psi_{i+1,s} - \psi_{i-1,s} \\ 6\psi_{is} - 4\psi_{i-1,s} + \psi_{i-2,s} \end{cases} - \frac{A_{66}\pi}{4\lambda b}\begin{cases} -6w_{ic} + 4w_{i+1,c} - w_{i+2,c} \\ w_{i+1,c} - w_{i-1,c} \\ 6w_{ic} - 4w_{i-1,c} + w_{i-2,c} \end{cases} \tag{A.47}$$

$$- \frac{3A_{16}\pi^2}{2\lambda^2}w_{is} - \frac{A_{12}\pi}{\lambda}\psi_{ic} \tag{A.48}$$

Equilibrium equation 10:

$$\frac{\partial G(w_i)}{\partial w_{ic}} = \frac{A_{66}\pi}{4\lambda b}\begin{cases} -3\psi_{ic} + 4\psi_{i+1,c} - \psi_{i+2,c} \\ \psi_{i+1,c} - \psi_{i-1,c} \\ 3\psi_{ic} - 4\psi_{i-1,c} + \psi_{i-2,c} \end{cases} + \frac{3A_{16}\pi^2}{2\lambda^2}\psi_{is} - \frac{A_{11}\pi^3}{\pi^3}w_{ic} \tag{A.49}$$

$$\frac{\partial G(w_i)}{\partial w_{is}} = -\frac{A_{66}\pi}{4\lambda b}\begin{cases} -3\psi_{is} + 4\psi_{i+1,s} - \psi_{i+2,s} \\ \psi_{i+1,s} - \psi_{i-1,s} \\ 3\psi_{is} - 4\psi_{i-1,s} + \psi_{i-2,s} \end{cases} + \frac{3A_{16}\pi^2}{2\lambda^2}\psi_{ic} + \frac{A_{11}\pi^3}{\pi^3}w_{is} \quad \text{(A.50)}$$

$$\frac{\partial G(w_i)}{\partial \psi_{ic}} = -\frac{A_{26}}{4b}\begin{cases} -6\psi_{is} + 4\psi_{i+1,s} - \psi_{i+2,s} \\ \psi_{i+1,s} - \psi_{i-1,s} \\ 6\psi_{is} - 4\psi_{i-1,s} + \psi_{i-2,s} \end{cases} - \frac{A_{66}\pi}{4\lambda b}\begin{cases} 3w_{ic} \\ 0 \\ -3w_{ic} \end{cases} \quad \text{(A.51)}$$

$$+ \frac{3A_{16}\pi^2}{2\lambda^2}w_{is} + \frac{A_{66}\pi}{\lambda}\psi_{ic} + \frac{A_{12}\pi}{\lambda}\psi_{ic} \quad \text{(A.52)}$$

$$\frac{\partial G(w_i)}{\partial \psi_{is}} = -\frac{A_{26}}{4b}\begin{cases} -6\psi_{ic} + 4\psi_{i+1,c} - \psi_{i+2,c} \\ \psi_{i+1,c} - \psi_{i-1,c} \\ 6\psi_{ic} - 4\psi_{i-1,c} + \psi_{i-2,c} \end{cases} - \frac{A_{66}\pi}{4\lambda b}\begin{cases} -3w_{is} \\ 0 \\ 3w_{is} \end{cases} \quad \text{(A.53)}$$

$$+ \frac{3A_{16}\pi^2}{2\lambda^2}w_{ic} - \frac{A_{66}\pi}{\lambda}\psi_{is} + \frac{A_{12}\pi}{\lambda}\psi_{is} \quad \text{(A.54)}$$

$$\frac{\partial G_{i+1}}{\partial w_i} \quad \text{(A.55)}$$

$$\text{(A.56)}$$

1<i<n

Equilibrium equation 1:

$$\frac{\partial G(w_{i+1})}{\partial w_{ic}} = -\frac{A_{26}\pi}{4\lambda b}\psi_{i+1,s} \quad \text{(A.57)}$$

$$\frac{\partial G(w_{i+1})}{\partial w_{is}} = \frac{A_{26}\pi}{4\lambda b}\psi_{i+1,c} \quad \text{(A.58)}$$

$$\frac{\partial G(w_{i+1})}{\partial \psi_{ic}} = \frac{A_{22}}{4b}\psi_{i+1,c} + \frac{A_{26}\pi}{4\lambda b}w_{i+1,s} \quad \text{(A.59)}$$

$$\frac{\partial G(w_{i+1})}{\partial \psi_{is}} = \frac{A_{22}}{4b}\psi_{i+1,s} - \frac{A_{26}\pi}{4\lambda b}w_{i+1,c} \tag{A.60}$$

Equilibrium equation 2:

$$\frac{\partial G_{i+1}}{\partial w_{ic}} = 0 \tag{A.61}$$

$$\frac{\partial G_{i+1}}{\partial w_{is}} = 0 \tag{A.62}$$

$$\frac{\partial G_{i+1}}{\partial \psi_{ic}} = \frac{B_{22}}{b^2} \tag{A.63}$$

$$\frac{\partial G_{i+1}}{\partial \psi_{is}} = -\frac{B_{26}\pi}{\lambda b} - \frac{B_{26}\pi}{2\lambda b} \tag{A.64}$$

Equilibrium equation 3:

$$\frac{\partial G_{i+1}}{\partial w_{ic}} = 0 \tag{A.65}$$

$$\frac{\partial G_{i+1}}{\partial w_{is}} = 0 \tag{A.66}$$

$$\frac{\partial G_{i+1}}{\partial \psi_{ic}} = \frac{B_{26}\pi}{\lambda b} + \frac{B_{26}\pi}{2\lambda b} \tag{A.67}$$

$$\frac{\partial G_{i+1}}{\partial \psi_{is}} = \frac{B_{22}}{b^2} \tag{A.68}$$

Equilibrium equation 4:

$$\frac{\partial G_{i+1}}{\partial w_{ic}} = \frac{A_{26}\pi}{4\lambda b}\psi_{i+1,s} \tag{A.69}$$

$$\frac{\partial G_{i+1}}{\partial w_{is}} = \frac{A_{26}\pi}{4\lambda b}\psi_{i+1,c} \tag{A.70}$$

$$\frac{\partial G_{i+1}}{\partial \psi_{ic}} = \frac{A_{22}}{4b}\psi_{i+1,c} + \frac{A_{26}\pi}{4\lambda b}w_{i+1,s} \tag{A.71}$$

$$\frac{\partial G_{i+1}}{\partial \psi_{is}} = -\frac{A_{22}}{4b}\psi_{i+1,s} + \frac{A_{26}\pi}{4\lambda b}w_{i+1,c} \tag{A.72}$$

Equilibrium equation 5:

$$\frac{\partial G_{i+1}}{\partial w_{ic}} = 0 \tag{A.73}$$

$$\frac{\partial G_{i+1}}{\partial w_{is}} = 0 \tag{A.74}$$

$$\frac{\partial G_{i+1}}{\partial \psi_{ic}} = \frac{A_{22}}{4b}\psi_{i+1,s} - \frac{A_{26}\pi}{4\lambda b}w_{i+1,c} \tag{A.75}$$

$$\frac{\partial G_{i+1}}{\partial \psi_{is}} = \frac{A_{22}}{4b}\psi_{i+1,c} + \frac{A_{26}\pi}{4\lambda b}w_{i+1,s} \tag{A.76}$$

Equilibrium equation 6:

$$\frac{\partial G_{i+1}}{\partial w_{ic}} = -\frac{A_{66}\pi}{4\lambda b}\psi_{i+1,s} \tag{A.77}$$

$$\frac{\partial G_{i+1}}{\partial w_{is}} = \frac{A_{66}\pi}{4\lambda b}\psi_{i+1,c} \tag{A.78}$$

$$\frac{\partial G_{i+1}}{\partial \psi_{ic}} = \frac{A_{26}}{4b}\psi_{i+1,c} + \frac{A_{66}\pi}{4\lambda b}w_{i+1,s} \tag{A.79}$$

$$\frac{\partial G_{i+1}}{\partial \psi_{is}} = \frac{A_{26}}{4b}\psi_{i+1,s} - \frac{A_{66}\pi}{4\lambda b}w_{i+1,c} \tag{A.80}$$

Equilibrium equation 7:

$$\frac{\partial G_{i+1}}{\partial w_{ic}} = 0 \tag{A.81}$$

$$\frac{\partial G_{i+1}}{\partial w_{is}} = 0 \tag{A.82}$$

$$\frac{\partial G_{i+1}}{\partial \psi_{ic}} = \frac{B_{26}}{b^2} \tag{A.83}$$

$$\frac{\partial G_{i+1}}{\partial \psi_{is}} = -\frac{4(B_{66} + B_{12})\pi}{2\lambda b} \tag{A.84}$$

Equilibrium equation 8:

$$\frac{\partial G_{i+1}}{\partial w_{ic}} = 0 \tag{A.85}$$

$$\frac{\partial G_{i+1}}{\partial w_{is}} = 0 \tag{A.86}$$

$$\frac{\partial G_{i+1}}{\partial \psi_{ic}} = \frac{(B_{12} + 2B_{66})\pi}{2\lambda b} \tag{A.87}$$

$$\frac{\partial G_{i+1}}{\partial \psi_{is}} = \frac{B_{26}}{b^2} \tag{A.88}$$

Equilibrium equation 9:

$$\frac{\partial G_{i+1}}{\partial w_{ic}} = \frac{A_{66}\pi}{4\lambda b}\psi_{i+1,s} \tag{A.89}$$

$$\frac{\partial G_{i+1}}{\partial w_{is}} = \frac{A_{66}\pi}{4\lambda b}\psi_{i+1,c} \tag{A.90}$$

$$\frac{\partial G_{i+1}}{\partial \psi_{ic}} = \frac{A_{26}}{4b}\psi_{i+1,c} + \frac{A_{66}\pi}{4\lambda b}w_{i+1,s} \tag{A.91}$$

$$\frac{\partial G_{i+1}}{\partial \psi_{is}} = -\frac{A_{26}}{4b}\psi_{i+1,s} + \frac{A_{66}\pi}{4\lambda b}w_{i+1,c} \tag{A.92}$$

Equilibrium equation 10:

$$\frac{\partial G_{i+1}}{\partial w_{ic}} = 0 \tag{A.93}$$

$$\frac{\partial G_{i+1}}{\partial w_{is}} = 0 \tag{A.94}$$

$$\frac{\partial G_{i+1}}{\partial \psi_{ic}} = \frac{A_{26}}{4b}\psi_{i+1,s} - \frac{A_{66}\pi}{4\lambda b}w_{i+1,c} \tag{A.95}$$

$$\frac{\partial G_{i+1}}{\partial \psi_{is}} = \frac{A_{26}}{4b}\psi_{i+1,c} + \frac{A_{66}\pi}{4\lambda b}w_{i+1,s} \tag{A.96}$$

$$\frac{\partial G_{i-1}}{\partial w_i} \tag{A.97}$$

(A.98)

1<i<n
Equilibrium equation 1:

$$\frac{\partial G_{i-1}}{\partial w_{ic}} = \frac{A_{26}\pi}{4\lambda b}\psi_{i-1,s} \tag{A.99}$$

$$\frac{\partial G_{i-1}}{\partial w_{is}} = -\frac{A_{26}\pi}{4\lambda b}\psi_{i-1,c} \tag{A.100}$$

$$\frac{\partial G_{i-1}}{\partial \psi_{ic}} = -\frac{A_{22}}{4b}\psi_{i-1,c} - \frac{A_{26}\pi}{4\lambda b}w_{i-1,s} \tag{A.101}$$

$$\frac{\partial G_{i-1}}{\partial \psi_{is}} = -\frac{A_{22}}{4b}\psi_{i-1,s} + \frac{A_{26}\pi}{4\lambda b}w_{i-1,c} \tag{A.102}$$

Equilibrium equation 2:

$$\frac{\partial G_{i-1}}{\partial w_{ic}} = 0 \tag{A.103}$$

$$\frac{\partial G_{i-1}}{\partial w_{is}} = 0 \tag{A.104}$$

$$\frac{\partial G_{i-1}}{\partial \psi_{ic}} = \frac{B_{22}}{b^2} \tag{A.105}$$

$$\frac{\partial G_{i-1}}{\partial \psi_{is}} = \frac{3B_{26}\pi}{2\lambda b} \tag{A.106}$$

Equilibrium equation 3:

$$\frac{\partial G_{i-1}}{\partial w_{ic}} = 0 \tag{A.107}$$

$$\frac{\partial G_{i-1}}{\partial w_{is}} = 0 \tag{A.108}$$

$$\frac{\partial G_{i-1}}{\partial \psi_{ic}} = -\frac{3B_{26}\pi}{2\lambda b} \tag{A.109}$$

$$\frac{\partial G_{i-1}}{\partial \psi_{is}} = \frac{B_{22}}{b^2} \tag{A.110}$$

Equilibrium equation 4:

$$\frac{\partial G_{i-1}}{\partial w_{ic}} = -\frac{A_{26}\pi}{4\lambda b}\psi_{i-1,s} \tag{A.111}$$

$$\frac{\partial G_{i-1}}{\partial w_{is}} = -\frac{A_{26}\pi}{4\lambda b}\psi_{i-1,c} \tag{A.112}$$

$$\frac{\partial G_{i-1}}{\partial \psi_{ic}} = -\frac{A_{22}}{4b}\psi_{i-1,c} - \frac{A_{26}\pi}{4\lambda b}w_{i-1,s} \tag{A.113}$$

$$\frac{\partial G_{i-1}}{\partial \psi_{is}} = \frac{A_{22}}{4b}\psi_{i-1,s} - \frac{A_{26}\pi}{4\lambda b}w_{i-1,c} \tag{A.114}$$

Equilibrium equation 5:

$$\frac{\partial G_{i-1}}{\partial w_{ic}} = 0 \tag{A.115}$$

$$\frac{\partial G_{i-1}}{\partial w_{is}} = 0 \tag{A.116}$$

$$\frac{\partial G_{i-1}}{\partial \psi_{ic}} = -\frac{A_{22}}{4b}\psi_{i-1,s} + \frac{A_{26}\pi}{4\lambda b}w_{i-1,c} \tag{A.117}$$

$$\frac{\partial G_{i-1}}{\partial \psi_{is}} = -\frac{A_{22}}{4b}\psi_{i-1,c} - \frac{A_{26}\pi}{4\lambda b}w_{i-1,s} \tag{A.118}$$

Equilibrium equation 6:

$$\frac{\partial G_{i-1}}{\partial w_{ic}} = \frac{A_{66}\pi}{4\lambda b}\psi_{i-1,s} \tag{A.119}$$

$$\frac{\partial G_{i-1}}{\partial w_{is}} = -\frac{A_{66}\pi}{4\lambda b}\psi_{i-1,c} \tag{A.120}$$

$$\frac{\partial G_{i-1}}{\partial \psi_{ic}} = -\frac{A_{26}}{4b}\psi_{i-1,c} - \frac{A_{66}\pi}{4\lambda b}w_{i-1,s} \tag{A.121}$$

$$\frac{\partial G_{i-1}}{\partial \psi_{is}} = -\frac{A_{26}}{4b}\psi_{i-1,s} + \frac{A_{66}\pi}{4\lambda b}w_{i-1,c} \tag{A.122}$$

Equilibrium equation 7:

$$\frac{\partial G_{i-1}}{\partial w_{ic}} = 0 \tag{A.123}$$

$$\frac{\partial G_{i-1}}{\partial w_{is}} = 0 \tag{A.124}$$

$$\frac{\partial G_{i-1}}{\partial \psi_{ic}} = \frac{B_{26}}{b^2} \tag{A.125}$$

$$\frac{\partial G_{i-1}}{\partial \psi_{is}} = \frac{(4B_{66} + B_{12})\pi}{2\lambda b} \tag{A.126}$$

Equilibrium equation 8:

$$\frac{\partial G_{i-1}}{\partial w_{ic}} = 0 \tag{A.127}$$

$$\frac{\partial G_{i-1}}{\partial w_{is}} = 0 \tag{A.128}$$

$$\frac{\partial G_{i-1}}{\partial \psi_{ic}} = \frac{(2B_{66} + B_{12})\pi}{b^2} \tag{A.129}$$

$$\frac{\partial G_{i-1}}{\partial \psi_{is}} = \frac{B_{26}}{b^2} \tag{A.130}$$

Equilibrium equation 9:

$$\frac{\partial G_{i-1}}{\partial w_{ic}} = -\frac{A_{66}\pi}{4\lambda b}\psi_{i-1,s} \tag{A.131}$$

$$\frac{\partial G_{i-1}}{\partial w_{is}} = -\frac{A_{66}\pi}{4\lambda b}\psi_{i-1,c} \tag{A.132}$$

$$\frac{\partial G_{i-1}}{\partial \psi_{ic}} = -\frac{A_{26}}{4b}\psi_{i-1,c} - \frac{A_{66}\pi}{4\lambda b}w_{i-1,s} \tag{A.133}$$

$$\frac{\partial G_{i-1}}{\partial \psi_{is}} = \frac{A_{26}}{4b}\psi_{i-1,s} - \frac{A_{66}\pi}{4\lambda b}w_{i-1,c} \tag{A.134}$$

Equilibrium equation 10:

$$\frac{\partial G_{i-1}}{\partial w_{ic}} = 0 \tag{A.135}$$

$$\frac{\partial G_{i-1}}{\partial w_{is}} = 0 \tag{A.136}$$

$$\frac{\partial G_{i-1}}{\partial \psi_{ic}} = -\frac{A_{26}}{4b}\psi_{i-1,s} + \frac{A_{66}\pi}{4\lambda b}w_{i-1,c} \tag{A.137}$$

$$\frac{\partial G_{i-1}}{\partial \psi_{is}} = -\frac{A_{26}}{4b}\psi_{i-1,c} + \frac{A_{66}\pi}{4\lambda b}w_{i-1,s} \tag{A.138}$$

$$\frac{\partial G_{i+1}}{\partial w_i}(i = n) \tag{A.139}$$

$$\tag{A.140}$$

Equilibrium equation 1:

$$\frac{\partial G_{i+1}}{\partial w_{ic}} = -\frac{A_{26}\pi}{\lambda b}\psi_{i+1,s} \tag{A.141}$$

$$\frac{\partial G_{i+1}}{\partial w_{is}} = \frac{A_{26}\pi}{\lambda b}\psi_{i+1,c} \tag{A.142}$$

$$\frac{\partial G_{i+1}}{\partial \psi_{ic}} = \frac{A_{22}}{b}\psi_{i+1,c} + \frac{A_{26}\pi}{\lambda b}w_{i+1,s} \tag{A.143}$$

$$\frac{\partial G_{i+1}}{\partial \psi_{is}} = \frac{A_{22}}{b}\psi_{i+1,s} - \frac{A_{26}\pi}{\lambda b}w_{i+1,c} \tag{A.144}$$

Equilibrium equation 2:

$$\frac{\partial G_{i+1}}{\partial w_{ic}} = 0 \tag{A.145}$$

$$\frac{\partial G_{i+1}}{\partial w_{is}} = 0 \tag{A.146}$$

$$\frac{\partial G_{i+1}}{\partial \psi_{ic}} = -\frac{5B_{22}}{b^2} \tag{A.147}$$

$$\frac{\partial G_{i+1}}{\partial \psi_{is}} = -\frac{6B_{26}\pi}{\lambda b} \tag{A.148}$$

Equilibrium equation 3:

$$\frac{\partial G_{i+1}}{\partial w_{ic}} = 0 \tag{A.149}$$

$$\frac{\partial G_{i+1}}{\partial w_{is}} = 0 \tag{A.150}$$

$$\frac{\partial G_{i+1}}{\partial \psi_{ic}} = \frac{6B_{26}\pi}{\lambda b} \tag{A.151}$$

$$\frac{\partial G_{i+1}}{\partial \psi_{is}} = -\frac{5B_{22}}{b^2} \tag{A.152}$$

Equilibrium equation 4:

$$\frac{\partial G_{i+1}}{\partial w_{ic}} = \frac{A_{26}\pi}{\lambda b}\psi_{i+1,s} \tag{A.153}$$

$$\frac{\partial G_{i+1}}{\partial w_{is}} = \frac{A_{26}\pi}{\lambda b}\psi_{i+1,c} \tag{A.154}$$

$$\frac{\partial G_{i+1}}{\partial \psi_{ic}} = \frac{A_{22}}{b}\psi_{i+1,c} + \frac{A_{26}\pi}{\lambda b}w_{i+1,s} \tag{A.155}$$

$$\frac{\partial G_{i+1}}{\partial \psi_{is}} = \frac{A_{22}}{b}\psi_{i+1,s} - \frac{A_{26}\pi}{\lambda b}w_{i+1,c} \tag{A.156}$$

Equilibrium equation 5:

$$\frac{\partial G_{i+1}}{\partial w_{ic}} = 0 \tag{A.157}$$

$$\frac{\partial G_{i+1}}{\partial w_{is}} = 0 \tag{A.158}$$

$$\frac{\partial G_{i+1}}{\partial \psi_{ic}} = \frac{A_{22}}{b}\psi_{i+1,s} - \frac{A_{26}\pi}{\lambda b}w_{i+1,c} \tag{A.159}$$

$$\frac{\partial G_{i+1}}{\partial \psi_{is}} = \frac{A_{22}}{b}\psi_{i+1,c} + \frac{A_{26}\pi}{\lambda b}w_{i+1,s} \tag{A.160}$$

Equilibrium equation 6:

$$\frac{\partial G_{i+1}}{\partial w_{ic}} = -\frac{A_{66}\pi}{\lambda b}\psi_{i+1,s} \tag{A.161}$$

$$\frac{\partial G_{i+1}}{\partial w_{is}} = \frac{A_{66}\pi}{\lambda b}\psi_{i+1,c} \tag{A.162}$$

$$\frac{\partial G_{i+1}}{\partial \psi_{ic}} = \frac{A_{66}\pi}{\lambda b}w_{i+1,s} \tag{A.163}$$

$$\frac{\partial G_{i+1}}{\partial \psi_{is}} = -\frac{A_{66}\pi}{\lambda b}w_{i+1,c} \tag{A.164}$$

Equilibrium equation 7:

$$\frac{\partial G_{i+1}}{\partial w_{ic}} = 0 \tag{A.165}$$

$$\frac{\partial G_{i+1}}{\partial w_{is}} = 0 \tag{A.166}$$

$$\frac{\partial G_{i+1}}{\partial \psi_{ic}} = -\frac{5B_{26}}{b^2} \tag{A.167}$$

$$\frac{\partial G_{i+1}}{\partial \psi_{is}} = -\frac{(8B_{66} + 2B_{12})\pi}{\lambda b} \tag{A.168}$$

Equilibrium equation 8:

$$\frac{\partial G_{i+1}}{\partial w_{ic}} = 0 \tag{A.169}$$

$$\frac{\partial G_{i+1}}{\partial w_{is}} = 0 \tag{A.170}$$

$$\frac{\partial G_{i+1}}{\partial \psi_{ic}} = \frac{(4B_{66} + 2B_{12})}{\lambda b} \tag{A.171}$$

$$\frac{\partial G_{i+1}}{\partial \psi_{is}} = -\frac{5B_{26}}{b^2} \tag{A.172}$$

Equilibrium equation 9:

$$\frac{\partial G_{i+1}}{\partial w_{ic}} = \frac{A_{66}\pi}{\lambda b}\psi_{i+1,s} \tag{A.173}$$

$$\frac{\partial G_{i+1}}{\partial w_{is}} = \frac{A_{66}\pi}{\lambda b}\psi_{i+1,c} \tag{A.174}$$

$$\frac{\partial G_{i+1}}{\partial \psi_{ic}} = \frac{A_{66}\pi}{\lambda b}w_{i+1,s} + \frac{A_{26}}{b}\psi_{i+1,c} \tag{A.175}$$

$$\frac{\partial G_{i+1}}{\partial \psi_{is}} = \frac{A_{66}\pi}{\lambda b}w_{i+1,c} - \frac{A_{26}}{b}\psi_{i+1,s} \tag{A.176}$$

Equilibrium equation 10:

$$\frac{\partial G_{i+1}}{\partial w_{ic}} = 0 \tag{A.177}$$

$$\frac{\partial G_{i+1}}{\partial w_{is}} = 0 \tag{A.178}$$

$$\frac{\partial G_{i+1}}{\partial \psi_{ic}} = -\frac{A_{66}\pi}{\lambda b} w_{i+1,c} + \frac{A_{26}}{b} \psi_{i+1,s} \tag{A.179}$$

$$\frac{\partial G_{i+1}}{\partial \psi_{is}} = -\frac{A_{66}\pi}{\lambda b} w_{i+1,s} + \frac{A_{26}}{b} \psi_{i+1,c} \tag{A.180}$$

$$\frac{\partial G_{i-1}}{\partial w_i}(i=1) \tag{A.181}$$

$$\tag{A.182}$$

Equilibrium equation 1:

$$\frac{\partial G_{i-1}}{\partial w_{ic}} = -\frac{A_{26}\pi}{\lambda b} \psi_{i-1,s} \tag{A.183}$$

$$\frac{\partial G_{i-1}}{\partial w_{is}} = \frac{A_{26}\pi}{\lambda b} \psi_{i-1,c} \tag{A.184}$$

$$\frac{\partial G_{i-1}}{\partial \psi_{ic}} = -\frac{A_{26}\pi}{\lambda b} w_{i-1,s} - \frac{A_{22}}{b} \psi_{i-1,c} \tag{A.185}$$

$$\frac{\partial G_{i-1}}{\partial \psi_{is}} = \frac{A_{26}\pi}{\lambda b} w_{i-1,c} - \frac{A_{22}}{b} \psi_{i-1,s} \tag{A.186}$$

Equilibrium equation 2:

$$\frac{\partial G_{i-1}}{\partial w_{ic}} = 0 \tag{A.187}$$

$$\frac{\partial G_{i-1}}{\partial w_{is}} = 0 \tag{A.188}$$

$$\frac{\partial G_{i-1}}{\partial \psi_{ic}} = -\frac{5B_{22}}{b^2} \tag{A.189}$$

$$\frac{\partial G_{i-1}}{\partial \psi_{is}} = \frac{6B_{26}\pi}{\lambda b} \tag{A.190}$$

Equilibrium equation 3:

$$\frac{\partial G_{i-1}}{\partial w_{ic}} = 0 \tag{A.191}$$

$$\frac{\partial G_{i-1}}{\partial w_{is}} = 0 \tag{A.192}$$

$$\frac{\partial G_{i-1}}{\partial \psi_{ic}} = -\frac{6B_{26}\pi}{\lambda b} \tag{A.193}$$

$$\frac{\partial G_{i-1}}{\partial \psi_{is}} = -\frac{5B_{22}}{b^2} \tag{A.194}$$

Equilibrium equation 4:

$$\frac{\partial G_{i-1}}{\partial w_{ic}} = -\frac{A_{26}\pi}{\lambda b}\psi_{i-1,s} \tag{A.195}$$

$$\frac{\partial G_{i-1}}{\partial w_{is}} = -\frac{A_{26}\pi}{\lambda b}\psi_{i-1,c} \tag{A.196}$$

$$\frac{\partial G_{i-1}}{\partial \psi_{ic}} = -\frac{A_{22}}{b}\psi_{i-1,c} - \frac{A_{26}\pi}{\lambda b}w_{i-1,s} \tag{A.197}$$

$$\frac{\partial G_{i-1}}{\partial \psi_{is}} = \frac{A_{22}}{b}\psi_{i-1,s} - \frac{A_{26}\pi}{\lambda b}w_{i-1,c} \tag{A.198}$$

Equilibrium equation 5:

$$\frac{\partial G_{i-1}}{\partial w_{ic}} = \frac{A_{26}\pi}{\lambda b}\psi_{i-1,c} \tag{A.199}$$

$$\frac{\partial G_{i-1}}{\partial w_{is}} = -\frac{A_{26}\pi}{\lambda b}\psi_{i-1,s} \tag{A.200}$$

$$\frac{\partial G_{i-1}}{\partial \psi_{ic}} = -\frac{A_{22}}{b}\psi_{i-1,s} + \frac{A_{26}\pi}{\lambda b}w_{i-1,c} \tag{A.201}$$

$$\frac{\partial G_{i-1}}{\partial \psi_{is}} = -\frac{A_{22}}{b}\psi_{i-1,c} - \frac{A_{26}\pi}{\lambda b}w_{i-1,s} \tag{A.202}$$

Equilibrium equation 6:

$$\frac{\partial G_{i-1}}{\partial w_{ic}} = \frac{A_{66}\pi}{\lambda b}\psi_{i-1,s} \tag{A.203}$$

$$\frac{\partial G_{i-1}}{\partial w_{is}} = -\frac{A_{66}\pi}{\lambda b}\psi_{i-1,c} \tag{A.204}$$

$$\frac{\partial G_{i-1}}{\partial \psi_{ic}} = -\frac{A_{66}\pi}{\lambda b}w_{i-1,s} \tag{A.205}$$

$$\frac{\partial G_{i-1}}{\partial \psi_{is}} = \frac{A_{66}\pi}{\lambda b}w_{i-1,c} \tag{A.206}$$

Equilibrium equation 7:

$$\frac{\partial G_{i-1}}{\partial w_{ic}} = 0 \tag{A.207}$$

$$\frac{\partial G_{i-1}}{\partial w_{is}} = 0 \tag{A.208}$$

$$\frac{\partial G_{i-1}}{\partial \psi_{ic}} = -\frac{5B_{26}}{b^2} \tag{A.209}$$

$$\frac{\partial G_{i-1}}{\partial \psi_{is}} = \frac{4B_{66}\pi}{\lambda b} + \frac{2B_{12}\pi}{\lambda b} \tag{A.210}$$

Equilibrium equation 8:

$$\frac{\partial G_{i-1}}{\partial w_{ic}} = 0 \tag{A.211}$$

$$\frac{\partial G_{i-1}}{\partial w_{is}} = 0 \tag{A.212}$$

$$\frac{\partial G_{i-1}}{\partial \psi_{ic}} = -\frac{4B_{66}\pi}{\lambda b} - \frac{2B_{12}\pi}{\lambda b} \tag{A.213}$$

$$\frac{\partial G_{i-1}}{\partial \psi_{is}} = -\frac{5B_{26}}{b^2} \tag{A.214}$$

Equilibrium equation 9:

$$\frac{\partial G_{i-1}}{\partial w_{ic}} = -\frac{A_{66}\pi}{\lambda b}\psi_{i-1,s} \tag{A.215}$$

$$\frac{\partial G_{i-1}}{\partial w_{is}} = -\frac{A_{66}\pi}{\lambda b}\psi_{i-1,c} \tag{A.216}$$

$$\frac{\partial G_{i-1}}{\partial \psi_{ic}} = -\frac{A_{26}}{b}\psi_{i-1,c} - \frac{A_{66}\pi}{\lambda b}w_{i-1,s} \tag{A.217}$$

$$\frac{\partial G_{i-1}}{\partial \psi_{is}} = \frac{A_{26}}{b}\psi_{i-1,s} - \frac{A_{66}\pi}{\lambda b}w_{i-1,c} \tag{A.218}$$

Equilibrium equation 10:

$$\frac{\partial G_{i-1}}{\partial w_{ic}} = \frac{A_{66}\pi}{\lambda b}\psi_{i-1,c} \tag{A.219}$$

$$\frac{\partial G_{i-1}}{\partial w_{is}} = -\frac{A_{66}\pi}{\lambda b}\psi_{i-1,s} \tag{A.220}$$

$$\frac{\partial G_{i-1}}{\partial \psi_{ic}} = -\frac{A_{26}}{b}\psi_{i-1,s} + \frac{A_{66}\pi}{\lambda b}w_{i-1,c} \tag{A.221}$$

$$\frac{\partial G_{i-1}}{\partial \psi_{is}} = -\frac{A_{26}}{b}\psi_{i-1,c} - \frac{A_{66}\pi}{\lambda b}w_{i-1,s} \tag{A.222}$$

$$\frac{\partial G_{i+2}}{\partial w_i}(i = n) \tag{A.223}$$

(A.224)

Equilibrium equation 1:

$$\frac{\partial G_{i+2}}{\partial w_{ic}} = \frac{A_{26}\pi}{4\lambda b}\psi_{i+2,s} \tag{A.225}$$

$$\frac{\partial G_{i+2}}{\partial w_{is}} = -\frac{A_{26}\pi}{4\lambda b}\psi_{i+2,c} \tag{A.226}$$

$$\frac{\partial G_{i+2}}{\partial \psi_{ic}} = -\frac{A_{22}}{4b}\psi_{i+2,c} - \frac{A_{26}\pi}{4\lambda b}w_{i+2,s} \tag{A.227}$$

$$\frac{\partial G_{i+2}}{\partial \psi_{is}} = -\frac{A_{22}}{4b}\psi_{i+2,s} + \frac{A_{26}\pi}{4\lambda b}w_{i+2,c} \tag{A.228}$$

Equilibrium equation 2:

$$\frac{\partial G_{i+2}}{\partial w_{ic}} = 0 \tag{A.229}$$

$$\frac{\partial G_{i+2}}{\partial w_{is}} = 0 \tag{A.230}$$

$$\frac{\partial G_{i+2}}{\partial \psi_{ic}} = \frac{4B_{22}}{b^2} \tag{A.231}$$

$$\frac{\partial G_{i+2}}{\partial \psi_{is}} = \frac{B_{26}\pi}{\lambda b}\frac{B_{26}\pi}{2\lambda b} \tag{A.232}$$

Equilibrium equation 3:

$$\frac{\partial G_{i+2}}{\partial w_{ic}} = 0 \tag{A.233}$$

$$\frac{\partial G_{i+2}}{\partial w_{is}} = 0 \tag{A.234}$$

$$\frac{\partial G_{i+2}}{\partial \psi_{ic}} = -\frac{B_{26}\pi}{\lambda b} - \frac{B_{26}\pi}{2\lambda b} \tag{A.235}$$

$$\frac{\partial G_{i+2}}{\partial \psi_{is}} = \frac{4B_{22}}{b^2} \tag{A.236}$$

Equilibrium equation 4:

$$\frac{\partial G_{i+2}}{\partial w_{ic}} = -\frac{A_{26}\pi}{4lambdab}\psi_{i+2,s} \tag{A.237}$$

$$\frac{\partial G_{i+2}}{\partial w_{is}} = -\frac{A_{26}\pi}{4\lambda b}\psi_{i+2,c} \tag{A.238}$$

$$\frac{\partial G_{i+2}}{\partial \psi_{ic}} = -\frac{A_{22}}{4b}\psi_{i+2,c} - \frac{A_{26}\pi}{4\lambda b}w_{i+2,s} \tag{A.239}$$

$$\frac{\partial G_{i+2}}{\partial \psi_{is}} = \frac{A_{22}}{4b}\psi_{i+2,s} - \frac{A_{26}\pi}{4\lambda b}w_{i+2,c} \tag{A.240}$$

Equilibrium equation 5:

$$\frac{\partial G_{i+2}}{\partial w_{ic}} = \frac{A_{26}\pi}{4\lambda b}\psi_{i+2,c} \tag{A.241}$$

$$\frac{\partial G_{i+2}}{\partial w_{is}} = -\frac{A_{26}\pi}{4\lambda b}\psi_{i+2,s} \tag{A.242}$$

$$\frac{\partial G_{i+2}}{\partial \psi_{ic}} = -\frac{A_{22}}{4b}\psi_{i+2,s} + \frac{A_{26}\pi}{4\lambda b}w_{i+2,c} \tag{A.243}$$

$$\frac{\partial G_{i+2}}{\partial \psi_{is}} = -\frac{A_{22}}{4b}\psi_{i+2,c} + \frac{A_{26}\pi}{4\lambda b}w_{i+2,s} \tag{A.244}$$

Equilibrium equation 6:

$$\frac{\partial G_{i+2}}{\partial w_{ic}} = \frac{A_{66}\pi}{4\lambda b}\psi_{i+2,s} \tag{A.245}$$

$$\frac{\partial G_{i+2}}{\partial w_{is}} = -\frac{A_{66}\pi}{4\lambda b}\psi_{i+2,c} \tag{A.246}$$

$$\frac{\partial G_{i+2}}{\partial \psi_{ic}} = -\frac{A_{66}\pi}{4\lambda b}w_{i+2,s} \tag{A.247}$$

$$\frac{\partial G_{i+2}}{\partial \psi_{is}} = -\frac{A_{66}\pi}{4\lambda b}w_{i+2,c} \tag{A.248}$$

Equilibrium equation 7:

$$\frac{\partial G_{i+2}}{\partial w_{ic}} = 0 \tag{A.249}$$

$$\frac{\partial G_{i+2}}{\partial w_{is}} = 0 \tag{A.250}$$

$$\frac{\partial G_{i+2}}{\partial \psi_{ic}} = \frac{4B_{26}}{b^2} \tag{A.251}$$

$$\frac{\partial G_{i+2}}{\partial \psi_{is}} = \frac{B_{66}\pi}{\lambda b} + \frac{B_{12}\pi}{2\lambda b} \tag{A.252}$$

Equilibrium equation 8:

$$\frac{\partial G_{i+2}}{\partial w_{ic}} = 0 \tag{A.253}$$

$$\frac{\partial G_{i+2}}{\partial w_{is}} = 0 \tag{A.254}$$

$$\frac{\partial G_{i+2}}{\partial \psi_{ic}} = -\frac{B_{66}\pi}{\lambda b} - \frac{B_{12}\pi}{2\lambda b} \tag{A.255}$$

$$\frac{\partial G_{i+2}}{\partial \psi_{is}} = \frac{4B_{26}}{b^2} \tag{A.256}$$

Equilibrium equation 9:

$$\frac{\partial G_{i+2}}{\partial w_{ic}} = -\frac{A_{66}\pi}{4\lambda b}\psi_{i+2,s} \tag{A.257}$$

$$\frac{\partial G_{i+2}}{\partial w_{is}} = -\frac{A_{66}\pi}{4\lambda b}\psi_{i+2,c} \tag{A.258}$$

$$\frac{\partial G_{i+2}}{\partial \psi_{ic}} = -\frac{A_{26}}{4b}\psi_{i+2,c} - \frac{A_{66}\pi}{4\lambda b}w_{i+2,s} \tag{A.259}$$

$$\frac{\partial G_{i+2}}{\partial \psi_{is}} = \frac{A_{26}}{4b}\psi_{i+2,s} - \frac{A_{66}\pi}{4\lambda b}w_{i+2,c} \tag{A.260}$$

Equilibrium equation 10:

$$\frac{\partial G_{i+2}}{\partial w_{ic}} = \frac{A_{66}\pi}{4\lambda b}\psi_{i+2,c} \tag{A.261}$$

$$\frac{\partial G_{i+2}}{\partial w_{is}} = -\frac{A_{66}\pi}{4\lambda b}\psi_{i+2,s} \tag{A.262}$$

$$\frac{\partial G_{i+2}}{\partial \psi_{ic}} = -\frac{A_{26}}{4b}\psi_{i+2,s} + \frac{A_{66}\pi}{4\lambda b}w_{i+2,c} \tag{A.263}$$

$$\frac{\partial G_{i+2}}{\partial \psi_{is}} = -\frac{A_{26}}{4b}\psi_{i+2,c} - \frac{A_{66}\pi}{4\lambda b}w_{i+2,s} \tag{A.264}$$

$$\frac{\partial G_{i-2}}{\partial w_i}(i=1) \tag{A.265}$$

(A.266)

Equilibrium equation 1:

$$\frac{\partial G_{i-2}}{\partial w_{ic}} = -\frac{A_{26}\pi}{4\lambda b}\psi_{i-2,s} \tag{A.267}$$

$$\frac{\partial G_{i-2}}{\partial w_{is}} = \frac{A_{26}\pi}{4\lambda b}\psi_{i-2,c} \tag{A.268}$$

$$\frac{\partial G_{i-2}}{\partial \psi_{ic}} = \frac{A_{22}}{4b}\psi_{i-2,c} + \frac{A_{26}\pi}{4\lambda b}w_{i-2,s} \tag{A.269}$$

$$\frac{\partial G_{i-2}}{\partial \psi_{is}} = \frac{A_{22}}{4b}\psi_{i-2,s} - \frac{A_{26}\pi}{4\lambda b}w_{i-2,c} \tag{A.270}$$

Equilibrium equation 2:

$$\frac{\partial G_{i-2}}{\partial w_{ic}} = 0 \tag{A.271}$$

$$\frac{\partial G_{i-2}}{\partial w_{is}} = 0 \tag{A.272}$$

$$\frac{\partial G_{i-2}}{\partial \psi_{ic}} = \frac{4B_{22}}{B^2} \tag{A.273}$$

$$\frac{\partial G_{i-2}}{\partial \psi_{is}} = -\frac{B_{26}\pi}{\lambda b} - \frac{B_{26}\pi}{2\lambda b} \tag{A.274}$$

Equilibrium equation 3:

$$\frac{\partial G_{i-2}}{\partial w_{ic}} = 0 \tag{A.275}$$

$$\frac{\partial G_{i-2}}{\partial w_{is}} = 0 \tag{A.276}$$

$$\frac{\partial G_{i-2}}{\partial \psi_{ic}} = \frac{B_{26}\pi}{\lambda b} + \frac{B_{26}\pi}{2\lambda b} \tag{A.277}$$

$$\frac{\partial G_{i-2}}{\partial \psi_{is}} = \frac{4B_{22}}{b^2} \tag{A.278}$$

Equilibrium equation 4:

$$\frac{\partial G_{i-2}}{\partial w_{ic}} = \frac{A_{26}\pi}{4\lambda b}\psi_{i-2,s} \tag{A.279}$$

$$\frac{\partial G_{i-2}}{\partial w_{is}} = \frac{A_{26}\pi}{4\lambda b}\psi_{i-2,c} \tag{A.280}$$

$$\frac{\partial G_{i-2}}{\partial \psi_{ic}} = \frac{A_{22}}{4b}\psi_{i-2,c} + \frac{A_{26}\pi}{4\lambda b}w_{i-2,s} \tag{A.281}$$

$$\frac{\partial G_{i-2}}{\partial \psi_{is}} = -\frac{A_{22}}{4b}\psi_{i-2,s} + \frac{A_{26}\pi}{4\lambda b}w_{i-2,c} \tag{A.282}$$

Equilibrium equation 5:

$$\frac{\partial G_{i-2}}{\partial w_{ic}} = -\frac{A_{26}\pi}{4\lambda b}\psi_{i-2,c} \tag{A.283}$$

$$\frac{\partial G_{i-2}}{\partial w_{is}} = \frac{A_{26}\pi}{4\lambda b}\psi_{i-2,s} \tag{A.284}$$

$$\frac{\partial G_{i-2}}{\partial \psi_{ic}} = \frac{A_{22}}{4b}\psi_{i-2,s} - \frac{A_{26}\pi}{4\lambda b}w_{i-2,c} \tag{A.285}$$

$$\frac{\partial G_{i-2}}{\partial \psi_{is}} = \frac{A_{22}}{4b}\psi_{i-2,c} + \frac{A_{26}\pi}{4\lambda b}w_{i-2,s} \tag{A.286}$$

Equilibrium equation 6:

$$\frac{\partial G_{i-2}}{\partial w_{ic}} = -\frac{A_{66}\pi}{4\lambda b}\psi_{i-2,s} \tag{A.287}$$

$$\frac{\partial G_{i-2}}{\partial w_{is}} = \frac{A_{66}\pi}{4\lambda b}\psi_{i-2,c} \tag{A.288}$$

$$\frac{\partial G_{i-2}}{\partial \psi_{ic}} = \frac{A_{66}\pi}{4\lambda b}w_{i-2,s} \tag{A.289}$$

$$\frac{\partial G_{i-2}}{\partial \psi_{is}} = -\frac{A_{66}\pi}{4\lambda b}w_{i-2,c} \tag{A.290}$$

Equilibrium equation 7:

$$\frac{\partial G_{i-2}}{\partial w_{ic}} = 0 \tag{A.291}$$

$$\frac{\partial G_{i-2}}{\partial w_{is}} = 0 \tag{A.292}$$

$$\frac{\partial G_{i-2}}{\partial \psi_{ic}} = \frac{4B_{26}}{b^2} \tag{A.293}$$

$$\frac{\partial G_{i-2}}{\partial \psi_{is}} = -\frac{B_{66}}{\lambda b} - \frac{B_{12}\pi}{2\lambda b} \tag{A.294}$$

Equilibrium equation 8:

$$\frac{\partial G_{i-2}}{\partial w_{ic}} = 0 \tag{A.295}$$

$$\frac{\partial G_{i-2}}{\partial w_{is}} = 0 \tag{A.296}$$

$$\frac{\partial G_{i-2}}{\partial \psi_{ic}} = \frac{B_{66}}{\lambda b} + \frac{A_{12}\pi}{2\lambda b} \tag{A.297}$$

$$\frac{\partial G_{i-2}}{\partial \psi_{is}} = \frac{4B_{26}}{b^2} \tag{A.298}$$

Equilibrium equation 9:

$$\frac{\partial G_{i-2}}{\partial w_{ic}} = \frac{A_{66}\pi}{4\lambda b}\psi_{i-2,s} \tag{A.299}$$

$$\frac{\partial G_{i-2}}{\partial w_{is}} = \frac{A_{66}\pi}{4\lambda b}\psi_{i-2,c} \tag{A.300}$$

$$\frac{\partial G_{i-2}}{\partial \psi_{ic}} = \frac{A_{26}}{4b}\psi_{i-2,c} + \frac{A_{66}\pi}{4\lambda b}w_{i-2,s} \tag{A.301}$$

$$\frac{\partial G_{i-2}}{\partial \psi_{is}} = -\frac{A_{26}}{4b}\psi_{i-2,s} + \frac{A_{66}\pi}{4\lambda b}w_{i-2,c} \tag{A.302}$$

Equilibrium equation 10:

$$\frac{\partial G_{i-2}}{\partial w_{ic}} = -\frac{A_{66}\pi}{4\lambda b}\psi_{i-2,c} \tag{A.303}$$

$$\frac{\partial G_{i-2}}{\partial w_{is}} = \frac{A_{66}\pi}{4\lambda b}\psi_{i-2,s} \tag{A.304}$$

$$\frac{\partial G_{i-2}}{\partial \psi_{ic}} = \frac{A_{26}}{4b}\psi_{i-2,s} - \frac{A_{66}\pi}{4\lambda b}w_{i-2,c} \tag{A.305}$$

$$\frac{\partial G_{i-2}}{\partial \psi_{is}} = \frac{A_{26}}{4b}\psi_{i-2,c} + \frac{A_{66}\pi}{4\lambda b}w_{i-2,s} \tag{A.306}$$

$$\frac{\partial G_{i+3}}{\partial w_i}(i=n) \tag{A.307}$$

$$\tag{A.308}$$

Equilibrium equation 1:

$$\frac{\partial G_{i+3}}{\partial w_{ic}} = 0, \frac{\partial G_{i+3}}{\partial w_{is}} = 0, \frac{\partial G_{i+3}}{\partial \psi_{ic}} = 0, \frac{\partial G_{i+3}}{\partial \psi_{is}} = 0 \tag{A.309}$$

Equilibrium equation 2:

$$\frac{\partial G_{i+3}}{\partial w_{ic}} = 0, \frac{\partial G_{i+3}}{\partial w_{is}} = 0, \frac{\partial G_{i+3}}{\partial \psi_{ic}} = -\frac{B_{22}}{b^2}, \frac{\partial G_{i+3}}{\partial \psi_{is}} = 0 \tag{A.310}$$

Equilibrium equation 3:

$$\frac{\partial G_{i+3}}{\partial w_{ic}} = 0, \frac{\partial G_{i+3}}{\partial w_{is}} = 0, \frac{\partial G_{i+3}}{\partial \psi_{ic}} = 0, \frac{\partial G_{i+3}}{\partial \psi_{is}} = -\frac{B_{22}}{b^2} \tag{A.311}$$

Equilibrium equation 4:

$$\frac{\partial G_{i+3}}{\partial w_{ic}} = 0, \frac{\partial G_{i+3}}{\partial w_{is}} = 0, \frac{\partial G_{i+3}}{\partial \psi_{ic}} = 0, \frac{\partial G_{i+3}}{\partial \psi_{is}} = 0 \tag{A.312}$$

Equilibrium equation 5:

$$\frac{\partial G_{i+3}}{\partial w_{ic}} = 0, \frac{\partial G_{i+3}}{\partial w_{is}} = 0, \frac{\partial G_{i+3}}{\partial \psi_{ic}} = 0, \frac{\partial G_{i+3}}{\partial \psi_{is}} = 0 \tag{A.313}$$

Equilibrium equation 6:

$$\frac{\partial G_{i+3}}{\partial w_{ic}} = 0, \frac{\partial G_{i+3}}{\partial w_{is}} = 0, \frac{\partial G_{i+3}}{\partial \psi_{ic}} = 0, \frac{\partial G_{i+3}}{\partial \psi_{is}} = 0 \tag{A.314}$$

Equilibrium equation 7:

$$\frac{\partial G_{i+3}}{\partial w_{ic}} = 0, \frac{\partial G_{i+3}}{\partial w_{is}} = 0, \frac{\partial G_{i+3}}{\partial \psi_{ic}} = -\frac{B_{22}}{b^2}, \frac{\partial G_{i+3}}{\partial \psi_{is}} = 0 \tag{A.315}$$

Equilibrium equation 8:

$$\frac{\partial G_{i+3}}{\partial w_{ic}} = 0, \frac{\partial G_{i+3}}{\partial w_{is}} = 0, \frac{\partial G_{i+3}}{\partial \psi_{ic}} = 0, \frac{\partial G_{i+3}}{\partial \psi_{is}} = -\frac{B_{22}}{b^2} \tag{A.316}$$

Equilibrium equation 9:

$$\frac{\partial G_{i+3}}{\partial w_{ic}} = 0, \frac{\partial G_{i+3}}{\partial w_{is}} = 0, \frac{\partial G_{i+3}}{\partial \psi_{ic}} = 0, \frac{\partial G_{i+3}}{\partial \psi_{is}} = 0 \tag{A.317}$$

Equilibrium equation 10:

$$\frac{\partial G_{i+3}}{\partial w_{ic}} = 0, \frac{\partial G_{i+3}}{\partial w_{is}} = 0, \frac{\partial G_{i+3}}{\partial \psi_{ic}} = 0, \frac{\partial G_{i+3}}{\partial \psi_{is}} = 0 \tag{A.318}$$

$$\frac{\partial G_{i-3}}{\partial w_i}(i=1) \tag{A.319}$$

$$\tag{A.320}$$

Equilibrium equation 1:

$$\frac{\partial G_{i-3}}{\partial w_{ic}} = 0, \frac{\partial G_{i-3}}{\partial w_{is}} = 0, \frac{\partial G_{i-3}}{\partial \psi_{ic}} = 0, \frac{\partial G_{i-3}}{\partial \psi_{is}} = 0 \tag{A.321}$$

Equilibrium equation 2:

$$\frac{\partial G_{i-3}}{\partial w_{ic}} = 0, \frac{\partial G_{i-3}}{\partial w_{is}} = 0, \frac{\partial G_{i-3}}{\partial \psi_{ic}} = -\frac{B_{22}}{b^2}, \frac{\partial G_{i-3}}{\partial \psi_{is}} = 0 \tag{A.322}$$

Equilibrium equation 3:

$$\frac{\partial G_{i-3}}{\partial w_{ic}} = 0, \frac{\partial G_{i-3}}{\partial w_{is}} = 0, \frac{\partial G_{i-3}}{\partial \psi_{ic}} = 0, \frac{\partial G_{i-3}}{\partial \psi_{is}} = -\frac{B_{22}}{b^2} \tag{A.323}$$

Equilibrium equation 4:

$$\frac{\partial G_{i-3}}{\partial w_{ic}} = 0, \frac{\partial G_{i-3}}{\partial w_{is}} = 0, \frac{\partial G_{i-3}}{\partial \psi_{ic}} = 0, \frac{\partial G_{i-3}}{\partial \psi_{is}} = 0 \tag{A.324}$$

Equilibrium equation 5:

$$\frac{\partial G_{i-3}}{\partial w_{ic}} = 0, \frac{\partial G_{i-3}}{\partial w_{is}} = 0, \frac{\partial G_{i-3}}{\partial \psi_{ic}} = 0, \frac{\partial G_{i-3}}{\partial \psi_{is}} = 0 \tag{A.325}$$

Equilibrium equation 6:

$$\frac{\partial G_{i-3}}{\partial w_{ic}} = 0, \frac{\partial G_{i-3}}{\partial w_{is}} = 0, \frac{\partial G_{i-3}}{\partial \psi_{ic}} = 0, \frac{\partial G_{i-3}}{\partial \psi_{is}} = 0 \tag{A.326}$$

Equilibrium equation 7:

$$\frac{\partial G_{i-3}}{\partial w_{ic}} = 0, \frac{\partial G_{i-3}}{\partial w_{is}} = 0, \frac{\partial G_{i-3}}{\partial \psi_{ic}} = -\frac{B_{22}}{b^2}, \frac{\partial G_{i-3}}{\partial \psi_{is}} = 0 \tag{A.327}$$

Equilibrium equation 8:

$$\frac{\partial G_{i-3}}{\partial w_{ic}} = 0, \frac{\partial G_{i-3}}{\partial w_{is}} = 0, \frac{\partial G_{i-3}}{\partial \psi_{ic}} = 0, \frac{\partial G_{i-3}}{\partial \psi_{is}} = -\frac{B_{22}}{b^2} \tag{A.328}$$

Equilibrium equation 9:

$$\frac{\partial G_{i-3}}{\partial w_{ic}} = 0, \frac{\partial G_{i-3}}{\partial w_{is}} = 0, \frac{\partial G_{i-3}}{\partial \psi_{ic}} = 0, \frac{\partial G_{i-3}}{\partial \psi_{is}} = 0 \tag{A.329}$$

Equilibrium equation 10:

$$\frac{\partial G_{i-3}}{\partial w_{ic}} = 0, \frac{\partial G_{i-3}}{\partial w_{is}} = 0, \frac{\partial G_{i-3}}{\partial \psi_{ic}} = 0, \frac{\partial G_{i-3}}{\partial \psi_{is}} = 0 \tag{A.330}$$

References

[1] http://www.google.co.uk/search=a380+fuselage+wing. vii, 2

[2] http://www.google.co.uk/search=a380+boeing787. vii, 3

[3] M.Stein. *Analytical results for post-buckling behaviour of plates in compression and in shear.In:*Aspects of Analysis of Plate Structures, A volume in honour of W.H.Wittrick*(ed.D.J.Dawe, R.W.Horsington, A.G.Kamtekar and G.H.Little).* Clarendon Press, Oxford, 1984. vii, 3, 4, 5, 36, 37, 54, 57

[4] L.Euler. On the strength of columns. *Academie Royale des Sciences et Belle Lettres Memoires*, 13:252, 1759. English translation by A. J. Van den Broek, Euler's Classic Paper 'On the Strength of Columns', *American Journal of Physics*, Volume 15, Number 4, July-August 1947, pp. 309-318. 2, 7

[5] Y.K.Cheung. The finite strip method in the analysis of elastic plates with two opposite simply supported ends. *Proceedings of the Institution of Civil Engineers*, 40(1):1–7, 1968. 3

[6] F.W.Williams, D.Kennedy, and M.S.Anderson. Analysis features of VICONOPT, an exact buckling and vibration program for prismatic assemblies of anisotropic plates. Proceedings of 31st AIAA/ASME/ASCE/AHS/ASC Structure, Structural Dynamics, and Materials Conference, Long Beach, CA, pages 920–929, 1990. 3, 45, 49

[7] D.Kennedy. Formulation of equations for finding stress resultants (method 2). *unpublished report*, 2007. 3, 4, 54

[8] Karlsson, Hibbitt, and Inc. Sorensen. *"ABAQUS/Standard User's Manual", Version 6.8.* Pawtucket, RI, 2008. 4

[9] MSC/Software. *MSC/NASTRAN verstion 70.7, MSC.* Los Angeles, USA, 1999. 4

[10] G.H.Bryan. On the stability of a plane plate under thrusts in its own plane, with applications to the 'buckling' of the sides of a ship. volume 22, from November 1890 to November 1891 (read 11 December 1890) of *Proceedings of the London Mathematical Society*, pages 54–67. 7

[11] L.H.Donnell. Stability of thin-walled tubes under torsion. *NACA Report 479, National Advisory Committee on Aeronautics, Washington, D.C., 1933. Also, A New Theory for the Buckling of Thin Cylinders Under Axial Compression and Bending,* Transactions of the American Society of Mechanical Engineers, 56:795–806, 1934. 7

[12] T.Von Kármán and H.S.Tsien. The buckling of thin cylindrical shells under axial compression. *Journal of the Aeronautical Sciences*, 8(8):303–312, 1941. 7

[13] S.B.Batdorf. A simplified method of elastic-stability analysis for thin cylindrical shells. *NACA Report 874, National Advisory Committee on Aeronautics*, Washington, D.C., 1947. 7

[14] T.Von Kármán. Festigkeitsprobleme im maschinenbau. *Enzyklop´adie der Mathematischen Wissenschaften*, 4:311–385, 1910. 7, 28, 31

[15] W.T.Koiter. De meedragende breedte bij groote oversehrijding der dnikspanning voor versehillende inklemming der plaatranden. (the effective width of infinitely long, flat rectangular plates under various conditions of edge restraint.). Rep.S.287.Nationaal Luchtvaartlaboratorium, Amsterdam, 1943. 7, 29

[16] J.W.Hutchinson and B.Budiansky. Dynamic buckling estimates. *AIAA Journal*, 4:525–530, 1967. 7, 29

[17] R.M.Jones. *Buckling of bars, plates and shells.* Bull Ridge Publishing, Blacksburg, Virginia, 2006. 8, 21, 23

[18] T.V.Galambos. *Guide to Stability Design Criteria for Metal Structures.* John Wiley, New York, 4th ed. edition, 1988. 9

[19] W.F.Chen and E.M.Lui. *Structural Stability. Theory and Implementation.* PTR, Prentice-Hall, Englewood Cliffs, NJ, 1987. 9

[20] A.W.Leissa. *Buckling and postbuckling theory for laminated composite plates. In:* Buckling and postbuckling of composite plates*(ed. G. J. Turvey, I. H. Marshall).* Chapman Hall, London, 1995. 11, 17

[21] J.N.Reddy. *Mechanics of laminated composite plates and shells: Theory and analysis.* CRC Press, Florida, 2004. 11, 17

[22] C.H.Yoo and S.C.Lee. *Stability of structures: principles and applications.* Elsevier, Oxford, 2011. 12, 24

[23] E.Reissner. On the theory of bending of elastic plates. *Journal of Mathematical Physics*, 23:198–191, 1944. 16, 17

[24] E.Reissner. The effect of transverse shear deformation on the bending of elastic plates. *Transactions of ASME, Journal of Applied Mechanics*, 12:A69–A77, 1945. 16, 17

[25] R.D.Mindlin. Influence of rotatory inertia and shear on flexural motions of isotropic, elastic plates. *Transactions of ASME, Journal of Applied Mechanics*, 18:31–38, 1951. 16

[26] S.A.Ambartsumyan. *Theory of Anisotropic Plates.* Scientific Publishing House (English Translation by Technomic, Stamford, CT, 1970), Moscow, 1967. 17

[27] C.M.Wang, C.Y.Wang, and J.N.Reddy. *Exact solutions of structural members.* CRC Press, Florida, 2005. 17

[28] H.S.Shen. *Postbuckling behavior of plates and shells.* Science and Technology Press, Shanghai, 2002. 20

[29] J.W.Hutchinson and W.T.Koiter. Postbuckling theory. *Applied Mechanics Reviews*, 23(12):1353–1366, 1970. 21

[30] T.Von Kármán, E.E.Sechler, and L.H.Donnell. The strength of thin plates in compression. *Transactions of ASME*, 54:53–57, 1932. 29

[31] H.L.Cox. *The buckling of thin plates in compression.* British Ministry of Aviation, Aeronautical Research Council, Reports and Memoranda, No. 1554, 1933. 29

[32] S.Timoshenko and J.M.Gere. *Theory of elastic stability.* Mcgraw-Hill Book Co., Inc., 1961. 29, 165

[33] K.Marguerre and E.Trefftz. ´Uber die tragf´ahigkeit cines l´angsbelasteten plattenstreifens nach ´Ubersehreiten der beullast. *Zeitschrift f´ur Angewandte Mathematik und Mechanik*, 17(2):85–100, 1937. 29

[34] A.Van der Neut. Post buckling behaviour of structures. V.T.H Rep.69, Technisehe Hogesechool Vliegtnigbonwkunde (Delft, Netherlands), 1956. 29

[35] A.Kromm and K.Marguerre. Behaviour of a plate strip under shear and compressive stresses beyond the buckling limit. *NACA TM*, (870), 1937. 29

[36] S.Levy. Bending of rectangular plates with large deflections. NACA Report 737, 1942. 29

[37] J.Mayers and B.Budiansky. Analysis of behaviour of simply supported flat plates compressed beyond the buckling load in the plastic range. *NACA TM*, (3368), 1955. 29

[38] G.Smith. *in: Thin-walled steel structures.* C. K. Rockey and H. V. Hill, Eds., Crosby Lockwood and Son Ltd, London, 1967. 29

[39] E.Reissner and Y.Stavsky. Bending and stretching of certain types of heterogeneous aelotropic elastic plates. *ASME Journal of Applied Mechanics*, 28:402–408, 1961. 29

[40] Y.Stavsky. Bending and stretching of laminated aelotropic plates. *Transactions ASCE*, 127, 1962. 29

[41] Y.Stavsky. Thermoelasticity of heterogeneous aeolotropic plates. *ASCE Journal of Engineering Mechanics*, 89, 89-105. 29

[42] B.Budiansky. Dynamic buckling of elastic structures: criteria and estimates. "Dynamic stability of structures," Proceedings of an International Conference, Northwestern University, Evanston, Illinois, Pergamon Press, 1965. 29

[43] B.Budiansky and J.W.Hutchinson. Dynamic buckling of imperfection-sensitive structures. Proceedings of XI International Congress on Applied Mechanics, Munich, Julius Springer-Verlag, pages 636–651, 1966. 29

[44] J.M.T.Thompson. Basic concepts of elastic stability. Technical report No.6, perpared for the National Aeronautics and Space Administration, under Grant NsG 93-60, 1963. 29

[45] J.M.T.Thompson. Basic principles in the general theory of elastic stability. *Journal of the Mechanics and Physics of Solids*, 11(1):13–20, 1963. 29

[46] J.M.T.Thompson. Towards a general statistical theory of imperfection-sensitivity in elastic post-buckling. *Journal of the Mechanics and Physics of Solids*, 15(6):413–417, 1967. 29

[47] J.M.T.Thompson and A.C.Walker. The non-linear perturbation analysis of discrete structural systems. *International Journal of Solids and Structures*, 4(8):757–768, 1968. 29

[48] M.J.Sewell. A general theory of elastic and inelastic plate failure-i. *Journal of the Mechanics and Physics of Solids*, 11(6):377–393, 1963. 29

[49] P.R.Hill. A general theory of uniqueness and stability of elastic plastic solids. *Journal of the Mechanics and Physics of Solids*, 6:236–249, 1959. 29

[50] M.J.Sewell. A general theory of elastic and inelastic plate failure-ii. *Journal of the Mechanics and Physics of Solids*, 12(5):279–297, 1964. 30

[51] M.J.Sewell. A method of post-buckling analysis. *Journal of the Mechanics and Physics of Solids*, 17(4):219–233, 1969. 30

[52] H.G.Allen. Analysis of sandwich panels: the significance of shear deformation. *Composites*, 1(4):215–220, 1970. 30

[53] S.Wang and D.J.Dawe. Finite strip large deflection and post-overall-buckling analysis of diaphragm-supported structures. *Computers and Structures*, 61(1):155–170, 1996. 30, 41

[54] S.Wang and D.J.Dawe. Spline FSM postbuckling analysis of shear-deformable rectangle laminates. *Thin-Walled Structures*, 34:163–178, 1999. 30, 41

[55] Y.Ge, W.Yuan, and D.J.Dawe. Thermomechanical postbuckling of composite laminated plates by the spline finite strip method. *Computers and Structures*, 71:115–129, 2005. 30, 41

[56] J.Rhodes. Some observations on the post-buckling behaviour of thin plates and thin-walled members. *Thin-Walled Structures*, 41:207–226, 2003. 30

[57] K.Marguerre. Zur theorie der gekreummter platte grosser formaenderung. Proceedings of Fifth International Congress for Applied Mechanics, Cambridge, UK, 1938. 31

[58] L.Librescu and W.Q.Lin. Postbuckling and vibration of shear deformable flat plat and curved panels on a non-linear elastic foundation. *International Journal of Non-linear Mechanics*, 32(2):211–225, 1996. 31

[59] P.R.Everall and G.W.Hunt. Arnold tongue predictions of secondary buckling in thin elastic plates. *Journal of the Mechanics and Physics of Solids*, 47(10):2187–2206, 1999. 31

[60] S.B.Singh and A.Kumar. Postbuckling response and strength of laminates under combined in-plane loads. *Composites Science and Technology*, 59:727–736, 1999. 31

[61] G.Srikanth and A.Kumar. Postbuckling response and failure of symmetric laminates under uniform temperature rise. *Composite Structures*, 59:109–118, 2003. 31

[62] P.Jain and A.Kumar. Postbuckling response of square laminates with a central circular/elliptical cutout. *Composite Structures*, 65:179–185, 2004. 31

[63] A.Kumar and S.B.Singh. Postbuckling strengths of composite laminate with various shaped cutouts under in-plane shear. *Composite Structures*, 92:2966–2978, 2010. 31

[64] K.M.Liew, J.Wang, M.J.Tan, and S.Rajendran. Postbuckling analysis of laminated composite plates using the mesh-free kp-ritz method. *Computer Methods in Applied Mechanics and Engineering*, 195:551–570, 2006. 31

[65] J.Yang, K.M.Liew, and S.Kitipornchai. Imperfection sensitivity of the postbuckling behavior of higher-order shear deformable functionally graded plates. *International Journal of Solids and Structures*, 43:5247–5266, 2006. 31

[66] K.M.Liew, J.Yang, and S.Kitipornchai. Postbuckling of piezoelectric fgm plates subject to thermo-electro-mechanical loading. *International Journal of Solids and Structures*, 40:3869–3892, 2003. 32

[67] J.Woo, S.A.Meguid, J.C.Stranart, and K.M.Liew. Thermomechanical postbucklinganalysis of moderately thick functionally graded plates and shallow shells. *International Journal of Mechanical Sciences*, 47:1147–1171, 2005. 32

[68] H.S.Shen and F.W.Williams. Termal postbuckling analysis of imperfect laminated plates on softening non-linear elastic foundations. *Composites Science and Technology*, 57:719–728, 1997. 32

[69] H.S.Shen. Thermomechanical postbuckling analysis of imperfect shear deformation laminated plates on elastic foundations. *Computer Methods in Applied Mechanics and Engineering*, 189:761–784, 2000. 32

[70] H.S.Shen. Thermal postbuckling behavior of shear deformable fgm plates with temperature-dependent properties. *International Journal of Mechanical Sciences*, 49:466–478, 2007. 32

[71] P.Kere and M.Lyly. Reissner-mindlin-von kármán type plate model for nonlinear analysis of laminated composite structures. *Composite Structures*, 71:289–292, 2005. 32

[72] C.G.Diaconu and P.M.Weaver. Postbuckling of long unsymmetrically laminated composite plates under axial compression. *International Journal of Solids and Structures*, 43:6978–6997, 2006. 32

[73] M.Stein. Postbuckling of orthotropic composite plates loaded in compression. *AIAA Journal*, 21(12):1729–1735, 1983. 32

[74] A.D.Muradova and G.E.Stavroulaki. Buckling and postbuckling analysis of rectangular plates resting on elastic foundations with the use of the spectral method.

Computer Methods in Applied Mechanics and Engineering, 205-208:213–220, 2012. 32

[75] H.Chen and W.B.Yu. Postbuckling and mode jumping analysis of composite laminates using an asymptotically correct,geometrically non-linear theory. *International Journal of Non-Linear Mechanics*, 41:1143–1160, 2006. 32

[76] S.C.Han, S.Y.Lee, and G.Rus. Postbuckling analysis of laminated composite plates subjected to the combination of in-plane shear, compression and lateral loading. *International Journal of Solids and Structures*, 43:5713–5735, 2006. 33

[77] M.Stein. Loads and deformations of buckled rectangular plates. NASA Tech. Rep. R-40, 1959. 33, 36

[78] M.Lentini and V.Pereyra. An adaptive finite difference solver for nonlinear two-point boundary problems with mild boundar layers. *SIAM Journal on Numerical Analysis*, 14(1), 1977. 38

[79] Y.K.Cheung. *Finite strip method in structural analysis*. Pergamon, Oxford, 1976. 40

[80] Y.K.Cheung and M.S.Cheung. Natural vibrations of thin flat-walled structures with different boundary conditions. *Journal of Sound and Vibration*, 18:325–337, 1971. 40

[81] P.V.T.Babu and D.V.Reddy. Frequency analysis of skew orthotropy plates by the finite strip method. *Journal of Sound and Vibration*, 18:465–474, 1974. 40

[82] G.J.Turvey and W.H.Wittrick. The influence of orthotropy on the stability of some multi-plate structures in compression. *Aeronautical Quarterly*, 24:1–8, 1973. 40

[83] D.J.Dawe. Finite strip bucling analysis of curved plate assemblies under biaxial loading. *International Journal of Solids and Structures*, 13:1141–1155, 1977. 40

[84] T.R.G.Smith and S.Sridharan. A finite strip method for the buckling of plate structures under arbitrary loading. *International Journal of Mechanical Sciences*, 20:685–693, 1978. 40

[85] W.H.Wittrick. A unified approach to the initial buckling of stiffened panels in compression. *Aeronautical Quarterly*, 12:265–283, 1968. 40, 41

[86] W.H.Wittrick. General sinusoidal stiffness matrices for buckling and vibration analysis of thin flat-walled structures. *International Journal of Mechanical Sciences*, 10:946–966, 1968. 40, 41

[87] W.H.Wittrick and F.W.Williams. Buckling and vibration of anisotropic or isotropic plate assemblies under combined loadings. *International Journal of Mechanical Sciences*, 16(4):209–239, 1974. 41, 43, 44, 49

[88] J.Kong and Y.K.Cheung. A generalized spline finite strip for the analysis of plates. *Thin-Walled Structures*, 22:181–202, 1995. 41

[89] D.J.Dawe and V.Peshkam. A note on finite strip buckling analysis of composite plate structures. *Composite Structures*, 34:163–168, 1996. 41

[90] D.Y.Tan and D.J.Dawe. Buckling and vibration analysis of composite laminated plates and shells using general spline function. *Composite Structures*, 10(1):25–42, 1998. 41

[91] D.J.Dawe and Y.S.Ge. Thermal buckling of shear-deformable composite laminated plates by the spline finite strip method. *Computer Methods in Applied Mechanics and Engineering*, 185:347–366, 2000. 41

[92] M.A.Bradford and M.Azhari. Buckling of plates with defferent end conditions using the finite strip method. *Computers and Structures*, 1:75–83, 1995. 41

[93] H.R.Ovesy, J.Loughlan, and H.Assaee. The compressive post-local bucking behaviour of thin plates using a semi-energy finite strip approach. *Thin-Walled Structures*, 42:449–474, 2004. 41

[94] H.R.Ovesy and H.Assaee. An investigation on the post-buckling behavior of symmetric cross-ply laminated plates using a semi-energy finite strip approach. *Composite Structures*, 71:365–370, 2005. 41

[95] H.R.Ovesy and H.Assaee. The effects of bendctwist coupling on the post-buckling characteristics of composite laminated plates using semi-energy finite strip approach. *Thin-Walled Structures*, 45:209–220, 2007. 42

[96] H.R.Ovesy and H.Assaee. Semi-energy finite strip post-buckling analysis of laminated plates concerning the effects of mechanical coupling. *Composite Structures*, 89:120–125, 2009. 42

[97] *ANSYS Academic Research, Release 14.0, Help System, Coupled Field Analysis Guide*. ANSYS, Inc. 42

[98] J.Loughlan. The influence of mechanical couplings on the compressive stability of anti-symmetric angle-ply laminates. *International Journal for Numerical Methods in Engineering*, 57:473–482, 2002. 42

[99] H.R.Ovesy, H.Assaee, and M.Hajikazemi. Post-buckling of thick symmetric laminated plates under end-shortening and normal pressure using semi-energy finite strip method. *Computers and Structures*, 89:724–732, 2011. 42

[100] H.R.Ovesy, J.Loughlan, and S.A.M.GhannadPour. Geometric non-linear analysis of thin flat plates under end shortening, using different versions of the finite strip method. *International Journal of Mechanical Sciences*, 47:1923–1948, 2005. 42

[101] H.R.Ovesy, J.Loughlan, and S.A.M.GhannadPour. Geometric non-linear analysis of channel sections under end shortening, using different versions of the finite strip method. *Computers and Structures*, 84:855–872, 2006. 42

[102] H.R.Ovesy, J.Loughlan, S.A.M.GhannadPour, and G.Morada. Geometric non-linear analysis of box sections under end shortening, using three different versions of the finite-strip method. *Computers and Structures*, 44:623–637, 2006. 42

[103] H.R.Ovesy, S.A.M.GhannadPour, and G.Morada. Post-buckling behavior of composite laminated plates under end shortening and pressure loading, using two versions of finite strip method. *Composite Structures*, 75:106–113, 2006. 42

[104] H.R.Ovesy, S.A.M.GhannadPour, and G.Morada. Geometric non-linear analysis of composite laminated plates with initial imperfection under end shortening, using two versions of finite strip method. *Composite Structures*, 71:307–314, 2005. 42

[105] H.R.Ovesy, S.A.M.GhannadPour, and G.Morada. Geometric non-linear analysis of imperfect composite laminated plates, under end shortening and pressure loading, using finite strip method. *Composite Structures*, 75:100–105, 2006. 42

[106] H.R.Ovesy and S.A.M.GhannadPour. An exact finite strip for the initial post-buckling analysis of channel section struts. *Computers and Structures*, 89:1785–1796, 2011. 43

[107] S.A.M.GhannadPour and H.R.Ovesy. The application of an exact finite strip to the buckling of symmetrically laminated composite rectangular plates and prismatic plate structures. *Composite Structures*, 89:151–158, 2009. 43

[108] S.Yuan, K.S.Ye, F.W.Williams, and D.Kennedy. Recursive second order convergence method for natural frequencies and modes when using dynamic stiffness matrices. *International Journal for Numerical Methods in Engineering*, 56:1795–1814, 2003. 43

[109] G.Eccher, K.J.R.Rasmussen, and R.Zandonini. Elastic buckling analysis of perforated thin-walled structures by the isoparametric spline finite strip method. *Thin-Walled Structures*, 46:165–191, 2008. 43

[110] G.Eccher, K.J.R.Rasmussen, and R.Zandonini. Geometric nonlinear isoparametric spline finite strip analysis of perforated thin-walled structures. *Thin-Walled Structures*, 47:219–232, 2009. 43

[111] Z.Y.Yao and K.J.R.Rasmussen. Material and geometric nonlinear isoparametric spline finite strip analysis of perforated thin-walled steel structuresanalytical developments. *Thin-Walled Structures*, 49:1359–1373, 2011. 43

[112] T.H.Lui and S.S.E.Lam. Finite strip analysis of laminated plates with general initial imperfection under end shortening. *Engineering Structures*, 23:673–686, 2011. 43

[113] W.H.Wittrick and F.W.Williams. A general algorithm for computing natural frequencies of elastic structures. *Quarterly Journal of Mechanics and Applied Mathematics*, 1(4):497–518, 1971. 43

[114] D.Kennedy, M.Fischer, and C.A.Featherston. Recent development in exact strip analysis and optimum design of aerospace structures. *Proceedings of the IMechE Part C: Journal of Mechanical Engineering Science*, 221:399–413, 2007. 43, 50

[115] F.W.Williams. Computation of natural frequencies and initial buckling stresses of prismatic plate assemblies. *Journal of Sound and Vibration*, 21(1), 1972. 45

[116] R.Butler F.W.Williams. Optimum design using VICONOPT, a buckling and strength constraint program for prismatic plate assemblies of anisotropic plates. *Computers and Structures*, 43(4):699–708, 1992. 46, 47, 51

[117] M.S.Anderson, F.W.Williams, and C.J.Wright. Buckling and vibration of any prismatic assembly of shear and compression loaded anisotropic plates with an arbitrary supporting structure. *International Journal of Mechanical Sciences*, 25(8):585–596, 1983. 46, 49

[118] F.W.Williams and M.S.Anderson. Incorporation of lagrangian mutipliers into an algorithm for finding exact natural frequencies or critical buckling loads. *International Journal of Mechanical Sciences*, 8:579–584, 1983. 47

[119] S.M.Powell. *Buckling and postbuckling of prismatic plate assemblies usingexact eigenvalue theory.* PhD thesis, Cardiff School of Engineering, Cardiff University, Cardiff, 1997. 49

[120] F.W.Williams, M.S.Anderson, D.Kennedy, R.Butler, G.Aston, and S.M.Hoh. User manual for VICONOPT: An exact analysis and optimum design program covering the buckling and vibration of prismatic assemblies of flat in-plane loaded, anisotropic plates, with approximations for curved and tapered plates, discrete supports and transverse stiffeners. *Release 1.3, School of Engineering, University of Wales Cardiff*, 1993. 49

[121] F.W.Williams, D.Kennedy, M.S.Anderson, and D.A.Edwards. User manual for VICONOPT: An exact analysis and optimum design program covering the buckling and vibration of prismatic assembies of flat in-plane loaded, anisotropic plates, with approximations for curved and tapered plates, discrete supports and connections, tansverse stiffeners and attachments to three-dimensional supporting frames. *Release 1.3, School of Engineering, University of Wales Cardiff*, 1996. 49

[122] G.N.Vanderplaats and O.Moses. Structural optimisation by methods of feasible directions. *Computers and Structures*, 3:739–755, 1973. 50

[123] S.M.Powell, F.W.Williams, A.S.Askar, and D.Kennedy. Local postbuckling analysis for perfect and imperfect longitudinally compressed plates and panels. Proceedings of the 39th AIAA/ASME/ASCE/AHS/ASC Structures, Structural Dynamics and Materials Conference, Long Beach, CA, pages 595–603, 1998. 50, 52

[124] M.Fischer. *Multilevel optimisation of aerospace and lightweight structures.* PhD thesis, Cardiff School of Engineering, Cardiff University, Cardiff, 2002. 50

[125] M.Fischer, D.Kennedy, and C.A.Featherston. Multilevel optimisation of a composite aircraft wing using viconopt mlo. Proceedings of the 9th AIAA/ISSMO Symposium on Multidisciplinary analysis and optimisation, Atlanta, GA, Paper AIAA 2002-5511, 2002. 50

[126] M.Fischer, D.Kennedy, and C.A.Featherston. Multilevel optimisation of aerospace and lightweight structures. Proceedings of the 23th International Congress of Aeronautical Science, Toronto, pages 344.1–344.9, 2002. 50

[127] MSC/Software. *MSC/NASTRAN version 70.7, MSC, Los Angeles, USA*. 1999. 50

[128] M.S.Anderson and D.Kennedy. Postbuckling of composite stiffened panels using exact strip analysis with Newton iteration. Proceedings of 49th AIAA/ASME/ASCE/AHS/ASC Structures, Structural Dynamics, and Materials Conference, Schaumburg, II, pages 1–8, 2008. 50, 52

[129] S.Qu, D.Kennedy, and C.A.Featherston. Multilevel optimisation of an aircraft wing incorporating postbuckling effects. Proceedings of CEAS European Air and Space Conference, Manchester, UK, pages 1–10, 2009. 50

[130] S.Qu. *Multilevel optimisation of aerospace and lightweight structures incorporating postbuckling effects.* PhD thesis, Cardiff School of Engineering, Cardiff University, Cardiff, 2011. 50, 52

[131] B.Che, D.Kennedy, and C.A.Featherston. Improved exact strip postbuckling analysis for anisotropic plates. Proceedings of 2nd Royal Aeronautical Society Conference on Aircraft Structural Design, London, UK, Paper 42, 2009. 50, 104

[132] D.Kennedy, T.J.Ong, O.J.O'Leary, and F.W.Williams. Practical optimisation of aerospace panels. Proceedings of 1st ASMO UK/ISSMO Conference, Ilkley, pages 217–224, 1999. 50

[133] O.J.O'Leary. *Optimisation of prismatic plate structures with natural frequency constraints*. PhD thesis, Cardiff School of Engineering, Cardiff University, Cardiff, 2000. 50

[134] O.J.O'Leary, F.W.Williams, and D.Kennedy. Optimum stiffened panel design with fundamental frequency constraint. *Thin-Walled Structures*, 39(7):555–569, 2001. 50

[135] D.Kennedy, O.J.O'Leary, and F.W.Williams. Optimum design of prismatic plate assemblies with spectral gap constraints. Proceedings of 5th International Symosium on Vibrations of Continuous Systems, Berchtesgaden, pages 36–38, 2005. 50

[136] A.Watson and D.Kennedy. Mode jumping in post-buckled stiffened panels. Proceedings of 4th International Conference on Thin-Walled Structures, Institute of Physics, Bristol, 2004. 52

[137] D.Kennedy and C.A.Featherston. Exact strip analaysis and optimum design of aerospace structures. *The Aeronautical Journal*, 114(1158):505–512, 2010. 52, 79